IDENTIFICATION OF MODULATORY FUNCTIONS OF TP53, ESTROGEN SIGNALING, AND 14q32.31 miRNA CLUSTER ON CHRNA5 KNOCK-DOWN EXPRESSION PROFILE AND DEVELOPMENT OF syneRgy APP

A DISSERTATION SUBMITTED TO
THE GRADUATE SCHOOL OF ENGINEERING AND SCIENCE
OF BILKENT UNIVERSITY
IN PARTIAL FULFILLMENT OF THE REQUIREMENTS FOR
THE DEGREE OF
DOCTOR OF PHILOSOPHY

IN

NEUROSCIENCE

By

AYŞE GÖKÇE KEŞKÜŞ

SEPTEMBER, 2021

IDENTIFICATION OF MODULATORY FUNCTIONS OF TP53, ESTROGEN SIGNALING, AND 14q32.31 miRNA CLUSTER ON CHRNA5 KNOCK-DOWN EXPRESSION PROFILE AND DEVELOPMENT OF syneRgy APP

By Ayşe Gökçe Keşküş

September, 2021

We certify that we have read this dissertation and that in our opinion it is fully adequate in scope and in quality, as a dissertation for the degree of Doctor of Philosophy.

_____

Özlen Konu Karakayalı

(Advisor)

_____

Michelle Marie. Adams

_____

Sreeparna Banerjee

_____

Hacı Hulusi Kafalıgönül

_____

Nurcan Tunçbağ

Approved for the Graduate School of Engineering and Science:

_____

Ezhan KARAŞAN

Director of the Graduate School of Engineering and Science

Abstract

IDENTIFICATION OF MODULATORY FUNCTIONS OF

TP53, ESTROGEN SIGNALING, AND 14q32.31 miRNA CLUSTER ON

CHRNA5 KNOCK-DOWN EXPRESSION PROFILE AND

DEVELOPMENT OF syneRgy APP

Ayşe Gökçe Keşküş

Ph.D. in Neuroscience

Supervisor: Özlen Konu Karakayalı

September 2021

Cholinergic receptor subunit alpha 5 (CHRNA5) is a ligand-gated ion channel expressed in not only the nervous system but also other tissues. Differential expression and the polymorphisms of CHRNA5 have been associated with addiction, particularly nicotine and various cancer types. The tumor-suppressive properties of CHRNA5 depletion, i.e., decrease in cell proliferation, induction of DNA damage response, and drug sensitivity, have been identified in breast cancer cell lines. This thesis focuses on identifying critical factors modulating or modulated by the knock-down of CHRNA5 in breast cancer cell lines using both wet-lab and bioinformatics approaches. Here I have first found the significant correlation between CHRNA5 and DNA damage response in breast cancer tumor datasets. Moreover, I discovered that the introduction of siTP53 antagonized the actions of siCHRNA5 and reverted the siCHRNA5-mediated cell cycle inhibition and drug sensitivity in the MCF7 breast cancer cell line.

Furthermore, siCHRNA5 was found to inhibit the secondary signaling of estrogen/ESR1 in time and dosage-dependent manners. CHRNA5 depletion also downregulated the conserved 14q32.31 miRNA

cluster expression. Among those miRNAs, miR495-3p appeared to be the most prominent candidate, exhibiting a similar expression profile with selective estrogen degraders and partially with siCHRNA5. However, the inhibitory effect of the combinatorial treatment with siCHRNA5 and miR495-3p on the secondary targets of estrogen signaling indicated that siCHRNA5 and miR495-3p might target converging pathways, evidenced by the antagonism (rather than addictiveness) between them.

In addition, the Shiny-based syneRgy app was developed to analyze the transcriptome-based synergy between treatments and/or genetic modifications. As a case study, syneRgy analysis using novel MDM2 inhibitor and/or temozolomide treated neuroblastoma cell lines revealed that although the tumor-suppressor effect of combination therapy was more than each individual treatment, it was less than additive. syneRgy was applied to understand the combinatorial treatment of siCHRNA5 with siTP53 as well as siCHRNA5 with miR495-3p mimic and enhanced our understanding of the TFs that might have a role in the crosstalk. To our knowledge, syneRgy is the first-ever online tool to perform statistical synergy analysis using RNAseq count or logFC transcriptomic data and *synreg*, i.e. our novel methodology allowing for statistical tests of TF target enrichment using regression models.

Keywords: CHRNA5, estrogen signaling, selective estrogen receptor degraders, selective estrogen receptor modulators, TP53 signaling, miRNA, 14q31.32 miRNA cluster, transcriptomics, synergy analysis.

Özet

TP53, ÖSTROJEN SİNYAL YOLAĞI, VE 14q32.31 miRNA GRUBU'NUN CHRNA5 DEPLESYON İFADE PROFİLİ ÜZERINE ETKİLERİNİN BELİRLENMESİ VE syneRgy UYGULAMASININ GELİŞTİRİLMESİ

Ayşe Gökçe Keşküş

Ph.D. in Neuroscience

Supervisor: Özlen Konu Karakayalı

September 2021

Kolinerjik reseptör nikotinik alfa 5 (CHRNA5) sadece sinir sisteminde değil diğer dokularda da ifade olunan ligand kapılı bir iyon kanalıdır. CHRNA5 ifade farklılığı ve polimorfizmi bağımlılık, özellikle nikotin, ve çeşitli kanser tipleriyle ilişkilendirilmiştir. CHRNA5 deplesyonunun tumor baskılayıcı özellikleri, hücre canlılığında düşme ve DNA hasarı ve onarımında ve ilaç hassasiyetinde artış olup meme kanseri hücre hatlarında belirlenmiştir. Bu tez, CHRNA5 deplesyonunu etkileyen ve ondan etkilenen anahtar faktörlerin, in-vitro ve in-siliko tekniklerle belirlenmesine odaklanılmıştır. Meme kanseri verisetleri kullanılarak, CHRNA5 ve DNA hasarı ve onarımı genleri arasındaki pozitif korelasyon ilk defa gösterilmiştir. Ek olarak, MCF7 meme kanseri hücre hattında, TP53 deplesyonun siCHRNA5 ile antagonistik olarak hareket ettiği ve siCHRNA5'ın hücre döngüsü ve ilaç hassasiyeti üzerindeki etkilerini geri çevirdiği gözlemlenmiştir. Ayrıca, siCHRNA5 ikincil östrojen sinyal yolağını zamana ve doza bağlı şekilde baskılayabilmektedir. CHRNA5 deplesyonu ayrıca evrimsel olarak korunmuş 14q32.31 miRNA grubunun ifade miktarını düşürmektedir. Bu miRNA'ların arasında,

miR495-3p, en önemli miRNA olarak öne çıkmakta olup selektif östrojen reseptör modülatörü ile benzer ifade profili sergilemektedir. Ancak, siCHRNA5 ve miR495-3p'nin ikincil östrojen sinyal yolağı üzerindeki antagonistik etkileri, siCHRNA5 ve miR495-3p'nin aynı protein/yolağı hedeflediklerini öne sürmektedir. Ek olarak, shiny temelli syneRgy uygulaması ilaçlar ve/veya gen modifikasyonları için gen ifade profili temelli sinerji analizi yapılması için geliştirmiştir. Örnek vaka çalışması olarak, MDM2 inhibitörü ve/veya DNA hasarı indükleyen temozolomide uygulanmış olup neuroblastoma hücre hatları kullanışmıştır. Elde edilen sonuçlara göre kombinasyon uygulamasının tumor baskılayıcı etkisi bireysel uygulamalardan daha fazla olsa da bireysel uygulamaların toplamlarından az olduğu bulgulanmıştır. Bildiğimiz kadarıyla, syneRgy, transkriptom temelli sinerji analizi ve *synreg* isimli yeni geliştirdiğimiz sinerji analiz metoduyla TF zenginleştirmesi analizi yapan tek online uygulamadır.

Keywords: CHRNA5, östrojen sinyal yolağı, selektif östrojen modulatörü, TP53 sinyal yolağı, miRNA, 14q31.32 miRNA grubu, transkriptomiks, sinerji analizi.

to my precious family and friends,

Acknowledgments

First of all, I would like to express my utmost gratitude toward my Ph.D. supervisor Ozlen Konu for accepting me into her team and her guidance, patience and for being accessible throughout my Ph.D. journey. On top of that, she always encouraged and supported me to explore new methods and approaches.

I would like to thank Dr. Sreepnarna Banerjee and Dr. Michelle Adams for being part of my TIK committee for all these years, sharing their experiences and insightful comments, and also involving me in their projects. I would like to thank Dr. Nurcan Tuncbağ and Dr. Hulusi Kafalıgönül for accepting my invitation to being in my thesis defense and their time to evaluate my thesis.

I would like to thank Sahika Cıngır-Köker, Huma Shehwana, and Said Tiryaki for their contributions to CHRNA5 projects, Farid Ahadli for his constructive comments and assistance in syneRgy app. I would like to thank current and former Konu lab members, Başak Özgürsoy, Sahika Cıngır-Köker, Seniye Targen, Murat Yaman, Said Tiryaki, Fatma Betül Dinçaslan, Damla Güneş, Büşra Korkmaz, Melike Tombaz, Burcin Irem Arıcı, Merve Vural, Kübra Çalışır, and Farid Ahadli for a friendly working environment and sharing their experiences in wet lab and dry lab.

I would like to thank my friends and bioinformatic room members, Rafed Said Tiryaki and Fatma Betül Dincaslan, for their fruitful brainstorms and help in the wet lab and dry lab, friendship and their support in all those hard times. I also want to thank my lab-mate and friend Seniye Targen for her friendship and laugh, giving all of us positive energy. Their friendship always courage me to continue. I would like to especially thank Burcin İrem Arıcı and Melike Tombaz for helping me in my projects, especially in my last year and for their company.

I would like to thank to my family, Hamza Keşküş, Avniye Keşküş, Taha Alperen Keşküş, Kübra Keşküş, Ömer Keşküş and Vasfiye Aktulga-Çatal for their unconditional love and support for all means. I would like to sincerely thank Hilal Nur Gülmez for always being there for me whenever I need, and keep me smiling.

I would like to thank Bilkent MBG and Neuroscience departments for providing us such an opportunity. CHRNA5 projects were supported by TUBITAK (siRNA and DNA damage project: 111T316, miRNA project; 114S367 and TP53 project; 219Z029), and the miRNA project was part of COST action (BM1406). I have received scholarships from TUBITAK 114S367 and 219Z029.

Table of Content

List of Figures

List of Tables

List of Appendix

1 Introduction

1.1 Breast cancer

Cancer is the leading cause of death worldwide. According to the GLOBOCAN report, cancer is the first or second cause of death before 70 in 112 countries (Sung, et al., 2021). The rates of cancer incidence and mortality are increasing with the aging population. However, due to the heterogenic nature of cancer, current therapeutic approaches remain limited.

In 2020, female breast cancer had the highest incidence rate (11.7%) among all cancer types (Sung, et al., 2021). Most breast cancers originate from epithelial cells. The normal breast epithelium has a bilayer structure in which the inner layer consists of luminal cells while the outer layer is myoepithelium (Sims, et al., 2007). The two most common histological subtypes of breast cancer are invasive ductal carcinoma (80%) and invasive lobular carcinoma (10%) (Arps, et al., 2013; Barroso-Sousa and Metzger-Filho, 2016).

1.1.1 Breast cancer subtypes

Apart from histological subtypes, breast cancer can be classified according to its molecular signatures, including molecular pathology, gene expression, and histology. Molecular classification exhibits prognostic importance since it helps to predict the tumor behavior and its response to therapies. Estrogen receptor alpha (ESR1) and human growth factor receptor 2 (HER2), Progesterone receptor (PGR), and Ki67 have been identified as valid stratification factors (Heng, et al., 2016; Himanshu Joshi, 2018; Perou, et al., 2000). According to their expression level, main clusters have been defined as: Luminal A, Luminal B, Her2, Basal, and normal-like (**Figure 1.1**). Several studies have proposed different molecular signatures for the classification of the subtypes. Perou et al. (2000) used 469 genes to classify breast cancer patients into four groups (Perou, et al., 2000). PAM50 is another prediction model based on the expression pattern of 50 genes (Parker, et al., 2009).

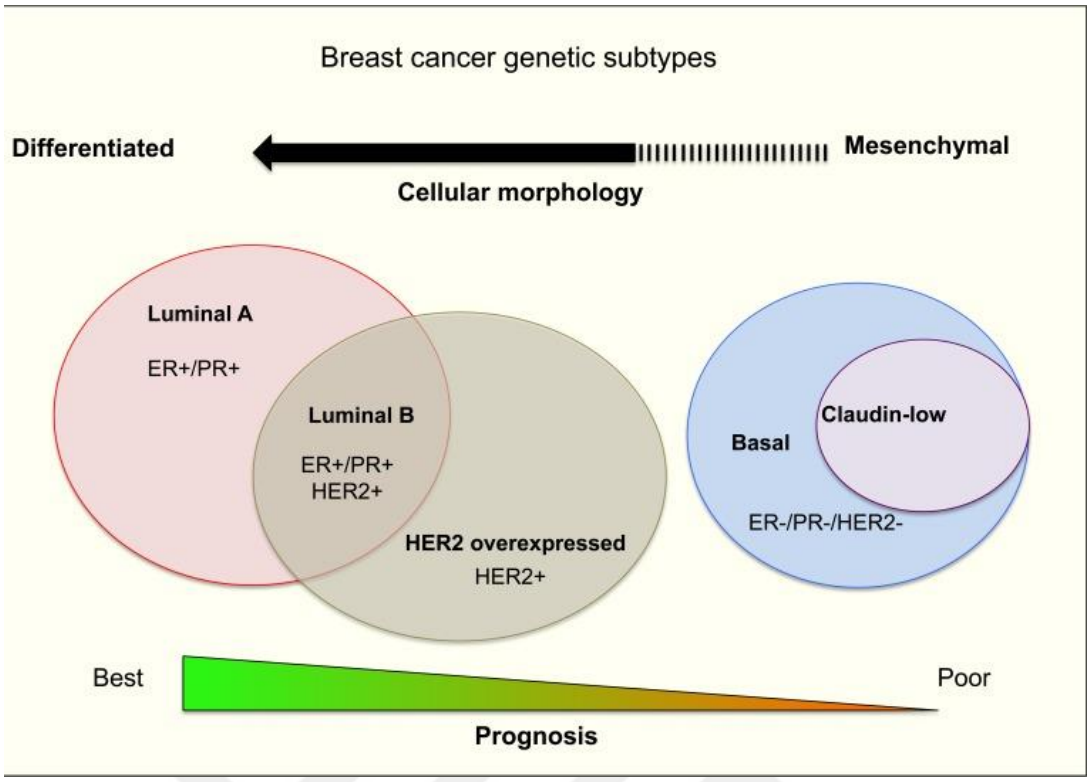

Figure 1.1 Molecular classification of breast cancer.

(This image was reproducible without the need of copyright permission and required citation and it was obtained from Heng B., Lim C. K., Lovejoy D. B., Bessede A., Gluch L., Guillemin G. J. Understanding the role of the kynurenine pathway in human breast cancer immunobiology. Oncotarget. 2016; 7: 6506-6520. Retrieved from https://www.oncotarget.com/article/6467/text/)

Luminal A, the most common subtype, is ER/PR+ and HER2 negative breast cancer subtype. Since proliferative marker Ki67 and other proliferation-related genes are low expressed, cellular growth is slower than other subtypes; therefore, it exhibits a better prognosis (Early Breast Cancer Trialists' Collaborative, et al., 2011; Gao and Swain, 2018; Perou, et al., 2000). Luminal A subtype has been identified as sensitive to tamoxifen and aromatase inhibitors which disrupt estrogen signaling (Early Breast Cancer Trialists' Collaborative, et al., 2011).

The difference between luminal A and luminal B subtypes is HER2 and/or Ki67 expression (Cheang, et al., 2009). Therefore luminal B is slightly more aggressive (Dai, et al., 2017; Hennigs, et al., 2016). Although luminal B tumors are hormone receptor-positive, they are less responsive

to hormone therapy when compared to luminal A, yet they are more sensitive to neoadjuvant chemotherapy (Goncalves, et al., 2021).

HER2 is a growth factor identified as a proto-oncogene. HER2 positive (or enriched) subtype is characterized by high expression of HER2. Although HER2 tumors are ER+, the expression level of ESR1 is lower than luminal subtypes (Cancer Genome Atlas, 2012). HER2 subtype exhibits a high proliferation rate, thereby, poorer prognosis (Fragomeni, et al., 2018; Hennigs, et al., 2016; Slamon, et al., 1987). Studies have reported that the HER2 subtype is sensitive to anti-HER2 therapies, i.e., Trastuzumab and Lapatinib, and also DNA damage-inducing agents doxorubicin and other topoisomerase inhibitors (Montemurro, et al., 2007; Slamon, et al., 2001).

The basal or triple-negative subtype consists of ER/PR/HER2- tumors which exhibit higher histological and nuclear grades (Cancer Genome Atlas, 2012). Basal-like tumors have a high proliferation rate and are highly metastatic. The occurrence rate of BRCA1 mutation is more elevated in basal-like tumors (Rakha, et al., 2008). Therefore, therapies causing DNA damage are more effective. Claudin-low cluster is one of the subtypes of basal-like tumors (Herschkowitz, et al., 2007; Pommier, et al., 2020). They are characterized by low expression of cell adhesion genes like claudin. This subgroup exhibits a bad prognosis (Dias, et al., 2017).

Normal-like breast tumors have been reported to be ER/PR- and HER2/Ki67 – like basal like subtype (Dai, et al., 2015). Normal-like subtypes, as the name suggests, resemble normal breast tissue. Therefore in some studies, the normal-like subtype is skipped.

1.2 Nicotinic acetylcholine receptors and CHRNA5

1.2.1 Nicotinic acetylcholine receptors (nACHRs)

Acetylcholine receptors (ACHRs) are classic neurotransmitter receptors expressed widely in the central and peripheral nervous systems and mediate many functions in the nervous system, including the reward mechanism (Xiao, et al., 2020). Other than their functionality in the nervous system, today, it is known that they are widely expressed in different tissues and regulate cellular

growth (Wessler and Kirkpatrick, 2008). They respond to acetylcholine and its agonist nicotine, as well as other nicotine derivatives like nitrosamine. It has been shown that cancer cells can express acetylcholinesterase (AChE) to generate acetylcholine and stimulate the signaling cascade in the absence of acetylcholine or its agonists (Cheng, et al., 2008; Perez-Aguilar, et al., 2015; Song and Spindel, 2008; Xi, et al., 2015).

They have two main subtypes, namely, muscarinic (mACHRs) and nicotinic (nACHRs) acetylcholine receptors. mACHRs, G-protein coupled receptors, are activated upon ligand binding and act through secondary messenger signaling. Therefore mACHRs can mediate a wide range of signaling cascades regulating several functions including postsynaptic potential in ganglions and cognitive processes in the nervous system, and muscle contraction in the heart (Brown, 2010; Lebois, et al., 2018; Wang, et al., 2007). mACHRs have also been reported to be involved in carcinogenesis and cellular migration (Feng, et al., 2018; Kohn, et al., 1996; Lin, et al., 2014; Pacini, et al., 2014; Tang, et al., 2012; Tolaymat, et al., 2019; Wang, et al., 2000; Yu, et al., 2017; Zhao, et al., 2015).

nACHRs are ligand-gated cation channels. Their widely known function is through the calcium influx upon binding to their ligands. nACHRs are cation channels, yet their activity depolarizes the cellular membrane, which activates voltage-gated calcium channels (Grando, 2014). Calcium homeostasis is one of the primary regulatory mechanisms in the cell. In the nervous system, calcium influx can lead to neurotransmitter release and nerve growth. Therefore, nACHRs have been associated with several disorders like Alzheimer's and Parkinson's disease (Oddo and LaFerla, 2006; Quik, et al., 2011).

nACHRs form a cytosolic loop between M3 and M4 transmembrane domains which exhibits the low similarity between subunits while ligand binding sites are conserved (Castelan, et al., 2007). Site-directed mutagenesis studies have been shown that the M3-M4 loop consists of essential properties necessary for assembly and membrane localization (Bouzat, et al., 2000; Castelan, et al., 2007). Apart from that, nACHRs can interact with G proteins through M3-M4 loops (Kabbani, et al., 2013) (**Figure 1.2**).

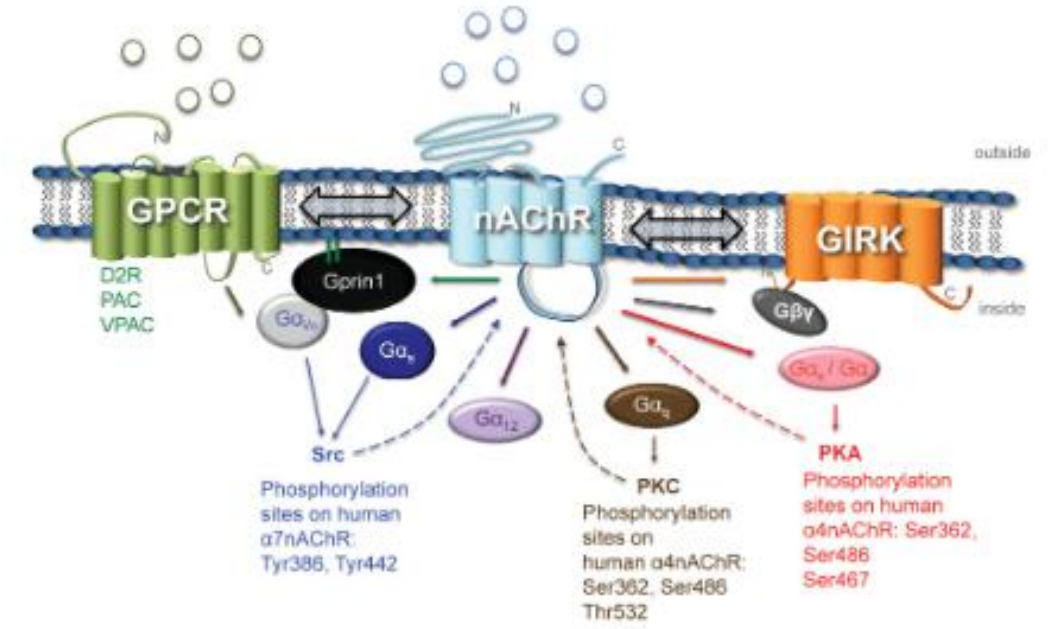

Figure 1.2 Interaction between G proteins and nACHRs

(This image was reproduced with the licence ID: 5139340382720 from Kabbani N, Nordman JC, Corgiat BA, Veltri DP, Shehu A, Seymour VA, Adams DJ. Are nicotinic acetylcholine receptors coupled to G proteins? Bioessays. 2013 Dec;35(12):1025-34. doi: 10.1002/bies.201300082. PMID: 24185813.)

1.2.2 Nicotinic acetylcholine receptors subunits

Seventeen subunits of nACHRs, twelve neuronal and five in muscles, have been identified in the human (Karlin, 2002). nACHRs form homo- or hetero-pentameric structures with different combinations of those subunits. α7 and α9 can form homomeric structures while heteromeric ones can be consist of other subunits (α2- α10 and β1-β4) in which α and β subunits are the primary binding site and complementary subunit, respectively (Brejc, et al., 2001; Grando, 2014; Karlin, 2002). Although it is not clear the regulatory mechanisms behind the preference over these subunits, the components of the nACHRs can alter the affinity and efficiency of the receptor, i.e., homomeric α7 and α9 exhibit higher affinity (Grando, 2014).

CHRNA5, α5 subunit, is located on chr15 along with other nACHRs; α3and β4. It can form heteromeric structures with α3β4 or α4β2 depending on cell types (Figure 1.3). Interestingly, the α5 subunit does not contain the ligand binding or the complementary site (Le Novere, et al., 2002;

Ramirez-Latorre, et al., 1996). Therefore the shift in the affinity, calcium permeability, desensitization of the receptors with and without α5 has been widely studied primarily on the nervous system by heterologous expression method using *Xenopus*, mouse, or chick (Fucile, et al., 1997; Kuryatov, et al., 2011; Nichols, et al., 2016; Prevost, et al., 2021; Ramirez-Latorre, et al., 1996; Tapia, et al., 2007). α4β2 can assemble in three different hetero-pentameric structures with α4, β2 or α5 subunits. Among these receptors α4 subunit exhibit the least sensitivity and efficacy, while β2 and α5 subunits are similar in efficacy. However, the α5 subunit leads to increased calcium permeability and reduced desensitization (Grady, et al., 2012; Jin, et al., 2014; Kuryatov, et al., 2008; Nichols, et al., 2016; Ramirez-Latorre, et al., 1996; Tapia, et al., 2007). In contrast, the involvement of α5 decreases calcium permeability in the receptors with the α3β4 backbone, although contradictory results have also been reported (Gerzanich, et al., 1998; Groot-Kormelink, et al., 2001; Stokes and Papke, 2012; Wang, et al., 1996).

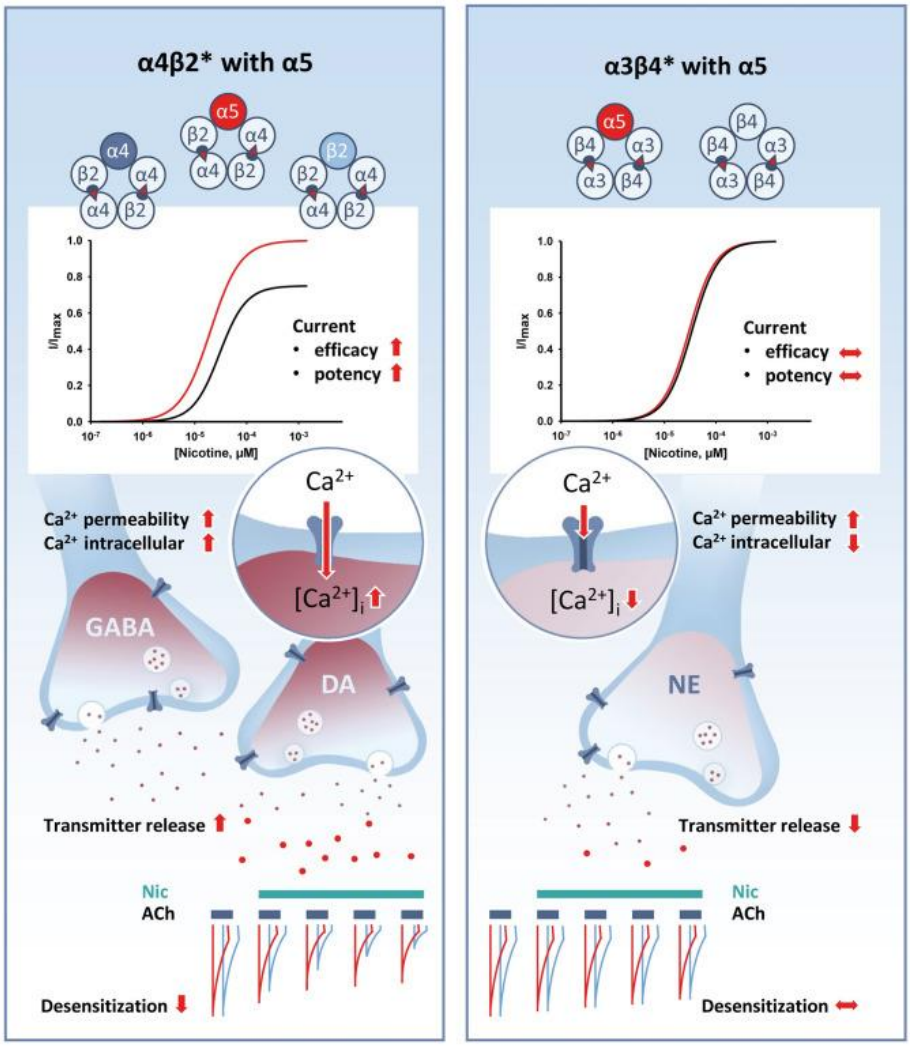

Figure 1.3 Schematic representation of the change in the efficacy, affinity, and calcium permeability of nACHRs consists of a5 subunit. Red arrows represent the direction of the shift when a5 is involved.

(This image was reproducible without the need of copyright permission and required citation and it was obtained from Scholze, P., & Huck, S. (2020). The α5 Nicotinic Acetylcholine Receptor Subunit Differentially Modulates α4β2* and α3β4* Receptors. *Frontiers in synaptic neuroscience*, *12*, 607959. https://doi.org/10.3389/fnsyn.2020.607959)

1.2.3 Nicotinic acetylcholine receptors in cancer

An increasing number of studies have been reported the involvement of nACHRs in cancer prognosis in several different types of cancer (Chen, et al., 2019). Although the functionality of

nACHRs can differ depending on cell type, calcium influx can lead to the secretion of growth factors that stimulates the growth of neighbor cells while inhibiting apoptosis (Improgo, et al., 2013; Medjber, et al., 2015; Min, et al., 2016; Rinner, et al., 1994; Sun, et al., 2017). The homomeric α7 receptor increases cell proliferation by activating the RAS/MEK/ERK pathway in non-small cell lung carcinoma and the JAK/STAT3 pathway in oral squamous cell carcinoma (Nishioka, et al., 2019; Zhang, et al., 2017). The homomeric α7 receptor also inhibits apoptosis via activation of NF-κB (Arredondo, et al., 2007; Li, et al., 2011; Stegemann and Bohm, 2019). Calcium influx can also stimulate angiogenesis through VEGF and FGF2 in lung cancer (Cooke, 2007; Heeschen, et al., 2002). Apart from α7, α4β2 and α4β3 have been reported to lead similar outcomes in non-small cell lung cancer and gastrointestinal adenocarcinoma (Falvella, et al., 2009; Improgo, et al., 2010; Schuller, 2009).

1.2.3.1 Breast cancer

The α9 subunit, overexpressed in breast tumors, has been reported to stimulate cyclin D3 expression while mediating lung metastasis in breast cancer (Chen, et al., 2011; Lee, et al., 2010). Knockdown of the α9 subunit has been reported to decrease cell proliferation, which the overexpression model increases (Lee, et al., 2010). α9 also modulates STAT3/TWIST pathway in breast cancer (Guha, et al., 2014). Several studies have reported increased migration with CHRNA9 expression (Guha, et al., 2014; Tu, et al., 2016). The α7 subunit is the other studied subunit in breast cancer (Lin, et al., 2012).

1.2.4 CHRNA5 in cancer

CHRNA5 (α5) subunit is associated with smoking and nicotine addiction. Nicotine itself is not classified as carcinogenic but as tumor-promoting; therefore, CHRNA5 is associated with lung and gastric cancer risk (Culverhouse, et al., 2020; Wang, et al., 2013; Wen, et al., 2016; Wu, et al., 2013; Yi, et al., 2021). In oral squamous cell carcinoma, CHRNA5 is found to increase radio-resistance via E2F signaling (Lin, et al., 2019). CHRNA5 inhibition in lung and bronchial cells increases p63 expression and migration (Krais, et al., 2011), whereas CHRNA7 (α7) knockdown

decreases migration. CHRNA5 level positively modulates nicotine-dependent activation of JAK/STAT3 pathway in lung cancer, while silencing of STAT3 decreases CHRNA5 expression levels (Zhang, et al., 2017). CHRNA5 expression level has also been shown to correlate with BIRC5 in lung cancer (Zhang, et al., 2021). CHRNA5 has also been associated with the PI3K/AKT, ERK 1/2 and NOTCH signaling pathways. CHRNA5 has been identified as a driver gene in a metanalysis in cervical cancer (Xu, et al., 2021). In our previous studies, we have discovered CHRNA5 knockdown decreases cell proliferation and increases drug sensitivity (Cingir Koker, et al., 2018).

Polymorphisms in α4β2 binding partners of CHRNA5 have been associated with nicotine dependence and heavy smoking in different populations (Bordas, et al., 2017; Hancock, et al., 2015; Perkins, et al., 2009; Thorgeirsson, et al., 2016). An interesting study on rats has reported a link between Klf5 and α4 in high-fat diet groups associated with reduced mammary cancer risk (Andrade Fde, et al., 2015). Inhibition of β2 through monoclonal antibody decreased tumor growths in gastric cancer, while β2 overexpression increased cell proliferation (Kanda, et al., 2021). On the contrary, β2 has been shown to be downregulated in *Helicobacter pylori*-positive gastric cancer (Hu, et al., 2018). Although their polymorphisms have been identified as risk factors for smoking-related lung cancer, comprehensive studies are scarce.

Other binding partners and chromosomal neighbors of CHRNA5, e.g., α3β4, have also been associated with smoking and nicotine addiction (Gu, et al., 2020; Silva, et al., 2019). Polymorphism, expression level, and methylation status of α5-α3-β4 gene cluster have been reported to exhibit prognostic importance in lung cancer (Liu, et al., 2017; Scherf, et al., 2013; Yi, et al., 2021; Zhang, et al., 2017). Polymorphism in the α5-α3-β4 gene cluster also correlates with DNA adduct levels and TP53 mutation. CHRNB4 (β4) knockdown in lung cancer cell lines increases cell proliferation, whereas CHRNA3 (α3) overexpression induces apoptosis (Paliwal, et al., 2010). CHRNA3 depletion in esophageal cancer cells increases cell proliferation and migration through YAP1 activation (Zhao, et al., 2014). The same region has also been identified as a risk factor for gastric cancer, esophageal squamous cell carcinoma, head and neck cancer,

cardiopulmonary disease (Balassiano, et al., 2011; Hallden, et al., 2016; Paliwal, et al., 2010; Silva, et al., 2019). Although several studies show the involvement of CHRNA5 via different mechanisms in multiple cancers, CHRNA5's relevance as a molecular modulator of breast cancer is yet to be uncovered. In addition, none of the nACHRs has been studied in the context of miRNA expression.

1.3 TP53 signaling and DNA damage response

1.3.1 TP53 and its regulation

TP53 is one of the most frequently studied genes in the cancer context due to its high mutation incidence rate and its wide range of function (Olivier, et al., 2010). TP53 is crucial for maintaining cell homeostasis via orchestrating the cellular response to stress, i.e., cell cycle arrest, DNA repair, apoptosis, senescence, ferroptosis, and shift in cell metabolism. TP53 harbors mutations in more than 50% of all cancers and 30% in breast cancer (Duffy, et al., 2018). In tumors with wildtype TP53, its regulatory mechanism is altered to inhibit its biological activity.

TP53 levels remain low in unstressed conditions through MDM2, a negative regulator. MDM2 and/or MDM4 ubiquitinates TP53 leading to its proteasomal degradation (Murray-Zmijewski, et al., 2008) (**Figure 1.4**). MDM2 as a transcriptional target of TP53 also involves a negative feedback loop to restore TP53 level after its activation (Harris and Levine, 2005). MDM2 mediated TP53 degradation is the primary regulatory mechanism in the absence of TP53 activating stimuli. The other upstream regulator of TP53 is p14ARF, a positive regulator (Agrawal, et al., 2006). Upon cellular stress, p14ARF inhibits MDM2-TP53 interaction, thereby stabilizes TP53 (**Figure 1.4**) (Llanos, et al., 2001). The early DNA damage response genes, ATM and ATR, along with CHEK1 and CHEK2, can also prevent MDM2-TP53 binding through phosphorylation of MDM2/4 and TP53 leading to TP53 stabilization (Kruse and Gu, 2009; Mayo, et al., 1997). Many tumors with wildtype TP53 harbor either duplication in MDM2 or silencing of p14ARF or DNA damage response genes (Olivier, et al., 2010)

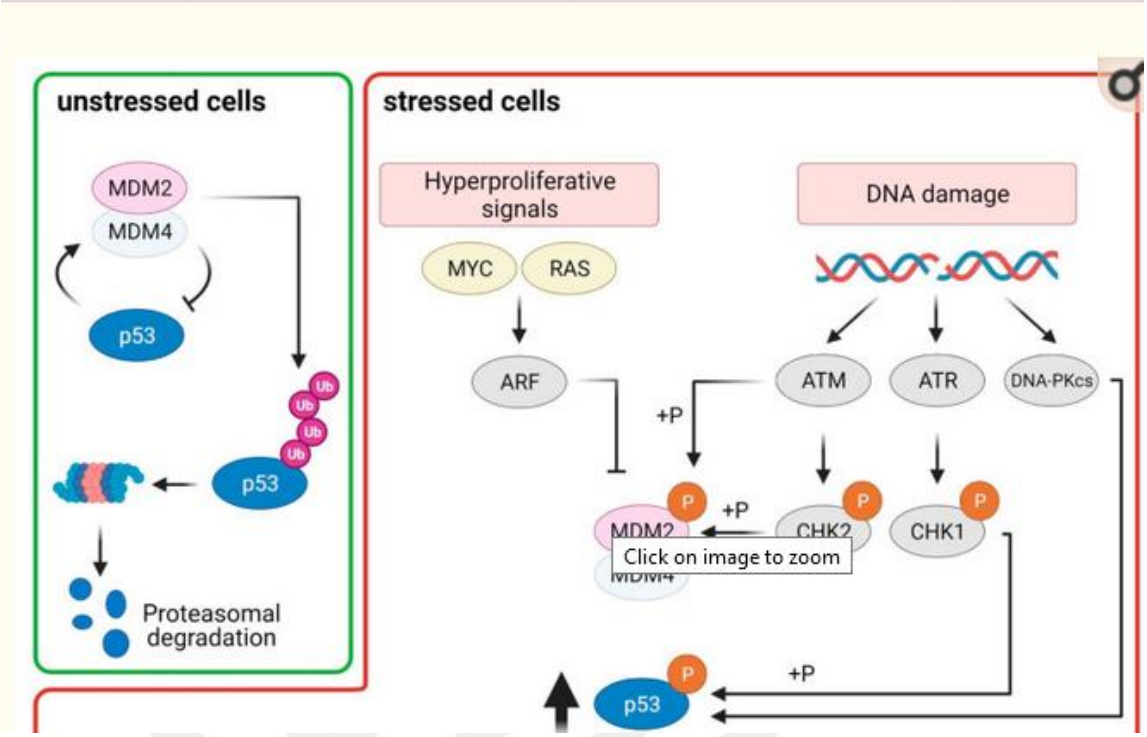

Figure 1.4 The regulatory mechanisms of TP53 in unstressed and stressed conditions.

(This image was reproducible without the need of copyright permission and required citation and it was obtained from Liebl, M. C., & Hofmann, T. G. (2021). The Role of p53 Signaling in Colorectal Cancer. *Cancers*, *13*(9), 2125. https://doi.org/10.3390/cancers13092125)

1.3.2 Downstream effects of TP53

Under stressed conditions, including DNA damage, oncogenic signals, oxidative stress, and hypoxia, TP53 is stabilized. Most canonical functions of TP53 are through its transcriptional factor activity, yet there are also studies reporting direct protein binding of TP53, especially to mitochondrial proteins (Chipuk, et al., 2004). Primary outcomes of TP53 activation are cell cycle arrest, DNA damage repair, apoptosis, senescence, ferroptosis, autophagy, and a shift in cellular metabolism (**Figure 1.5**) (Moulder, et al., 2018). Although the decision mechanism between these outcomes is still unclear, posttranslational modifications, availability of binding counterparts, and the level of stress-inducing stimuli have been reported to play a role (Carvajal and Manfredi, 2013; Hafner, et al., 2019).

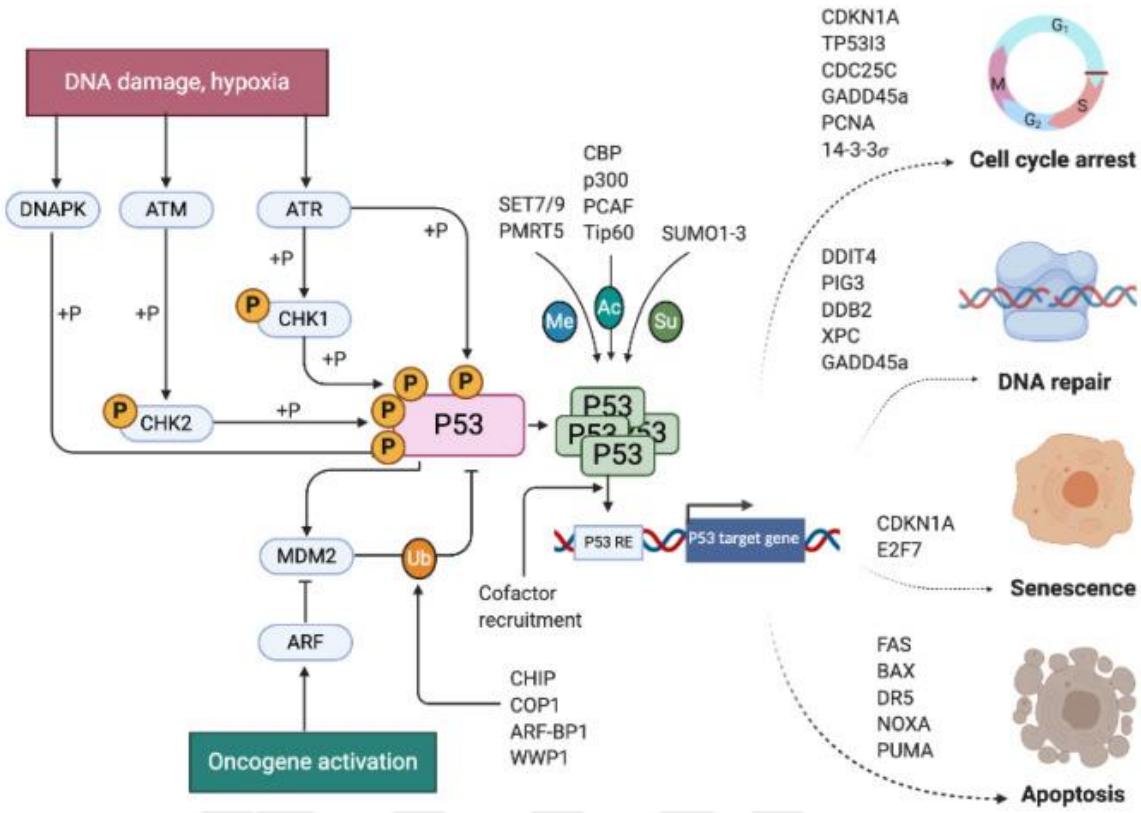

Figure 1.5 Overview of TP53 regulation, activation, and outcome

(This image was reproducible without the need of copyright permission and required citation and it was obtained from Hernández Borrero LJ, El-Deiry WS. Tumor suppressor p53: Biology, signaling pathways, and therapeutic targeting. Biochim Biophys Acta Rev Cancer. 2021 Aug;1876(1):188556. doi: 10.1016/j.bbcan.2021.188556. Epub 2021 Apr 29. PMID: 33932560.)

1.3.2.1 Cell cycle arrest

Cell cycle arrest is the earliest and the most prominent effect of TP53 activation. The phosphorylation of TP53(Ser20) through DNA damage response proteins or p14ARF induces TP53 dependent p21-RB1 pathway (McGowan, et al., 2011; McGowan, et al., 2012). p21 inhibits CDK4/6, primary mediators for G1/S progression. Inhibition of CDK4/6 prevents the disassociation of E2F from RB1, thereby transcription of E2F targets (Becker, et al., 2009; He, et al., 2005). TP53 mediated cell cycle arrest can be temporal or prolonged.

1.3.2.2 DNA damage response

Since the primary cellular stress stimuli activating TP53 is DNA damage, the repair pathway is induced upon cell cycle arrest (Wang, 2007). Activation of ATM and ATR by stalled replication fork mediates the activation of proper DNA damage repair cascade, i.e., nucleotide excision and homologous recombination (Musgrove, et al., 2011; Wang, 2007). Many DNA damage repair genes have also been reported as TP53 targets. The repair of the respected region needs to be completed before re-entering the cell cycle. In the physiological levels of DNA damage, this pathway protects cells from accumulation of mutation and genomic instability (Poletto, et al., 2016; Smith and Seo, 2002).

1.3.2.3 Senescence

Senescence is the irreversible state of cell cycle arrest which can prevent cell cycle entry of the damaged cells, i.e., telomere shortening and DNA damage. Induction and maintenance of cellular senescence is the fundamental role of TP53 as a tumor suppressor (Chen, et al., 2005; Rufini, et al., 2013). DNA damage response pathway can acetylate TP53 via RAS and NOREA1, bypassing its phosphorylation, leading to cellular senescence (Mijit, et al., 2020).

1.3.2.4 Apoptosis

Depending on the levels of cellular stress, TP53 can mediate apoptosis via induction of NOXA, PUMA or BAX (Aubrey, et al., 2018). NOXA and PUMA are transcriptional targets of TP53 and pro-apoptotic members of BCL2 protein family (Chota, et al., 2021). Activation of NOXA and PUMA inhibits pro-survival BCL2 family members, i.e., BCL2, BCL-XL, and release BAX, an apoptotic regulator (Zhang, et al., 2013). Apart from transcriptional activity, TP53 induces BAX translocation to mitochondria via direct binding (Chipuk, et al., 2004). The increase in BAX/BCL2 ratio is widely used as apoptosis marker (Naseri, et al., 2015). TP53 can also modulate apoptotic response indirectly via transcription of FAS, DR5, and miR34a (Aubrey, et al., 2018).

1.4 Estrogen signaling

1.4.1 Physiological functions of estrogens

Estrogens are a group of steroid hormones, i.e., estrone, estriol, estetrol, and the dominant form estradiol (Fuentes and Silveyra, 2019). Estrogen is mainly secreted from the ovaries, adrenal gland, and adipose tissue while estrogen biosynthesis is primarily mediated by HSD17B1, CYP17/19, and CYP1A1 (Olivo-Marston, et al., 2010).

Although estrogens are female steroid hormones, they have a plethora of physiological roles. They regulate the menstrual cycle, secondary sexual characteristics, i.e., development of breast tissue and sexual organs and fertility in females (Fuentes and Silveyra, 2019). In addition, estrogen is functional in maintaining bone density, cognitive functioning, and even reduction of inflammation (Cauley, 2015; Luine, 2014; Vegeto, et al., 2008). Since estrogens promote cell growth in breast epithelium, it is a crucial modulator for breast cancer, as discussed in Chapter 1.1.1.

1.4.2 Estrogen receptor signaling

Like other steroid hormones, estrogens can pass through the cellular membrane and bind to estrogen receptors or interact with membrane-bound G protein-coupled estrogen receptors (GPER) and activate secondary messengers (**Figure 1.6**). The classical signaling cascade for estrogen is through ESR1 (ER-alpha) and ESR2 (ER-beta). Although there are studies on ESR2 and GPER activity, ESR1 is still considered as the primary receptor for estrogen signaling.

1.4.2.1 Estrogen-mediated direct genomic signaling

The estrogen-mediated transcriptional activity of ESR1 can be classified as direct and indirect genomic signaling. As the name suggests, direct genomic interaction requires nuclear localization of the ESR1-Estrogen complex and directly binding to the genome. A 13-bp long palindromic sequence, namely estrogen response element (ERE), has been identified as an ESR1 binding site (Beato, et al., 1996). O'Lone et al. (2004) comprehensively compared the EREs in different

estrogen-responsive genes (O'Lone, et al., 2004). Palindromic EREs have been reported as the dominant motif for ER binding while they have also identified half-EREs that are functional with the assistance of a cofactor. The range of EREs, from full consensus ERE to half ERE, can be a marker for estrogen responsiveness through affinity to ERs and conformational change of bound ER. However, estrogen also functions together with many coactivators, which also alter the functionality of ERs. In a comprehensive study, Bourdeau et al. (2004) have identified more than 17000 EREs in the promoter region (15kb upstream of TSS) in the whole human genome (Bourdeau, et al., 2004). The same study has employed a comparative approach and filtered the EREs conserved between mouse and human. However, even those could not fully cover the estrogen-responsive genes.

1.4.2.2 Estrogen-mediated indirect genomic signaling

Another challenge to identifying genomic targets of ESR1 is that more than 30% of the identified targets have no EREs (O'Lone, et al., 2004). For those genes, the ER-Estrogen complex interacts with other transcriptional factors to bind the genome; and this is called transcriptional cross-talk. The primary transcription partner of ER is SP1 (Li, et al., 2001; Safe, 2001). Well-known estrogen-responsive genes, i.e., CCND1, GATA1, and LDL, are SP1-ER-estrogen targets. O'Lone et al. (2004) have identified most half EREs accompany the SP1 binding site (O'Lone, et al., 2004), while Bajic et al. (2003) have shown that the presence of estrogen-ER complex enhances the SP1 activity (Bajic, et al., 2003).

The other prominent mediator for the ER-estrogen complex is AP1 which regulates a wide range of cellular functions, including cellular differentiation, growth, and apoptosis (Fujimoto and Kitamura, 2004; Paech, et al., 1997). AP1 has a heterodimer structure consisting of Jun and Fos primarily. Intrestingly, Paech et al. (1997) have reported that AP1-ESR1 has activatory while AP1-ESR2 has repressor functions (Paech, et al., 1997). Therefore, several studies have reported competing interplay between ESR1 and ESR2 in the presence of high levels of ESR2 (Mal, et al., 2020; Marino, et al., 2006). CCND1, a critical cell cycle regulator during G1 to S transition, is subject to this inhibitory interplay (Liu, et al., 2002; Marino, et al., 2006). The ER-estrogen

complex can interact with other transcription factors like ATF1, ATF2, and NF-kB yet to a lesser extent. In some cases, the ER-estrogen complex can play a repressor role, i.e., the ER-estrogen complex can bind to NF-kB inhibiting its binding to the IL6 promoter (Kalaitzidis and Gilmore, 2005).

1.4.2.3 Transcriptional coregulators of estrogen receptors

Transcriptional coregulators exhibit a pivotal role in estrogen signaling. They usually directly bind to ERs and enhance or repress their activity. The first cofactor identified for ERs is SRC-1, and later on, the other SRC family members, SRC-2 and SRC-3, are found (Cavailles, et al., 1995; Johansson, et al., 2000; Treuter, et al., 1999). Several chromatin remodeling complexes, i.e., p300, SWI/SNF, and TRAP/DRIP, have also been shown as coregulators (Cottone, et al., 2001; Smith and O'Malley, 2004; Yuan, et al., 1998). The duality in co-regulator binding to ESR1 and ESR2 has been reported (Kim, et al., 2006; Paech, et al., 1997).

The ER-estrogen complex also exhibits repressor activity through binding to specific cofactors. The ER-estrogen complex has been reported to interact with DNMTs, i.e., TETs and CXXs, and induce demethylation. Dumasia et al. (2017) has shown ESR2 prevents DNMT expression and DNA methylation (Dumasia, et al., 2017). The ER-estrogen complex also binds to Sin3A to construct an inhibitory feedback loop for ESR1 itself (Ellison-Zelski, et al., 2009).

1.4.2.4 Estrogen mediated non-genomic signaling

Apart from classical actions of estrogen through estrogen receptors (ESR1, ESR2), estrogen can also bind to GPER1, which refers to the non-genomic function of estrogen (Prossnitz and Barton, 2011). The signaling through GPER1 and secondary messengers are through cAMPs and kinase activation, which can be classified into four signaling pathways: protein kinase C (PKC), protein kinase A (PKA), RAS/RAF, and PI3K/AKT (Chuang, et al., 2020; Deng, et al., 2018; Liu, et al., 2021; Qiu, et al., 2021; Wang, et al., 2021).

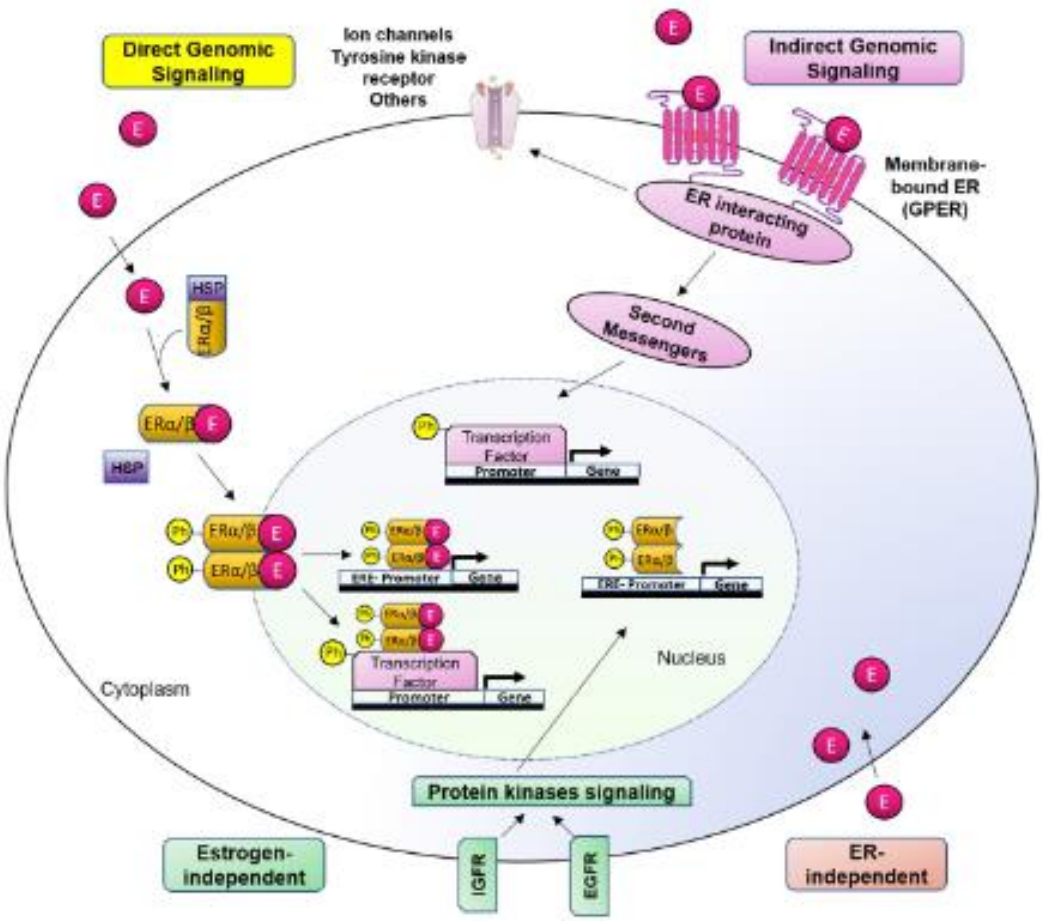

Figure 1.6 Schematic representation of estrogen signaling through direct genomic signaling, indirect genomic signaling, non-genomic signaling.

(This image was reproduced with the licence number: 5139650980669 from Fuentes N, Silveyra P. Estrogen receptor signaling mechanisms. Adv Protein Chem Struct Biol. 2019;116:135-170. doi: 10.1016/bs.apcsb.2019.01.001. Epub 2019 Feb 4. PMID: 31036290; PMCID: PMC6533072.)

1.4.3 Estrogen signaling and nACHRs

There is a limited number of studies focusing on the cross-talk between cholinergic and estrogen signaling pathways. CHRNA4 is regulated by estrogen in a site-specific manner in the mouse brain (Xu, et al., 2008). CHRNA7 levels can be controlled by estradiol in macaque brains (Centeno, et al., 2006). Lee et al. (2011) have reported an increase in the expression levels of CHRNA9 upon estrogen treatment in MCF7 cells (Lee, et al., 2011).

1.4.4 Selective estrogen receptor modulators and degraders

Estrogen signaling is one of the critical modulators in breast cancer and exerts its function in various cellular processes. Therefore, estrogen biosynthesis and estrogen receptor signaling have been targeted as therapeutic approaches, especially for the luminal A subtype. Several selective estrogen receptor modulators (SERMs) and degraders (SERD) have been proposed (**Figure 1.7)**.

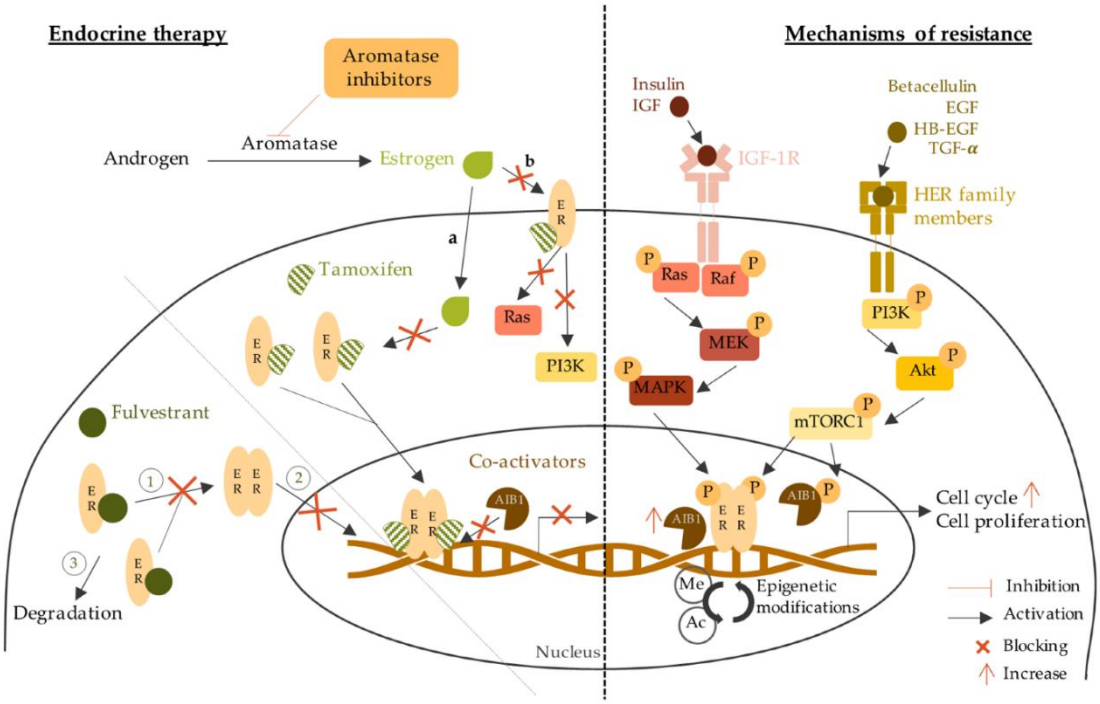

Figure 1.7 Mechanism of action of the widely used endocrine therapy agents in breast cancer.

(This image was reproducible without the need of copyright permission and required citation and it was obtained from Burguin A, Diorio C, Durocher F. Breast Cancer Treatments: Updates and New Challenges. *Journal of Personalized Medicine*. 2021; 11(8):808. https://doi.org/10.3390/jpm11080808)

1.4.4.1 Tamoxifen

Tamoxifen is the first developed (1977) and the most widely used estrogen antagonist. It competes with estrogen for estrogen receptor binding and prevents the recruitment of coactivators. However, tamoxifen also exhibits estrogenic activity by promoting activation function domain; AF1, activation (Frasor, et al., 2004). Therefore, although it competes with E2 and leads to

decreased transcriptional activation, it cannot completely block ESR1 activity. In the uterus, it can induce polyp production and increases the risk for endometrial cancer (Bergman, et al., 2000).

1.4.4.2 Raloxifene

Raloxifene is a second-generation estrogen receptor antagonist primarily used against osteoporosis (Zhang, et al., 2021). It does not induce endometrial cancer; however, its efficacy as a therapeutic agent for breast cancer is lower than tamoxifen and due to its low bioavailablity, and raloxifene is not favored for long term usage (Vogel, et al., 2006).

1.4.4.3 Bazedoxifen

Bazedoxifen is a third-generation SERM that can prevent pro-proliferative pathways, i.e., STAT3, PI3K, and, when combined with paclitaxel, increases apoptosis (Fu, et al., 2020; Komm, et al., 2005; Zhang, et al., 2021). In combinatorial treatment with Palbociclib, CDK4/6 inhibitor, the cell growth inhibitory effect is enhanced to a higher degree than Fulvestrant (Jeselsohn, et al., 2019). In addition, bazedoxifen exhibits estrogen receptor degrading properties, therefore widely used to overcome acquired tamoxifen resistance (Zafar, et al., 2021). Bazedoxifen also functions in an estrogen receptor-independent manner, thus commonly used in other types of cancer as well (Fu, et al., 2020; Lewis-Wambi, et al., 2011).

1.4.4.4 Fulvestrant

Fulvestrant is a selective estrogen receptor degrader designed to overcome the agonistic activity of tamoxifen and other estrogen antagonists and the acquired resistance throughout the treatment (Wakeling and Bowler, 1988). Therefore, estrogen degraders have been proposed to eliminate estrogen receptors instead of preventing its action. Fulvestrant is the only FDA-approved selective estrogen degrader, yet its mode of action is still unclear. Several fulvestrant variants have been proposed, i.e., GDC-0810, AZD9496, and GDC-0927 (Chow, et al., 2020; Hamilton, et al., 2018; Joseph, et al., 2016; Kahraman, et al., 2019).

Guan et al. (2019), and Wardell (2012) have compared the known SERMs and SERDs in wide range of breast cancer cell lines and xenograft model in mice (Guan, et al., 2019; Wardell, et al.,

2012). Fulvestrant yields less E2 activity compared to tamoxifen in breast cancer cell lines. In a xenograft study, fulvestrant and other derivatives have been found to inhibit tumor growth more than tamoxifen (Simoes, et al., 2015). Fulvestrant has also been shown to decrease ESR1 binding and induce ESR1 immobility and chromatin accessibility, yet minimal inhibition has been observed with tamoxifen and other E2 antagonists (Guan, et al., 2019). Bazedoxifen and raloxifene exhibit higher inhibition when compared to tamoxifen, yet is less efficacacious than fulvestrant. Selective estrogen degraders like Fulvestrant have been shown to increased E2 inhibition yet, its application through intra-muscular injection limits its clinical use (Nathan and Schmid, 2017).

1.5 miRNAs

microRNAs (miRNAs) are small non-coding RNAs exhibiting post-transcriptional and post-translational inhibition of their targets (Winter, et al., 2009). Since their discovery in mammalian cells, an increasing number of studies have reported their involvement in crucial biological processes, i.e., neurodevelopment, epithelial to mesenchymal transition, aging, metabolism, regulation of the immune system (de Lencastre, et al., 2010; Gregory, et al., 2008; Mehta and Baltimore, 2016; Park, et al., 2008; Ristori, et al., 2015; Zhao, et al., 2009). miRNAs are also critical regulators for a wide range of pathologies, including Alzheimer's disease, systemic lupus erythematosus, obesity, and cancer (de Lencastre, et al., 2010; Gregory, et al., 2008; Jafari Ghods, et al., 2017; Jiang, et al., 2012; Lischka, et al., 2021; Mehta and Baltimore, 2016; Park, et al., 2008).

1.5.1 miRNA biogenesis and function

miRNAs can be stratified into two groups depending on their localization. miRNAs located within a transcribed region are called intergenic, and those found outside are intragenic miRNAs. Intergenic miRNAs are often transcribed with their host gene (Hajarnis, et al., 2015; Winter, et al., 2009). The transcription of both groups of miRNAs requires the recruitment of either RNA polymerase II or RNA polymerase III (**Figure 1.8**) whose product is called pri-miRNA, which is

often polyadenylated and capped. The pri-mRNA is then recognized by DROSHA/DGCR8 complex to cleave pri-miRNA and generate pre-miRNA with a hairpin stem of ~33 nucleotides. Pre-miRNAs transported from nucleus to cytoplasm by exportin5. In the cytoplasm, Dicer mediates the generation of ~20bp long mature miRNA through cleavage of the loop. After cleavage, mature miRNA is recognized by Ago2, which recruits the rest of the RISC complex (Figure 1.8). Each mature miRNA contains a seed sequence in which it binds to mRNA. The miRNA-RISC complex binds to mRNA with a complementary sequence to the miRNA seed sequence, which leads to mRNA degradation or translational repression.

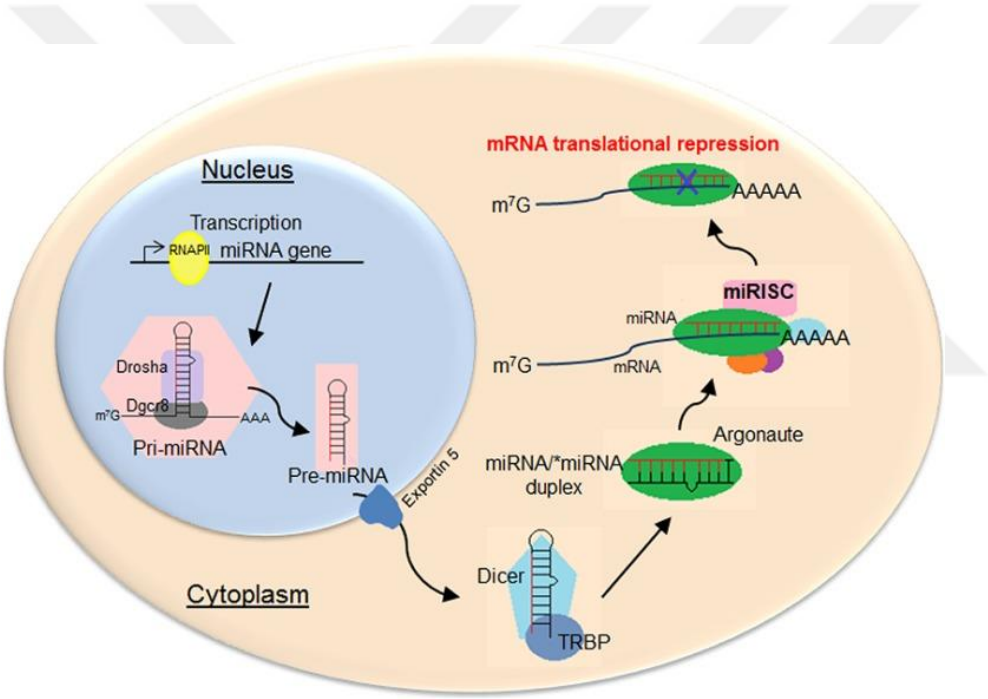

Figure 1.8 Schematic representation of miRNA biogenesis

(This image was reproducible without the need of copyright permission and required citation and it was obtained from Hajarnis S, Lakhia R, Patel V. MicroRNAs and Polycystic Kidney Disease. In: Li X, editor. Polycystic Kidney Disease [Internet]. Brisbane (AU): Codon Publications; 2015 Nov. Chapter 13. Available from: https://www.ncbi.nlm.nih.gov/books/NBK373371/ doi: 10.15586/codon.pkd.2015.ch13)

1.5.2 miRNAs in estrogen receptor signaling

Although estrogen signaling is one of the primary regulatory pathways in breast cancer, studies focusing on the regulatory roles of miRNAs on estrogen signaling are scarce. miRNAs in the context of estrogen signaling can be classified into three groups miRNAs targeting ESR1, miRNAs targeting estrogen biosynthesis, and miRNAs in endocrine resistance, as exemplified below in further detail.

1.5.2.1 miRNAs targeting estrogen biosynthesis

Aromatases are functional in the conversion of testosterone to estrogen compounds. Several aromatases have been identified, primarily, CYP19A1 and CYP17; and aromatase inhibitors, i.e., letrozole and anastrozole, are also proposed to be therapeutic agents in breast cancer (Bhatnagar, et al., 1990; Goss and Tye, 1997). Several miRNAs associated with aromatase function have been reported in the literature. Shibahara et al. (2012) have demonstrated let-7f, a tumor suppressor miRNA, targets CYP19A1 and exerts a negative correlation with CYP19A1 in ER-positive breast cancer cell lines (Shibahara, et al., 2012). miR-4463, miR-146a and miR-26a are other miRNAs directly targeting CYP19A1 (Lee, et al., 2020; Li, et al., 2021; Li, et al., 2019; Yu, et al., 2020). There are also miRNAs inhibiting aromatases indirectly. Vilquin et al. (2015) have reported a high level of miR125b is associated with aromatase inhibitor resistance (Vilquin, et al., 2015).

1.5.2.2 miRNAs targeting ESR1

miR221/222 family miRNAs are the widely studied regulators of ESR1 (Di Leva, et al., 2010; Miller, et al., 2008). Zhao et al. (2016) have demonstrated their high expression in ER-negative breast cancer cell lines and their role in tamoxifen resistance (Zhao, et al., 2016). This miRNA family have also been reported to bind 3'-UTR of ESR1 and decrease its expression in both mRNA and protein levels. miR9-5p, miR142-3p, miR301a-3p, miR22, miR335-5p, miR335-3p, and miR1280 are the other miRNAs directly binding to ESR1 (Lettlova, et al., 2018; Mansoori, et al., 2019; Martin, et al., 2017; Meng, et al., 2016; Pandey and Picard, 2009; Wang, et al., 2021).

1.5.2.3 miRNAs in endocrine resistance

miRNAs targeting ESR1 have also been shown to induce re-sensitization to tamoxifen, indicating the importance of miRNA regulation on estrogen signaling (Rao, et al., 2011; Zhao, et al., 2016). Several others, i.e., miR205, miR575, miR192, miR152, miR27b, regulate tamoxifen resistance indirectly (Barazetti, et al., 2021; Kim, et al., 2016; Liu, et al., 2020; Song, et al., 2020; Zhu, et al., 2016). On the contrary, overexpression of miR500 and miR873 can re-sensitize tamoxifen-resistant breast cancer cell lines (Cui, et al., 2015; Kim, et al., 2016).

1.5.3 14q32.31 miRNA cluster

The 14q32 region, also called DLK1-DIO3 or DLK1-MEG3 region, is one of the largest miRNA clusters in human genome, consisting of 54 miRNAs (**Figure 1.9**) (Gardiner, et al., 2012). This region houses coding DLK1 and RTL genes and several lncRNAs, namely, MEG3, MEG8, and RTL1, along with clusters of miRNAs. miRNAs located in this cluster can be further divided into two; miRNA cluster A has ten miRNAs and miRNA cluster B contains the rest. DLK1-DIO3 region in an imprinted region and miRNAs are expressed from the maternal allele while DLK1 and DIO from the paternal (shown with pink and blue color in **Figure 1.9**).

The 14q32 region exerts a plethora of physiological functions, including neurodevelopment, embryonic development, and immune response (Groeneveld, et al., 2018; Holder, et al., 2012; Youngs, et al., 2011). In addition, deletions in this region lead to congenital abnormalities and defects, i.e., Temple disease and Silver-Russel syndrome (Bruck, et al., 2020; Geoffron, et al., 2018; Prasasya, et al., 2020). However, 14q32 activity in cancer can be both oncogenic and tumor-suppressor, depending on the cell/tissue type (see Section 1.5.3.2).

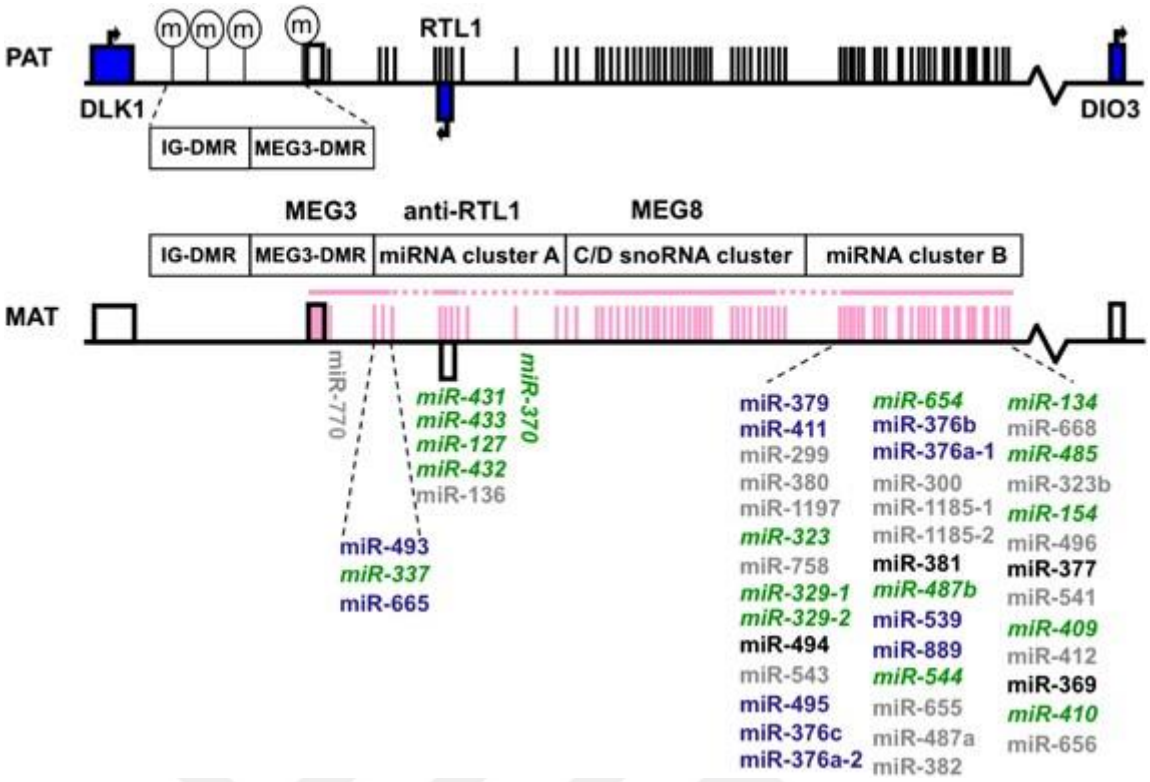

Figure 1.9 Genomic organization of 14q31.32 miRNA family. PAT and MAT refer to paternal and maternal alleles, while genes colored blue and pink are paternally and maternally expressed. DMR refers to the differentially methylated region in which DLK1-MEG3 is regulated.

(This image was reproducible without the need of copyright permission and required citation and it was obtained from Gardiner E, Beveridge NJ, Wu JQ, Carr V, Scott RJ, Tooney PA, Cairns MJ. Imprinted DLK1-DIO3 region of 14q32 defines a schizophrenia-associated miRNA signature in peripheral blood mononuclear cells. Mol Psychiatry. 2012 Jul;17(8):827-40. doi: 10.1038/mp.2011.78. Epub 2011 Jul 5. PMID: 21727898; PMCID: PMC3404364.)

1.5.3.1 Regulation of 14q32.31 miRNA cluster

The primary regulatory mechanism has been identified as methylation through a differentially methylated region (DMR) in the MEG3 and DLK1 genes. DNMT1/DNMT3B double knockout HCT116 lung cancer cells exhibit increased expression of 14q32.31 miRNA cluster, while 5-Aza-dC treatment can induce expression in time- and dose-dependent manners, suggesting methylation-dependent expression of miRNA cluster (Oshima, et al., 2019). CTCF binding sites spanning MEG3 (MEG3 DMR in **Figure 1.9**) have been reported to control methylation-

dependent miRNA cluster expression (Rosa, et al., 2005; Sellers, et al., 2019). Deletion of that particular region has been associated with several disorders. In accord with that, CTCF knockdown reverts 5-Aza-dC dependent overexpression of 14q32.31 miRNA cluster (Oshima, et al., 2019). In another study on mice, deletion of the intergenic differentially methylated region (IG-DMR) has been associated with the downregulation of the miRNA cluster (Zhu, et al., 2019). Another epigenetic modulator cluster of drugs, HDAC inhibitors, has been shown to induce expression of the miRNA cluster alone and in combination with 5-Aza-dC (Zehavi, et al., 2012). PRC2, a methylation complex, can suppress the miRNA cluster expression via methylation (Shivram, et al., 2019). UHRF1 and Rb can also regulate the methylation level of MEG3-DMR via recruiting DNMT1 in hepatocellular carcinoma and gastric cancer (Kruer, et al., 2016; Zhuo, et al., 2016). In another study with gastric cancer cell lines, E2F3 knockdown decreases the MEG3 expression level while overexpression of SNAIL1 increases MEG3 expression in lung cancer cell lines, suggesting transcription factors could be regulators of this miRNA cluster (Groeneveld, et al., 2018; Zhou, et al., 2015).

Apart from methylation, DNA copy number is another factor regulating the 14q32.31 miRNA cluster expression. Since regulatory elements, MEG3-DMR and IG-DMR, are on the maternal chromosome, the loss of heterozygosity has been observed in melanoma and neuroblastoma cancer cell lines and patients with low or no 14q32.31 miRNA cluster expression (Bando, et al., 1999; Gattolliat, et al., 2011; Zehavi, et al., 2012).

Besides above-mentioned transcriptional regulators, and chromosomal modifications and copy number alterations, very little is known how the 14q.32.31 miRNA cluster is regulated, except MEF2A which can also regulate the miRNA cluster expression (Kumar, et al., 2018; Wang, et al., 2019) and RNA binding proteins, CIRBP and HADHB for post-transcriptional regulation in vascular regeneration (Downie Ruiz Velasco, et al., 2019). Therefore, in many pathological conditions, including cancer, copy number alterations, and methylation status has been studied and reported to vary but there is still many unknowns left to be discovered for understanding 14q32 transcriptional and post-transcriptional regulation.

1.5.3.2 14q32.31 miRNA cluster in cancer

Dysregulation of the 14q32 miRNA cluster has been reported in various cancers, yet as oncogenic in some and tumor-suppressor in others. 14q32 miRNA cluster can drive metastatic and aggressive lung carcinoma and its expression increases in the metastatic hepatocarcinoma. Molina-Pinelo et al. (2010) has reported hypermethylation in MEG3-DMR in smoking-associated lung cancer (Molina-Pinelo, et al., 2018). The 14q32.31 miRNA cluster is also found dysregulated in uterine carcinosarcoma (Devor, et al., 2012). In another study in neuroblastoma, the 14q32.31 miRNAs are identified as high-risk markers (Gattolliat, et al., 2011). On the contrary, in osteosarcoma and myeloid leukemia, high expression of 14q32 miRNA cluster is associated with a better prognosis (Hill, et al., 2017; Sarver, et al., 2013; Sellers, et al., 2019). The same region is downregulated in glioblastoma, papillary thyroid carcinomas, metastatic prostate cancer, and melanoma (Krokker, et al., 2021; Sellers, et al., 2019; Shivram, et al., 2019).

14q32 miRNA cluster also upregulated in aromatase inhibitor-resistant breast cancer cell lines (Hoppe, et al., 2016). The overexpression of 14q32.31 miRNA cluster suppresses metastasis of lung and liver cancer cells in both in-vitro and xenograft studies. MEG3 methylation level can predict the aggressiveness of the osteosarcoma cell lines (Hill, et al., 2017). Lenalidomide, an immunomodulatory and antiangiogenic compound used for multiple myeloma, can suppress 14q32.31 expression (Krejcik, et al., 2015). Curcumin which has been reported to suppress cell growth in prostate cancer also modulates the expression levels of 14q32.31 (Zhang, et al., 2018). In breast cancer, 14q32.31 miRNAs along with miR-200 and miR-199 have been proposed as a modulator of epithelial-mesenchymal transition (EMT) through network analysis (Drago-Garcia, et al., 2017). Haga et al. (2012) have shown miRNAs located in the 14q32.31 region can suppress EMT via targeting TWIST1 and TGFB in breast cancer cell lines (Haga and Phinney, 2012). MEG3 expression level also correlates positively with stromal markers and negatively with survival in breast cancer (Budkova, et al., 2020).

The 14q32.31 miRNA cluster is among one of the widely studied miRNA clusters in cancer. Although the direction of its functionality, oncogenic or tumor suppressor, is cell/cancer type-

specific, its dysregulation of the expression level and involvement in critical pathways have been reported in a wide range of cancer types. However, very little is known about the underlying mechanism of th regulation and modulatory function of this miRNA cluster. Therefore, there is a need to address the context-dependent activity of 14q32.31 miRNA cluster and individual miRNAs.

1.5.3.3 miR495-3p in cancer

miR495-3p is a member of the 14q32 miRNA cluster. Like other members, its function in carcinogenesis and prognosis vary depending on cancer type (Jishnu, et al., 2020). The current literature for miR495-3p expression change in tumors when compared to healthy tissues and the validated targets through functional studies or binding assays are summarized in **Figure 1.10** and **Appendix Table 1** (Ahmadi, et al., 2017; Alqurashi, et al., 2019; Bai, et al., 2017; Cao, et al., 2014; Chen and Xie, 2018; Chen, et al., 2018; Chen, et al., 2013; Chen, et al., 2017; Chu, et al., 2014; Du, et al., 2020; Eun, et al., 2018; Feng, et al., 2018; Guan, et al., 2018; Hwang-Verslues, et al., 2011; Jiang, et al., 2017; Kumar, et al., 2021; Lee, et al., 2015; Li, et al., 2016; Li, et al., 2018; Li, et al., 2012; Li, et al., 2015; Lin, et al., 2021; Liu, et al., 2019; Lv, et al., 2015; Lv, et al., 2019; Mao, et al., 2016; Nie, et al., 2015; Qiu, et al., 2015; Song, et al., 2014; Sun, et al., 2019; Tan, et al., 2017; Tang, et al., 2021; Wang, et al., 2015; Wang, et al., 2017; Wang, et al., 2018; Wang, et al., 2015; Wang, et al., 2021; Wang, et al., 2019; Wei, et al., 2017; Widodo, et al., 2016; Xia, et al., 2019; Xu, et al., 2013; Yan, et al., 2017; Yang, et al., 2013; Ye, et al., 2017; Ye, et al., 2018; Yin, et al., 2019; You, et al., 2020; Zhang, et al., 2016; Zheng, et al., 2018; Zou, et al., 2017). miR495 expression is downregulated in glioma, colorectal cancer, endometrial cancer, and lung cancer while upregulated in hepatocellular carcinoma and gastric cancer (Appendix Table 1). In support of miR495's anticancer effects, Chen et al. (2017) have demonstrated that miR495 induces apoptosis and inhibits cellular growth by targeting STAT3 in MCF7 and HCC1973 cells (Chen, et al., 2017). miR-495-3p mimic treatment reduces cell viability in cervical cancer cell lines via targeting CDK1 (Tang, et al., 2021). Furthermore, the miR495-3p-TOP2A axis has been found to be associated with low-grade gliomas (Wang, et al., 2021). In another study

in MCF7 and MDA-MB-231 cell lines, miR495-3p promotes cell cycle arrest through Bmi1 (Wang, et al., 2015).

Apart from cell cycle modulatory roles, miR495-3p can also repress E-cadherin and REDD1 and could be important in acquired resistance (Hwang-Verslues, et al., 2011). In the multi-drug-resistant (MDR) triple-negative breast cancer line, miR495 expression has been found to be downregulated, and its overexpression could re-sensitize cells via downregulation of FOXC1 and TGFB2 (Kumar, et al., 2021). In another study in gastric cancer, miR-495-3p inhibits MDR through modulation of mTOR pathway. miR-495-3p has been found to be overexpressed in ER+/PR- tumors (Chen, et al., 2018).

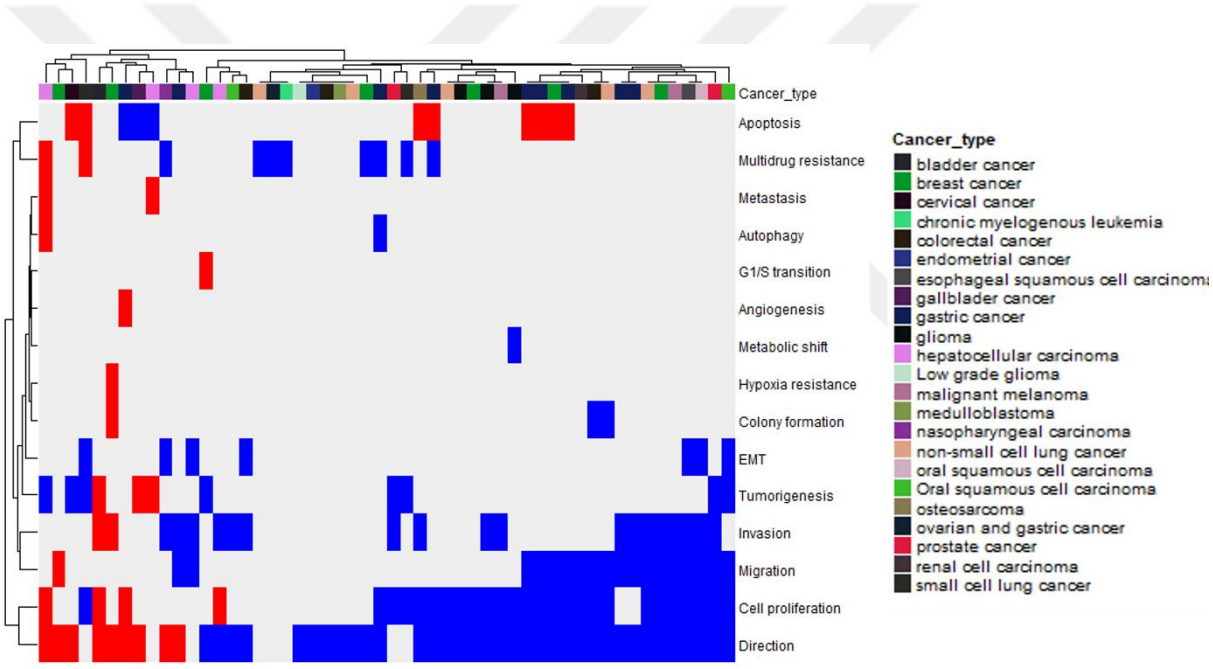

Figure 1.10 Heatmap representation of the change in miR495-3p expression level and the altered pathways in cancer in which each column represents a different study using cell lines or tumors indicated in the column annotation. Blue represents inhibition and red represents induction.

Several lncRNAs have also been reported to regulate miR495-3p expression via sponging. GATA3-AS1 can inhibit miR495-3p in breast cancer cell lines and modulate FOXM1/PLK1 signaling (Lin, et al., 2021). FAM83A-AS1 in lung and esophageal cancers, RNCR2 in melanoma, LUNAR1 in colorectal cancer, NEAT1 in colorectal cancer and melanoma, LINC01133 in ovarian cancer, NORAD in prostate cancer, LGMN and HOTAIRM1 in

glioblastoma, SNHG20 in gastric cancer, LUCAT1 in renal carcinoma, circ_0000215 in glioma, and circKRT1 in oral squamous cell carcinoma can sponge miR-495-3p (Chen, et al., 2020; Cui, et al., 2019; Duan, et al., 2021; He, et al., 2019; Huang, et al., 2020; Liang, et al., 2019; Liao, et al., 2020; Liu and Xi, 2020; Mutalifu, et al., 2020; Qian, et al., 2020; Wang, et al., 2021; Yang, et al., 2021).

1.6 Synergy analysis

1.6.1 Combinatorial therapy

Combinatorial therapy is a treatment approach in which more than one drug/therapy is combined to treat a single disease. Combinatorial therapy has been employed in several malignancies, including tuberculosis, HIV infection, and cancer (Al-Lazikani, et al., 2012; Bass, et al., 1994; Maenza and Flexner, 1998; Zhu, et al., 2021). In combinatorial treatment, the most common methodology is to identify compounds/therapies targeting two different molecular pathways in order to increase the efficiency of the treatment while reducing cellular toxicity (Diaz, et al., 2020; He, et al., 2021; Li, et al., 2020).

Cancer therapy has been challenging since it exhibits inter and intra-tumor heterogeneity by modifications in various molecular pathways. One of the primary challenges of chemotherapy is de novo or acquired resistance. Several mechanisms have been demonstrated for the acquired resistance (Vasan, et al., 2019; Wang, et al., 2019). Therapies based on a single drug primarily target a key modulatory factor, e.g., a protein or hormone. Alteration in gene expression levels of the target can induce resistance. In those cases, restoring the target gene(s) expression re-sensitizes cells in which miRNAs have been proposed as a valuable tool. Alternatively, a compensatory pathway can be activated to bypass the targeted mechanism by the treatment through alteration in drug intake and metabolism.

Targeting multiple pathways, independent or compensatory, can increase the efficiency of the therapy. In ovarian cancer, PARP inhibitors, an established therapy repressing DNA damage repair, have been reported to be more efficient along with an estrogen receptor inhibitor,

bazedoxifen (Zhang, et al., 2021). CDK inhibitor Dinaciclib combined with PD1 antibodies enhances the anti-proliferative effect in different cancer cells (Hossain, et al., 2018).

Apart from chemotherapy, increased sensitivity to radiotherapy can be achieved through drug combinations. Edwards et al. (2002) have demonstrated targeting PI3K/AKT signaling pathway can increase sensitivity to radiation (Edwards, et al., 2002). Later on, several other mTOR inhibitors have been reported to overcome resistance (Bo, et al., 2021; Mardanshahi, et al., 2021; Sun, et al., 2021; Yao, et al., 2021). In another study, ERBB, along with other tyrosine kinases, have been found to induce sensitivity (Kulukian, et al., 2020; Yu, et al., 2020).

1.6.1.1 Combinatorial therapy using miRNAs and siRNAs

As a negative regulator of their target genes hence the pathways, miRNAs have been proposed as therapeutic agents. Their interaction with mutations in other genes, drugs, and other miRNAs has been studied in various types of cancer. There is a number of studies focusing on co-delivery methods for miRNA, siRNA, and drugs (Babu, et al., 2017; Larsson, et al., 2017; Wang, et al., 2021).

miRNA-miRNA synergy has been under focus for a long time. Several computational methods have been proposed to calculate miRNA synergy score indicating the possibility of two miRNAs exhibiting synergistic effect on a particular gene, i.e., their common target or a gene downstream of their targets (Li, et al., 2014; Zhu, et al., 2013). Zhao et al.(2017) has scanned nine miRNAs significantly altered in glioma in pairs (Zhao, et al., 2017). They have identified synergy between upregulated miRNAs through miRNA mimics while the effect for downregulated miRNAs was additive. In another study in prostate cancer, the synergistic effect between miR-331-3p and Aurora Kinase Inhibitor has been reported (Epis, et al., 2017). miR-34a, a widely studied miRNA in cancer, synergizes with EGFR inhibitors, afatinib, rociletinib, and osimertinib in EGFR mutant cell lines, while no synergy is observed between miR-34a and afatinib in EGFR positive cell lines indicating the existence of a tertiary factor (Zhao, et al., 2017). Combinatorial treatment of miR-1 and miR21 inhibits hypoxia-induced apoptosis of cardiomyocytes (Xu, et al., 2015) .

As in the case of miR34a and EGFR inhibitors, the synergistic interplay between siRNAs and drugs has also been reported. Doxorubicin exhibits synergistic effects with siBCL2, or siMDR1 in various cancer types (Nourbakhsh, et al., 2015; Xu, et al., 2015). siMCL1 and MEK inhibitor (PD0325901) reduces cell viability in mice xenografts (Kang, et al., 2011). siGRSF and miR-346 overexpression increases the invasion capacity of cervical cancer cells (Guo, et al., 2015). In another study, siEphA2 and miR520d-3p synergistically exhibit tumor suppressor properties (Nishimura, et al., 2013). Combinatorial treatment with BMP9 overexpression vectors and miR-21 mimic increases osteogenic differentiation synergistically (Song, et al., 2015).

1.6.2 Synergy analysis

Many human diseases, particularly neurodegeneration and neurodevelopmental diseases, exhibit complex interactions between genetic variations and environmental factors. In a comprehensive study with 11260 patients and 24542 healthy controls, Pardinas et al. (2018) has identified 145 loci associated with schizophrenia (Pardinas, et al., 2018). Several other studies identified a number of mutations in autism, congenital abnormalities, and developmental delay (Deciphering Developmental Disorders, 2017; Kosmicki, et al., 2017; Samocha, et al., 2014). Apart from single-gene mutations, the interaction between the mutations has also been studied. The co-occurrence of the PRNP and ATP7B has been associated with severity with Wilson's disease, a neuropsychiatric disorder (Forbes, et al., 2014). LRRK2 and a-Synuclein have also been reported to exhibit a synergistic effect on Parkinson's disease (O'Hara, et al., 2020). In another interesting study in mice, neonatal exposure to iron along with a-Synuclein increases the susceptibility for age-related neurotoxicity (Peng, et al., 2010). Taken all together, the synergy analysis of the environmental and genetic variations is needed to understand the nature of the disease and the driving factors better and to develop new therapeutic strategies. As an example, Schrode et al. (2019) have developed and applied the limma-based synergy analysis method to dissect the synergy between common genetic variations in schizophrenia (Schrode, et al., 2019). They have introduced four common mutations alone or in combination using CRISPR technology, and they

have identified synergistically regulated genes and pathways. The synergy analysis method can facilitate our understanding of neurodevelopmental, neurodegeneration diseases.

The outcome of the combinatorial treatment is based on the synergistic interaction between individual treatments when combined. The interaction is called synergistic, if the effect of the combination is superior to the sum of individual therapies. The most common metric to measure synergy is through cell viability assays. Several methodologies have been proposed to identify synergistic and antagonistic therapies (Chou, 2010; Liu, et al., 2018). However, these approaches fail to uncover the underlying mechanism. Although there is an increasing number of transcriptomics data containing individual and combinatorial treatments, the methodologies to analyze such high-throughput data have yet to be systematic.

A widely-used approach is to identify the treatments altered in combinatorial but not with the individual therapies (Diaz, et al., 2020; Nassiri, et al., 2019; Ord, et al., 2021). This approach ignores the genes affected antagonistically, i.e., changed in the individual but not in the combinatorial, or changed in both treatments but not in the combinatorial. Another method is to use Venn diagrams to identify common and uniquely altered genes. In this method, down and upregulated genes are separated for each treatment (Han, et al., 2013; Kwon, et al., 2017; Mathison, et al., 2017; Raynal, et al., 2017; Stevens, et al., 2017; Vichas, et al., 2021). Although this method is more comprehensive, the complexity increases with the increasing number of treatments. Another approach is through comparison between enriched networks in individual treatments and combinatorial treatment (Chen, et al., 2019; Mathison, et al., 2017; Nagaoka, et al., 2020; Nassiri, et al., 2019; Ord, et al., 2021). None of these methods could provide a statistical approach to measure the level or extent of synergistic and antagonistic behaviors. In a recent study, a limma-based method has been proposed to measure the synergy coefficient for each gene and is able cluster genes accordingly (Schrode, et al., 2021). Unfortunately, even using this method, it is hard to infer the overall direction and magnitude of the interaction and individual contribution of treatments to the combinatorial outcome.

Aims and Rationale

CHRNA5, a nicotinic cholinergic subunit, has been studied in various contexts, including cancer. In our lab, we have been investigating the role of CHRNA5 in breast cancer progression since early 2010s. Previously, Ermira Jahja and Sahika Cıngır-Koker have shown siCHRNA5 treatment leads to a decrease in cellular growth and an increase in DNA damage response and drug sensitivity (Cingir Koker, et al., 2018; Shehwana, et al., 2021). Sıla Özdemir, Azer Acıkgöz, and Huma Shehwana have demonstrated the association between CHRNA5 and estrogen signaling (Shehwana, et al., 2021). Furthermore, Mehtap Yılmaz, Basak Ozgursoy, Said Tiryaki and Sahika Cıngır-Koker have shown the miRNA profile of siCHRNA5 (Basak Ozgursoy, MS Thesis, 2017, Sahika Cingir-Koker, Ph.D. Thesis, 2019, Rafed Said Tiryaki, MS Thesis, 2019). As a follow-up study, I focused on deciphering several major regulatory factors in siCHRNA5 function in MCF7 cells and breast cancer, as a whole. Therefore, I aimed to:

1. analyze CHRNA5 levels in normal tissues and tumors, and its correlation with other nACHRs in breast cancer to test whether CHRNA5 is an oncogene.
2. investigate the role of CHRNA5 in DNA damage response with respect to:
    a. the correlation between CHRNA5 and DNA damage response markers in breast cancer datasets,
    b. the hypothesis that siCHRNA5 profile partially depends on the existence of functional TP53 using siTP53,
    c. statistically analyze the possible antagonism between siTP53 and siCHRNA5.
3. explore the role of CHRNA5 in estrogen signaling by
    a. examining the expression levels of primary and secondary targets of estrogen in breast cancer,
    b. examining the time and dose-dependent impact of CHRNA5 knockdown on estrogen targets.
4. test the hypothesis that siCHRNA5 differential expression profile is partially through the change in miRNA expression levels, by

a. investigating the behavior of 14q32.31 miRNA cluster using TCGA and METABRIC breast cancer datasets,
b. statistically analyzing the synergism between siCHRNA5 and mimics of selected miRNAs,
c. examining the expression profile of miRNA mimics in the context of estrogen signaling

5. develop a shiny-based web tool allowing user to perform synergy analysis based on a published recent method, coupled with a novel regression-based TF enrichment methodology.
6. demonstrate the applicability of the shiny app using a case study that investigates the synergy between a novel MDM2 inhibitor and temozolomide, a DNA alkalyting agent, in neuroblastoma cells.

Chapter 2

2 Materials and Method

2.1 In vitro studies

2.1.1 Materials

2.1.1.1 General laboratory solutions, reagents, and kits

Solutions and reagents used for cell culture maintenance and in vitro experiments are listed.

Table 2-1. Cell culture and maintenance materials

Products	**Company**	**Catalog No**
DMEM w/1.0 g/L glucose w/o L-Glut	Lonza	BE12-707F
DMEM, low glucose, pyruvate, no glutamine, no phenol red	GIBCO	11880028
PBS-1X w/o Ca, Mg	Lonza	BE17-516F
FBS	Biowest	S181G-500
NEAA 100X	Lonza	BE13-114E
Sodium Pyruvate Solution 100 mM	Lonza	BE13-115E
Pen/strep stock	Lonza	DE17-602E
L-glutamine 200 mM	Lonza	BE17-605E
Trypsin-Versene(EDTA) Mix(1X)	Lonza	BE17-161E

Table 2-2. Transfection related reagents and oligos

Product	**Description**	**Catalog Number (Qiagen, Germany)**
Hs_CHRNA5_5 FlexiTube siRNA	siCHRNA5	SI03051111
Hs_TP53_7 FlexiTube siRNA	siTP53	SI02623747
AllStars Negative Control siRNA	siCONTROL	SI03650318
Syn-hsa-miR-495-3p miScript miRNA Mimic	miR495-3p mimic	YM00472039
Hs_miR-495_1 miScript Primer Assay	miR495-3p primer	YM00472039
Syn-hsa-miR-409-3p miScript miRNA Mimic	miR409-3p mimic	YM00472688
Hs_miR-409_1 miScript Primer Assay	miR409-3p primer	YM00472688
Syn-hsa-miR-376a-3p miScript miRNA Mimic	miR376a-3p mimic	YM00472498
Hs_miR-376_1 miScript Primer Assay	miR76a-3p primer	YM00472498
HiPerfect Transfection Reagent	Transcfection reagent	301704

Table 2-3. mRNA, miRNA, and protein expression measurement related reagents

Product name	**Company (Country)**	**Catalog Number**
Water, molecular biology grade, nuclease free	HyClone, USA	SH30538.01
LightCycler® 480 SYBR Green I Master	Roche, Switzerland	4887352001
LightCycler 480 Multiwell Plate 96, White	Roche, Switzerland	4729692001
RNase-Free DNase Set (50)	Qiagen, Germany	79254
RevertAid First Strand cDNA Synthesis Kit	Fermentas,Canada	K1622

miRscript RT Kit	Qiagen, Germany	218160
RNeasy Mini Kit	Qiagen, Germany	74104
miRneasy Mini Kit	Qiagen, Germany	217004
miScript syber green kit	Qiagen, Germany	218073
QIAzol lysis reagent	Qiagen, Germany	79306
HiPerfect	Qiagen, Germany	301704
2-mercaptoethanol	Sigma Aldrich, USA	M3148
Glacial acetic acid	Sigma Aldrich, USA	27225
Glycine	Sigma Aldrich, USA	G8898
Ammonium persulfate	Sigma Aldrich, USA	A3678
TEMED	Applichem, Germany	A11480100
NP-40	Applichem,Germany	A16940250
cOmplete, EDTA-free	Roche, Switzerland	11873580001
TGX Stain-Free™ FastCast™ Acrylamide Kit, 10%	Bio-Rad	1610183
PageRuler Prestained Protein Ladder	ThermoScientific,USA	26616
PVDF membrane	Roche (Switzerland)	3010040
ECL Plus Western Blotting Detection System	GE Healthcare (UK)	RPN 2232
Amersham ECL Prime Western Blotting Detection Reagent	Sigma Aldrich, USA	RPN2232
Phosstop Easypack phosphatase inhibitor cocktail tablets	Roche, Switzerland	4906845001
BCA Protein Assay kit	ThermoScientific,USA	23227
Ponceau S solution	Sigma Aldrich, USA	P-7170
4X Laemmli Sample Buffer	Bio-Rad	161-0747
BSA	Sigma Aldrich, USA	A7905
6-Aminocaproic acid	Sigma Aldrich, USA	A2504

Table 2-4. MTT and drug response-related reagents

Product name	**Company (Country)**	**Catalog Number**
SDS	Sigma Aldrich, USA	71725
MTT	Invitrogen	M6494
S-(+)-Camptothecin (100mg)	Sigma Aldrich, USA	C9911-100MG
Doxorubicin	Cell Signaling, USA	5927S
Dimethyl sulfoxide (DMSO)	Applichem, Germany	A1584

2.1.1.2 qPCR primers

Primer pairs used in this thesis are listed in **Table 2-5**.

Table 2-5 List of primer pairs

Name	**Primer sequence (5'-3')**
CHRNA5	F: GGAAACTGAGAGTGGTAGTGGA
	R: CTTCAACAACCTCACGGACA
CLDN1	F: CTGTCATTGGGGGTGCGATA
	R: CTGGCATTGACTGGGGTCAT
WDHD1	F: AGCAGCCAAGGACGAGTAAA
	R: CTTCGGCTTTGGAATCAGAG
ANLN	F: TAAAGCAGGTGATTGTTCGG
	R: GTTCTTCATCAACACAGCAG

BIRC5	F: GTTGCGCTTTCCTTTCTGTC
	R: TCTCCGCAGTTTCCTCAAAT
CDKN1A	F: GTCACTGTCTTGTACCCTTGTG
	R: CGGCGTTTGGAGTGGTAGAA
GPNMB	F: TGCTGACTGTGAGACGAACC
	R: ACACCAAGAGGGAGATCACAG
GJA1	F: TCTGAGTGCCTGAACTTGCC
	R:CCCTCCAGCAGTTGAGTAGG
GADD45A	F:TCTCGGCTGGAGAGCAGAAGAC
	R:AGCTTGGCCGCTTCGTACAC
BAX	F:GGGTTGTCGCCCTTTTCTAC
	R:CTGGAGACAGGGACATCAGT
BCL2	F:TGAACTGGGGGAGGATTGTG
	R:CGTACAGTTCCACAAAGGCA
FAS	F:AATAAACTGCACCCGGACCC
	R:AGAAGACAAAGCCACCCCAA
CCND1	F:CTGCGAAGTGGAAACCATCC
	R:GCACTTCTGTTCCTCGCAGA
CCNE2	F:GTAGCTGGTCTGGCGAGGTTT
	R:GGGCTGCTGCTTAGCTTGTAA

CHEK1	F:TGGTCACAGGAGAGAAGGCA
	R:CAGATAAACCACCCCTGCCA
TPT1	F:GATCGCGGACGGGTTGT
	R:TTCAGCGGAGGCATTTCC

2.1.1.3 Antibody list

Antibodies used in this thesis are listed in **Table 2-6**.

Table 2-6. Antibodies used in western blot

Protein name	**Company**	**catalog No:**
CHRNA5	SantaCruz	sc-376979
TP53	SantaCruz	sc-126
GAPDH	SantaCruz	sc-47724
BAX	Cell signalling	#5023
BCL2	Cell Signalling	#2870
CHEK1	SantaCruz	sc-8408
pCHEK1[Ser345]	Cell Signalling	#2348
Phospho-RB1[Ser807/811]	Cell Signaling	#9308
Anti-rabbit IgG, HRP-linked	Cell Signaling	#7074
Anti-mouse IgG, HRP-linked	Cell Signaling	#7076

2.1.1.4 Equipment

The equipment used in this study is listed in **Table 2-7**.

Table 2-7 List of Equipment

Name of the instrument	**Company**
LightCycler 480 Instrument	Roche (Sweitzerland)
NanoDrop ND-1000	Thermo Scientific (USA)
DIC Microscope	Leica (DMi8)
Amersham (TM) Imager 600	GE Healthcare Life Sciences(USA)

2.1.1.5 Prepared solutions and recipes

Standard solutions used in in vitro experiments, i.e., western blot, are listed in **Table 2-8**.

Table 2-8 Common solutions and recipes

Solution	**Content**
MTT	0,01g MTT,2ml PBS
SDS-HCL solution	2 g SDS, 16µl HCl, 20ml ddH_2O
PI (25X)	2 tablets in 840µl ddH_2O
PhosStop(20 X)	2 tablets in 1ml ddH_2O
4X SDS Loading Dye	100uL 2-mercaptoethanol , 900 µl BioRad Laemmli Buffer

RIPA buffer	75 µl 2M NaCl, 50 µl 1M Tris-HCl, 10 µl 10% SDS, 40 µl 25x proteinase inhibitor, 40 µl 20X PhoStop,775 µl ddH_2O (for 1ml)
10x Running buffer	30.3 g Tris, 144.1 glycines, 100 ml 10% SDS, ddH_2O up to 1000ml
Anode I buffer	18.15g Tris, 100ml MetOH, ddH_2O up to 500ml
Anode II buffer	1.5g Tris, 100ml MetOH, ddH_2O up to 500ml
Cathode buffer	2.62 g aminocaproic acid, 100ml EtOH, ddH_2O up to 500ml
Blocking solution (5%)	5 g BSA, 100 ml TBS-T(2%)
10% APS	0,5 APS, 5ml ddH_2O
10X TBS	24 g Tris, 88 g NaCl dissolve in 900 ml ddH_2O. PH adjusted to 7.6, volume bring up to 1000ml.
1X TBS-T (Tween 0.2%)	100ml from 10X TBS, 900 ml ddH_2O, 2ml Tween-20.
10X Running Buffer	10.08 g SDS, 30.3 g Tris, 144g Glycine in 1000ml ddH2O.
Mild Stripping Buffer	1.5g Glycine, 0.1g SDS, 1ml Tween-20 volume up to 50 ml; adjust pH 2.2, complete up to 100ml

Table 2-9 Complete DMEM recipe

	Amount	**Ratio**
DMEM, Low Glucose	500 ml	
Fetal Bovine Serum (FBS)	50 ml	10%
Sodium pyruvate	10 ml	2%
L-Glutamine	10 ml	2%
NEAA 100X	5 ml	1%
Penicillin/Streptomycin	5 ml	1%

2.1.2 Methods

2.1.2.1 Cell culture maintenance and handling

2.1.2.1.1 Thawing cells

Cell stocks were kept at liquid nitrogen in cryovials. For thawing, cells were taken from liquid nitrogen and half thawed in the water bath (37°C). The rest was dissolved through slowly mixing with complete DMEM (**Table 2-9**). Cells were then transferred to 15 ml falcon and centrifuged for 5min at 1500rpm to remove freezing media. The cell pellet was resuspended in an adequate amount of complete DMEM and transferred to a T25 plate. After overnight incubation in the incubator (37°C with 5% CO_2), cells were inspected through microscopy, passaged to a T75 plate. Cells were maintained in the incubator.

2.1.2.1.2 Passaging cells

After cells reached a 70-80% confluency, old media was removed, and cells were washed with sterile pre-warmed PBS. Then cells were incubated with an adequate amount of 0.25% Trypsin/EDTA for 3-5 min in the incubator to detach cells from the plate. A double amount of complete DMEM was added to inactivate the trypsin, and cells were transferred to 15ml falcon. Cells were centrifuged for 5 min at 1500rpm. The cell pellet was then dissolved in fresh media,

and 1:6 of the resuspension was transferred to a new plate then completed with an adequate amount of complete DMEM.

2.1.2.1.3 Freezing cells

For the maintenance of the cell stock, in the second or third passage, the cells were frozen. Freezing media was prepared as 90% FBS and 10% DMSO. The cell pellet was obtained as passaging cells, dissolved in freezing media (2ml per 1million cells), and then transferred to cryovials (2 ml each). The cryovials were first kept at -20^{o}C for 1-2h, then moved to -80^{o}C for overnight incubation, finally transferred to liquid nitrogen for long-term preservation.

2.1.2.2 siRNA and miRNA mimic transfections

After cells reached a 70-80% confluency, the cell pellet was obtained as in passaging. The cell pellet was resuspended in 1 ml complete DMEM, and 20µl of cell suspension was further diluted in 180 ul DMEM (1:10). The diluted cell suspension was counted twice using a hematocytometer. Then cells were seeded to 6, 12, 24, or 96 well plates with the amount shown in **Table 2-10**. The cells were then incubated overnight in the incubator. The transfection mixture was prepared the next day with the conditions shown in **Table 2-10** (optimized by Ermira Jahja). For the double transfections, an equal amount of siCONTROL was added to individual treatments, i.e., siCONTROL (20nM), siCHRNA5(10nM siCHRNA5 + 10nM siCONTROL), siTP53 (10nM siTP53+ 10nM siCONTROL) and combinatorial (10nM siCHRNA5 + 10nM siTP53). In order to reduce pipetting errors, a single transfection mixture was prepared for biological replicates. Transfection reagent (HiPerfect) and oligo (siRNA and/or miRNA mimic) were mixed through pipetting followed by gentle vortexing. After a quick spindown, the transfection mixture was incubated for 10 min for the formation of the transfection complex under the hood. During incubation, old media was removed from plates and replenished with the new media. After incubation, the transfection mixture was distributed dropwise onto cells, swirled to the eight shape several times, and then carefully placed in the incubator. After 72h of incubation, cells were taken for the follow-up experiment, i.e., RNA isolation, protein isolation, or MTT. RNA and protein experiments were performed in duplicates, and cells were treated in five replicates for MTT.

Table 2-10. Transfection conditions for cell plates

Plate	Number of cells seeded	Transfection Reagent	10nm Oligo (siRNA/miRNA mimic)
6 well	200.000	12µl	1µl
12 well	100.000	6µl	0.5µl
24 well	50.000	3µl	0.25µl
96 well	2.000	1.2µl	0.1µl

2.1.2.3 RNA isolation and cDNA synthesis

For the RNA experiments, 6 or 12 well plates were used, and cells were transfected as described before. After 72h of incubation with the transfection mixture, old media was removed, and cells were washed with pre-warmed PBS.

2.1.2.3.1 mRNA isolation

For siTP53 and siCHRNA5 experiments, RNAeasy kit (Qiagen, Germany) was used. After washing with PBS, the cell pellet was obtained as in passaging, RNA was isolated according to manufacturers' instructions. At the final step, RNA was eluted in 35µl nuclease-free water. RNA amount and quality were measured using NanoDrop.

2.1.2.3.2 Total RNA isolation (for miRNA mimic studies)

For miRNA mimic studies, miRNeasy kit (Qiagen, Germany) was used. After washing with PBS, 700µl Qiazol (Trizol) was added, and cells were detached using a scrapper. Cell lysis was transferred to an eppendorf and snap-freezed in liquid nitrogen and kept at 80^{o}C overnight. The next day, RNA was isolated according to manufacturers' instructions. At the final step, total RNA was eluted in 35µl nuclease-free water. RNA amount and quality were measured using NanoDrop.

2.1.2.3.3 cDNA synthesis from mRNA

For the cDNA synthesis for mRNA from mRNA isolate or total mRNA isolate, the RevertAit RT Reverse transcriptase kit was used. 800 ng of RNA was used for all experiments. cDNA was

synthesized according to manufacturers' instructions. 800 ng of RNA was completed with nuclease-free water to 11µl, and 1µl Oligo (dT) primers were added. To 12µl mixture, 4µl 5X Reaction Buffer, 2µl dNTP mix and 1µl of RT and RiboLock RNase inhibitor were added. The reaction mixture was incubated 60min at 42ºC, and the reaction was terminated at 70ºC for 5min. For the qPCR experiments, 1:20 dilution was used, and cDNA stocks were kept at -80ºC.

2.1.2.3.4 cDNA synthesis from miRNA

For the miRNA mimic studies, cDNA was also synthesized from miRNA using the miScript II RT kit (Qiagen, Germany). 800ng of RNA was mixed with 2µl 5X HiSpec Buffer, 1µl Nucleus mix, 1µl RT enzyme and completed to 10µl with nuclease-free water. The reaction mixture was incubated at 37ºC for 60min and terminated at 95ºC for 5 min. For the qPCR experiments, 1:20 dilution was used, and cDNA stocks were kept at -80ºC.

2.1.3 Expression analysis with qPCR

Expression analysis of mRNA and miRNA was performed using qPCR. qPCR analysis for both mRNA and miRNA expression was performed with two biological and two technical replicates.

2.1.3.1 mRNA qPCRs

The master mix for the mRNA qPCR was prepared with the recipe per sample; 5µl SYBR Green (Roche, Switzerland), 1µl forward primer, 1µl reverse primer, and 1µl nuclease-free water. 8µl of the master mix was distributed to the qPCR plate. 2ul of 1:20 diluted cDNA was mixed. After centrifuging for 2 min at 1500rpm, the reaction was conducted at LightCycler 480 qPCR instrument with optimized annealing temperature of the primer pairs for 50cycle with the conditions summarized in **Table 2-11**. TPT1 was used as a housekeeping gene for mRNA qPCRs.

Table 2-11 Reaction conditions for mRNA qPCR

Step	**Temperature (°C)**	**Time (mm:ss)**	**Cycles**
Pre-incubation	95	05:00	1
Amplification	95	00:10	50

	58-62	00:20	
	72	00:20	
Melting Curve	95	00:05	1
	55	01:00	
	95	Acquisition per 5 °C	
Cooling	40	00:30	1

2.1.3.2 miRNA qPCRs

For the miRNA qPCRs, a commercially designed protocol, miScript primer assays (Qiagen, Germany) and miScript SYBR Green PCR kit (Qiagen, Germany), was employed. The first master mix was prepared with the recipe per sample; 5µl SYBR Green, 1µl miRNA primer, 1µl miScript Universal primer, and 1µl nuclease-free water. 2ul of 1:20 diluted miRNA cDNA was added, and after centrifuging for 2 min at 1500rpm, the reaction was conducted at LightCycler 480 qPCR instrument with conditions **Table 2-12**. RNAU6 was used as a housekeeping gene.

Table 2-12 Reaction conditions for miRNA qPCR

Step	**Temperature (°C)**	**Time (mm:ss)**	**Cycles**
Pre-incubation	95	15:00	1
Amplification	94	00:15	45
	55	00:30	
	70	00:30	
Melting Curve	95	00:05	1
	55	01:00	
	95	Acquisition per 5 °C	
Cooling	40	00:30	1

2.1.3.3 qPCR analysis

ΔΔCT method was employed for the analysis of both types of qPCR (Livak and Schmittgen, 2001). Raw CT and TM values were obtained from the LightCycler 480 qPCR instrument through "AbsQuant 2nd Derivative Max" and "TM calling" analysis methods provided in instrument software. TM values and peaks were used to detect the contamination.

The mean of the technical replicates was calculated for each sample. Then all samples were normalized with the average of the control samples ($control_{mean}$ – sample). Next, genes were normalized with the housekeeping gene (TPT1 for mRNA and RNAU6 for miRNA) through subtraction. Log transformed ΔΔCT values were used for the statistical analysis.

2.1.4 RNAseq studies

After confirming the siCHRNA5 and siTP53 treatments and their combination downregulated their targets through qPCRs, samples were sent for the RNAseq (BmLabosis). Assessment of the RNA quality was performed by the company through measuring Phred Quality Score. After confirming the quality of the samples, they were taken for the RNAseq. The additional quality controls and analysis of the results were described in **Section 2.2.3.**

2.1.5 Microarray studies

After confirming the siCHRNA5 and miR409-3p treatments and their combination altered their targets through qPCRs, samples were sent for the gene expression analysis using Affymetrix hgu133aplus2 platform (AY-KA Ltd.). The analyses of the microarrays were described in **Section 2.2.2.**

2.1.6 Protein isolation and quantification

Cells were seeded to 6 well plates in duplicates for protein experiments. Fresh RIPA buffer was prepared before protein extraction **Table 2-8**. After 72h of treatment, as described before, old media was collected, and cells were washed with ice-cold PBS twice, and that PBS was added to old media and centrifuged at 5000rpm for 5min to collect dead cells. Cells were scraped with 50µl RIPA buffer, and cell lysate was contained in a 1.5ml tube. The cell pellet from old media was

resuspended with 15µl RIPA buffer and mixed to the cell lysate. The cell lysate was kept on ice for 30min and vortexed at every 5min. Then, samples were centrifuged at 13000rpm for 20min, and the supernatant was transferred to a fresh tube.

After protein isolation, protein concentration was measured through the BCA Protein Assay Reagent kit (Thermo Scientific, USA). Standards and solutions were prepared according to manufacturers' instructions. After incubation at 37ºC for 30min, absorbance values were measured using the BD Accuri C6 instrument. The total amount of protein was calculated with the regression line formula between the concentration of standards and their corresponding absorbance.

2.1.7 Western blot

15µg protein of each sample was transferred to a fresh tube. The concentration was equalized for all samples through completing to the max volume by RIPA. Then protein solution was mixed with 4X SDS Loading Dye and denatured at 95ºC for 5 min. Undenatured proteins were stored at -80ºC.

10% BioRad Fast Casting gels were prepared according to manufacturers' instructions for 1mm gel. After gels were prepared and proteins were denatured, a 6µl protein ladder was added to the first well and the samples to the rest of the wells. For the empty wells, 6µl of 4X SDS Loading Dye was added. Proteins were run at 80V until the stacking border; then, it was increased to 120V. Proteins were then transferred to a PVDF membrane using semi-dry transfer using the Anode I, Anode II, and Catode solutions in **Table 2-8**. After 55 min of transfer (1.3A, 25V), membranes were stained with the Ponceau S solution to visualize the transfer quality. Then, membranes were washed with dH_2O and cut according to the sizes of the proteins of interest. Membranes were incubated in blocking solution with 5% BSA at room temperature for 60min. Membranes were then incubated with primary antibodies at 4ºC overnight on a shaker or rotator. The next day, membranes were washed with TBST for 10min three times and moved to secondary antibody

incubation at room temperature for 1-4h. Then, membranes were again washed with TBST for 10min three times. Proteins were visualized using ECL and Amersham (TM) Imager 600.

Mild stripping was used to re-use the membranes. The mild stripping buffer was prepared fresh, and its pH was adjusted to 2.2. Membranes were washed with the buffer for 10 min twice, TBS for 5 min twice, and finally 10min TBST once. Then membranes were moved to blocking and the rest of the western protocol.

2.1.8 MTT cell viability assay

Cells were seeded to 96 well plates for the MTT cell viability assays. After 72h treatment, MTT experiments were carried out following manufacturers' instructions. 0.01gr MTT was dissolved in 2ml of PBS and filtered. Old media was removed and replenished with 100ul fresh phenol-free media and 10ul of MTT mixture. After 4h of incubation in the incubator, 100 ul freshly prepared SDS-HCl solution was added to each well and incubated for 16-18h. Then, the absorbance was measured using a microplate reader at 570nm.

2.1.9 Drug sensitivity assays with MTT

Cells were seeded to 96 well plates a day before the treatment. On the treatment day, cells were treated with an increasing amount of doxorubicin (0 uM (DMSO-control), 0.06 uM, 0.125uM, 0.25 uM) and siCHRNA5 and/or siTP53 as described in **Section 2.1.2.2**. After 72h of incubation, cell viability was measured with the MTT assay.

2.1.10 Statistical analysis

All the statistical analyses were done using GraphPad Prism 6.0. For qPCR data with two groups, Student's t-test and qPCR and MTT analysis with multiple groups Tukey HSD corrected ONE-WAY ANOVA were employed.

2.2 In silico analysis

2.2.1 Datasets used

Datasets used in this thesis, their platform and their accession ID, if applicable, are provided in Table 3-13 (Bisio, et al., 2014; Carroll, et al., 2006; Chen, et al., 2019; Cingir Koker, et al., 2018; Guan, et al., 2019; Hah, et al., 2011; Janky, et al., 2014; Lin, et al., 2007; Nikulenkov, et al., 2012; Shatz, et al., 2015; Wardell, et al., 2012; Welboren, et al., 2009; Zaccara, et al., 2014).

Table 2-13 List of datasets used in this study

GSE ID	Platform	PMID	Title
GSE24065	Agilent-014850 Whole Human Genome Microarray	25401416	Crossroads of the p53, ER, NFkB stress response networks
GSE30183	Affymetrix Human Genome U219 Array	22790872	Expression profiling of MCF7 cells upon nutlin3a treatment
GSE47042	RNAseq	25058159	Discovery of the p53 targetome in MCF7 cells from RNA-seq data
GSE50650	Agilent-014850 Whole Human Genome Microarray	24926617	Transcriptome and translatome profiling of MCF7 vector cells after p53 activation
GSE72359	Affymetrix Human Genome U133 Plus 2.0 Array	26220208	p53 amplifies Toll-like receptor 5 response in MCF-7 cells

GSE86880	Affymetrix Human Genome U219 Array		Expression data from MCF7 cells treated with RITA or Nutlin
GSE104917	RNAseq	30536898	RNASeq analysis of NB1691 neuroblastoma cells treated with MDM2-p53 inhibitor RG7388 alone and in combination with temozolomide
GSE35428	Affymetrix Human Genome U133 Plus 2.0 Array	22570330	Transcriptional profiling of clinically relevant SERMs and SERM/estradiol complexes in a cellular model of breast cancer
GSE117942	RNAseq	31353221	RNA-seq of breast cancer cell lines post ligand treatment I
GSE11506	Affymetrix Human Genome U133 Plus 2.0 Array	17510434	Novel Estrogen Receptor-alpha Binding Sites and Estradiol Target Genes Identified by ChIP Cloning in Breast Cancer.
GSE11324	Affymetrix Human Genome U133 Plus 2.0 Array	17013392	Genome-wide analysis of estrogen receptor binding sites
GSE89333	Affymetrix Human Genome U133 Plus 2.0 Array	30543688	Downregulation of Cholinergic Receptor Alpha 5 (CHRNA5) in MCF7 breast cancer cells
GSE117941	ChIP-seq	31353221	ChIP-seq of ER in MCF-7 cells post ligand treatment

GSE14664	ChIP-seq	19339991	ChIP-Seq of ERalpha and RNA polymerase II defines genes differentially responding to ligands
GSE27463	GRO-seq	21549415	Global Analysis of the Immediate Transcriptional Effects of Estrogen Signaling Reveals a Rapid, Extensive, and Transient Response

2.2.2 Microarray data normalization and differentially expressed gene analysis

Several microarray datasets, both publicly available and in-house, were used throughout this study in different contexts **Table 2-13**. Raw CEL files for public datasets were obtained from NCBI/GEO.

For the miRNA microarray dataset, raw CEL files were normalized using the rma function from the oligo package. Since Affymetrix miRNA microarrays contain probes for non-human miRNAs as well, human miRNAs were filtered after normalization. Differential expression analysis was performed using limma (Ritchie, et al., 2015). Results were visualized using the EnhancedVolcano package (Blighe K, 2021).

Affymetrix hgu133aplus2 platform was used for the miRNA mimic studies. In each study, experiments were designed as; siCONTROL, miRNA mimic, i.e., miR-495-3p (Sahika Cıngır-Koker Thesis, 2019), miR-376a-3p (Said Tiryaki Thesis, 2019) and miR-409-3p and miRNA mimic with siCHRNA5. Quality control of CEL files was performed using the AffyQCReport and the affyplm packages (Brettschneider, et al., 2008; Craig Parman). After confirmation of the data quality, data were normalized using the rma function from the affy package (Gautier, et al., 2004). Log fold change (logFC) values were calculated with subtraction of siCONTROL results. For the different probes of the same gene, the best jetset probes were used.

Raw CEL files for publicly available Affymetrix datasets were obtained from GEO then normalized using the rma function from the affy package (Gautier, et al., 2004). Differential gene expression analysis was done using the limma package. For the different probes of the same gene, the best jetset probes were used.

For Agilent datasets, normalized expression data (series matrix) was obtained through GEO. After log2 transformation, limma was employed for the differential gene expression analysis.

2.2.3 RNAseq analysis

To investigate the transcriptomic effects of siCHRNA5, siTP53, and their combination, MCF7 cells were treated with siCONTROL, siCHRNA5, siTP53, and their combination in duplicates. RNA was isolated as described previously, then sent for the RNAseq analysis with Novaseq technology with 150bp paired-end and 20M read depth parameters. The company prepared Poly-A enriched cDNA library and performed the initial quality control analyses.

Raw fastq files were uploaded to Seven Bridges Cancer Genomics Cloud (https://www.cancergenomicscloud.org/). CGC allows users to analyze their data using publicly available tools and pipelines in a user-friendly interface. FastQC tool was employed for the quality control of the RNAseq data. FastQC, the most commonly used quality control analysis tool, examines read data in twelve metrics and produces a report (**Figure 2.1**). Basic statistics provide a general summary, i.e., sequence length, %GC, Total sequence. Per base sequence quality is an important measure that shows the quality scores according to their position in the reads. Per sequence quality score plot is the histogram of the quality scores, the skewness to the right represents higher quality. Per base sequence content gives error for all RNAseq experiments because sequencing is initiated with random hexamers, altering the enrichment score for some bases. However, through visual inspection of the plot, quality can be assessed. Per sequence GC content is a histogram plot of the distribution of %GC and compared against theoretical distribution. Sharp peaks imply contamination or over-representation of a specific gene, i.e., lncRNA. Sequence Duplication Levels metric is about the library preparation and mostly not

relevant to RNAseq data results. The other important metric is overrepresented sequence, which helps to detect contamination of adaptors etc. According to FastQC reports, the quality of the RNAseq results was high enough for the downstream analysis.

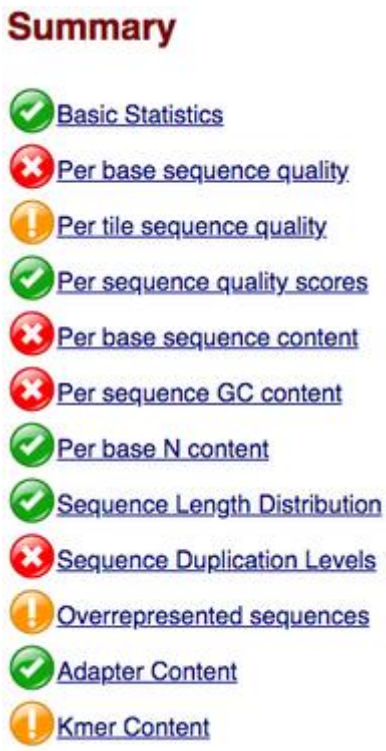

Figure 2.1 The metrics used by FastQC for the quality assessment. The green ticks and red crosses represent quality control tests that read data passed and failed while warnings were labeled yellow.

After quality control analysis, reads were aligned to human genome hg19 assembly using the Star alignment tool with default parameters in CGC (Dobin, et al., 2013). Raw read counts were then obtained using the HTSeq Count tool in CGC with Ensemble Gene IDs and genomic location (Anders, et al., 2015).

For the publicly available datasets, raw count data (**Table 2-13**) were obtained from GEO. Normalization and differential gene expression analysis was performed using the limma package following developers' instructions. For the PCA and MDS plots, voom transformed count data was used.

2.2.4 TCGA data analyses

mRNA and miRNA expression data along with copy number alteration and clinical information of samples were obtained from FireBrowser. Subtype information and methylation data for the TCGA BRCA dataset were downloaded from the XENA and cBioPortal (Gao, et al., 2013; Goldman, et al., 2020).

Log2 transformed expression data (RSEM +1) were used during PCA plots, distribution plots, and correlation analysis. For the pairwise correlation analyses, Spearman's method was employed.

2.2.5 METABRIC data analyses

METABRIC dataset is the largest breast cancer expression cohort stored in European Genome-Phenome Archive (EGA) with the accession ID EGAS0000000012 (Curtis, et al., 2012; Lappalainen, et al., 2015). Unlike TCGA, Access to METABRIC is controlled, and permission is required.

METABRIC data provide mRNA and miRNA expression data from microarrays, copy number alterations, mutations, and clinical information. The expression data provided was pre-processed and log-transformed. Therefore, the data was used directly without any other processing.

2.2.6 STRING database and Cytoscape network analyses

The STRING is a well-established and widely used protein-protein interaction (PPI) database (Szklarczyk, et al., 2019). PPI network for the altered genes with miR-495-3p treatment (abs(logFC)>0.5) was obtained and uploaded to Cytoscape for the network analysis (Shannon, et al., 2003). Markow Cluster Algorithm (MCL) with default parameters was used to identify network clusters (Morris, et al., 2011). The iRegulon plugin was employed to understand the regulatory components further (Janky, et al., 2014).

2.2.7 miRNA-mRNA network

Experimentally validated targets of the miRNAs located 14q32.31 miRNA cluster were obtained from miRNET (Chang, et al., 2020). miRNA-mRNA network was constructed in Cytoscape, in

which nodes were colored according to the logFC values obtained from siCHRNA5 treatment (GSE89338). Primary and secondary targets of ESR1 were shown with larger nodes.

2.2.8 Enrichment analysis

Various enrichment and overrepresentation analyses were performed to understand the altered biological processes and pathways. Gene Set Enrichment Analysis (GSEA) is a java-based standalone tool to perform enrichment analysis for the user-given dataset (Subramanian, et al., 2005). It allows users to select gene sets, i.e., Gene Ontology (GO) terms, KEGG pathways (Kanehisa, et al., 2016; Mi, et al., 2019). GSEA for the KEGG pathway enrichment analysis was employed for siCHRNA5 microarray data with default parameters. Results were visualized using the ggplot2 package.

The clusterprofiler package was used to perform overrepresentation analysis for GO terms, and KEGG pathways in R (Wu, et al., 2021). Results were visualized using ggplot2 and enrichplot packages.

2.2.9 Ingenuity pathway analyses

Ingenuity Pathway Analysis (IPA) tool allows users to perform enrichment analysis with manually curated gene sets (QIAGEN Inc., https://www.qiagenbioinformatics.com/products/ingenuity-pathway-analysis). For microarray results of miR-495-3p mimic and its combination with siCHRNA5 was uploaded to IPA, and the analysis was performed for the genes (abs(logFC) >0.5 using "Core Analysis" and "Analysis Comparison" functions. Other canonical pathways were also investigated.

2.2.10 SyneRgy app

syneRgy is a shiny-based web tool to perform synergy analysis using transcriptome data. syneRgy was designed to accept raw count data from an RNAseq experiment or differential gene expression results from any platform.

2.2.10.1 Limma-based synergy analyses

Limma-based syneRgy analysis was adapted from a recently published method (Schrode, et al., 2021). In this method, regular limma analysis was performed for the treatment groups as well as additive and synergy coefficients with the contrast matrix shown in **Figure 2.2**.

ID	Contrast
Treatment 1	Treatment1- Control1
Treatment 2	Treatment2- Control2
Combination	Combinatorial Treatment -Control3
Additive	Treatment1- Control1 + Treatment2 - Control2
Synergy	Combinatorial Treatment -Control3 - (Treatment1- Control1 + Treatment2 - Control2)

Figure 2.2 Example contrast matrix used for synergy analysis

After limma analysis, the synergy cluster for each gene was calculated following the pseudocode in

Figure 2.3. The meanSE is calculated as the average standard error for all treatment groups. Visualization of the clusters and the distribution was done using ggplot2, Waterfalls, ComplexHeatmap packages (Gu, et al., 2016).

```
Input logFC matrix m;
for every gene in m do;
 if Synergy.logFC > meanSE
       if additive.logFC < -meanSE
          if combinatorial.logFC > meanSE
               gene -> More up
          else   gene -> Less down
      else     gene  ->More up
 else if Synergy.logFC < -meanSE
         if additive.logFC > meanSE
           if combinatorial.logFC < meanSE
               gene -> More down
           else   gene -> Less up
       else     gene  ->More down
else gene -> Additive
```

Figure 2.3 Pseudocode for synergy analysis generated from (Schrode, et al., 2021).

2.2.10.2 *Synreg*: a regression-based synergy analysis

In the regression analysis module for the regression, lmfit function from the glmfit function was employed. Statistical analysis of the difference between the regression line and the y=x line was performed by adding an offset value 1. The ggplot2 package was used for the visualization.

2.2.10.3 DoRothEA analysis

DoRothEA is an R package containing TF-Target data with evidence score and the direction of the interaction (Garcia-Alonso, et al., 2019). The developers have curated the TF-Target pairs manually using various sources and calculated an evidence score ranging from A to E in which A is the highest and E is the lowest. In syneRgy, TF-Target pairs with the evidence scores A and B were used. Since DoRothEA also contains the direction information, enrichment analysis was performed using the run_viper function, a wrapper function for the viper from the Viper package (Alvarez, et al., 2016). Viper function was designed to perform enrichment analysis for the Aracne regulons derived from transcription data. For the statistical analysis permutation-based FDR was

calculated. In this method, genes were randomly matched with the logFC values 100 times, and the viper function was called for each. The ratio of the enrichment scores higher than the original score was reported, i.e., if the enrichment score in five out of 100 trials were higher than the original enrichment score, the FDR value is calculated as 0.05.

In addition to enrichment analysis, overrepresentation analysis using Fisher's exact test was performed for treatment results as well as synergy clusters (Shen L, 2021). For the treatment analysis, significantly altered genes (adj p-value <0.05) were stratified according to the direction of the logFC values (up and downregulated), and overrepresentation analysis for the targets of each TF was performed. For the synergy clusters that were obtained using limma-based synergy analysis, the same method was used.

For both of the analysis types, regression analysis results between additive logFC and combinatorial logFC for the targets of selected TF were reported. Hierarchical clustering and heatmap representation through the ComplexHeatmap package was also included.

2.2.10.4 ChEA3 analysis

ChEA3 is another well-known TF-Target database (Keenan, et al., 2019). As oppose to DoRothEA, they report the actual scores from each data they have curated in addition to their two scoring metrics, namely, meanRank and topRank. In collaboration with Farid Ahadli, on-fly ChEA3 analysis for synergy clusters was included. The enrichment scores and the relevant statistical analysis results were reported and visualized using ggplot2.

CHAPTER 3

3 Results

3.1 Part 1. CHRNA5 expression in tissues

3.1.1 CHRNA5 is expressed in various tissues.

CHRNA5, as a cholinergic receptor, was not only expressed in the nervous system, but its function was shown in various tissues in different contexts. Therefore I first explored the expression level of CHRNA5 in 31 normal tissues using the public GTEX dataset (**Figure 3.1**). Testis, bone marrow, colon, muscle, and pancreas exhibited high levels of CHRNA5 expression while it was low expressed in the kidney, liver, thyroid, spleen, and pituitary. CHRNA5 was found to be expressed in the breast tissue in the mid-range along with the brain, esophagus, heart, vagina, prostate, and uterus supporting its wide range of function.

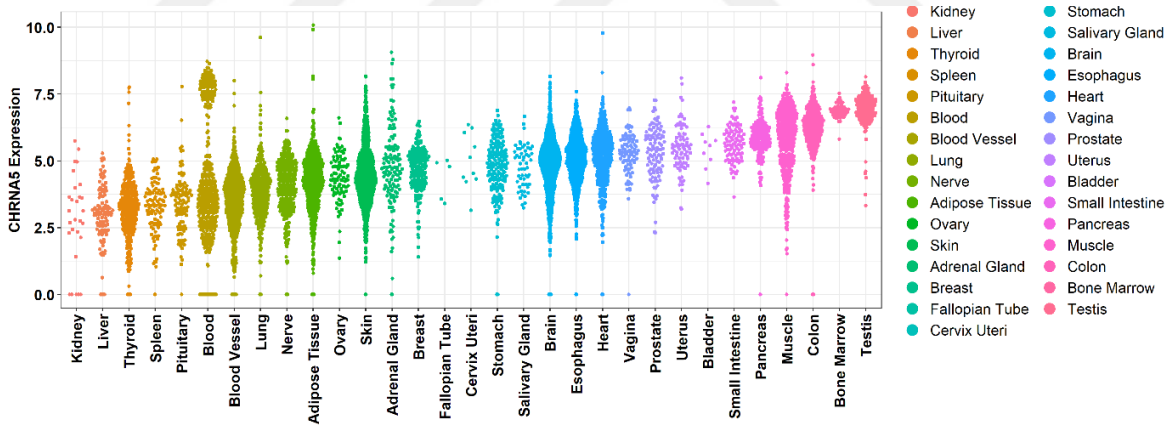

Figure 3.1 CHRNA5 expression in the normal tissue samples in the GTEX dataset.

3.1.2 CHRNA5 is highly and variably expressed in tumor tissues in different cancer types.

I next investigated the CHRNA5 expression levels in different cancer types (**Figure 3.2**). All cancer types in TCGA with normal tissue samples exhibited higher or, for some, equal levels of CHRNA5 when compared to their normal tissues. As expected, CHRNA5 expression was the

highest in the lung adenocarcinoma (LUAD), and pheochromocytoma and paraganglioma (PCPG). In bladder cancer (BLCA), in which smoking is one of the main risk factors, CHRNA5 expression was higher. Low-grade glioma (LGG) and glioblastoma multiforme exhibited mid to low CHRNA5 expression. Interestingly, CHRNA5 expression was variable in breast cancer (BRCA).

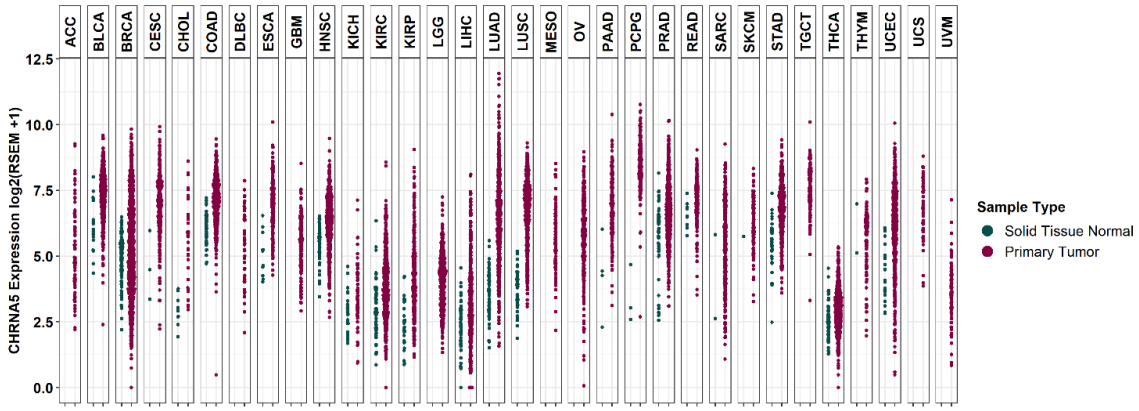

Figure 3.2 CHRNA5 expression in the tumor samples in the TCGA dataset.

3.1.3 CHRNA5 expression positively correlates with CHRNA3 and CHRNB4 expressions

nACHRs form homo- or hetero-pentameric structures to be functional. CHRNA5 have shown to bind CHRNA4-CHRNB2 and CHRNA3-CHRNAB4 subunits. Pairwise correlation analysis with nACHRs in TCGA BRCA dataset revealed that CHRNA5 was positively and significantly correlated with its chromosomal neighbors CHRNA3 and CHRNB4 (**Figure 3.3**). Interestingly, CHRNB2, another binding partner of CHRNA5 along with CHRNA4, exhibited no correlation with CHRNA5; and the low correlation with CHRNA4 might indicate CHRNA3-CHRNB4 could be the dominant assembly for CHRNA5. CHRNA7, known to form a homomeric structure, also exhibited a positive correlation with CHRNA5.

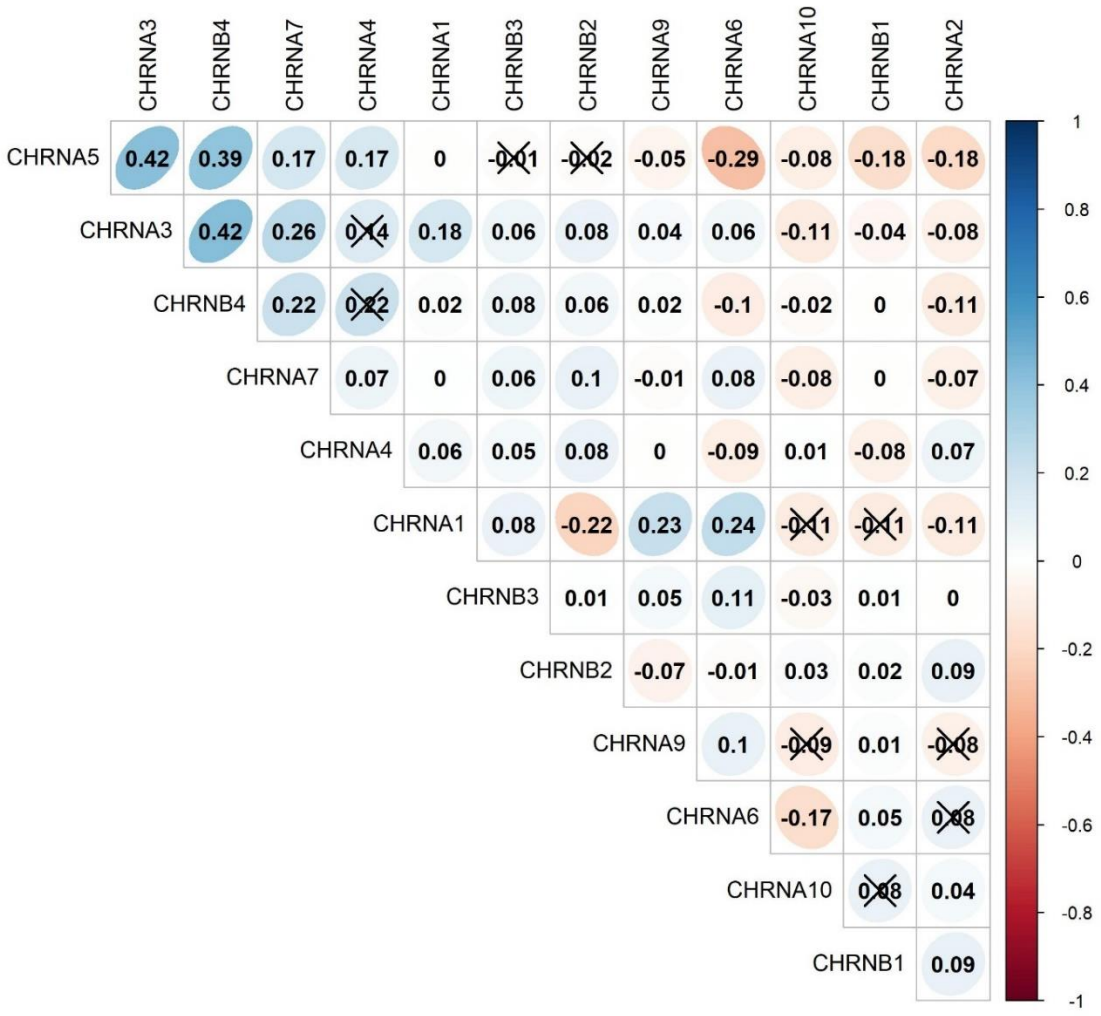

Figure 3.3 Pairwise Spearman's correlation coefficients of nACHRs in the TCGA BRCA dataset. Dots were colored according to the correlation coefficient, and insignificant results were labeled with a cross (p-value < 0.05).

3.1.4 CHRNA5 is highly expressed in the basal subtype

In order to further evaluate the CHRNA5 expression pattern in breast cancer, CHRNA5 expression in breast cancer subtypes was investigated. CHRNA5 was highly expressed in the basal subtype, which contains ER-negative and mostly TP53 mutant tumors, and expressed at lower levels in the LumA subtype. No difference was observed between Her2, LumB, and Normal-like subtypes (**Figure 3.4**).

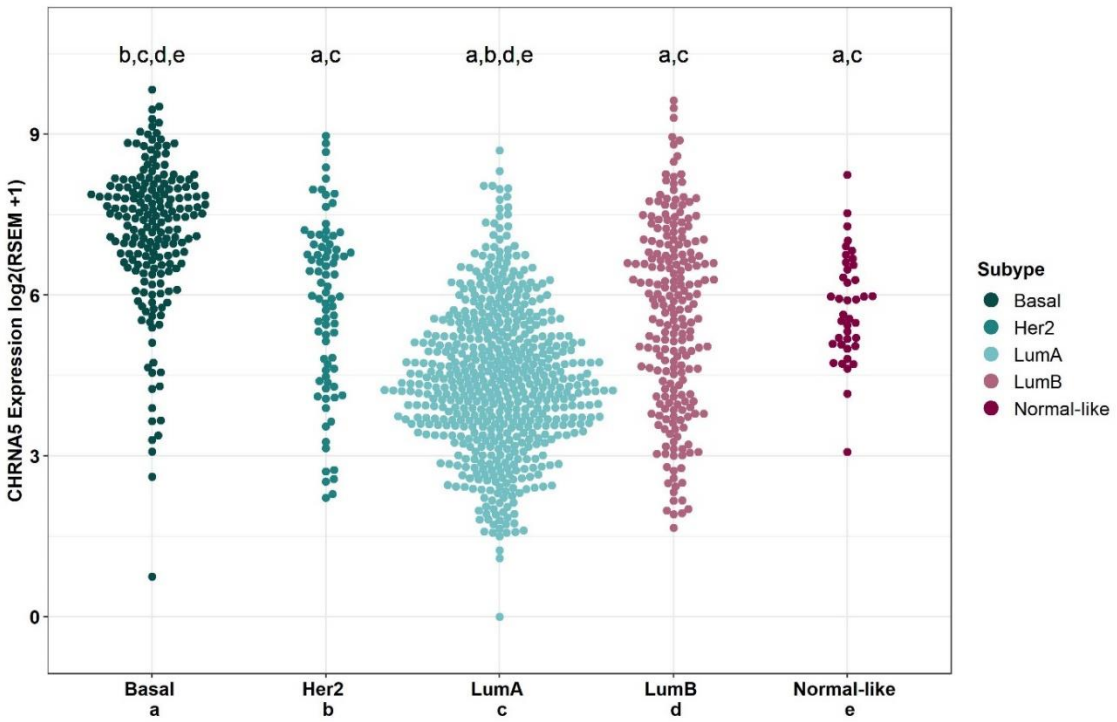

Figure 3.4 CHRNA5 expression in breast cancer subtypes. Tukey HSD following One-way anova was employed for statistical analysis. Significantly different groups were reported on top of each group (Adj. p-value < 0.05).

3.2 Part 2. CHRNA5 modulates the DNA damage repair pathway

3.2.1 siCHRNA5 downregulates expression of DNA damage pathway genes.

In the previous studies from our lab, CHRNA5 was successfully downregulated by three different siRNAs, and siCHRNA5 transcriptome was profiled using Affymetrix hgu133a.plus2 microarray (Ermira Jahja Ph.D. thesis, Bilkent University 2017; GSE89333). KEGG pathway enrichment analysis of siCHRNA5 profile using GSEA revealed that DNA replication and DNA damage response and repair (DDR) related pathways were significantly enriched with downregulated genes, whereas TP53 signaling, one of the primary regulators of DDR, was the most upregulated pathway (**Figure 3.5**). Therefore, I focused on exploring the interplay between CHRNA5 and DNA damage pathway and TP53 signaling.

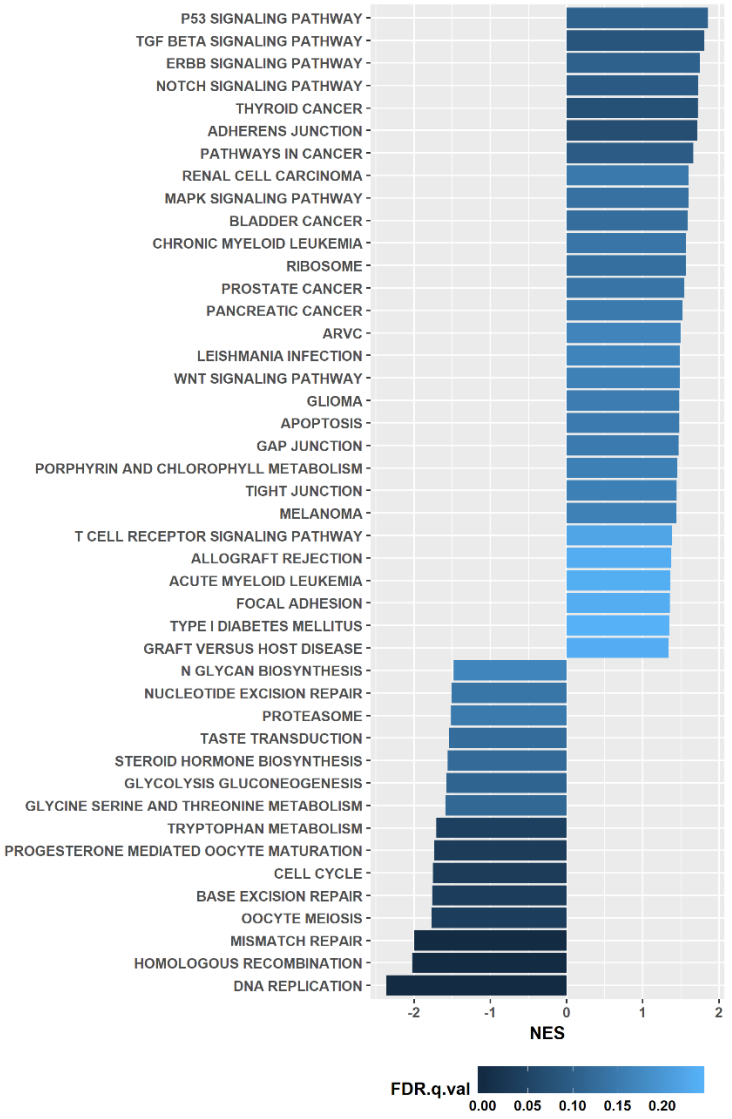

Figure 3.5 KEGG pathway enrichment analysis of siCHRNA5 transcription profile. Negative normalized enrichment scores (NES) were used for pathway enriched for downregulated genes.

(This image was reproducible without the need of copyright permission and required citation and it was obtained from Cingir Koker S, Jahja E, Shehwana H, Keskus AG, Konu O (2018) Cholinergic Receptor Nicotinic Alpha 5 (CHRNA5) RNAi is associated with cell cycle inhibition, apoptosis, DNA damage response and drug sensitivity in breast cancer. PLoS ONE 13(12): e0208982. https://doi.org/10.1371/journal.pone.0208982)

3.2.2 CHRNA5 is co-expressed with DNA damage repair genes.

Manually curated 60 essential DDR genes were obtained from Lin et al. (2016). Hierarchical clustering with those DDR genes and CHRNA5 using METABRIC and TCGA BRCA datasets revealed CHRNA5 clustered together with a subgroup of DDR genes, including PCNA, BRCA1, and CHEK1 (**Figure 3.6** A-D). Genes clustered together with CHRNA5 were also highly expressed in TP53 mutant tumors consistent in both datasets (**Figure 3.6** B, D). The pairwise correlation coefficient was calculated between CHRNA5 and DDR genes. I found that the correlation coefficient was negative with respect to the change in expression of the gene in response to siCHRNA5 in both datasets (**Figure 3.6** E-F).

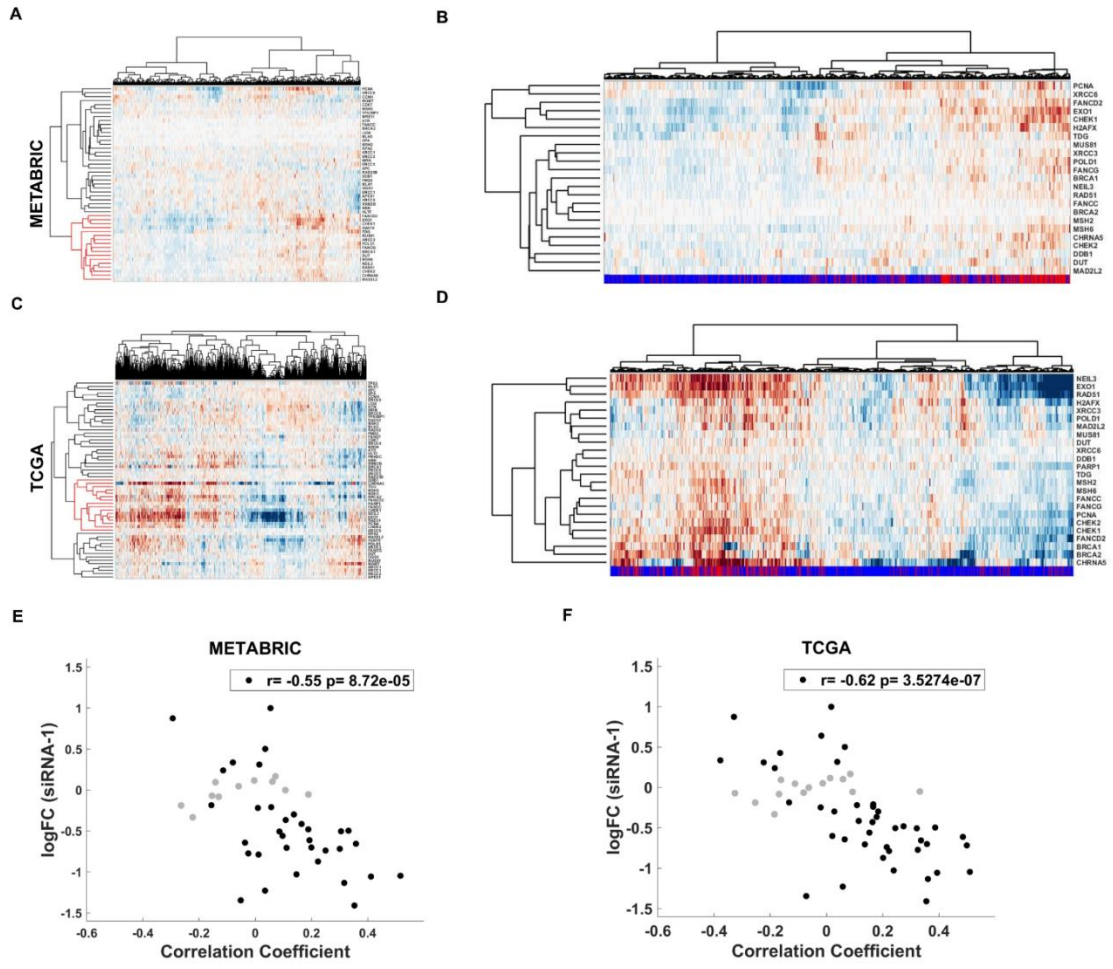

Figure 3.6 DNA damage response and CHRNA5 expression in METABRIC (A) and TCGA BRCA (C) datasets. Clusters with CHRNA5 were labeled with red (A, C) and reclustered. TP53

mutant tumors were annotated with red (B, D). The pairwise correlation coefficient between CHRNA5 and DDR genes and the change in their expression level in response to CHRNA5 (E, F). Pearson correlation coefficient and p-value were reported on plots.

(This image was reproducible without the need of copyright permission and required citation and it was obtained from Cingir Koker S, Jahja E, Shehwana H, Keskus AG, Konu O (2018) Cholinergic Receptor Nicotinic Alpha 5 (CHRNA5) RNAi is associated with cell cycle inhibition, apoptosis, DNA damage response and drug sensitivity in breast cancer. PLoS ONE 13(12): e0208982. https://doi.org/10.1371/journal.pone.0208982)

The expression level of CHEK1 mRNA, one of the key DDR modulators, was downregulated in response to siCHRNA5 treatment, and pCHEK1 level decreased even further (Sahika Cingir-Koker Ph.D. thesis, Bilkent University 2018). CHEK1, a member of the subgroup with CHRNA5 in both TCGA and METABRIC datasets (**Figure 4.6**), was found to be positively correlated in CCLE, TCGA, and METABIC (**Figure 3.7 A-C**). In accord with these findings. The CHRNA5 expression level was positively correlated with altered genome fraction in cell line and TCGA tumor data (**Figure 3.7D-E**). Altogether, these findings support the involvement of CHRNA5 in DDR.

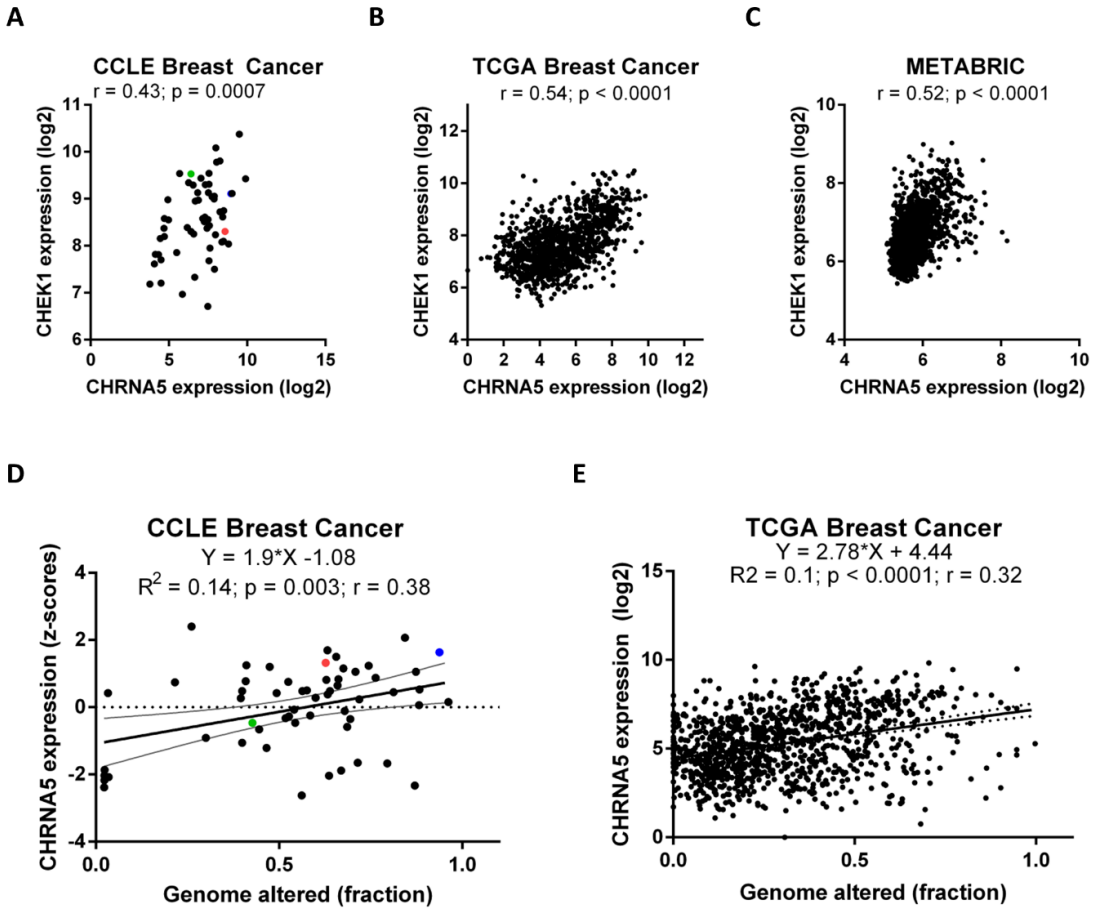

Figure 3.7 Correlation between CHEK1 and CHRNA5 expression in CCLE (A), TCGA (B), and METABRIC (C). Correlation between altered genome fraction and CHRNA5 expression in breast cancer cell lines in CCLE (D) and TCGA breast cancer dataset (E). Pearson correlation coefficient and p-value were reported on plots.

(This image was reproducible without the need of copyright permission and required citation and it was obtained from Cingir Koker S, Jahja E, Shehwana H, Keskus AG, Konu O (2018) Cholinergic Receptor Nicotinic Alpha 5 (CHRNA5) RNAi is associated with cell cycle inhibition, apoptosis, DNA damage response and drug sensitivity in breast cancer. PLoS ONE 13(12): e0208982. https://doi.org/10.1371/journal.pone.0208982)

3.2.3 CHRNA5 siRNA alters TP53 signaling.

KEGG pathway enrichment analysis revealed TP53 signaling as a primary upregulated pathway in response to CHRNA5 depletion in the MCF7 cell line. TP53 is one of the critical regulators of

the cell cycle and DDR. Our previous results showed that the siCHRNA5 transcription profile is not conserved between TP53 wild-type and mutant breast cancer cell lines for DDR and cell cycle related genes. I also found that CHRNA5 expression was higher in TP53 mutant tumors in comparison to those wild-type in both TCGA and METABRIC datasets along with other DDR genes (**Figure 3.6, Figure 3.8**).

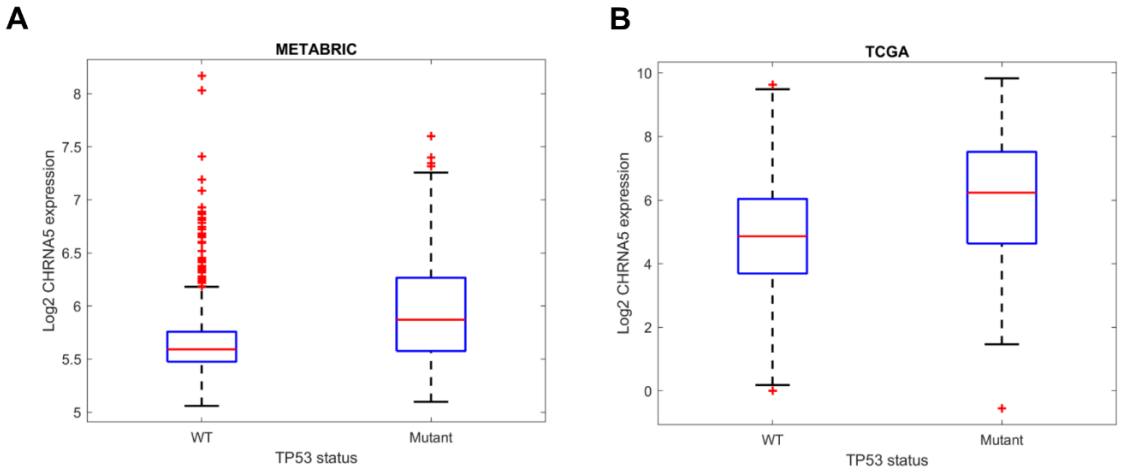

Figure 3.8 CHRNA5 expression in TP53 wild-type and mutant tumors in METABRIC (A) and TCGA (B).

(This image was reproducible without the need of copyright permission and required citation and it was obtained from Cingir Koker S, Jahja E, Shehwana H, Keskus AG, Konu O (2018) Cholinergic Receptor Nicotinic Alpha 5 (CHRNA5) RNAi is associated with cell cycle inhibition, apoptosis, DNA damage response and drug sensitivity in breast cancer. PLoS ONE 13(12): e0208982. https://doi.org/10.1371/journal.pone.0208982)

3.2.4 CHRNA5 siRNA and TP53 siRNA transcriptome profiled with RNAseq.

In-silico analysis and previous findings from our lab suggest that siCHRNA5 transcription profile and downstream effects may depend on the presence of functional TP53. Therefore, TP53 wild-type MCF7 cells were treated with different concentrations of siTP53 in order to find the optimal concentration through a decrease in the expression levels of TP53 and its selected targets using qPCR (**Figure 3.9**). For 72h treatment, the optimal duration for siCHRNA5 treatment, 10nM of siTP53 was identified as ideal due to a consistent decrease in TP53 and its selected targets.

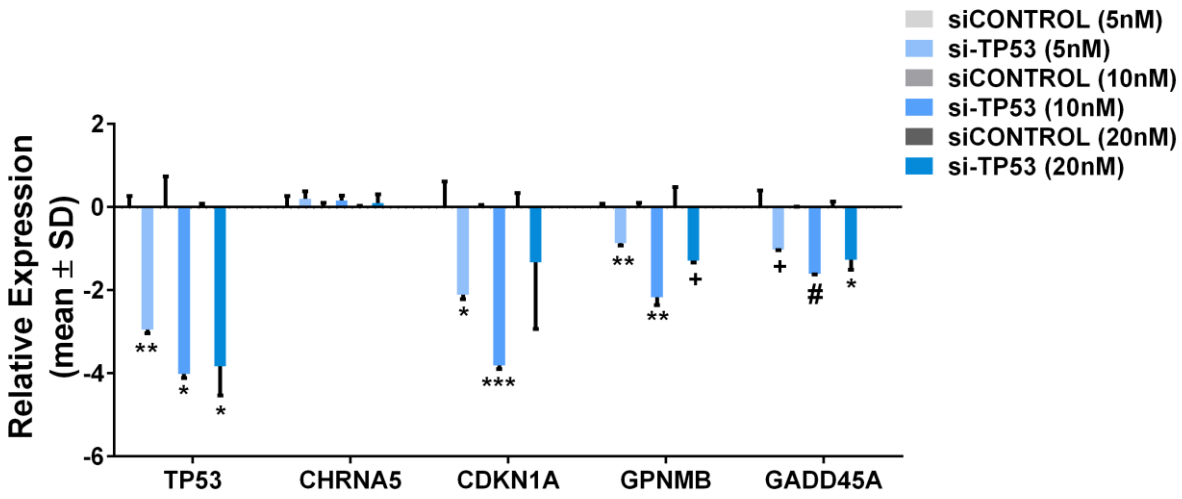

Figure 3.9 qPCR validation of the decrease in CHRNA5 and TP53 levels along with known TP53 targets in response to siCHRNA5 and siTP53. Mean ΔΔCT (±SD) was reported. One-way-ANOVA results were shown on plots.

Next, TP53 wild-type MCF7 cells were treated with siTP53 with or without siCHRNA5 for 72h. Their phenotype was investigated under DIC microscopy (**Figure 3.10**). In accord with the previous studies, siCHRNA5 phenotype was observed in siCHRNA5 alone treatment. In siTP53 treated cells, the confluency was >95%, whereas it was ~85% in siCONTROL, indicating an increased proliferation rate. The siCHRNA5 phenotype was partially inhibited in the combinatorial treatment, as opposed to the once in siTP53 or siCHRNA5 alone treatments (**Figure 3.10**).

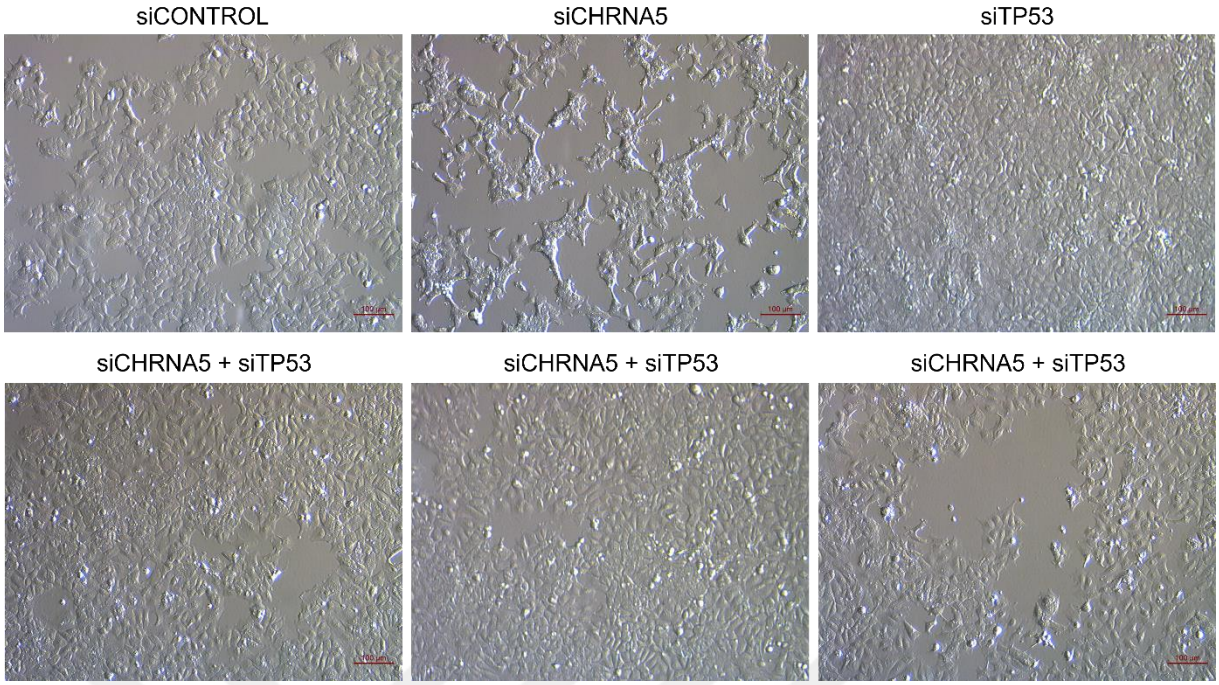

Figure 3.10 Microscopy images of siCONTROL, siCHRNA5(10nM), siTP53(10nM), and their combination after 72h of treatment.

After microscopic examination, the groups' transcriptomes were profiled through RNAseq. FastQC tool in Cancer Genomics Cloud (CGC) was used for quality control analysis. An example of quality control reports was shown in **Figure 3.11**.

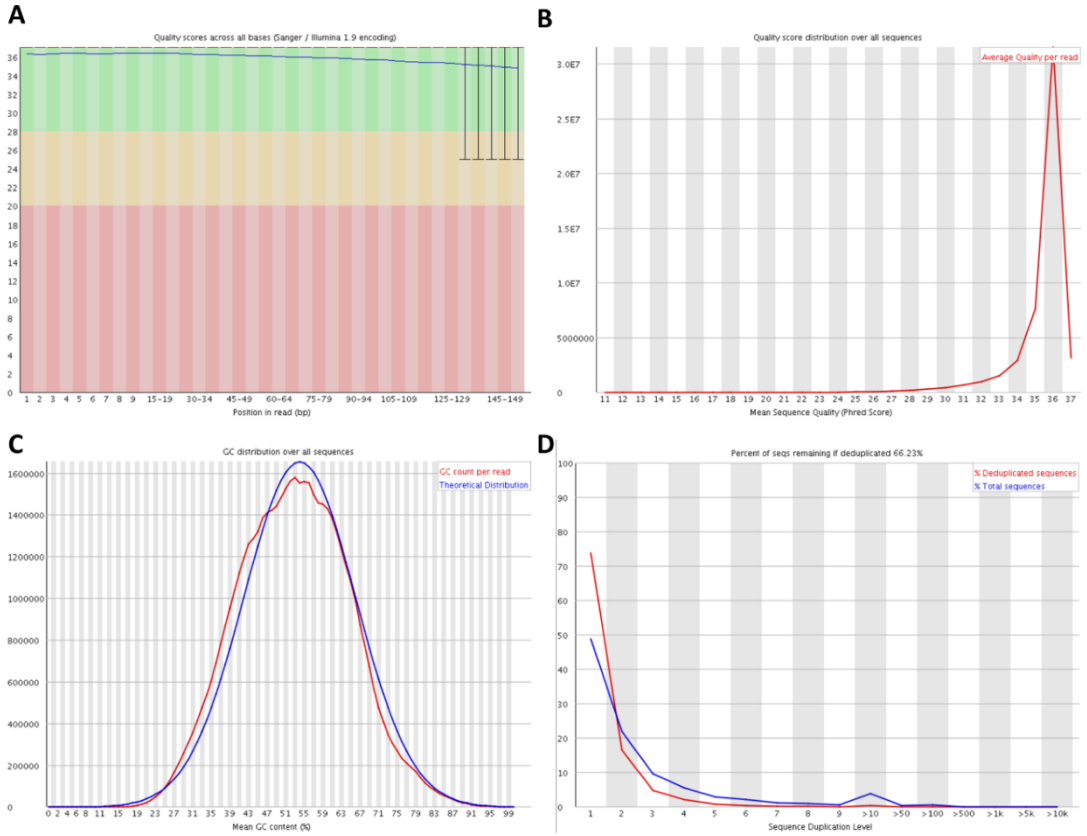

Figure 3.11 Example quality control results. Per base sequence quality (A), Per sequence quality score plot (B), Per sequence GC content (C), and Sequence Duplication Levels (D).

After confirming the quality of the data, reads were aligned with STAR alignment, and counts for each gene were obtained through HTseq count. After voom transformation using limma package, Principal Component Analysis (PCA) and Multiple Dimensional Scaling (MDS) were employed to visualize the results (**Figure 3.12**). In both analyses, although siCHRNA5 samples exhibited more divergence, the treatment groups were clustered together. Combinatorial treatment groups were clustered closer to siTP53 than siCHRNA5, implying a relatively dominant or rescue effect of siTP53 on siCHRNA5. PC1 in PCA analysis was able to distinguish treatments with and without TP53, whereas treatments with siCHRNA5 were separated along PC2.

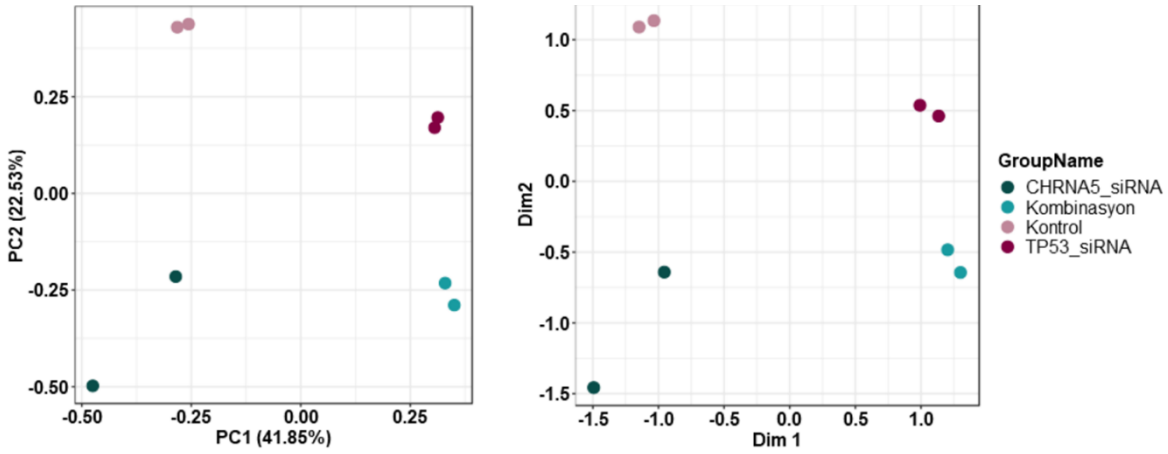

Figure 3.12 PCA (A) and MDS (B) results of RNAseq results. Percentages in the parentheses indicate the percent variation explained by the given component.

In accord with the PCA and MDS analyses, the combinatorial treatment exhibited a higher positive correlation with siTP53 when compared to siCHRNA5. Interestingly, siCHRNA5 and siTP53 were also positively correlated with each other, although it is not as high as the one with combinatorial treatment (**Figure 3.13A**). The regression analysis of siTP53 and siCHRNA5 alone treatments showed that although there was a positive relationship between the two siRNAs, the coefficients were low yet significant (**Figure 3.13**B; a = 0.309, p<2e-16). Although both correlation and regression analysis suggest the positive association between the two siRNAs, a cluster of genes was altered only in siTP53.

The distribution of genes significant in any of the three treatments was investigated to evaluate the combinatorial action of two siRNAs further. Interestingly, most genes were not altered in siTP53 or siCHRNA5, but the combinatorial treatment of them implied a synergistic effect between these two siRNAs (**Figure 3.13C).** Regression analysis between individual siRNA treatments and combinatorial treatment showed that siTP53 exhibits a coefficient higher than 1 while the coefficient in siCHRNA5 is 0.694, implied siTP53 alleviates the effect of siCHRNA5 to a certain degree (**Figure 3.13D-E**).

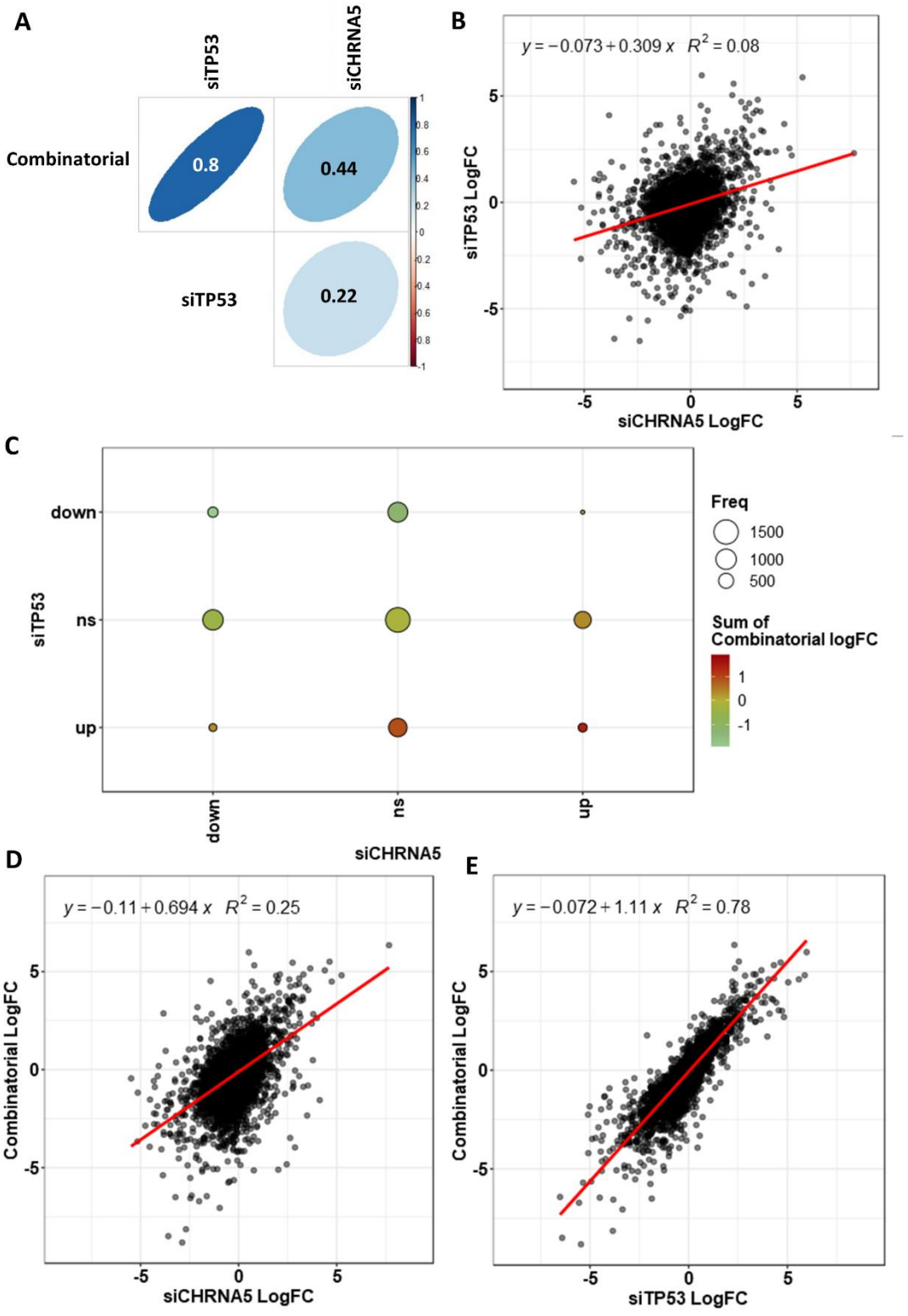

Figure 3.13 RNAseq results of siCHRNA5, siTP53, and their combinational treatments. Pairwise correlation between groups (A). Regression analysis between siCHRNA5 and siTP53 treatments (B). Distribution of genes altered in at least of the groups (C). Regression analysis between

combination treatment and siCHRNA5 (D) and siTP53(E). Regression line formulas and corresponding R-squared results were reported on plots.

3.2.5 CHRNA5 siRNA profile is positively correlated with TP53 inducer profiles.

Several TP53 inducers have been reported in the literature, i.e., nutlin3a (nutlin), doxorubicin (doxo), 5-Fluorouracil(FU5), and Rita (**Table 2-13**). Apart from direct inducers, several indirect factors have been proposed, including estrogen (E2), NFkB signaling, STAT3, and MDM2 inducers. Comparative transcriptome analysis I performed with TP53 inducers revealed that siCHRNA5 exhibited a positive correlation while siTP53 and combinatorial treatment displayed a negative or no correlation (**Figure 3.14**). E2 profile clustered together with siTP53 and combinatorial treatments and showed a negative correlation with TP53 inducers. TNF, an NFkB inducer, was positively correlated with E2 and showed no correlation with TP53 inducers.

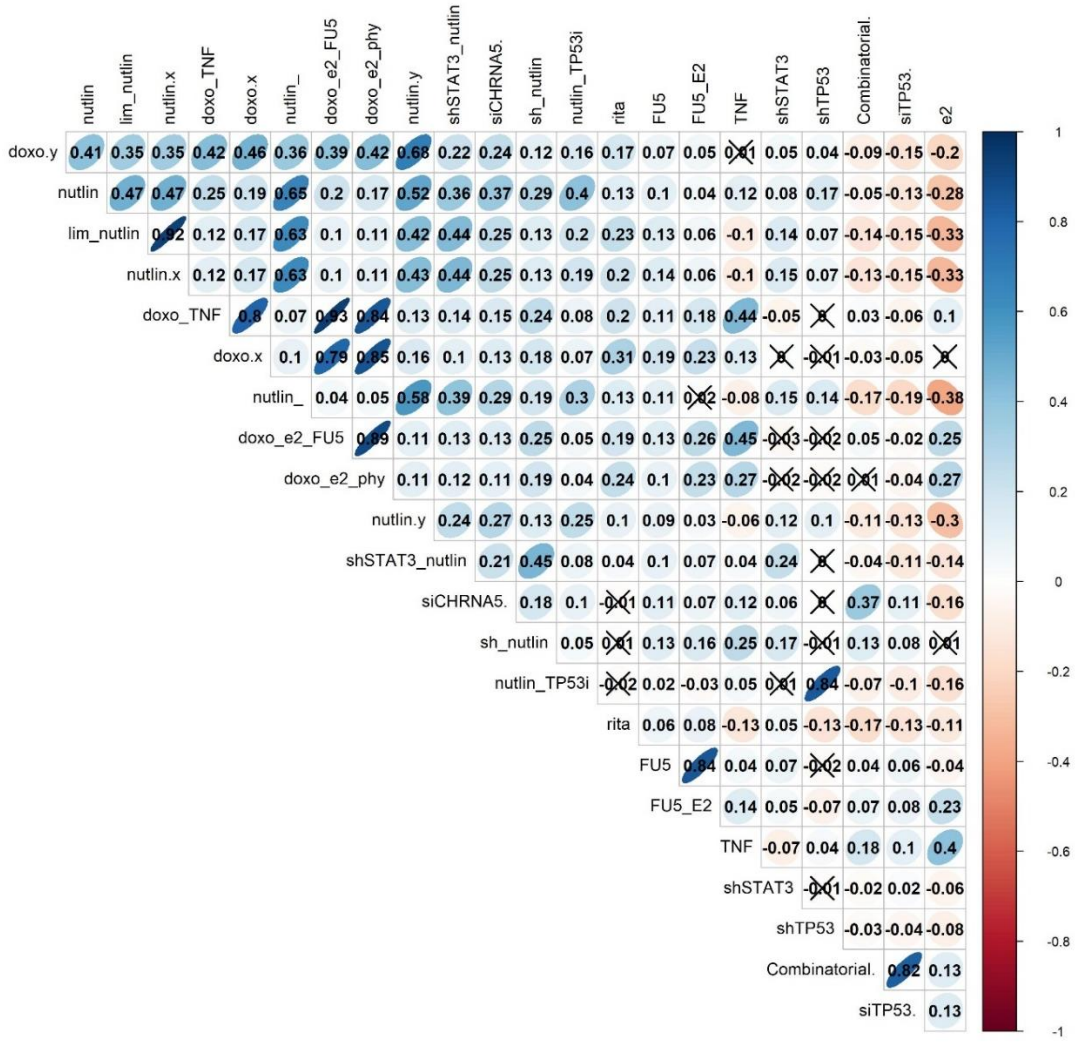

Figure 3.14 Pairwise Spearman's correlation analysis with TP53 inducers and others. Dots were colored according to the correlation coefficient, and insignificant results were shown with a cross.

Fischer et al. (2017) identified TP53 targets through a comprehensive literature search. They provided an evidence score for the TP53 targets ranging from one to 17 based on the number of studies reporting the interaction, which was used for filtering out those supported with less than five studies. As expected, TP53 inducers doxorubicin and nutlin3a increased the expression of TP53 targets shown as the rows of the hierarchical cluster (**Figure 3.15).** E2 and TNF reversed the doxorubicin mediated TP53 induction for a cluster of TP53 targets. 5-Fluorouracil and Rita appeared to be less effective in incuding TP53 when compared to doxorubicin and nutlin3a.

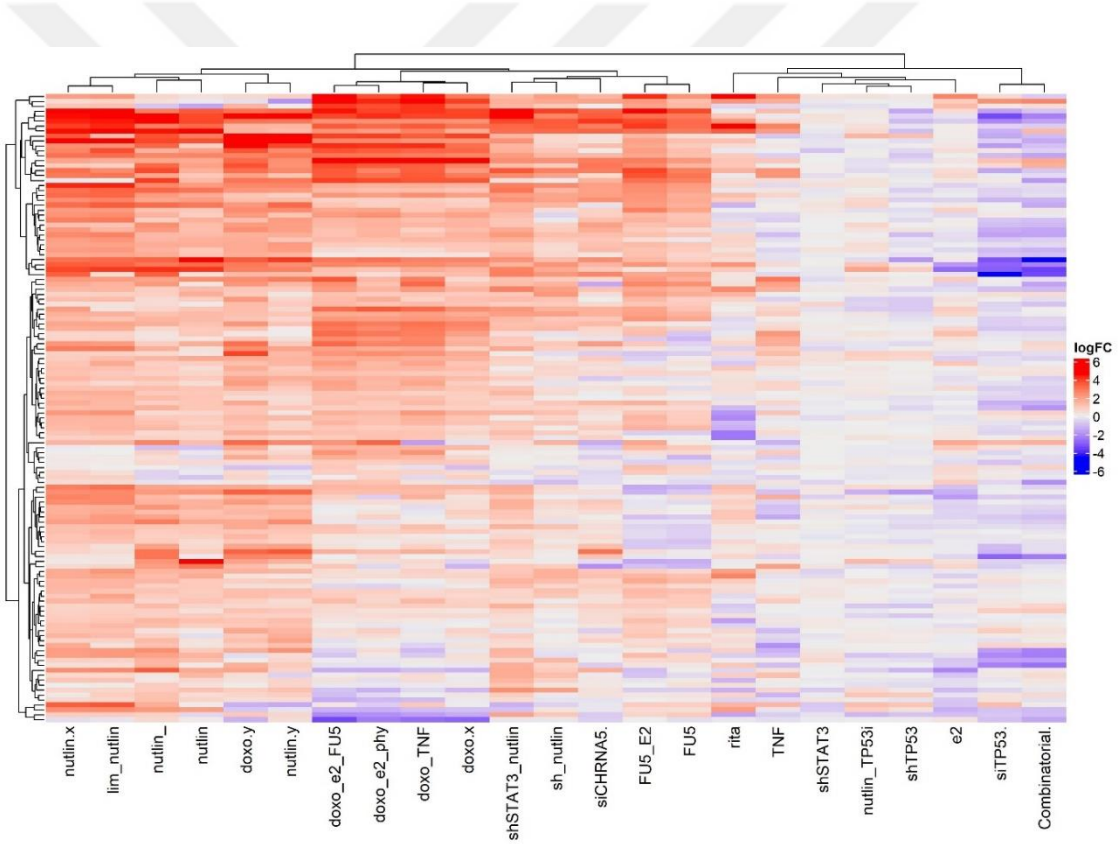

Figure 3.15 The change in the expression levels of TP53 targets in response to TP53 inducers, doxorubicin (doxo), nutlin3a (nutlin), Rita, 5-Fluorouracil (FU5), indirect influencers, shSTAT3, estradiol (E2), TNF, siCHRNA5, siTP53, and their combination. Evidence scores higher than five were used as a threshold for the TP53 targets.

The change of expression in TP53 targets was validated using qPCR. CDKN1A (p21), GADD45A, and RRM2 expressions increased with siCHRNA5 and TP53 but not changed in the combinatorial treatment suggesting TP53 was needed (**Figure 3.16**). Interestingly, TP53INP1, CCNG1, and ZMAT3 were downregulated by siTP53 alone and in combination with siCHRNA5. In silico analysis indicated a negative correlation between E2 treatment and TP53 induction. Therefore, the change in selected E2 targets, i.e., LAMC1, DTL, FOXC1, and SCNN1A, was examined. The siCHRNA5 effect in the LAMC1, a vital cell junction gene, was preserved in combinatorial treatment. CLDN1, another cell junction gene, was even further upregulated in combinatorial treatment. DTL, an estrogen target and negative regulator of CDKN1A, was downregulated with siCHRNA5 and not changed in combinatorial treatment indicated the induction dependent on TP53. Another gene involved in crosstalk between estrogen and TP53 signaling, FOXC1, followed a similar pattern with CDKN1A.

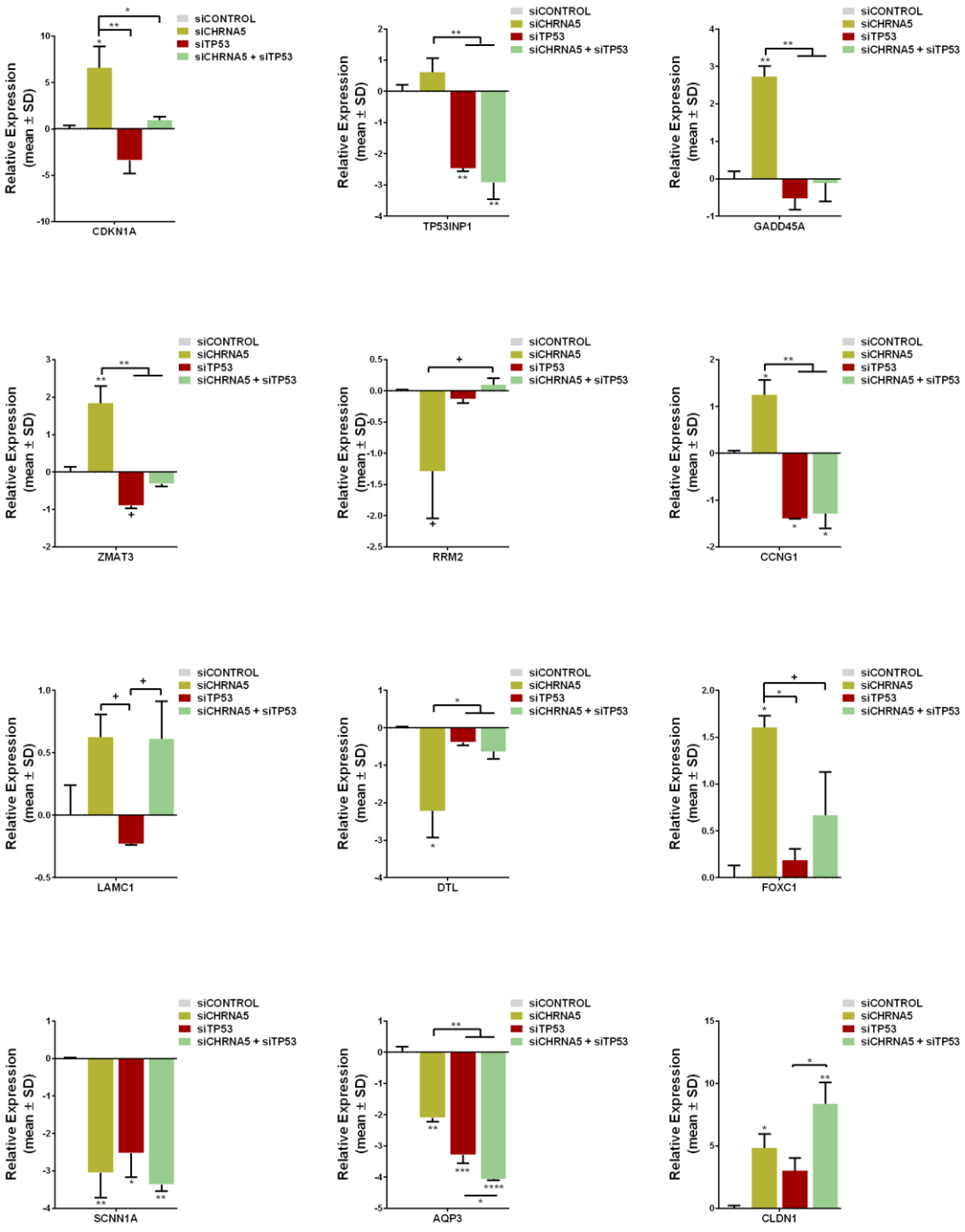

Figure 3.16 qPCR validation of expression changes (in logarithmically transform fold changes, log2FC) in TP53 targets (upper panel), E2 targets, AQP3, and CLDN1. Mean ΔΔCT (±SD) was reported. One-way-ANOVA results were shown on plots.

3.2.6 TP53 siRNA reverts the drug sensitivity to doxorubicin induced by siCHRNA5.

siCHRNA5 had been shown to induce sensitivity to DNA damage-inducing agents, doxorubicin and camptothecin (Cingir Koker, et al., 2018). Therefore, I further treated MCF7 cells with doxorubicin with siCHRNA5 and/or siTP53 for 72h. The cell viability was measured with an MTT assay. Although there was variation in the results in the DMSO treated group, as expected, there was an increasing trend in siTP53, whereas decreasing one in siCHRNA5 and in the combinatorial treatment rescue effect was observed. In doxorubicin-treated groups, the rescue effect was observed in low dosages, i.e., 0.06 uM and 0.125uM.

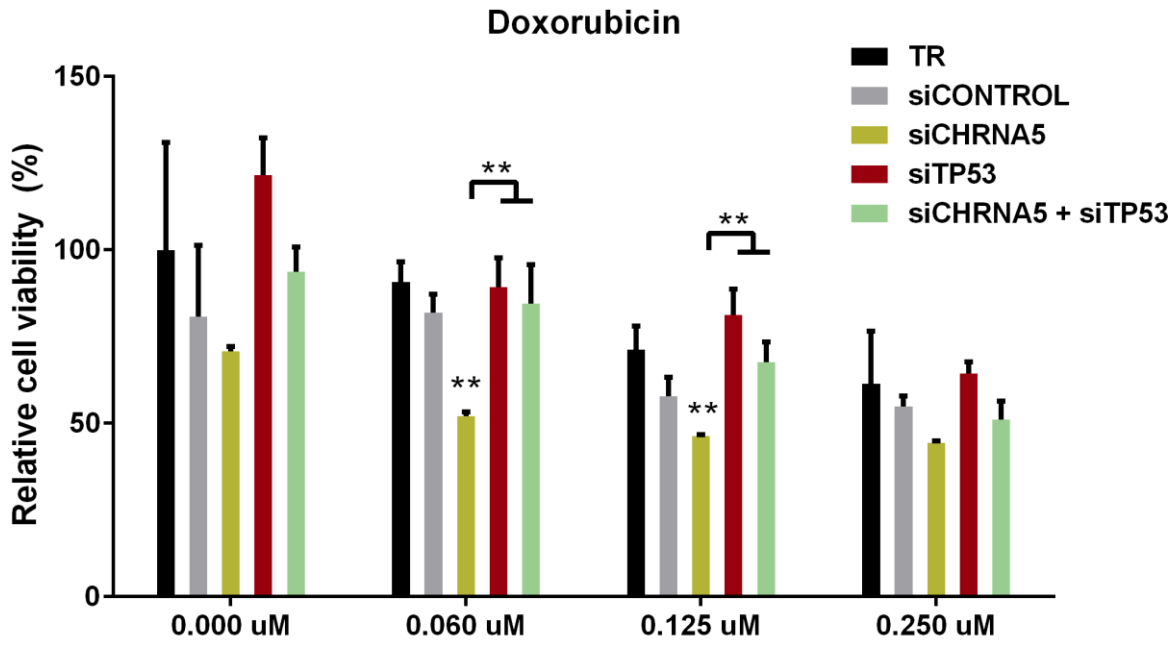

Figure 3.17 MTT cell viability assay results with increasing dosage (uM) of doxorubicin for 72h. TR: Transfection reagent. Mean relative cell viability (±SD) was reported. One-way-ANOVA results were shown on plots.

3.2.7 CHRNA5 siRNA and TP53 siRNA exhibit synergic and antagonistic effects.

3.2.7.1 The regression-based synergy analysis: *synreg*

To address the synergistic and antagonistic behavior of siTP53 and siCHRNA5, I first applied the regression-based synergy method called *synreg* we developed in our lab to evaluate the overall

interplay between two treatments. In this method, the additive logFC value was calculated as described in Chapter 2.3, corresponding to the expected results if the effect between siRNAs were additive. A regression line was fitted between the calculated additive logFC and the combinatorial logFC for the genes significantly altered in at least one group (**Figure 3.18A**). Slope less than one (0.72) shows the overall antagonistic effect between two siRNAs. Next, an x=y line was plotted with a +/-0.3 interval corresponding to the additivity region on the additive logFC vs. combinatorial logFC plot (**Figure 3.18A-B).** The interaction between two siRNAs was additive for the genes in that region. The blue line (y = 0) separated up and downregulated genes in combinatorial treatment, which helped distinguish synergistically (labeled with green) and antagonistically (labeled with red) affected genes. The regression-based analysis method showed that overall action between two siRNAs, i.e., siTP53 and siCHRNA5 was inhibitory, yet with a coefficient, additive logFC could predict combinatorial logFC, significantly.

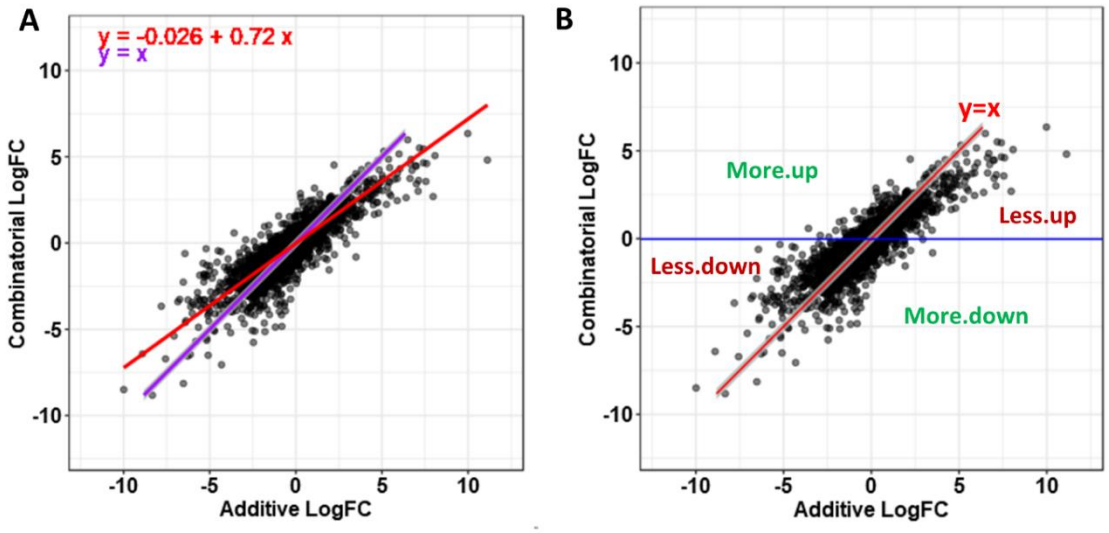

Figure 3.18 *synreg*, a regression-based synergy analysis results of siTP53 and siCHRNA5 and their combination. The regression line between additive and combinatorial logFC values for the genes significantly altered in at least one group was plotted with red and a y=x line representing additivity with purple. The formulas for the lines were reported on plots (A). A y=x line was plotted with red, and the synergy groups were labeled with green for synergistic and red for antagonistic genes (B).

3.2.7.2 Limma-based synergy analysis

A recently published limma-based synergy analysis method was employed next. Additive logFC calculated as in the abovementioned regression-based model. Then synergy groups were identified with the threshold calculated using the mean standard error in treatment groups (**Figure 3.19A**). more.up and more.down groups corresponded to the synergistic groups, whereas less.down and less.up groups were antagonistic. Genes altered at least in one of the three treatment groups were investigated given the threshold; most of the genes were additive (n = 2607), and 1868 of them were antagonistic (Less up; n= 703, less down; n= 1165), while only 1076 (More up; n= 446, more down; n= 630) genes were synergistic (**Figure 3.19B**).

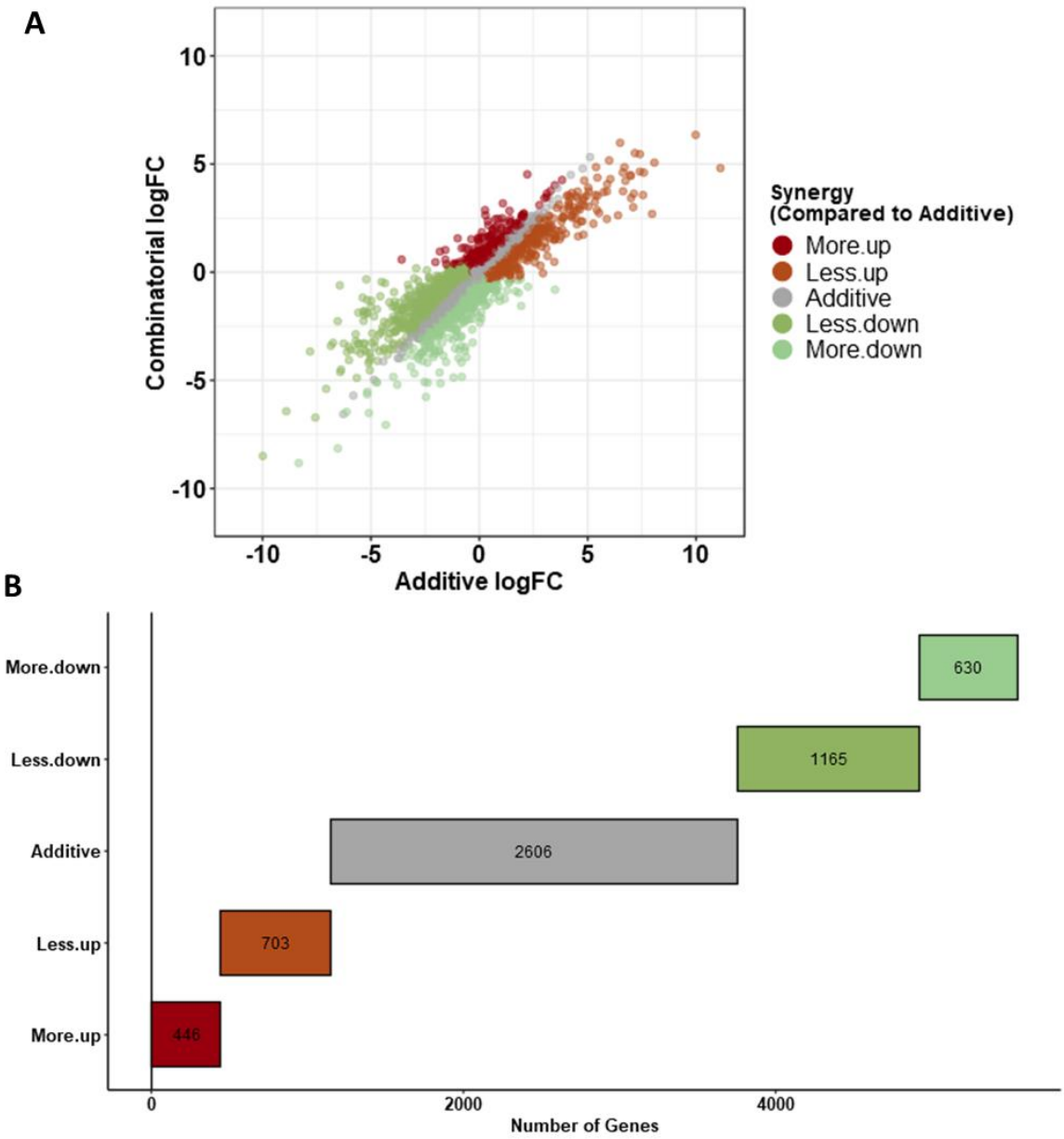

Figure 3.19 Limma-based synergy analysis results. Scatter plot of calculated additive logFC and combinatorial logFC for genes altered at least in one group (A). Waterfall plot of the genes in A (B). Boxes are proportional to the gene number, indicated inside the boxes.

Hierarchical clustering with a heatmap representation was used to understand the gene expression pattern better (**Figure 3.20**). Accordingly, in the more.up (synergistic) cluster, most genes were downregulated by siCHRNA5 and upregulated by siTP53.

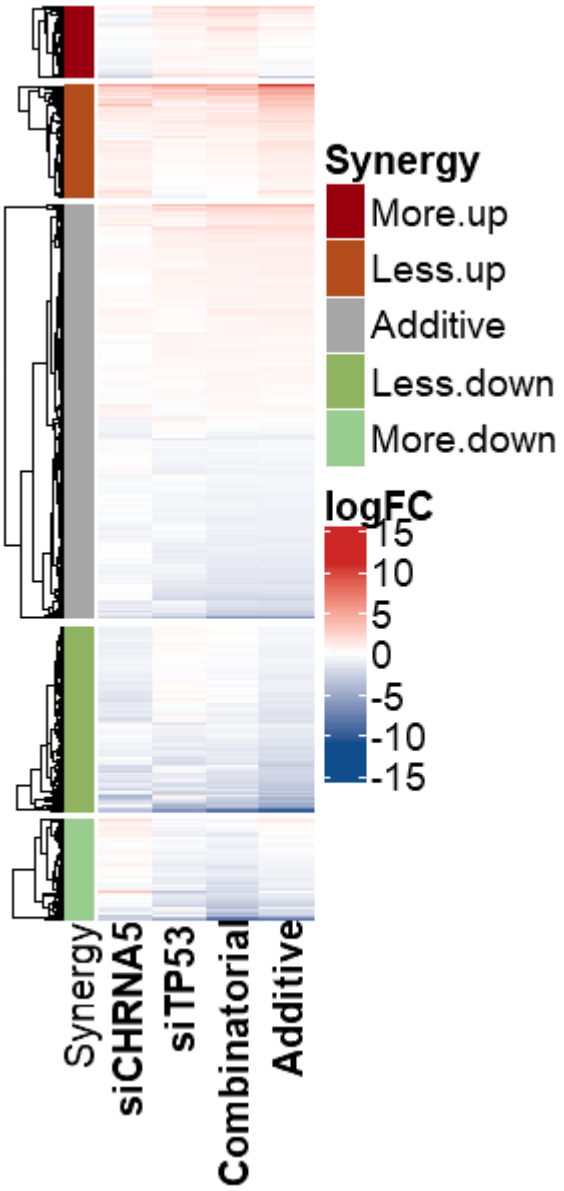

Figure 3.20 Hierarchical clustering and heatmap representation of the synergy clusters for genes altered in at least one group. Gene clusters are marked with different colors in the cluster row legend while logarithmically transformed expression fold changes (logFC) indicate an increase with red and a decrease with blue colors.

3.2.8 Pathway enrichment analysis of synergy groups

KEGG enrichment analysis was performed for each synergy group using clusterprofiler in R; and the results were detailed below.

3.2.8.1 DNA damage repair gene expression was downregulated less in the combinatorial treatment.

The genes in the less.down synergy group were downregulated with siCHRNA5 and the combinatorial treatment mostly (**Figure 3.20**). However, there was a cluster of genes that were upregulated with siTP53. Those genes were downregulated less than the expected outcome suggesting an inhibitory interaction between the individual siRNAs when combined. DNA replication and DNA repair-related pathways were found as enriched with the less.down genes (**Figure 3.21**). This finding further supported the hypothesis that functional TP53 was required for the siCHRNA5 profile, at least partially.

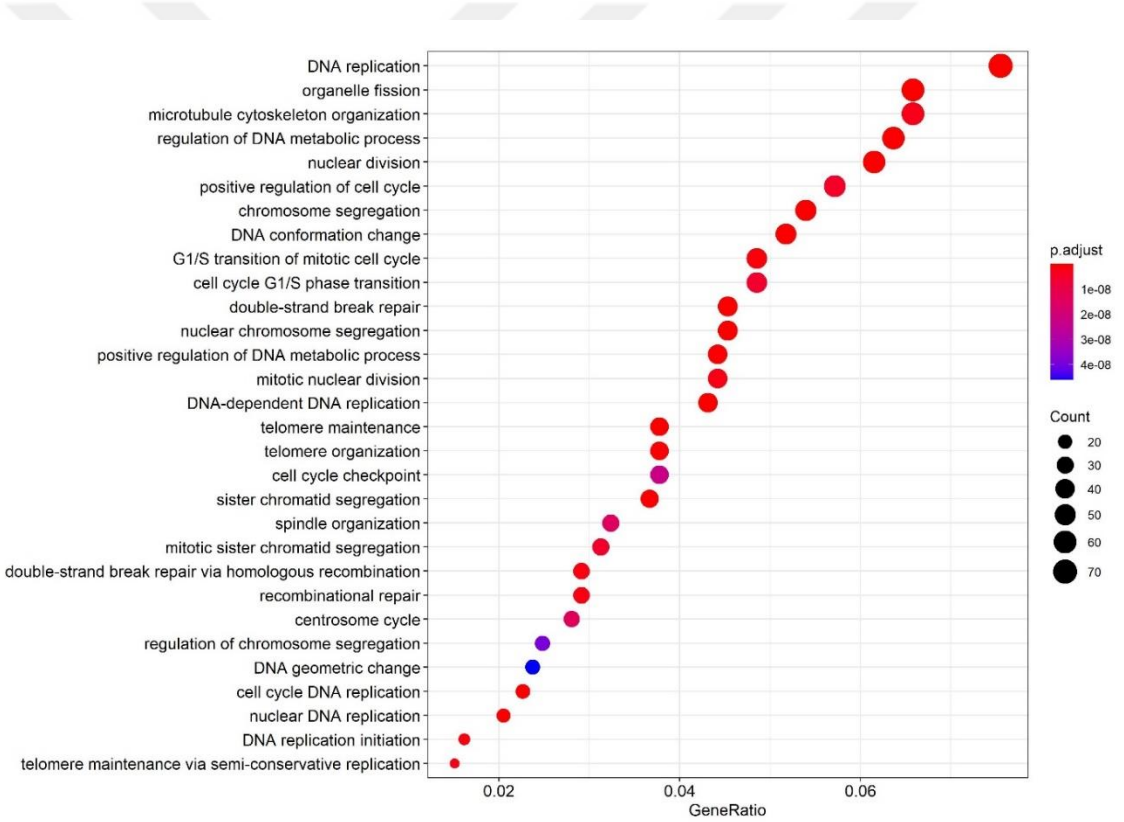

Figure 3.21 KEGG pathway enrichment analysis results for genes less downregulated in the combinatorial treatment when compared to the expected (additive).

Next, transcription factors enriched for these genes were analyzed using ChEA3 and DoRothEA (**Figure 3.22**). Integrated mean ranks for the top 10 enriched TFs were plotted. FOXM1, CENPA, a target of FOXM1, E2Fs, and TFDP1, E2F coactivator, were among the highest-ranked TFs. In

accord with that, E2F and MYC targets in DoRothEA were overrepresented among the less.down genes.

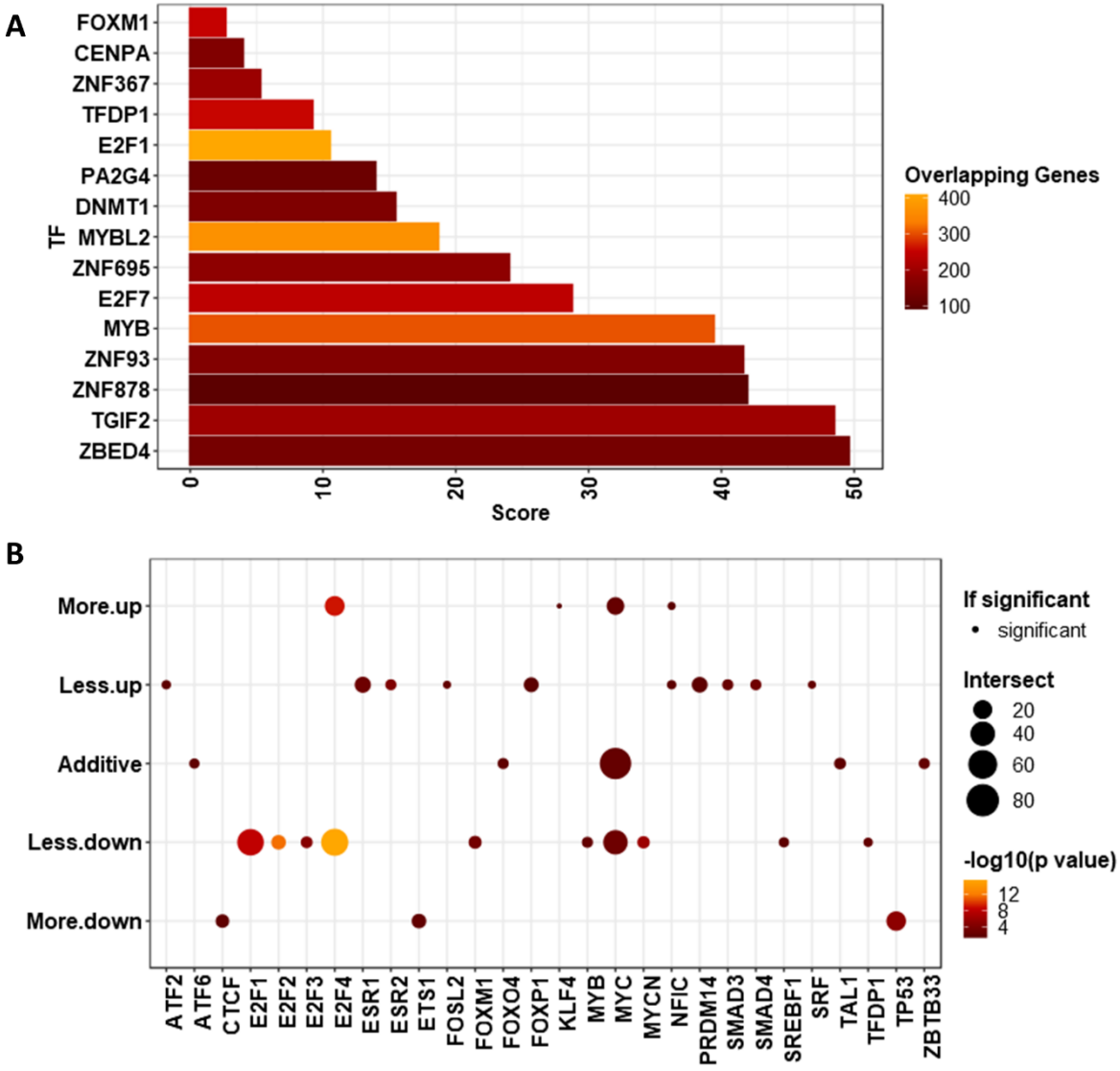

Figure 3.22 Transcription factor overrepresentation analysis of the less.down cluster using ChEA3 (A). The top 10 TFs ranked according to integrated mean rank were plotted. Transcription factor overrepresentation analysis of all synergy clusters using DoRothEA (B). The sizes of the balloons correlate with the number of targets found in given synergy cluster.

3.2.8.2 G2/M cell cycle control genes were upregulated more in the combinatorial treatment.

In the more.up synergy group, many genes were downregulated with siCHRNA5 yet upregulated in both siTP53 and combinatorial, suggesting an overwhelming effect of siTP53 over siCHRNA5 for those genes (**Figure 3.20**). Interestingly, chromosome segregation and cell division related-pathways were enriched, suggesting a possible alteration in G2/M transition (**Figure 3.23A**). In accord with that, TF overrepresentation analysis showed that similar TFs were enriched in the more.up and the less.down clusters (**Figure 3.23 B**).

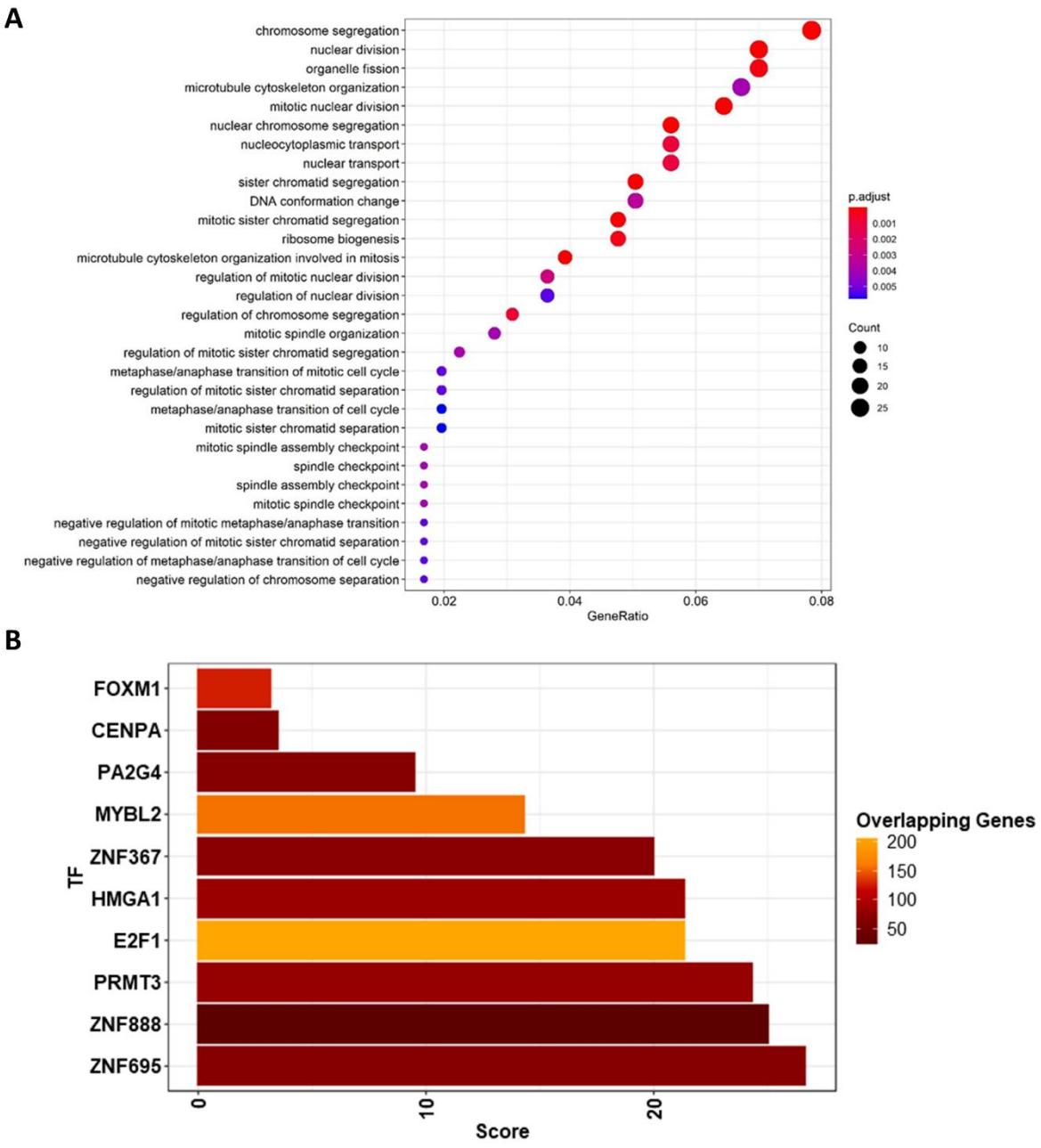

Figure 3.23 KEGG pathway enrichment analysis results for genes more upregulated in the combinatorial treatment when compared to expected (additive), where the circle size is correlated with number of genes found in the terms (A). Transcription factor overrepresentation analysis cluster using ChEA3, where the bars indicate the enrichment score (B).

Since FOXM1 and E2F1 appeared in both clusters, the expression levels of their targets were further analyzed (**Figure 3.24**). The regression analysis revealed that the overall behavior of E2F targets was antagonistic. E2F1 targets in the less.down cluster were downregulated with

siCHRNA5 and not altered with siTP53, while E2F1 targets in the more.up cluster were upregulated with siTP53, potentially indicating the involvement of other coregulators', i.e., TFDB1, which was also overrepresented only in the less.down group. As E2F1, FOXM1 targets were mostly downregulated with siCHRNA5, yet a subset of them was reversed in the combinatorial treatment.

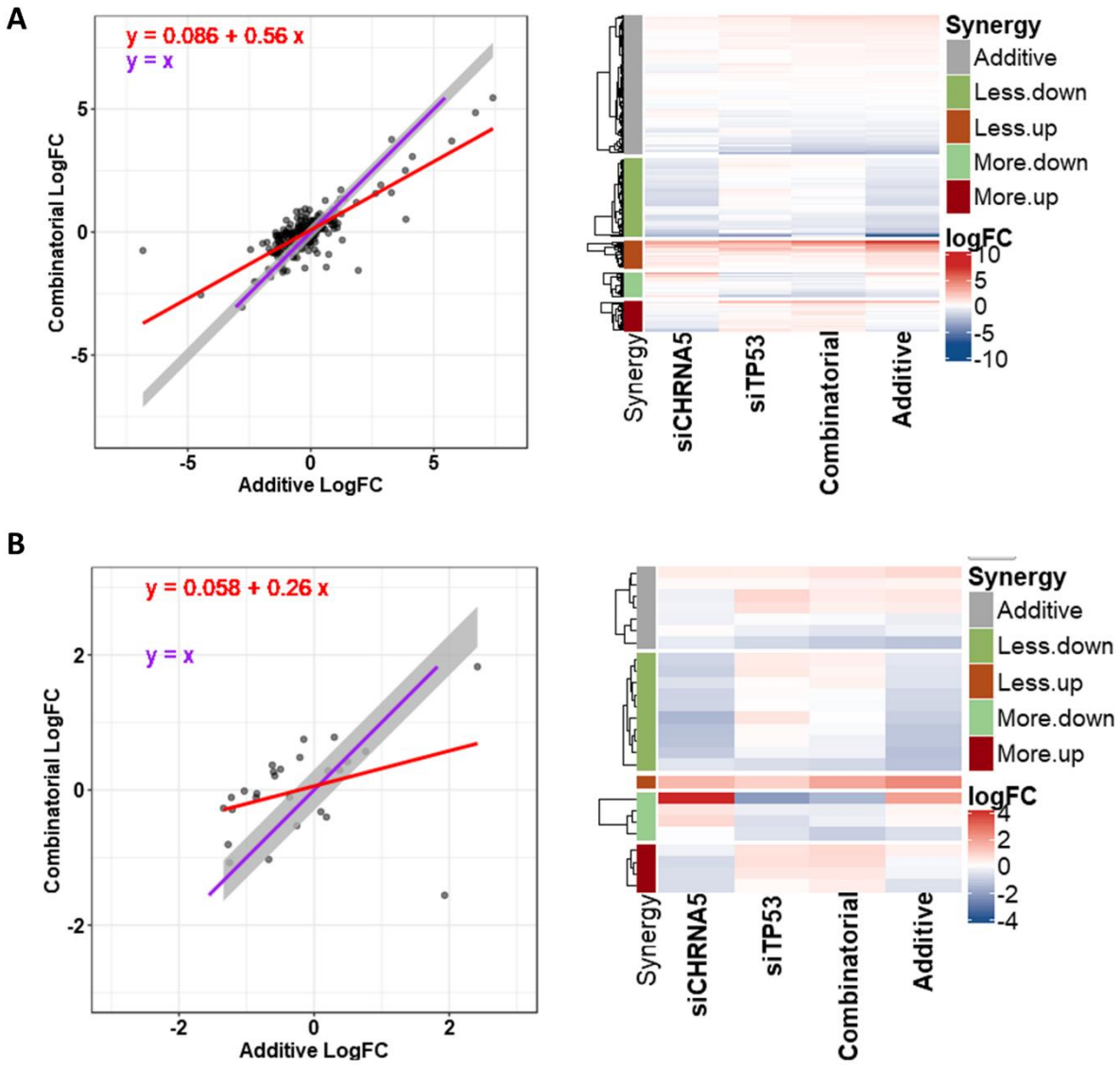

Figure 3.24 Regression analysis between additive logFC and combinatorial logFC and the heatmap representation of hierarchical clustering of the targets of E2F1 (A) and FOXM1 (B).

3.2.9 Transcription factor enrichment analysis

Transcription factor enrichment analysis using DoRothEA and the viper algorithm revealed that the top five TFs enriched in the combinatorial treatment were altered in the same direction yet to a lesser extent compared to additive. ESR1 and its important coregulator JUN were positively enriched in all three groups (**Figure 3.25A**). As overrepresentation analysis for synergy groups suggested, E2F targets were negatively enriched in siCHRNA5 while positively in siTP53 and combinatorial treatments (**Figure 3.25B, C**).

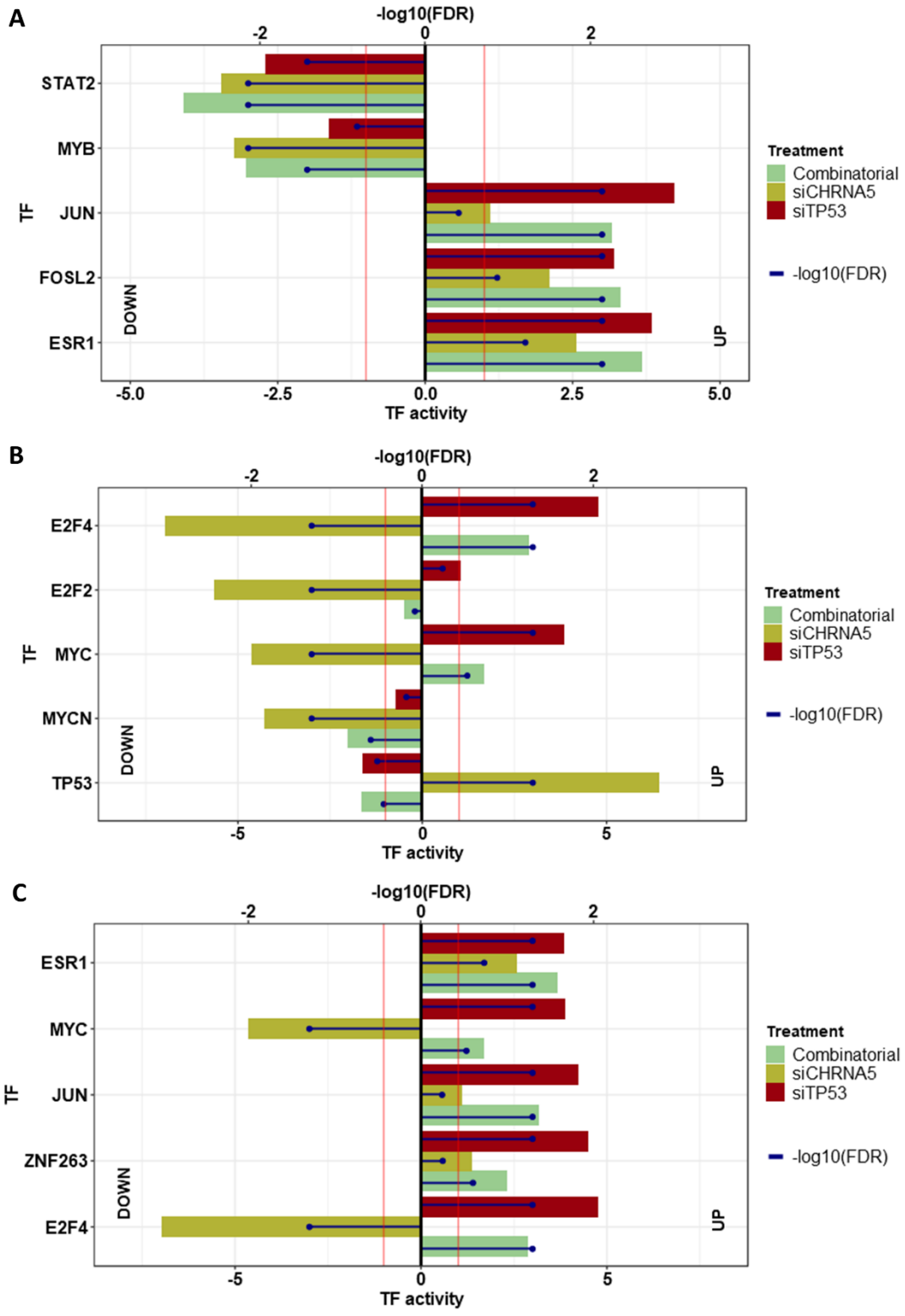

Figure 3.25 Transcription factor enrichment analysis was performed using the DoRothEA data and the viper algorithm. The top five transcription factors were plotted for treatments indicated by different colors, i.e., combinatorial (green) (A), siCHRNA5 (yellow) (B), and siTP53 (red) (C). The significance threshold (0.05) was represented with a red vertical line on plots, where

horizontal blue lines show the treatments p-value corresponding to the TF activity shown by a bar.

3.2.10 siTP53 antagonizes with siCHRNA5 in response to DNA damage-inducing drugs.

Since targets of FOXM1 and E2Fs were altered differentially with siCHRNA5 and siTP53, the expression levels of their regulators, PLK1 and pRB, respectively, were investigated at the protein level (**Figure 3.26**). pRB decreased with siCHRNA5 and exhibited a decreasing pattern with siTP53 as well as in the combinatorial treatment. Also, essential cell cycle proteins CDK2 and CCND1 were downregulated in the combinatorial treatment. CDKN1A levels increased with siCHRNA5 and decreased with siTP53 in the combinatorial treatment. CHEK1 level decreased in siCHRNA5, and its expression was rescued to a certain degree in the combinatorial treatment. BAX/BCL2 ratio, an indicator of apoptosis, decreased in the combinatorial treatment when compared to the siCHRNA5 alone treatment.

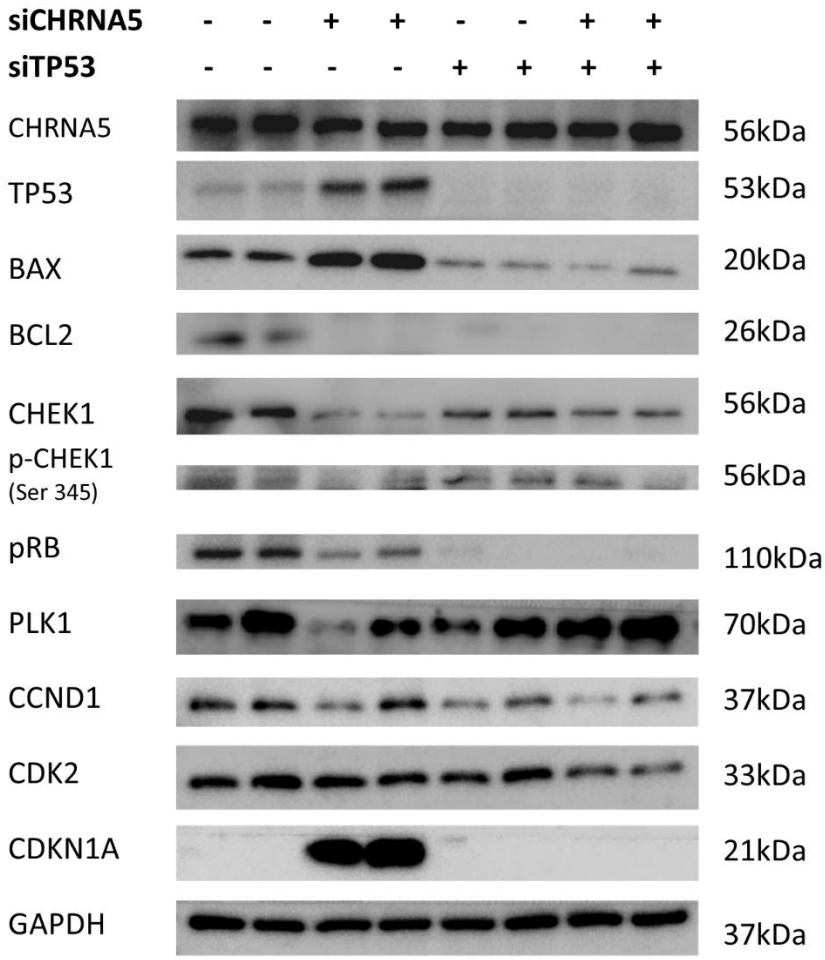

Figure 3.26 Western Blot analysis of selected cell cycle-related proteins in siCHRNA5 and/or siTP53 treatments.

3.3 Part 3. CHRNA5 and estrogen

3.3.1 Primary and secondary targets of estrogen in TCGA dataset.

3.3.1.1 Primary estrogen targets are strictly defined via analysis of three different datasets.

Publicly available two ChIP-seq (GSE117941 and GSE14664) datasets for ESR1 binding and a GRO-seq (GSE27463) dataset for newly transcribed mRNAs upon E2 treatment for 40 min were analyzed to obtain a consensus for the primary targets for ESR1. Genes significantly

altered/enriched in all three datasets were considered primary targets for the rest of the study (**Figure 3.27**; n =722).

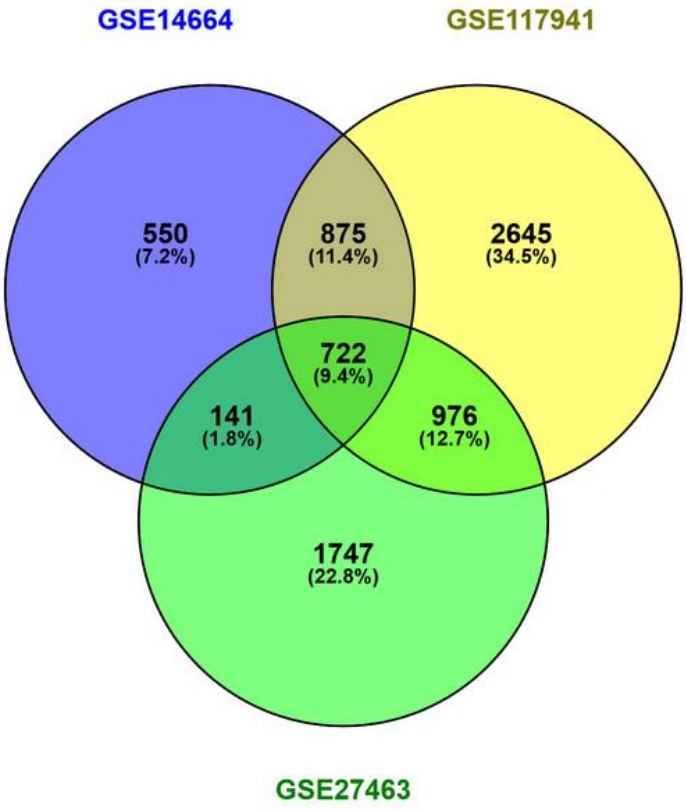

Figure 3.27 The Venn diagram representation of two Chip-seq and one GRO-seq datasets were analyzed to identify ESR1 primary targets. The numbers indicate the common and shared primary targets followed by percentage of them in the parentheses.

Secondary targets were identified with the methods developed in our lab previously, as described in Shehwana et al. (2021). The publicly available GSE8597 dataset consisted of microarray data for MCF7 cells treated with E2 with or without cycloheximide (CHX) used in this method. E2 and E2 + CHX treated samples were normalized with their control groups, EtOH vehicle and CHX treated samples, respectively. Since CHX inhibits protein translation, the difference between E2 only and E2 + CHX groups, called Predicted Secondary (PS) score, can unveil the secondary targets. Therefore limma analysis was performed between E2 and E2 + CHX treated samples after normalization with their respective control groups. Genes upregulated significantly

in E2 treatment only (adj. p-value <0.05 and logFC > 0.5) and with a PS score above the threshold (adj. p-value <0.05 and PS score > 0.5) were identified as secondary targets (n=446).

3.3.1.2 TCGA data analysis

PCA analysis of the expression levels of the primary and secondary targets of ESR1 in the TCGA breast cancer dataset revealed that the secondary targets were more tightly clustered when compared to the primary targets (**Figure 3.28**). A group of primary targets was clustered closer to secondary targets while the rest were dispersed through the PC1 and PC2 axis, implying differential expression of primary targets. Primary targets were more variable than the secondary and could be distinguished across both PC1 and PC2 into groups.

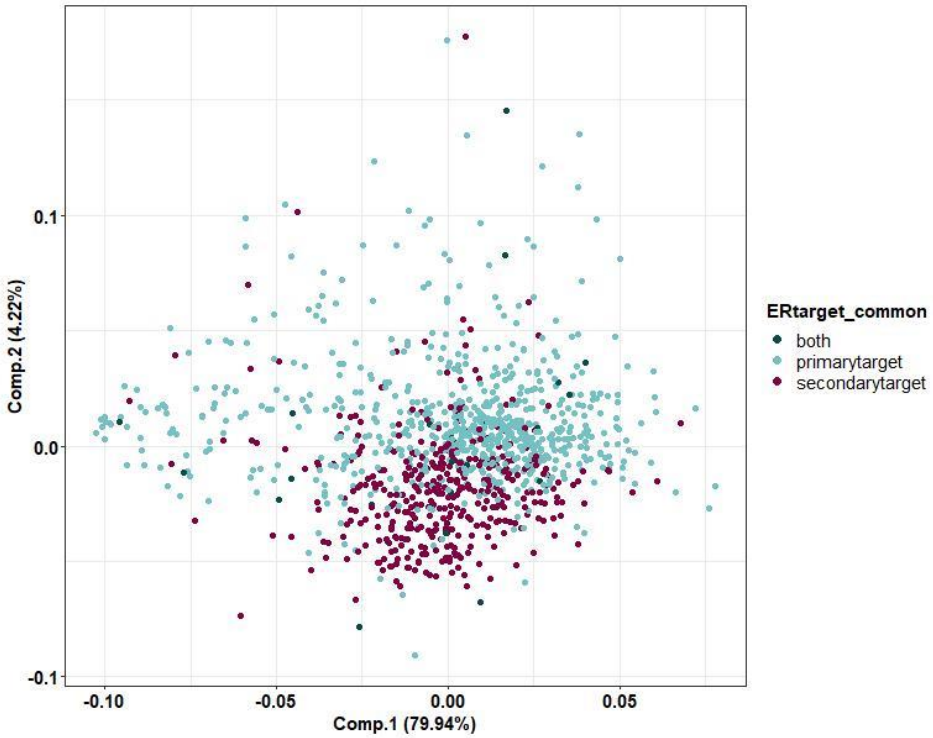

Figure 3.28 PCA analysis of expression levels of primary and secondary targets of E2 in TCGA breast cancer dataset.

Moreover, pairwise Spearman's correlation coefficient between each primary and secondary target was calculated. Hierarchical clustering and the heatmap representation of the coefficients further supported that secondary targets formed a tight cluster while primary targets were more

dispersed (**Figure 3.29**). Interestingly, secondary targets exhibited a negative correlation for the majority of the primary targets.

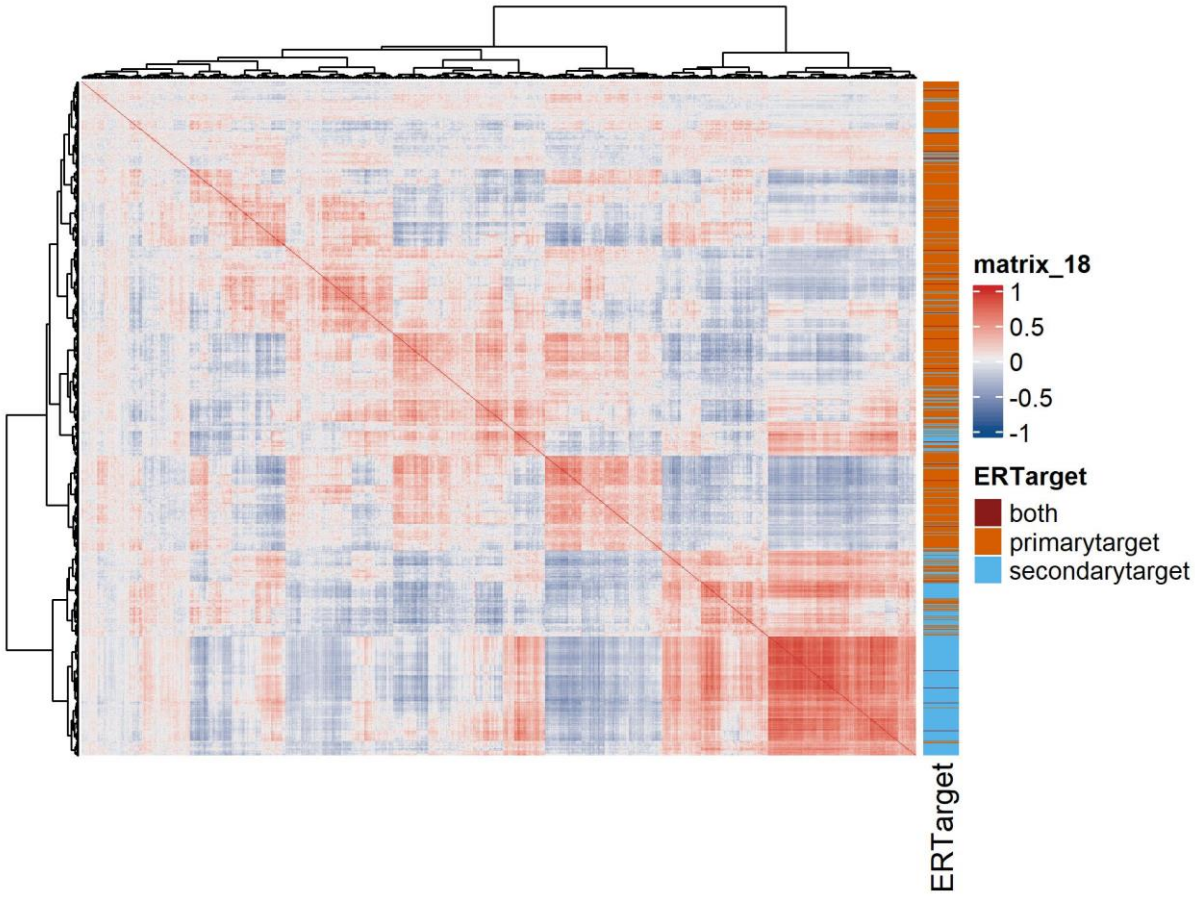

Figure 3.29 Hierarchical clustering analysis of the pairwise correlation between primary and secondary targets of estrogen. Correlation matrix is represented by red and blue, for positive and negative correlation values.

To further understand the expression dynamics of E2 targets in different breast cancer subtypes, the scaled expression levels of them were visualized through a heatmap **(Figure 3.30**). In accord with the PCA and coexpression analyses, the majority of the secondary targets were clustered together. The second cluster was mainly primary targets, while the third cluster consisted of both primary and secondary targets. ER-negative/basal patients formed a set where secondary target expression was higher, where expression levels of the primary target were relatively low. Interestingly, the ER-positive luminal B subtype exhibited a similar expression pattern with the ER-negative/basal subtype and the HER2 subtype in the context of E2 target expression. Normal

and Normal-like patients were clustered together with a cluster of Luminal A exhibiting lower expression of cluster 1 and higher that of cluster 2. Subtypes and ESR1 status failed to explain the other patient clustering, implying that other modulators may be involved in E2 target expression.

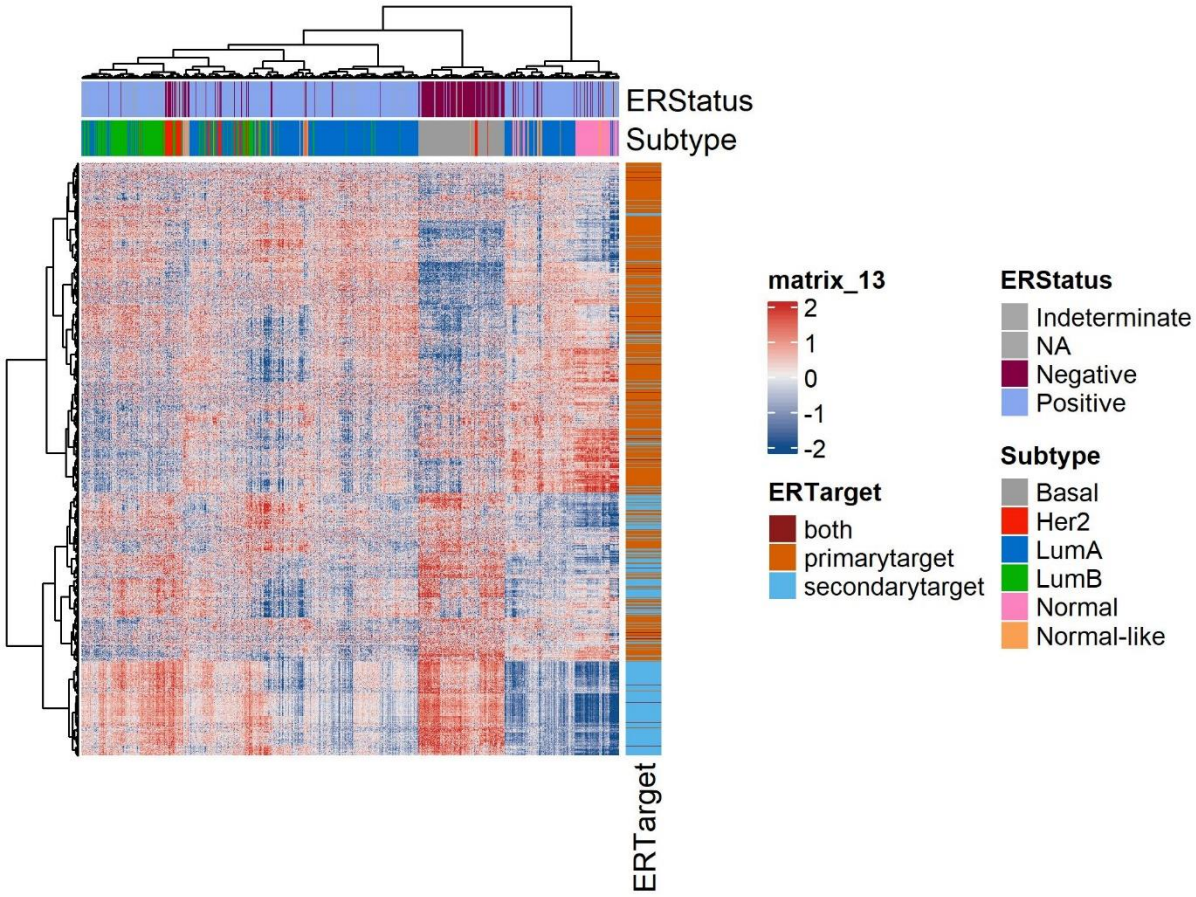

Figure 3.30 Heatmap of scaled expression values of ESR1 primary (orange) and secondary (blue) targets across TGCA breast cancer dataset labeled with ESR1 status, tissue, and subtypes. Correlation matrix is represented by red and blue, for positive and negative correlation values.

3.4 siCHRNA5 modulates estrogen targets.

3.4.1 siCHRNA5 exhibits a negative correlation with E2 treatment.

I next analyzed the alteration in expression levels of primary and secondary targets of E2 in the siCHRNA5 profile (**Figure 3.31**). Primary targets with a negative PS score were upregulated in the siCHRNA5 treatment while the ones with positive PS scores were more likely to be

downregulated. E2 signaling was modulated with feedback inhibition through secondary signaling. Primary targets with negative PS scores were those subjected to negative inhibition, while the ones with positive PS scores further activated through secondary signaling. siCHRNA5 treatment also downregulated the secondary targets. siCHRNA5 exhibited a similar expression pattern with the starvation dataset and an opposite one with theE2 treatment (**Figure 3.31**).

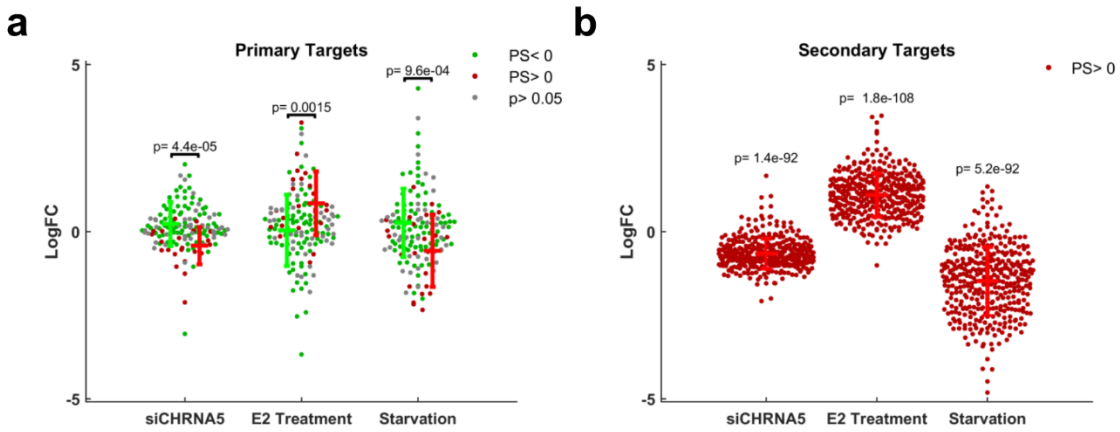

Figure 3.31 Change in the expression levels of primary and secondary targets in the siCHRNA5, E2 treatment, and the starvation profile.

(This image was reproduced with the licence ID: 5161460968853 from Shehwana, H., Keskus, A.G., Ozdemir, S.E. et al. CHRNA5 belongs to the secondary estrogen signaling network exhibiting prognostic significance in breast cancer. Cell Oncol. 44, 453–472 (2021). https://doi.org/10.1007/s13402-020-00581-x.)

The Spearman's correlation coefficient between CHRNA5 and every other gene was calculated for the TCGA breast cancer dataset. The comparison between the siCHRNA5 profile and the TCGA coexpression profile revealed that the secondary targets downregulated with siRNA treatment were also positively correlated with CHRNA5 (**Figure 3.32**). A negative correlation was found between the correlation coefficient of CHRNA5 and every other gene and siCHRNA5 profile (r = -0.44, p = 2.2e-16). In accord with that, regression analysis calculated the slope as -0.91 (p-value = 0.37, compared to -1), implying a correlation coefficient that could predict the

outcome of siCHRNA5 treatment yet with relatively low R squared (0.22). However, primary targets exhibited a more dispersed pattern.

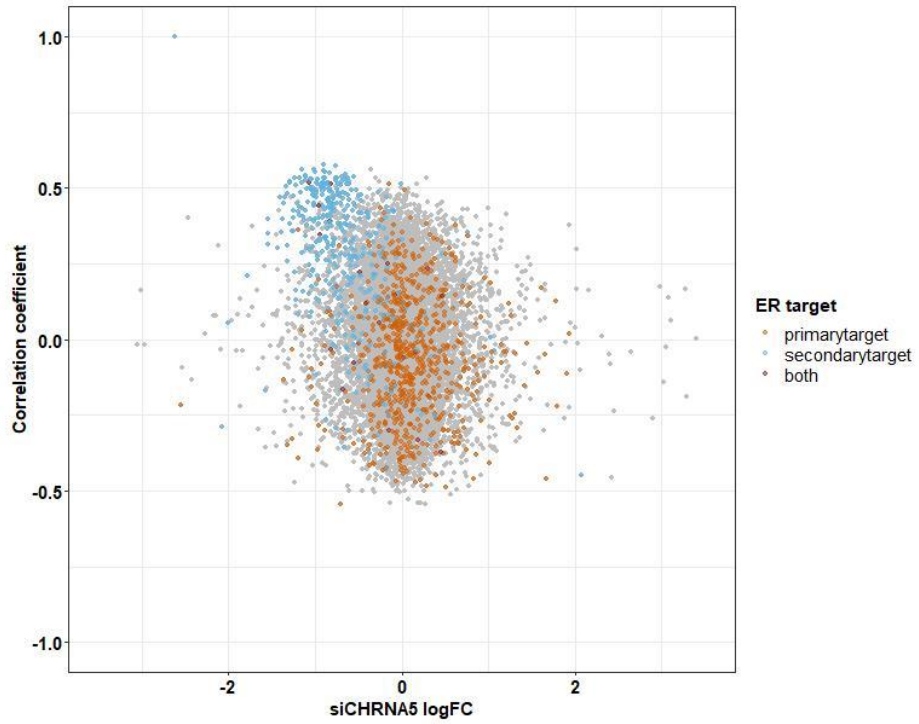

Figure 3.32 Scatter plot of pairwise correlation coefficient and siCHRNA5 logFC values in TCGA breast cancer dataset.

3.4.2 siCHRNA5 modulates estrogen targets in a time and dosage-dependent manner.

For the validation of the microarray results, ER-positive MCF7 cells were treated with 10nm, 20nm, and 50nm of siCHRNA5 for 72h and with 10nm for 120h (**Figure 3.33**). The expression changes for the selected primary and secondary targets were profiled via qPCR. All selected secondary targets except AREG, identified as a primary target in only two of the datasets (**Figure 3.27**), were downregulated in response to siCHRNA5 independent from the dose and the time. Primary targets with higher PS scores, i.e., MYBL1, TFF1, and DTL, were also downregulated. All primary targets with negative PS scores were upregulated in 72h treatments in a dose-dependent manner, yet not altered in 120h of treatment.

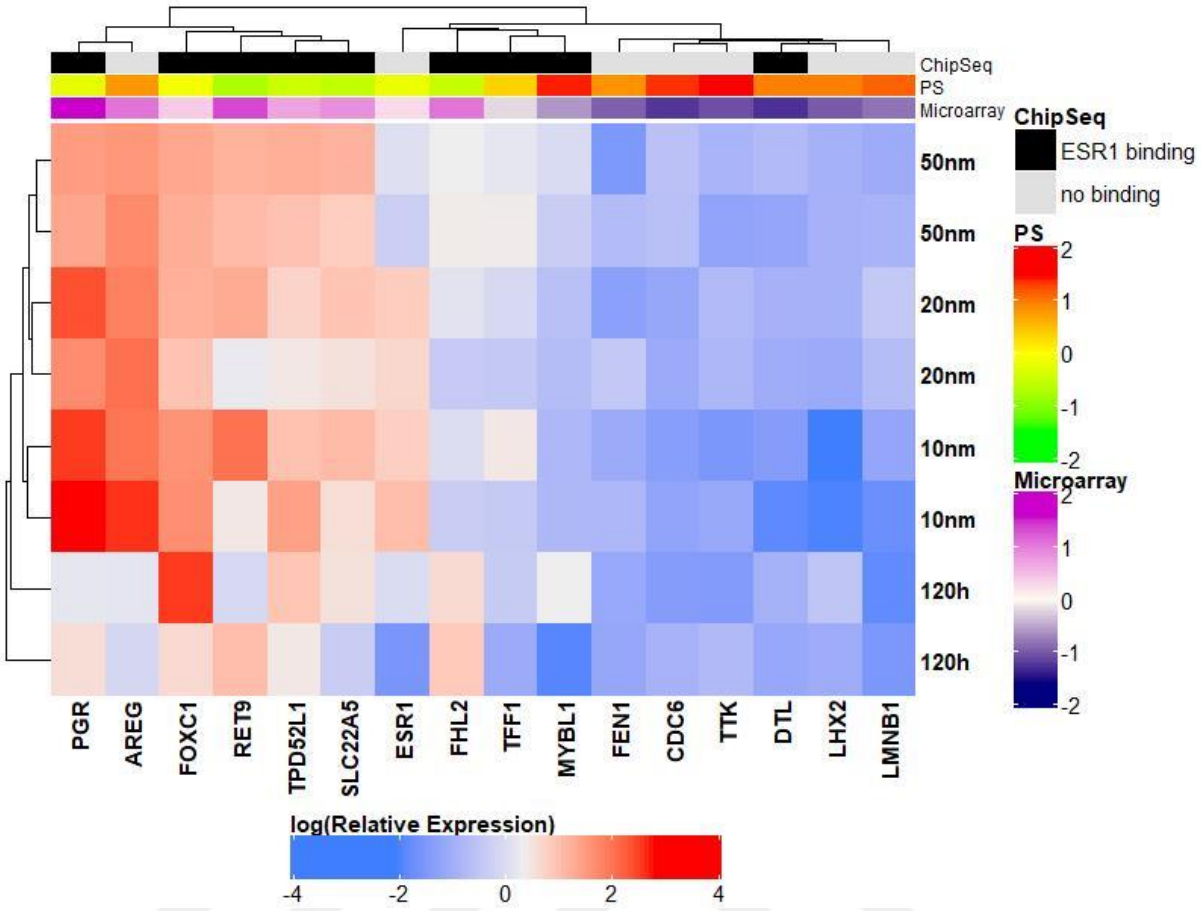

Figure 3.33 qPCR results for selected primary and secondary targets of ESR1 in response to siCHRNA5 in time- and dose-dependent manners. MCF7 cells were treated with different concentrations of siCHRNA5 for 72h (10nm, 20nm, and 50nm) and a single concentration for 120h (10nm), and indicated as row legends. ChipSeq, PSscore and microarray logFC values for genes were shown with colors as column legends.

(This image was reproduced with the licence ID: 5161460968853 from Shehwana, H., Keskus, A.G., Ozdemir, S.E. et al. CHRNA5 belongs to the secondary estrogen signaling network exhibiting prognostic significance in breast cancer. Cell Oncol. 44, 453–472 (2021). https://doi.org/10.1007/s13402-020-00581-x.)

3.5 Part 4. CHRNA5 miRNA expression

3.5.1 siCHRNA5 downregulates the 14q31.32 miRNA family.

In previous studies performed in our lab, CHRNA5 was successfully downregulated in both mRNA and protein levels through three different siRNAs (Cingir-Koker et al., 2018). The transcriptomic effects of siCHRNA5 were profiled through microarrays, and the results suggested alterations in key pathways, including TP53 and estrogen signaling. Later on, in order to further discover the regulatory factors involved in the siCHRNA5 profile, miRNA transcriptome was profiled through the microarray, and the selected miRNAs were investigated (Basak Özgürsoy, Sahika Cıngır-Koker, Rafet Said Tiryaki; TUBITAK 114S367). The hypothesis was that siCHRNA5 could affect mRNA profile via its effects on miRNAs since there were significant number of miRNA targets was observed (Ermira Jahja, 2018).

Chromosomal enrichment analysis of our miRNA microarray results performed with siCHRNA5 revealed that downregulated miRNAs belonged to a miRNA cluster located on chromosome 14, namely 14q31.32 miRNAs (**Figure 3.34**). The downregulation for those selected miRNAs were validated by Başar Özgürsoy, Şahika Cıngır-Köker and Said Tiryaki.

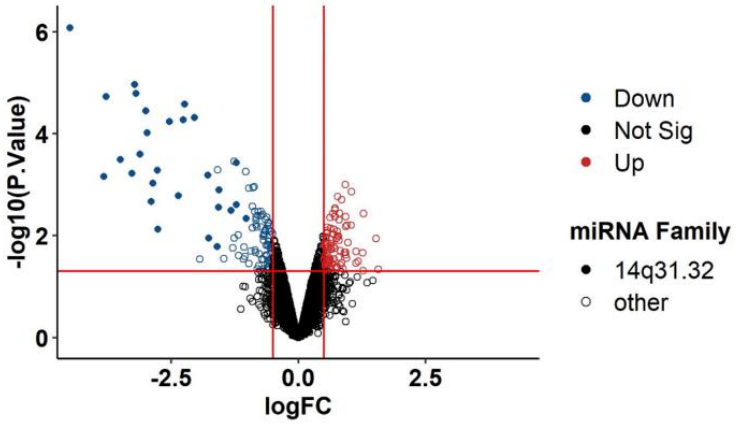

Figure 3.34 Volcano plot of miRNA microarray results. The x-axis refer to the logarithmically transformed expression fold changes in response to siCHRNA5 while the y-axis indicates the significance levels. The dots plotted, each refer to a miRNA, colored according to their direction of change while the closed circles indicate 14q31.32 cluster members.

3.5.1.1 14q31.32 miRNA family targets were enriched with the term estrogen signaling.

Enrichment analysis for targets using the miEAA tool and mirpathDB revealed that the top two enriched pathways for experimentally validated and/or predicted targets of 14q31.32 miRNA cluster were relaxin and estrogen signaling pathways (**Figure 3.35**A). In the network representation of the enriched pathways in which edge weights, node size, and node color represented numbers of shared miRNAs, the number of miRNAs, and the enrichment score, respectively, relaxin and estrogen signaling pathways shared a high number of miRNAs (**Figure 3.35**B)

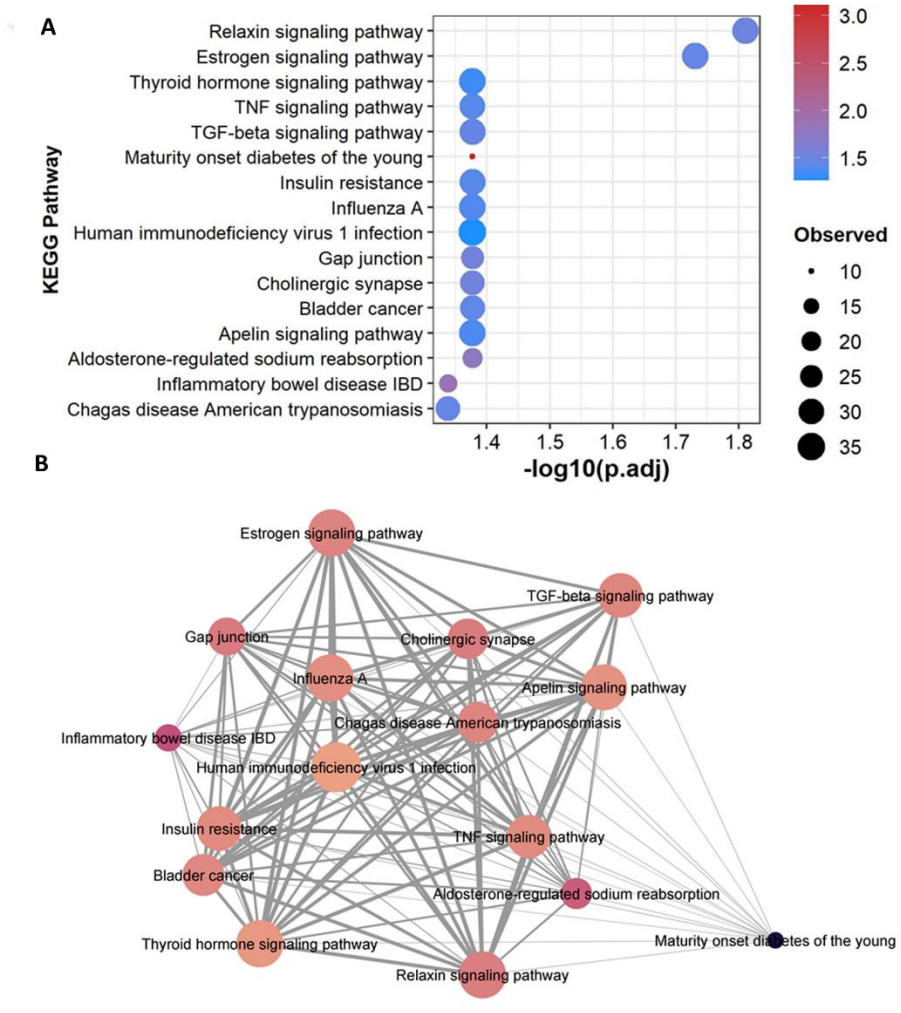

.

Figure 3.35 Functional analysis of 14q31.32 mirna cluster. KEGG pathway enrichment analysis of 14q31.32 miRNA cluster targets (A). Network of enriched KEGG pathways in which edge

weight represents common miRNAs between nodes and node size represents the number of miRNAs (B).

3.5.2 14q31.32 is a highly co-expressed miRNA cluster in TCGA and METABRIC datasets.

3.5.2.1 14q31.32 miRNA cluster members are coexpressed

The 14q31.32 miRNA cluster has been shown to be coregulated/coexpressed in various contexts, including breast cancer (Gonzalez-Vallinas, et al., 2018; Hoppe, et al., 2016; Uppal, et al., 2015). I have investigated their expression levels using the two largest breast cancer patient cohorts, i.e., TCGA and METABRIC. The RSEM normalized miRNA expression values for the TCGA BRCA dataset and miRNA microarray results of the METABRIC dataset were obtained from Firebrowse and Expression Atlas. The pairwise correlation coefficient between each miRNA from the 14q31.32 miRNA cluster was calculated for each dataset. Although their expression level was variable, the 14q31.32 miRNA expression was highly correlated with each other in both datasets except miR-494 and miR134, which were negatively correlated in the METABRIC dataset (**Figure 3.36**). The mature and pre-miRNA expression levels were concordant in the TCGA BRCA dataset.

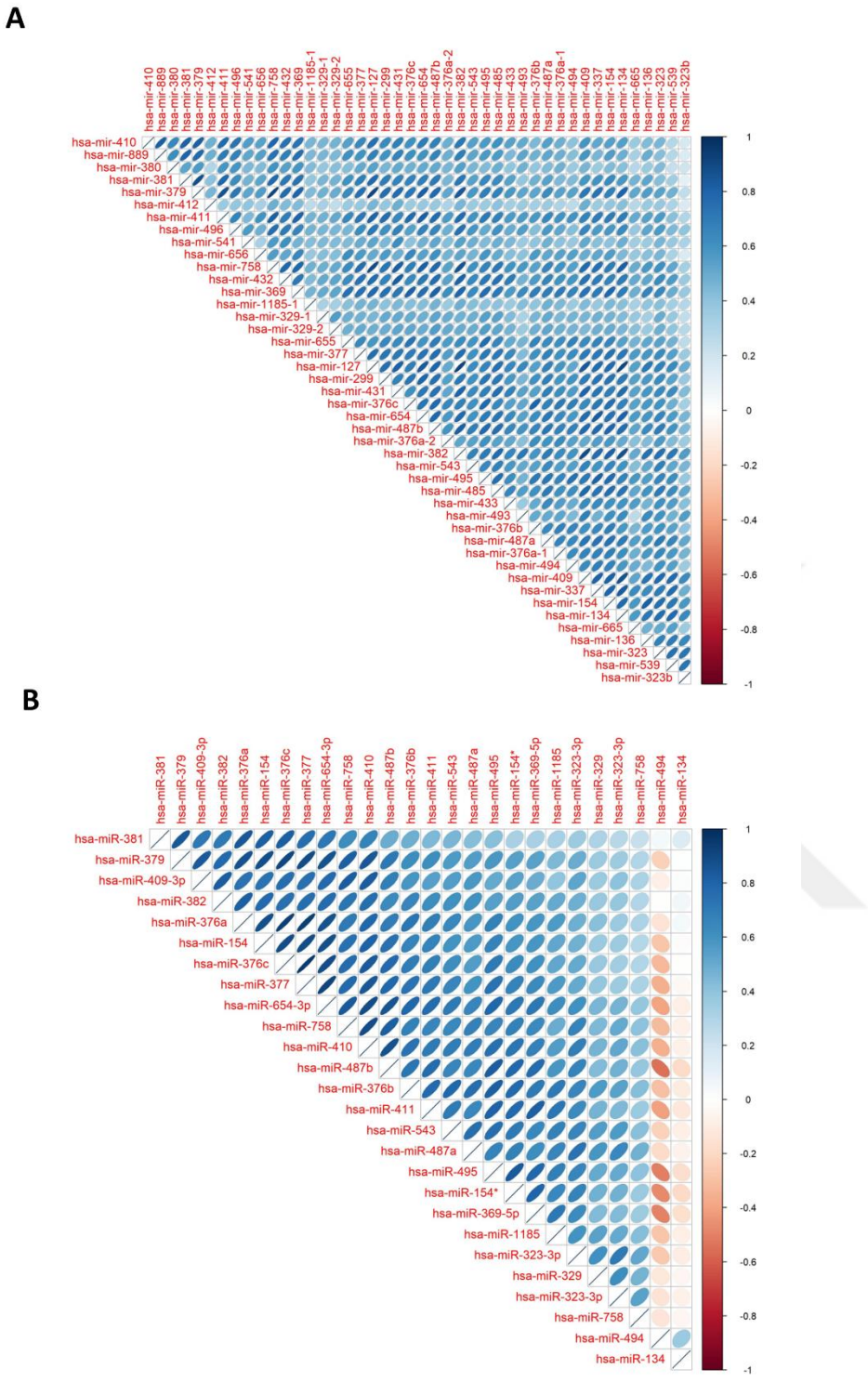

Figure 3.36 The pairwise correlation coefficient between 14q31.32 miRNA cluster miRNAs in TCGA (A) and METABRIC (B) datasets. Nodes were colored according to the correlation coefficient, if positive it was colored shades of blue and if negative those of red.

3.5.2.2 The composite 14q32.31 miRNA expression is lowest in Luminal B and Basal subtypes.

Since miRNA expression was highly correlated with each other, the 14q32.31 miRNA expression score for each patient was calculated. According to my previous findings, the miRNA expression level varied between the miRNAs in this cluster. Therefore, in order to prevent a bias toward the highly expressed miRNAs, a z-score based scoring metric was employed. The 14q32.31 miRNA expression score was found to be significantly lower in tumor samples than in solid normal breast tissues and also between tumor-normal pairs (**Figure 3.37**A-B). Enrichment analysis with miRNA targets using the miEAA also implicated the estrogen signaling. Therefore I compared the ESR1 protein expression level with 14q32.31 miRNA expression score. Our findings revealed a negative correlation in the luminal A subtype (**Figure 3.37**C). Next, the expression levels of the 14q32.31 miRNA cluster were further examined in different breast cancer subtypes. The 14q32.31 miRNA expression score was the lowest in luminal B and basal subtypes, whereas Normal-like patients exhibited the highest expression which may indicate involvement in breast cancer differentiation (**Figure 3.37**D).

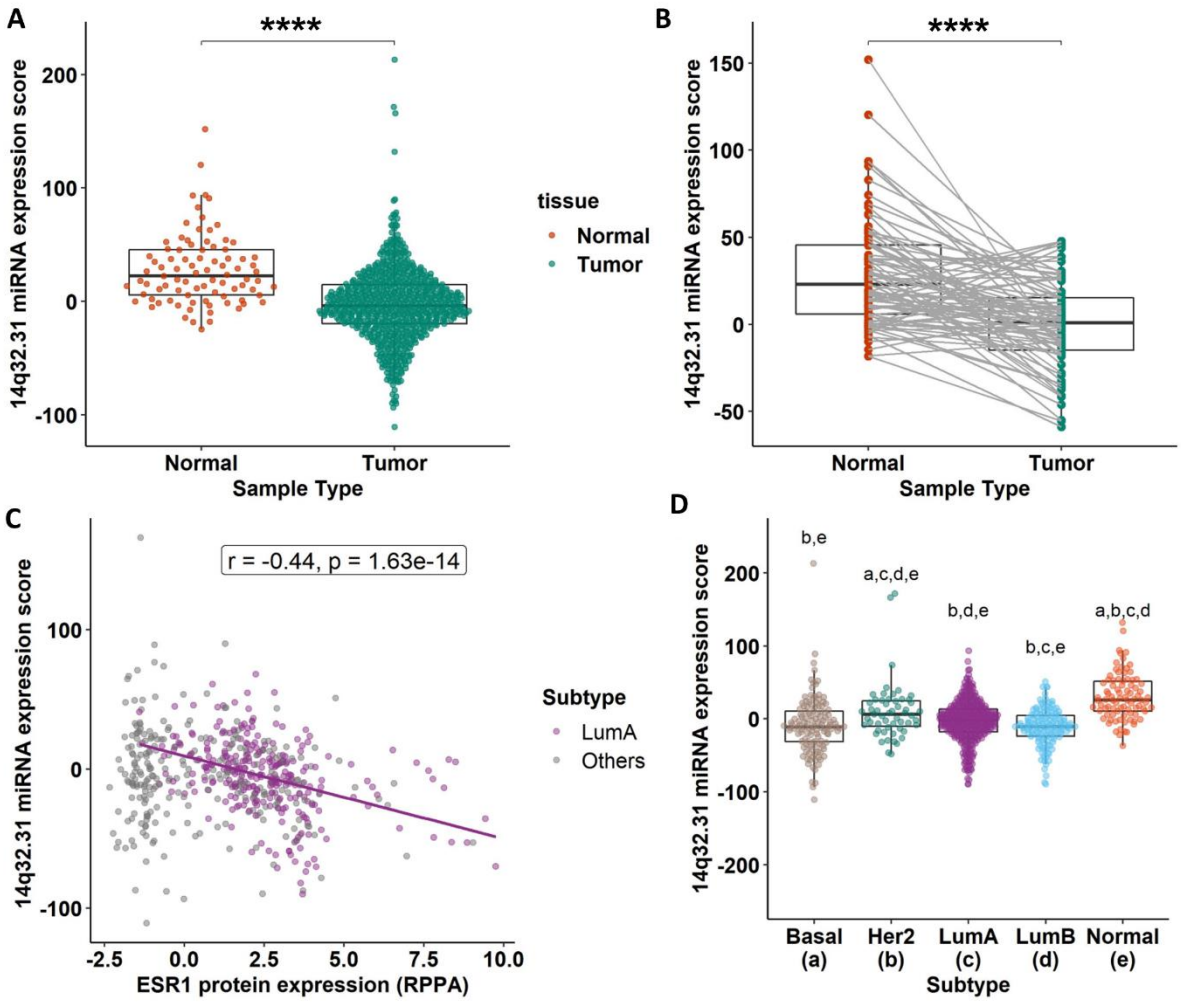

Figure 3.37 The 14q32.31 miRNA expression score in all (A) and paired (B) normal and tumor samples in the TCGA BRCA dataset. The 14q32.31 miRNA expression score compared to ESR1 protein levels in TCGA dataset (RPPA: Reverse-phase protein array). Luminal A samples were labeled, and Spearman's correlation coefficient with the p-value was reported on plot (C). The 14q32.31 miRNA expression score in breast cancer subtypes. Significantly different subtypes were represented above each group ($p < 0.05$). Samples were colored according to the subtype (D).

3.5.2.3 Methylation and copy number alteration levels of MEG3 and DLK1 differ with ER status in BRCA.

The 14q31.32 region, also called DLK1-MEG3 region, is a maternally imprinted region and coregulated with DLK1 and MEG3. In RNAseq results, both MEG3 and DLK1 were

downregulated in response to siCHRNA5 (MEG3; logFC = -5.16, FDR adj. p-value =0.019, DLK1; logFC = -3.19, FDR adj. p-value = 0.006). The primary regulatory mechanism of this region has been reported as the methylation of the DLK1-MEG3 region located upstream of the 14q31.32 miRNA family (Gardiner, et al., 2012; Sellers, et al., 2019; Zhu, et al., 2019). My previous analysis suggested the differential regulation of 14q32.31 miRNA family in between ER-positive and ER-negative patients. Therefore, I next investigated the methylation and copy number alterations (CNA) of DLK1 and MEG3 in ER-positive and ER-negative patients in the TCGA dataset (**Figure 3.38**). The CNA and the methylation score of DLK1 and MEG3 were obtained through cbioportal.org. In accord with previous reports, CNA for DLK1 and MEG3 was the same, and 48.8% of the ER-negative patients had a DLK1-MEG3 deletion, whereas it was only 22.4% for the ER-positive patients (**Figure 3.38**A, C). The percentage of amplification was similar in ER-positive and ER-negative patients. I also found that methylation levels of MEG3 and DLK1 were significantly higher in ER-negative patients. Together with previous findings, these results indicate a possible interaction between estrogen signaling and the 14q32.31 miRNA family and its chromatin regulators.

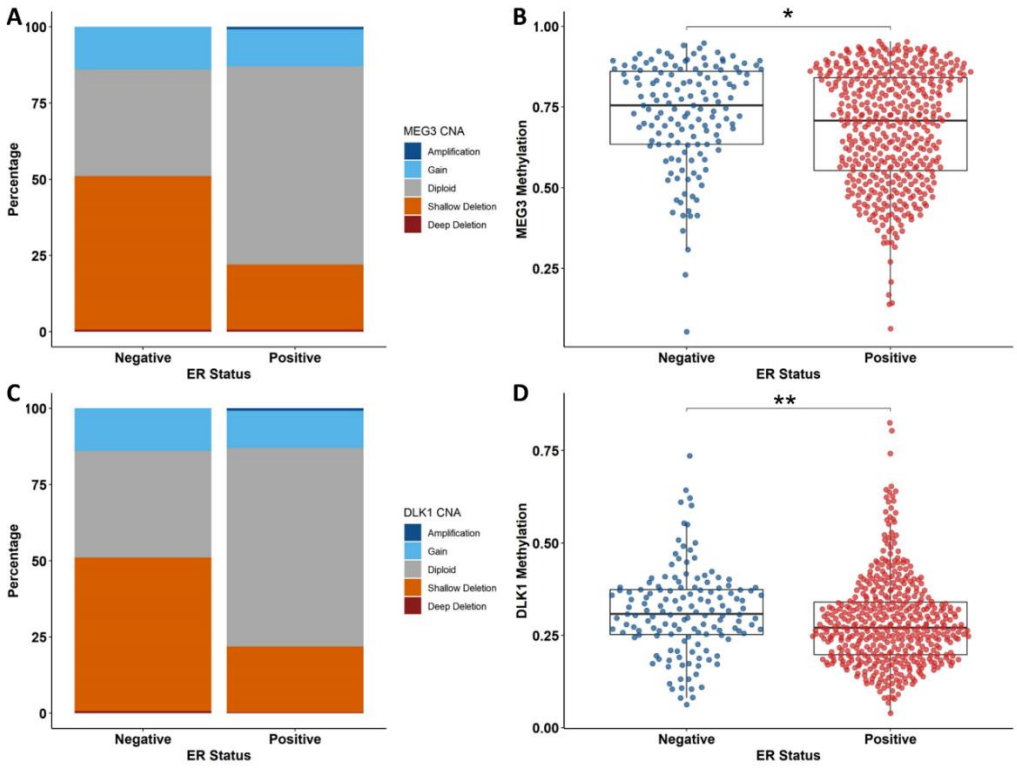

Figure 3.38 Analysis of DLK1 and MEG3 copy number alteration (CNA) and methylation status. MEG3 (A, B) and DLK1 (C, D) in ER-positive and ER-negative patients. Student t-test results were reported on B and D. In A and C, stacked bar plots show the percentage of patients with a given chromosomal alteration shown in the legend while in B and D, boxplots with 95% confidence interval are plotted for methylation values of different subtypes.

3.5.3 DLK1 expression does not change with E2 treatment in breast cancer cell lines.

Since in silico results suggested a regulatory role for E2-ESR1 signaling on the expression of 14q32.31 miRNA cluster, I examined the change in the expression level in DLK1 in E2-treated breast cancer cell lines (**Figure 3.39**; in cooperation with Sila Ozdemir and Damla Gunes). The decrease in the DLK1 expression level was demonstrated in siCHRNA5 treated MCF7 cells validating the usage of DLK1 as the representative regulator of the 14q32.31 miRNA cluster (**Figure 3.39A**). DLK1 expression however, did not change in response to E2 treatment for 24h

except for ZR75 indicating DLK1 expression may require co-regulatory factors in addition to E2 hence possibly requiring longer exposure times (**Figure 3.39B**).

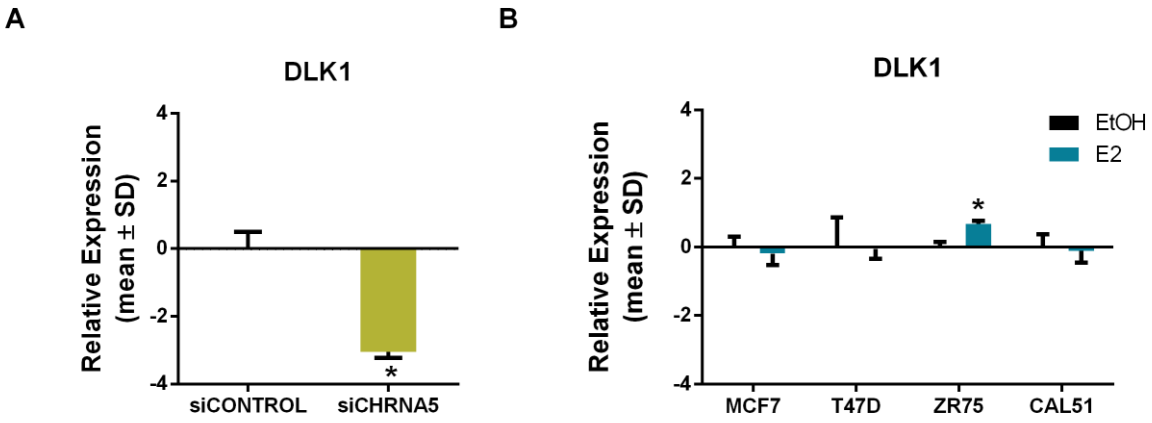

Figure 3.39 The change in the DLK1 expression level in response to siCHRNA5 in MCF7 cells (A) and E2 in ER-positive MCF7, T47D, and ZR75 and ER-negative CAL51 cell lines (B)

3.5.4 miRNA-mRNA networks of selected 14q31.32 miRNA cluster members suggest possible cooperation and inhibition between miRNAs.

Since 14q32.31 miRNA targets were enriched in the estrogen signaling pathway, I next analyzed the miRNA-target network with the 14q32.31 miRNA family and their experimentally validated targets obtained from miRNET. Previously defined estrogen targets (see Chapter 3.3) were used. Network analysis showed that 14q32.31 miRNAs shared targets and formed a single extensive network (**Figure 3.40**, **Table 3-1**). miR-495-3p, miR-329-3p, and miR-432-5p exhibited the highest closeness and betweenness score (**Table 3-1**). The network was overlayed with the logFC values from the siCHRNA5 profile in the microarray data, and larger nodes represented ESR1 targets. The distribution of up and downregulated targets was similar for miRNAs; however, miR495-3p emerged as a good candidate with its high network metrics as well as the number of ESR1 targets among its targets.

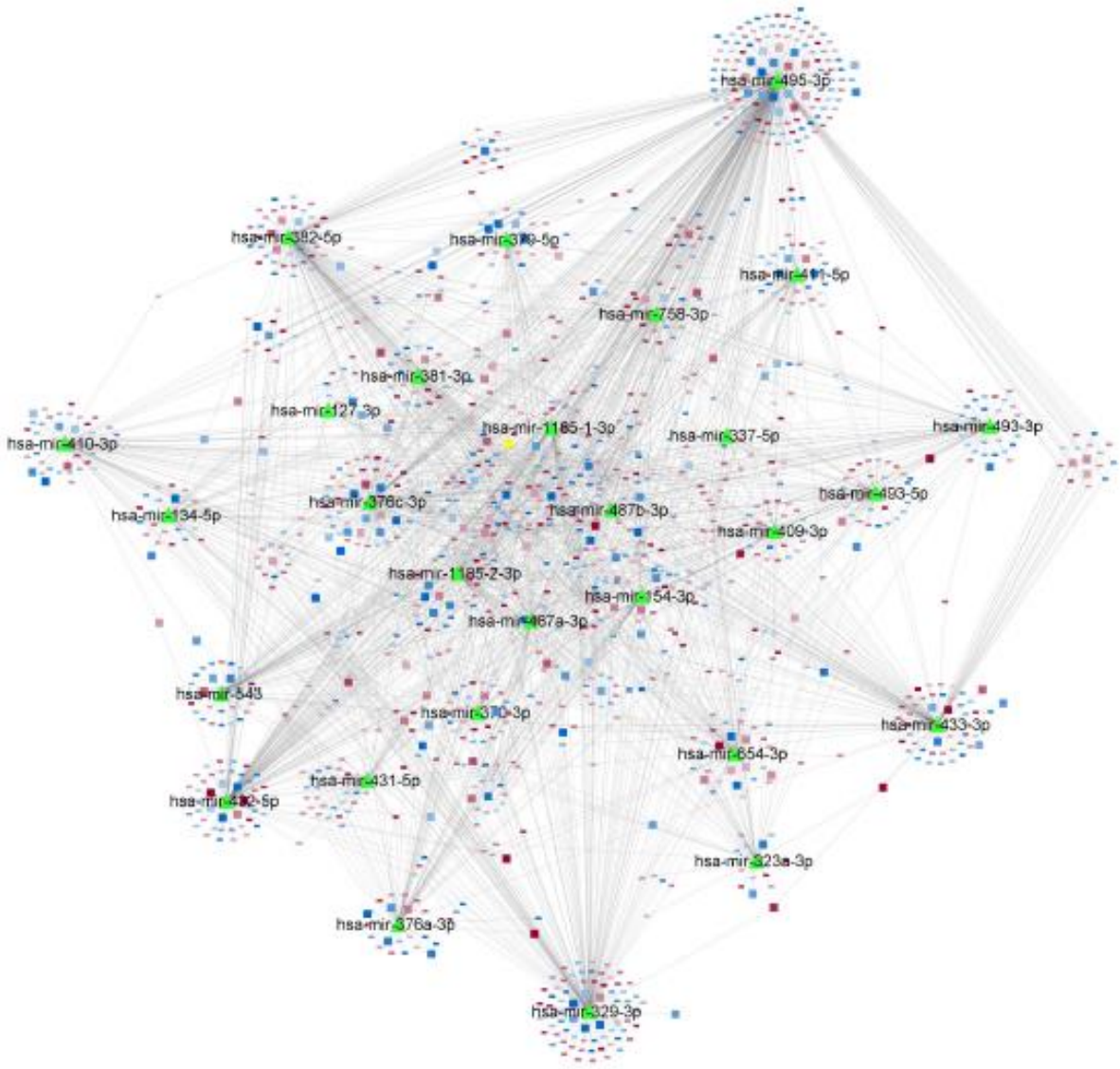

Figure 3.40 The miRNA – Target network for 14q32.31 miRNA family miRNAs and their experimentally validated targets. The network was overlayed with logFC values from siCHRNA5 microarray data (red, upregulation; blue, downregulation), and larger nodes represented primary and secondary ER targets.

Table 3-1 Network metrics for miRNA-mRNA network

node_name	**Degree**	**Closeness**	**Betweenness**
hsa-mir-495-3p	386	693.5	668548.0654
hsa-mir-329-3p	176	566.85	285356.7804
hsa-mir-382-5p	153	540.58333	189195.7576

hsa-mir-432-5p	148	541.91667	197339.8168
hsa-mir-376c-3p	132	536.16667	186206.6338
hsa-mir-433-3p	132	529.4	177099.2785
hsa-mir-410-3p	95	511.66667	125398.4278
hsa-mir-493-3p	90	505.5	124957.3151
hsa-mir-654-3p	80	490.65	106552.749
hsa-mir-543	80	502.58333	99136.90778
hsa-mir-411-5p	79	496.9	114738.9369
hsa-mir-493-5p	78	503.5	108628.3083
hsa-mir-376a-3p	76	495.51667	81262.92984
hsa-mir-381-3p	67	490.46667	79198.91638
hsa-mir-379-5p	64	484.76667	80284.64705
hsa-mir-758-3p	63	486.73333	75920.6833
hsa-mir-134-5p	61	484.9	76478.88489
hsa-mir-487a-3p	58	485.13333	45192.15167
hsa-mir-370-3p	57	482.61667	81936.41654
hsa-mir-409-3p	57	486.33333	78915.45324
hsa-mir-431-5p	55	486.08333	88255.2506
hsa-mir-1185-1-3p	54	480.21667	31321.2146
hsa-mir-1185-2-3p	54	480.21667	31321.2146
hsa-mir-323a-3p	53	482.33333	56037.43425
hsa-mir-154-3p	40	471.55	19227.6601
hsa-mir-127-3p	32	444	30647.1171
hsa-mir-487b-3p	30	452.91667	25988.78621
hsa-mir-337-5p	12	380.63333	13974.26225

3.5.5 The miR409-3p transcriptome in the presence or absence of siCHRNA5 is profiled.

Since there was an intense alteration in miRNA expression levels in response to siCHRNA5 treatment, we next treated MCF7 cells with miRNA mimics to understand the roles of miRNAs in siCHRNA5 transcriptome further. Previously Basak Ozgursoy and Mehtap Yılmaz optimized the miRNA mimic application as 10nm in MCF7 cells. Sahika Cıngır-Koker and Said Tiryaki successfully had increased the miR-495-3p and miR376a-3p expression levels in MCF7 cells using miRNA mimics (Sahika Cıngır-Köker, Ph.D Thesis,2019, Rafet Said Tiryaki, Ph.D Thesis, 2019). They profiled miRNA mimic transcriptome along with their combinatorial treatment siCHRNA5 using microarrays.

miR-409-3p has also emerged as a strong candidate since it is the second most downregulated miRNA, while its mean expression level was one of the highest among 14q32.31 miRNAs. Therefore, I treated MCF7 cells with 10nm miR409-3p mimics with or without siCHRNA5 in duplicates. The downregulation of siCHRNA5 and upregulation of miR409-3p were validated through qPCR (**Figure 3.41**). RNA quality of samples was measured with RIN and biological replicate with the best RIN value sent for the microarray.

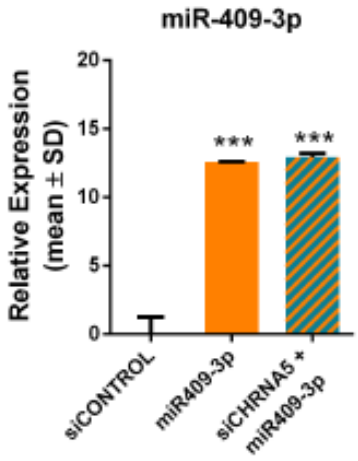

Figure 3.41 qPCR validation of miR409-3p mimic treatment with or without siCHRNA5. Mean ΔΔCT (±SD) was reported. One-way-ANOVA results were shown on plots.

3.5.6 miR495-3p acts antagonistically with siCHRNA5 in secondary estrogen targets.

The microarray results of miRNA mimic treated MCF7 cells were analyzed for each miRNA separately and normalized using the rma function from the oligo package. Their transcription profiles were compared with the siCHRNA5 transcriptome through hierarchical clustering and pairwise correlation analysis (**Figure 3.42**A, B). Accordingly, samples treated with siCHRNA5 along with miRNA mimic were clustered together with the siCHRNA5 alone group and exhibited a high correlation coefficient. All miRNA mimics had a positive correlation with their combinatorial group yet to a lesser degree compared to siCHRNA5, implying a relatively dominant effect of siCHRNA5. miR495-3p was the only miRNA mimic group showing a positive correlation with siCHRNA5.

miR495-3p expression profile exhibited a positive correlation with its combinatorial treatment for both primary and secondary targets of estrogen. I next employed the synergy analysis methods described in Chapter 3.2 separately for primary and secondary targets of ESR1. Regression-based synergy analysis for primary targets showed that the regression coefficient was lesser than 1, indicating an inhibitory interplay between siCHRNA5 and miR495-3p. Accordingly, 240 primary targets were found to be altered in siCHRNA5 treatment, while only 138 of them, 113 in the same direction and 25 in the opposite direction, were changed in combinatorial treatment. The limma-based synergy method was used to understand further the nature of the interaction between siCHRNA5 and miR495-3p. The effect was additive for the majority of the primary targets (43.5%, n=174), whereas 119 (29.8%) were upregulated less and 60 (15%) were downregulated more than expected. Heatmap representation helped digest the behavior of each cluster further. Primary targets downregulated more were the genes altered in the opposite direction in individual treatments. Except for a small cluster in the more.down group, primary targets upregulated in siCHRNA5 were also upregulated in combinatorial treatment.

We have previously found that siCHRNA5 downregulates secondary targets of estrogen (Chapter 3.2, Huma Shehwana, Ph.D. Thesis, 2018). Remarkably, the secondary targets of estrogen were

also downregulated in miR495-3p and so in combinatorial treatment. The regression analysis between miR495-3p and the combinatorial treatment showed that the slope was not statistically different than 1 (slope =1.01, intercept = -0.242). The regression analysis results indicated the downregulation of siCHRNA5 enhanced the effect of miRNA mimic on the downregulation of the secondary targets of estrogen signaling with 0.242 fold. However, the effect of siCHRNA5 on secondary targets was more potent than the calculated intercept. Therefore, the interplay between siCHRNA5 and miR495-3p was predicted as antagonistic. In accord with that, the limma-based synergy analysis revealed that most of the secondary targets were downregulated less than expected (71.8% n= 304), while only 105 (24.8%) were additively affected. Synergy analysis showed that combinatorial treatments were more efficient compared to individual treatments yet to a lesser degree than expected, indicating partial inhibition between miR495-3p and siCHRNA5.

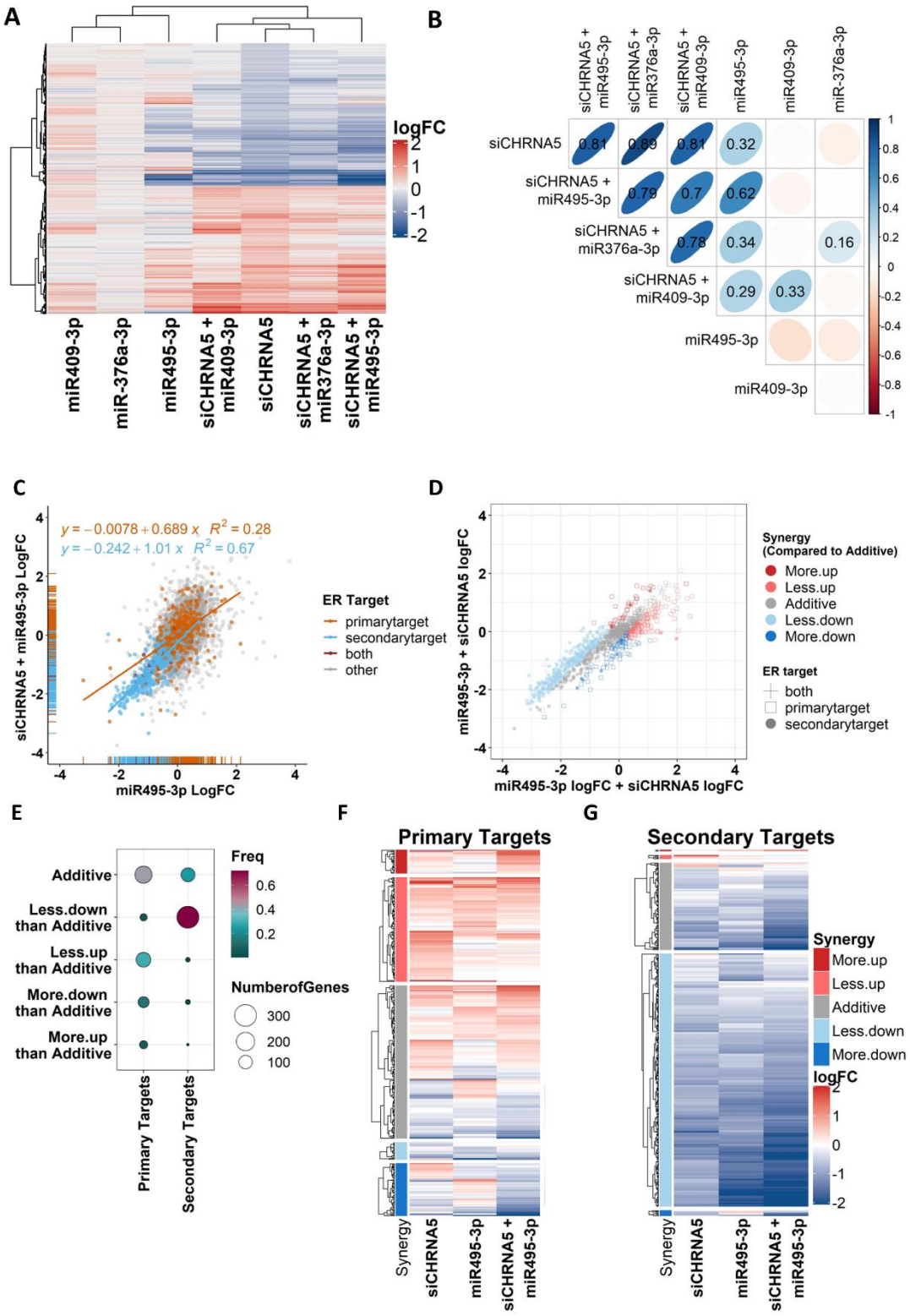

Figure 3.42 Microarray analysis of the mimic treatment for selected miRNAs with or without siCHRNA5. Heatmap representation of the hierarchical clustering of the expression of the genes significantly altered in siCHRNA5 treatment (A). Pairwise correlation analysis between logFC

values from miRNA mimics and their combinatorial treatments (B). The significant correlation coefficients were reported ($p < 0.05$). Regression analysis for primary and secondary targets of ESR1 between miR-495-3p and combination treatment with siCHRNA5 (C). Synergy analysis between siCHRNA5 and miR-495-3p mimic treatment (D). Dot plot representation of the distribution of primary and secondary targets in synergy groups (E). Heatmap representation of primary targets (F) and secondary targets (G) altered in at least one group.

3.5.7 miR409-3p acts synergistically with siCHRNA5 in primary estrogen targets.

On the other hand, miR409-3p exhibited a positive correlation with its combinatorial groups for primary targets of estrogen signaling. Regression analysis between miR-409-3p and combinatorial treatment revealed that the regression line was not significantly different from the x=y line (**Figure 3.43**, slope = 0.985, intercept = 0.006), indicating either the siCHRNA5 effect on primary targets was too low or miR409-3p inhibited it. The limma-based synergy analysis showed that 246 (62.1%) primary targets were affected additively in the combinatorial treatment. Hierarchical clustering with heatmap representation was employed to understand the nature of the additivity. Accordingly, only a small cluster (n=32) was altered in both treatments, and for the rest of the genes, the effect of individual treatments was preserved in combinatorial treatment. The results of the synergy analyses suggested the additivity between the two treatments was through separate pathways.

Regression analysis for secondary targets showed the slope between miR409-3p and its combinatorial treatment was not significantly different than 0 with the intercept -0.511, suggesting a minimal effect of miR409-3p on secondary targets. 240 (59.2%) secondary targets were additively affected, whereas 108 (26.6%) were downregulated more in combinatorial treatment compared to expected. Interestingly the majority of the secondary targets were either upregulated with miR409-3p treatment yet to a lesser degree. In the additive cluster, the potency of siCHRNA5 was partially inhibited with miR409-3p.

The effect of miR-376a-3p on estrogen receptor targets was less pronounced than miR-495-3p or miR-409-3p.

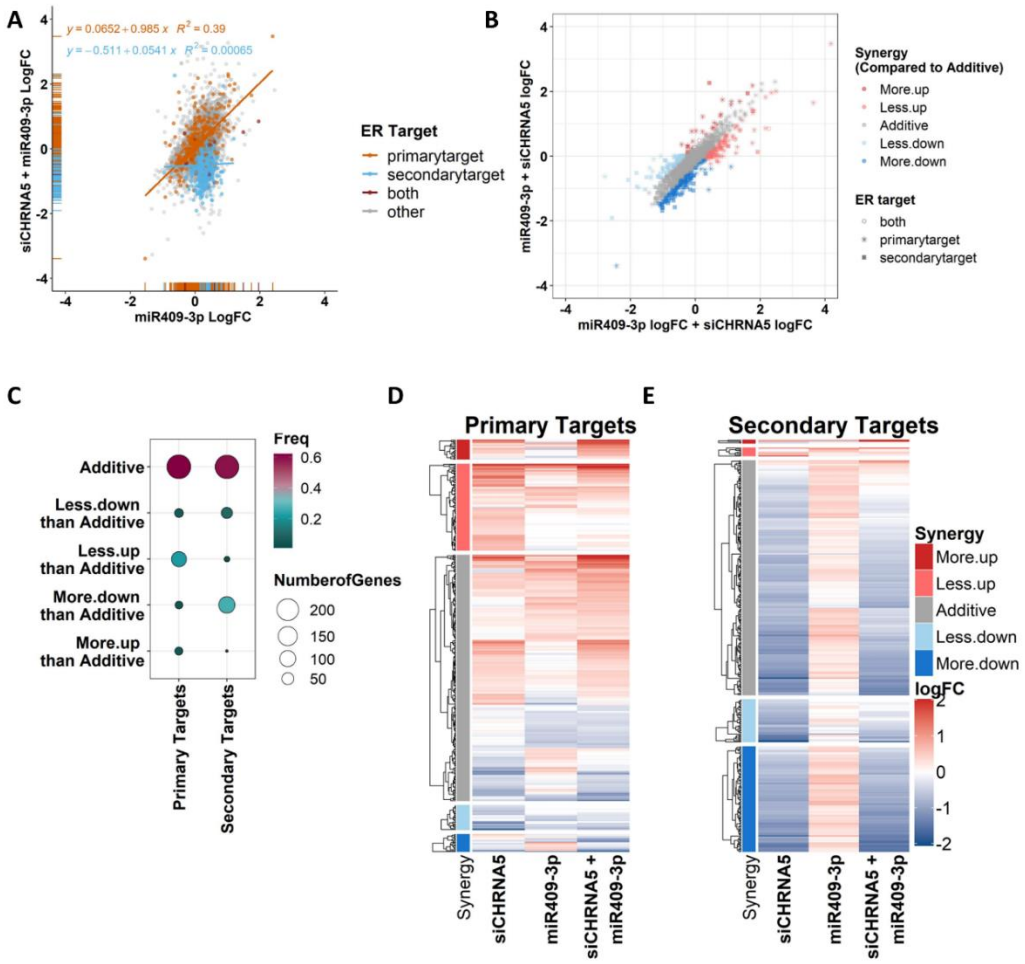

Figure 3.43 Regression analysis for primary and secondary targets of ESR1 between miR-409-3p and combination treatment with siCHRNA5 (A). Synergy analysis between siCHRNA5 and miR-409-3p mimic treatment (B). Dot plot representation of the distribution of primary and secondary targets in synergy groups (C). Heatmap representation of primary targets (D) and secondary targets (E) altered at least one group.

3.5.8 miR495-3p exhibits a negative correlation with the E2 profile.

Since primary and secondary targets of ESR1 were differentially modulated with miRNA mimics and/or their combinatorial treatment, I next analyzed two public datasets (GSE35428 and GSE117942) in which MCF7 cells were treated with either E2 or selective estrogen receptor modulators (SERMs) for 24h. miRNA mimic, siCHRNA5, and their combinatorial treatment transcriptome were compared with those (**Figure 3.44**). As synergy analysis suggested, miR495-3p exhibited a negative correlation with E2 and a positive one with SERMs. Fulvestrant (ICI)

reported to be 95% antagonist of E2 had the highest correlation with the miR495-3p profile. On the other hand, miR-409 positively correlated with the E2 profile and negatively with SERMs. Interestingly, secondary targets were downregulated with SERMs except for Tamoxifen and upregulated with E2.

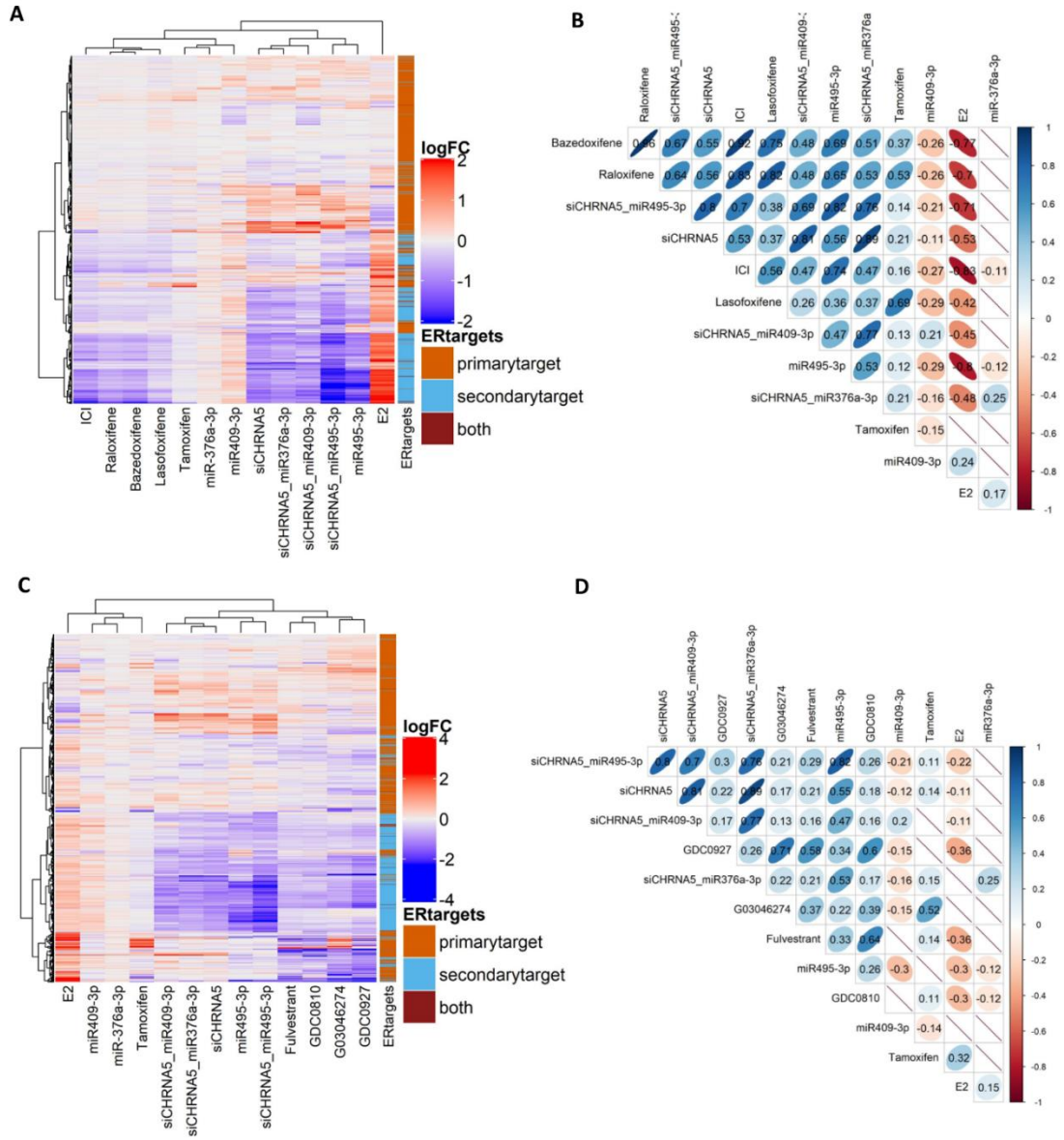

Figure 3.44 Comparative analysis of selective estrogen receptor modulators (SERMs) and siCHRNA5 and miRNA mimic transcriptomes. Heatmap representation of clustering analysis between logFC values of primary and secondary ESR1 targets in SERMs and miRNA mimic treatments with or without siCHRNA5 (A, C) and pairwise correlation analysis between samples in A and C respectively (B, D).

3.5.9 miR-495-3p differentially regulates early and late response targets

In silico analysis revealed that the response of secondary targets was more consistent than that of primary targets. Therefore, the expression profile of primary targets was further examined through time-course transcriptome datasets for the E2 response in MCF7 cells. The increase in the expression levels of primary targets started at 3hr (n =144), and the number of genes upregulated increased over time; additional 56 genes at 6hr and 25 genes at 12h were induced (**Figure 3.45**). Interestingly, transcriptional repression became more apparent at 12h (n=213), in which 40 of them were upregulated by miR-495-3p, while only seven were downregulated. siCHRNA5 and miR495-3p treatment changed the expression of those primary targets in the same direction, yet not additively including CXCL12 and CYP1B1. Among the early response primary targets (n=144), 52 were upregulated, and 15 were downregulated by siCHRNA5.

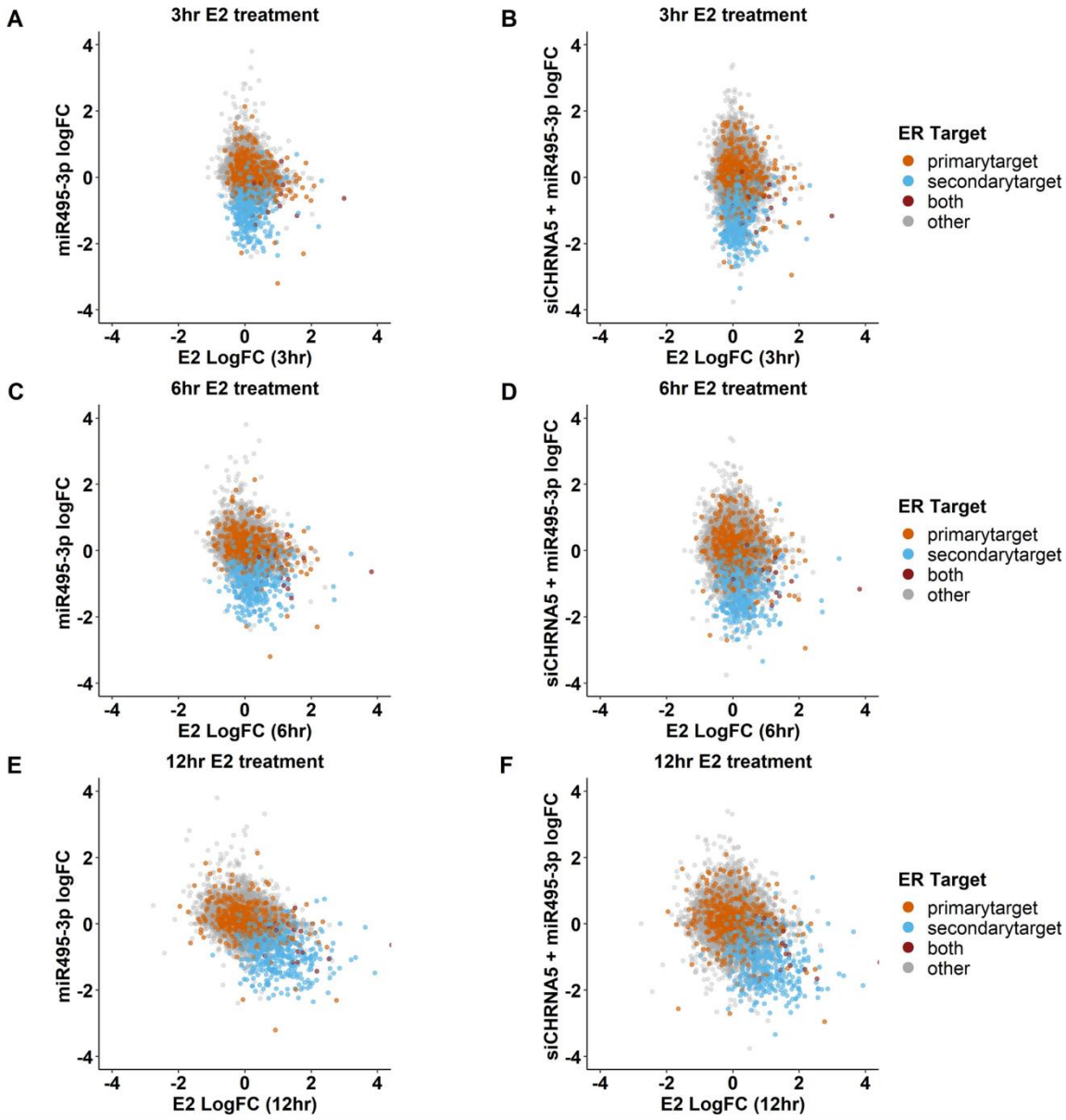

Figure 3.45 Time-course expression changes in primary and secondary targets in response to estrogen treatment for 3hr, 6hr, and 12hr in miR-495-3p (A, C, E) in miR-495-3p + siCHRNA5 (B, D, F), respectively.

In silico analysis showed that miR409-3p positively correlated with E2 and negatively with SERMs. In accord with that miR-409-3p and E2 profile was positively correlated in 3h of E2 treatment ($r = 0.27$, $p < 2.2e\text{-}16$) and remained significant for 6 and 12h treatments ($r = 0.21$, $p < 2.2e\text{-}16$). miR-495-3p and miR-409-3p was negatively correlated for primary targets altered in either of the mimic treatments ($r = -0.2$ $p = 0.0002$). For example, the early response genes, i.e.,

CXCL12 and PGR, were downregulated in miR-495-3p and upregulated in miR-409-3p treatment.

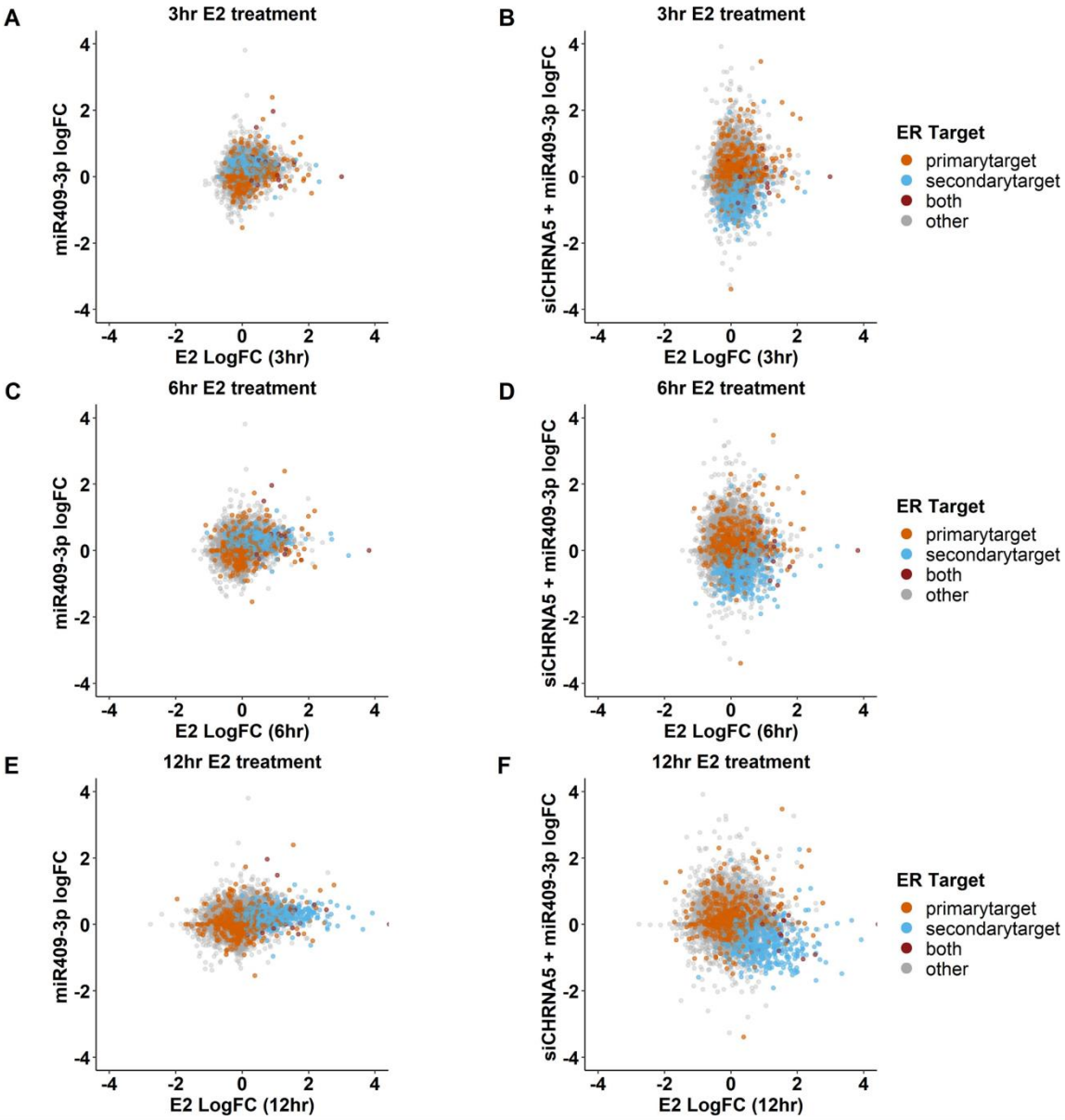

Figure 3.46 Time-course expression changes in primary and secondary targets in response to estrogen treatment for 3hr, 6hr, and 12hr in miR-495-3p (A, C, E) in miR-495-3p + siCHRNA5 (B, D, F), respectively.

3.5.10 qPCR validation of miR495-3p and siCHRNA5 synergy is performed

Synergy and comparative transcriptomic analysis suggested a possible interplay between miR409-3p and miR495-3p along with siCHRNA5. Therefore, MCF7 cells were treated with

individual mimics, their combination with siCHRNA5, their combination with each other, and 20nm siCHRNA5 (In cooperation with Sahika Cıngır-Koker). The microarray results for selected primary and secondary targets of estrogen were validated through qPCR (**Figure 3.47**). Heatmap representation of the hierarchical clustering and the PCA analysis of the qPCR results showed that miR409-3p clustered together with the siCONTROL groups, suggesting limited effectivity except for PGR. miR495-3p alone and miR495-3p with miR409-3p clustered together, offering a relatively dominant effect of miR495-3p on selected targets. All other samples with siCHRNA5 treatment were clustered together.

PGR, an essential primary target, upregulated in miR409-3p and exhibit a downregulation trend in miR495-3p, and wasn't altered in combinatorial treatment. STON2, a primary target, did not change in individual treatments yet displayed a decreasing trend in combinatorial treatment. CXCL12, another primary target, downregulated only in miR-495-3p treated groups and not any other groups. In accord with previous results, secondary targets were downregulated in miR495-3p and/or siCHRNA5 treated samples.

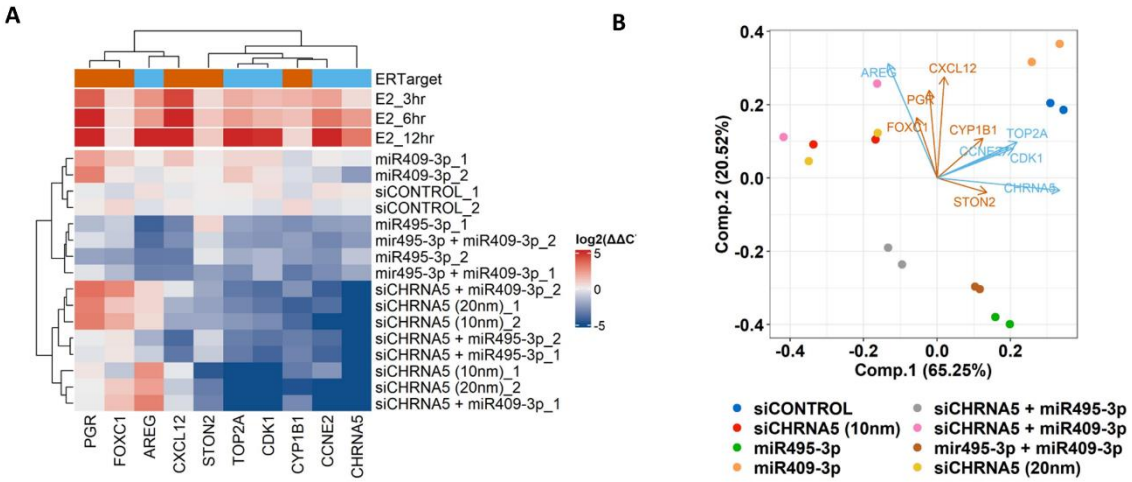

Figure 3.47 RT-qPCR validation of mirna mimic and siCHRNA5 interaction. Heatmap of qPCR results (logFC) of selected ESR1 primary and secondary targets (A, n=2 per group). PCA analysis for qPCR results in A shown with two dimensions; treatment groups are indicated by colors as genes with the vectors on the plot where axes indicate the percentage of the variation explained by each dimension in parenthesis. (B).

3.5.11 miR495-3p alters E2F targets.

In order to understand the regulatory mechanism behind miR495-3p transcriptome, protein-protein interaction (PPI) network for the genes altered with miR495-3p (abs(logFC)>0.5) were obtained through the String database. The PPI network was reconstructed in Cytoscape and clustered with Markov Clustering Algorithm (MCL). The largest network consisted of the downregulated genes, and TF enrichment analysis with iRegulon add-in in Cytoscape showed that those genes were enriched in E2F targets (**Figure 3.48** A). Ingenuity Pathway Analysis (IPA) with miR495-3p, siCHRNA5, and their combinatorial treatment showed that estrogen-mediated S-phase entry was the most enriched pathway (**Figure 3.48**B). E2Fs and their binding partner TFDP1 were downregulated in combinatorial treatment. The decrease in pRB level in all treatment groups provides further evidence to inhibition of E2Fs. Cell cycle, DNA replication, and DNA repair-related pathways were among the top enriched pathways (**Figure 3.48**C).

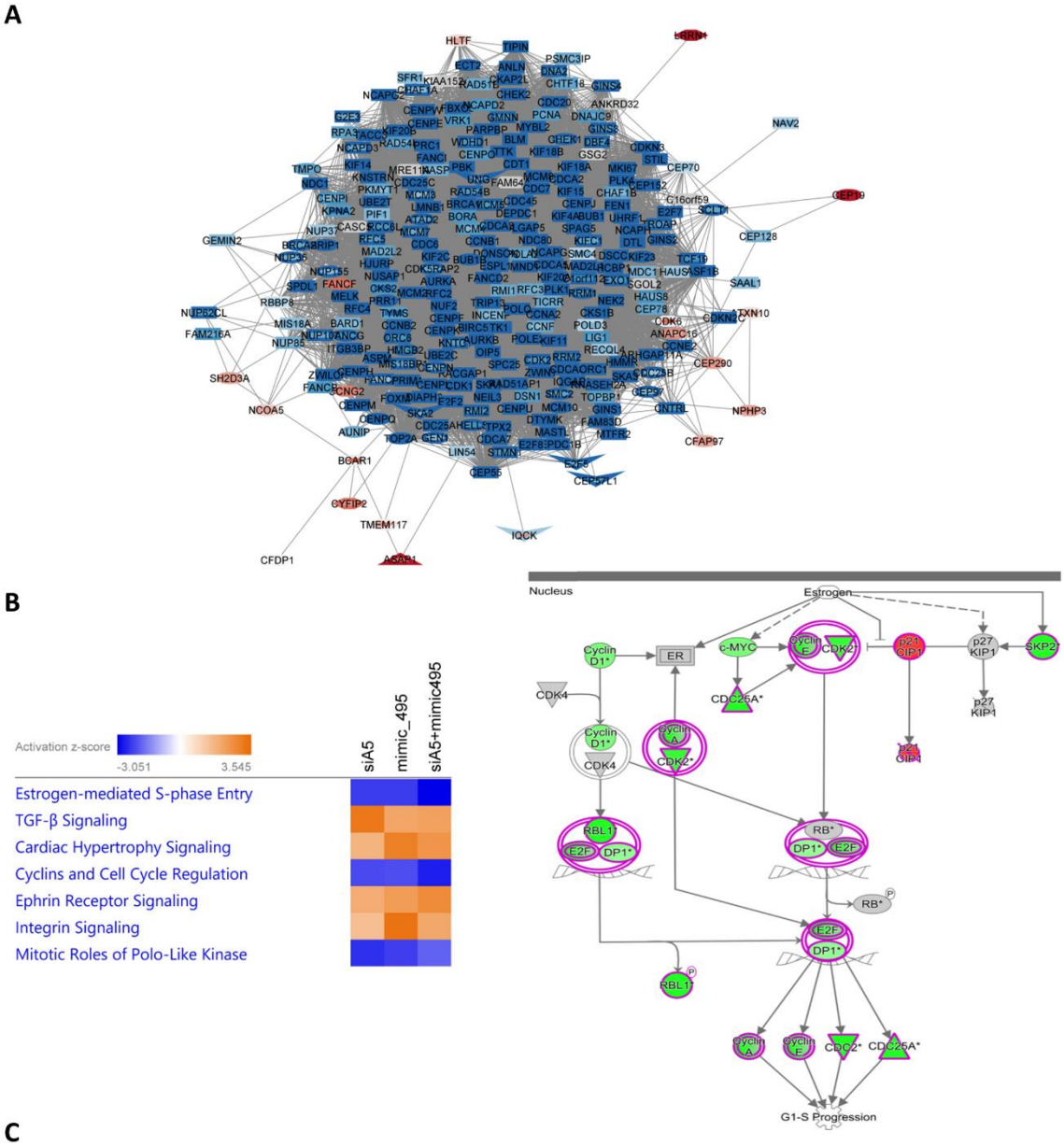
A
B
C
Activation z-score
-3.051
3.545
siA5
mimic_495
siA5+mimic495
Estrogen-mediated S-phase Entry
TGF-β Signaling
Cardiac Hypertrophy Signaling
Cyclins and Cell Cycle Regulation
Ephrin Receptor Signaling
Integrin Signaling
Mitotic Roles of Polo-Like Kinase
Nucleus
Estrogen
Cyclin D1*
ER
c-MYC
Cyclin E
CDK2*
p21 CIP1
p27 KIP1
SKP2
CDK4
CDC25A*
Cyclin A
RBL1
E2F
DP1*
RB*
G1-S Progression
Cell cycle
DNA replication
Oocyte meiosis
Cellular senescence
Fanconi anemia pathway
Progesterone-mediated oocyte maturation
Homologous recombination
Human T-cell leukemia virus 1 infection
p53 signaling pathway
MicroRNAs in cancer
Mismatch repair
Nucleotide excision repair
RNA transport
Base excision repair
Small cell lung cancer
FoxO signaling pathway
Pyrimidine metabolism
0.1
0.2
0.3
GeneRatio
p.adjust
0.01
0.02
0.03
Count
10
20
30

Figure 3.48 The functional analysis of mir495-3p profile. The largest network generated after MCL analysis of protein-protein interaction network of genes significantly altered in miR-495-3p treatment (A). Nodes were colored according to miR-495-3p logFC (inside) and miR-495-3p + siCHRNA5 logFC (border). Triangle represents more up; inverted triangle represents more-down, and ellipse represents additive results. Canonical pathway results from Ingenuity pathway analysis (IPA) where top seven pathways enriched in miR-495-3p treatment were shown (B). Estrogen-mediated S phase entry pathway from IPA analysis colored according to miR-495-3p + siCHRNA5 logFC values (C). KEGG pathway enrichment analysis of genes in A (D).

3.6 Part 5. syneRgy app

3.6.1 Overview of syneRgy app

syneRgy app is a Shiny-based web tool to analyze transcriptomic data to identify the synergistic and additive interplay between two or more treatments and possible underlying regulatory mechanisms. Current studies on synergy analysis are based on cell viability and cell toxicity assays. Although they provide a lead for therapy, the underlying mechanism of the synergistic or antagonistic behavior remains unclear. Transcriptomic data obtained from individual treatments and their combinatorial treatment can help uncover; however, there are limited methods to analyze transcriptomic data in the context of synergy systematically. Therefore, the syneRgy app has been designed to perform synergy analysis followed by TF enrichment analysis with transcriptomic data **(Figure 3.49**).

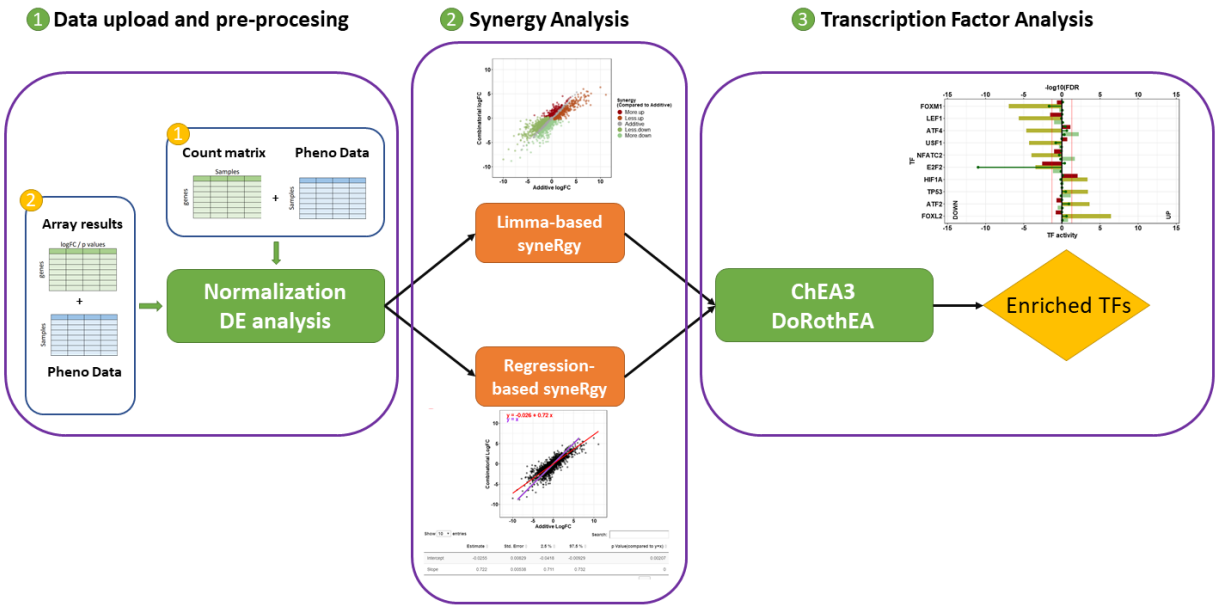

Figure 3.49 The flowchart for syneRgy App. Each box represent different modules starting from the left to right.

3.6.2 Input data

syneRgy app accepts input data in txt and csv formats in which rows are the genes and columns are either differential expression analysis results or raw count data from an RNAseq experiment (Step1 in **Figure 3.49**). For both input types (represented in step 1 in **Figure 3.49**), data for two or more treatments and their combinatorial group need to be provided. Input data also must contain a column with either HGCN gene symbols or Ensembl Gene IDs. In the case of duplicate gene IDs, the row with the highest total expression value for count data and the row with the highest number of significant adj p-value for logFC data will be used in later steps.

For RNAseq experiments, only count data is accepted and user asked to provide phenotype information. In the phenodata, the user is asked to fill a table by matching treatment ID with column name (**Figure 3.50**A). Suppose multiple control groups exist, as in the study shown in Figure 3.50B in which wildtype of TP53/RB1 knockout (vector control) LNCaP cells was treated with Enzalutamide (DMSO control). In that case, the user also needs to provide the contrast matrix by labeling treatment samples with "1" and corresponding control samples with "-1" (**Figure 3.50**B). After constructing the phenodata, syneRgy performs voom transformation followed by

differential expression analysis with limma for the user-defined comparisons, and additive and synergy coefficient calculations (For details, please see Methods). syneRgy also performs diagnostic analysis, i.e., MDS and PCA.

The second option for input data is directly providing differential expression analysis results, enabling users to analyze data from any platform with any normalization methods. In this option, the user needs to match column names with logFC and adj. p-value (or any statistics) for each treatment. syneRgy calculates additive and synergy coefficients with logFC values only; therefore, adj. p-value for those cannot be calculated in this option (For details, please see Methods).

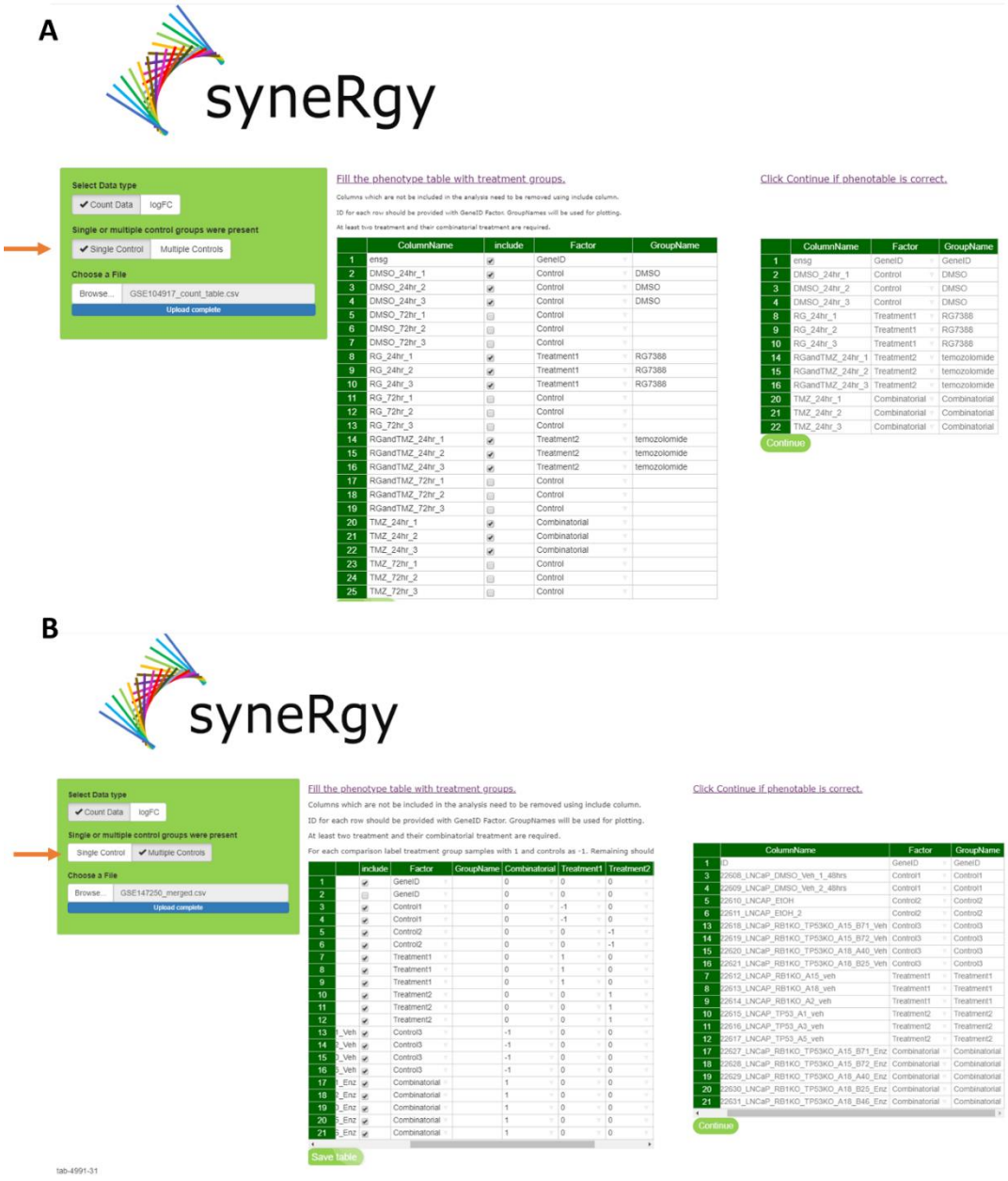

Figure 3.50 The syneRgy app pheno-data panel for studies with single control (A) and in multiple control (B).

3.6.3 Synergy analysis

After differential gene expression analysis and additive and synergy coefficient calculations, syneRgy performs synergy analysis by two different methods as described in methods. I have used as a case study GSE104917 dataset in which NB1691 neuroblastoma cells were treated with MDM2 inhibitor RG7388, DNA alkylating reagent temozolomide or their combination for 24h.

3.6.3.1 Regression-based synergy analysis: *synreg*

Regression-based synergy analysis is based on the hypothesis that if the effect of individual treatments is additive, the outcome of combinatorial treatment needs to be equal to the sum of individual treatments (Additive). Therefore in combinatorial vs. additive plot, the y=x line represents the null hypothesis and the regression line fitted is the alternative hypothesis. The divergence between the two lines represents the overall interplay between individual treatments. Lower the slope means more antagonistic, and higher means synergistic (**Figure 3.51**).

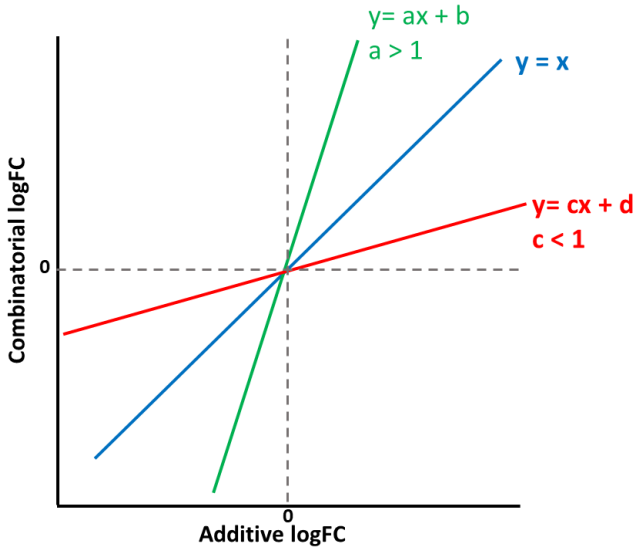

Figure 3.51 Schematic representation of regression-based synergy analysis. Blue, green and red lines represent the Additive/Null hypothesis, synergistic and antagonistic responses, respectively.

In the GSE104917 dataset, the slope is 0.7 and statistically different than one, indicating an antagonistic interplay between RG7388 and temozolomide. In addition to synergy analysis, the regression-based synergy analysis tab allows the user to perform a regression analysis in any

chosen two treatment groups. Comparison of individual treatments with their combinatorial treatment showed that the slope of RG7388 is greater than temozolomide, implying a more dominant effect of RG7388 over temozolomide **(Figure 3.52**).

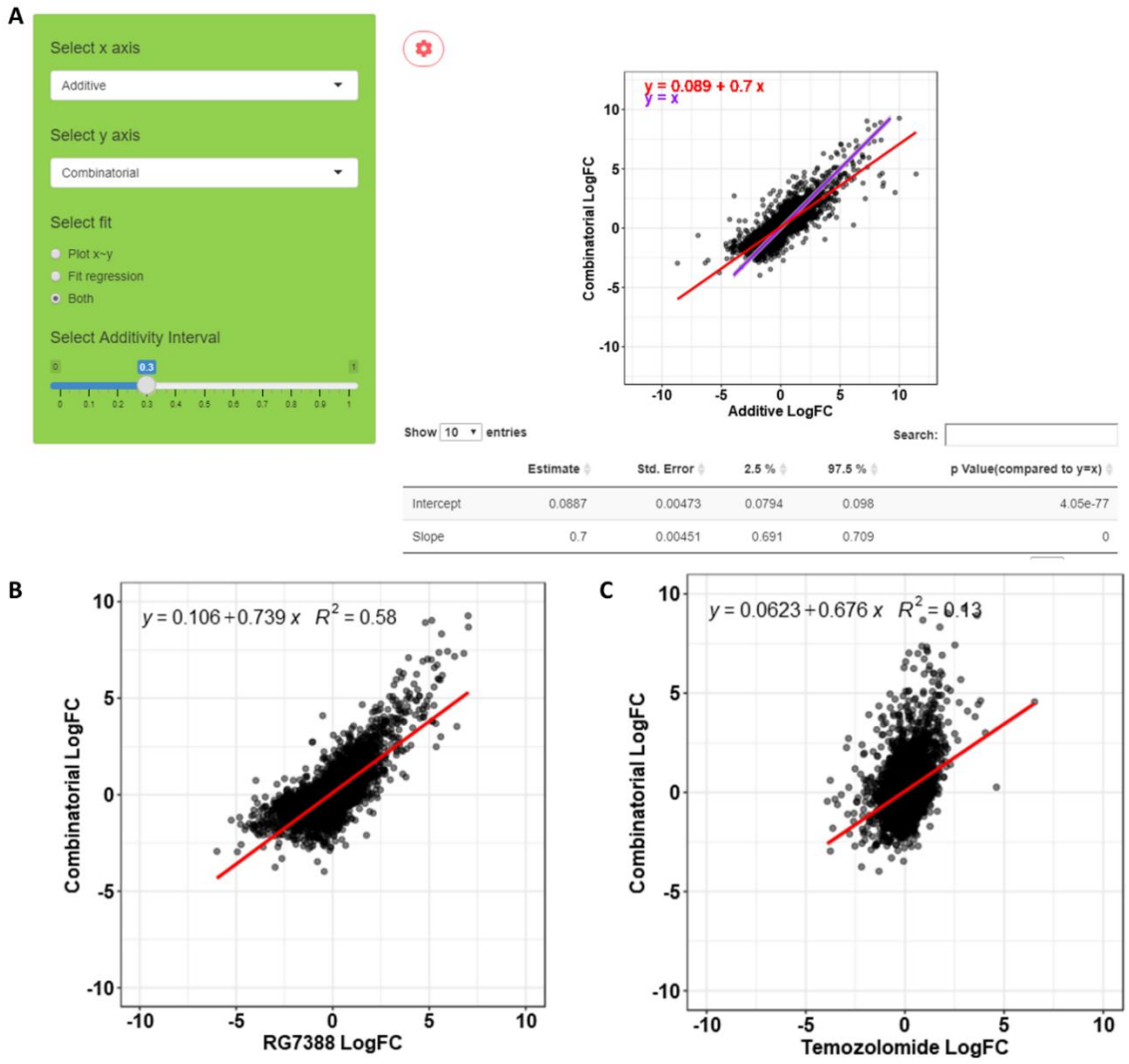

Figure 3.52 syneRgy app: Regression-based synergy analysis user interface (A). Example regression analysis results between combinatorial treatment and RG7388(B) and Temozolomide (C).

3.6.3.2 Limma-based synergy analysis

The recently published method has been implemented as a second synergy analysis option in the syneRgy app. This methodology is based on limma analysis and requires the construction of a contrast matrix (For details, see Methods). When a count matrix is provided, syneRgy performs

limma analysis with the contrast matrix generated; otherwise, it calculates only additive and synergy logFC/coefficients (**Figure 3.53**).

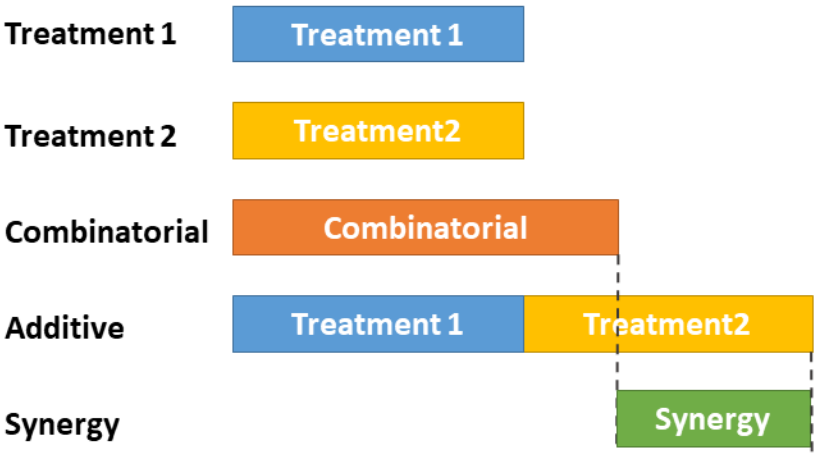

Figure 3.53 Schematic representation of limma-based synergy analysis contrasts. Treatment1, Treatment2, and Combinatorial boxes represent the logFC value obtained compared to the control group(s). The additive is calculated by adding Treatment1 and Treatment2, while Synergy Coefficient is calculated as the difference between the Combinatorial and the Additive.

Synergy coefficient is defined as the difference between additive, the sum of treatments, and combinatorial and is used to identify synergy clusters. The interaction is predicted as synergistic for more.up and more.down genes are while it is antagonistic for less.up and less.down genes. syneRgy generates summary plots for the synergy analysis (**Figure 3.54**).

Scatter plot representation shows the synergy groups' overall behavior and helps identify genes isolated from the rest. In GSE104917, the more.down cluster is smaller, while there are more genes separated from the bundle in more.up and less.up clusters. The second plot of the limma-based synergy analysis is a dot plot of the distribution of the genes significantly altered in at least one of the treatments. The majority of the genes were not changed in temozolomide, but RG7388 and combination. The direction of the change was compatible with each other indicating RG7388 exhibited a more dominant effect in combinatorial treatment. The waterfall plot shows the size of the synergy clusters. The additive cluster was the largest, and antagonistic clusters were more extensive than synergistic clusters. Synergy clusters alone cannot provide insights into how

individual treatments behaved in each synergy cluster. Therefore hierarchical clustering of the genes in each cluster with a heatmap is necessary. Interestingly, in the more.down cluster, both RG7388 and temozolomide alter gene expression to a lesser extent compared to other clusters, and they were more effective in the combinatorial.

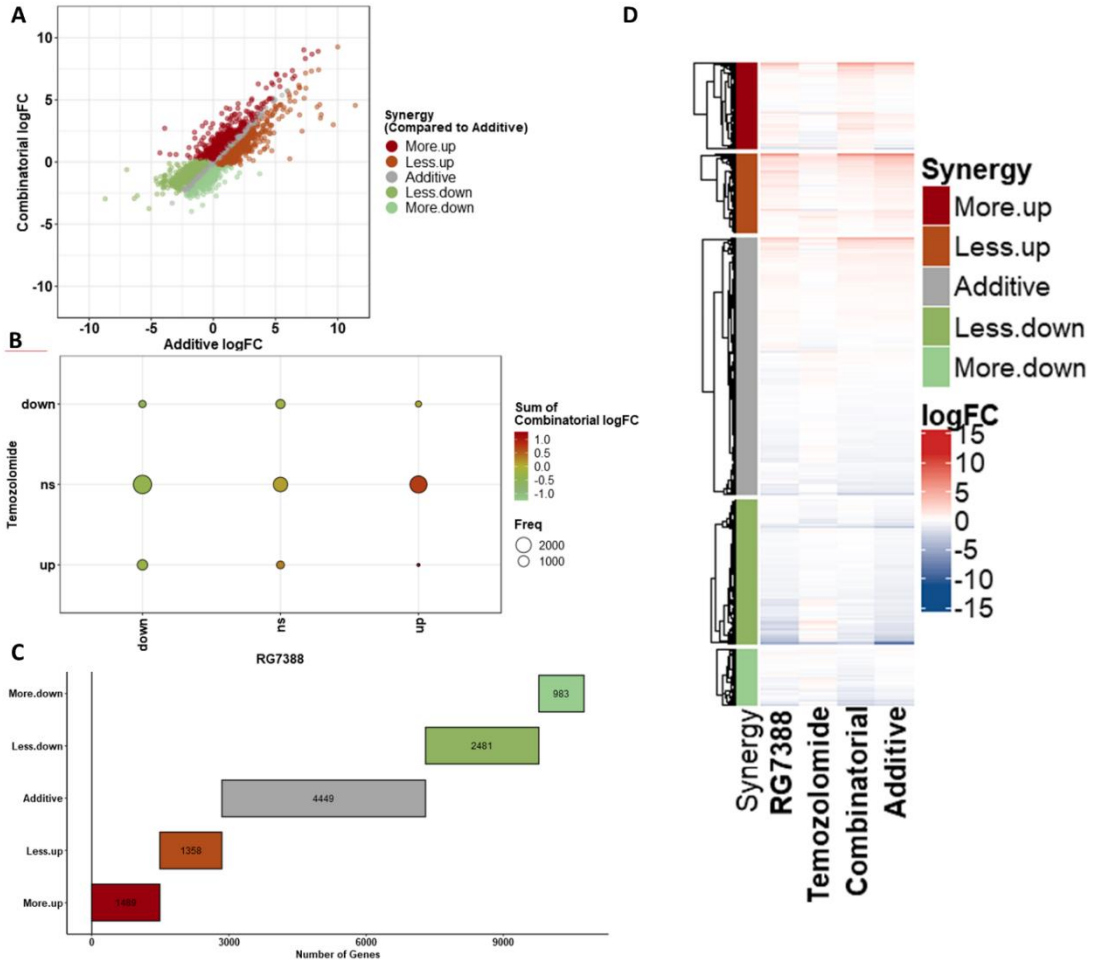

Figure 3.54 syneRgy app: limma-based synergy analysis results

3.6.4 Transcription factor analysis

The last step in the syneRgy app is TF enrichment and overrepresentation analysis. For this module, widely used ChEA3 and DoRothEA data were used.

3.6.4.1 ChEA3 analysis

ChEA3 exhibits an extensive collection of TF target data including, Chip-seq data from ENCODE, ReMap, and literature and coexpression data from ARCHS4 and GTEX. ChEA3 also

provides mean rank and top rank as integrative metrics for the datasets used. syneRgy performs ChEA3 analysis on-fly through connecting their web-server using json and reports the analysis results. E2F4 and FOSL2 were found to be the most significant TFs in the less.down and the more.up clusters in ENCODE database, respectively (**Figure 3.55**).

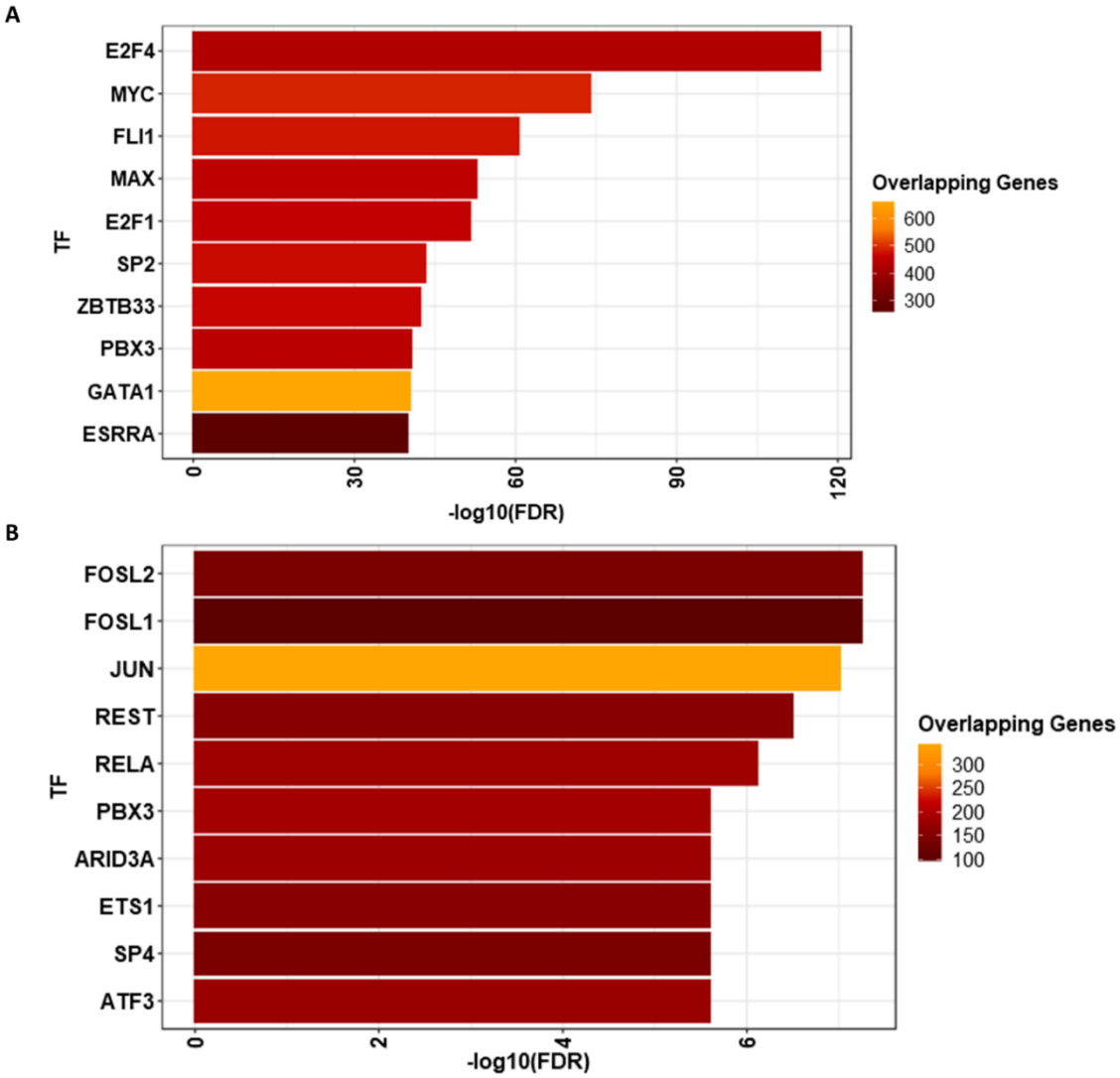

Figure 3.55 syneRgy App: ChEA3 results for the less.down (A) and the more.up (B) clusters using ENCODE database.

3.6.4.2 DoRothEA analysis

DoRothEA is another curated TF-target collection in which the confidence between TF and target was assigned as a letter ranging between A to E. As the authors suggested, syneRgy uses the TF

targets with confidence A and B. As oppose to ChEA3, DoRothEA also provides direction for TF activity in which "-1 "represents inhibition, and "1" represents activation. Since regular enrichment analysis tools cannot be used with the direction information, syneRgy uses the viper algorithm developed for the Aracne networks. For the statistical analysis of the scoring, it performs permutation-based FDR analysis (n=100). It reports the enrichment analysis results and a bar plot of the top user-selected number of enriched TFs in the user-selected group, i.e., top 5 TFs in combinatorial treatment (**Figure 3.56**).

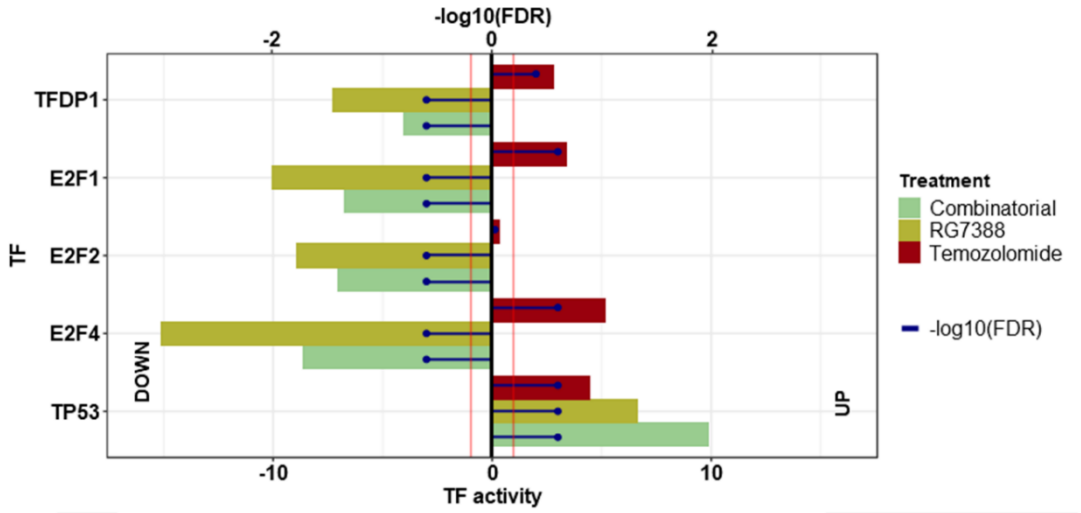

Show 5 entries Search:

	Combinatorial EScore	Combinatorial FDR	RG7388 EScore	RG7388 FDR	Temozolomide EScore	Temozolomide FDR
TP53	9.86	0	6.65	0	4.45	0
E2F4	-8.64	0	-15.1	0	5.14	0
E2F2	-7.02	0	-8.9	0	0.303	0.75
E2F1	-6.73	0	-10.1	0	3.39	0
TFDP1	-4.02	0	-7.26	0	2.78	0.01

Figure 3.56 syneRgy app: TF enrichment analysis using DoRothEA ordered according to enrichment score of combinatorial group.

syneRgy also provides publication-ready plots, i.e., heatmap and regression analysis of the targets of selected TF. Since both RG7388, MDM2 inhibitor, and temozolomide, DNA alkylating agent, are known TP53 activators, TP53 exhibited the highest enrichment score in combinatorial and

altered in the same direction in all treatments (**Figure 3.57**). The slope of the regression line is close to one, although it is significant, indicating their effect is primarily additive. R7388 exhibits more similarity with the combinatorial than temozolomide. On the other hand, E2F4, enriched in the negative direction in RG7388 and combinatorial and positively in temozolomide, suggesting that an inhibitory action of temozolomide in combinatorial treatment. As expected, according to regression analysis, the interplay between treatments was antagonistic (**Figure 3.57**). Interestingly, a group of E2F4 targets is in the more.up cluster, and they are upregulated only in the combinatorial treatment, indicating possible pure synergy, and warrants further study.

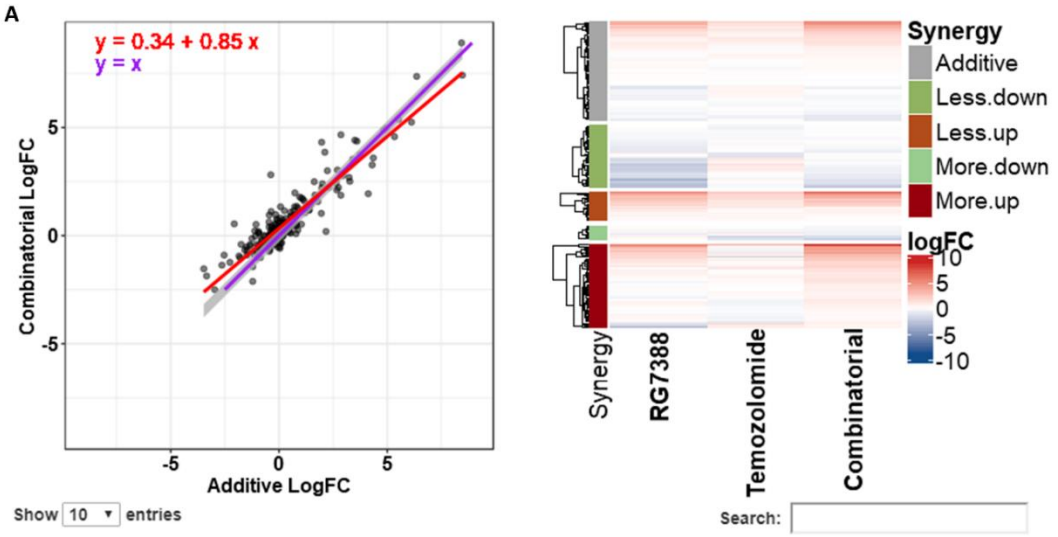

	Estimate	Std. Error	2.5 %	97.5 %	p Value(compared to y=x)
Intercept	0.341	0.0433	0.256	0.427	1.77e-13
Slope	0.85	0.024	0.802	0.897	2e-9

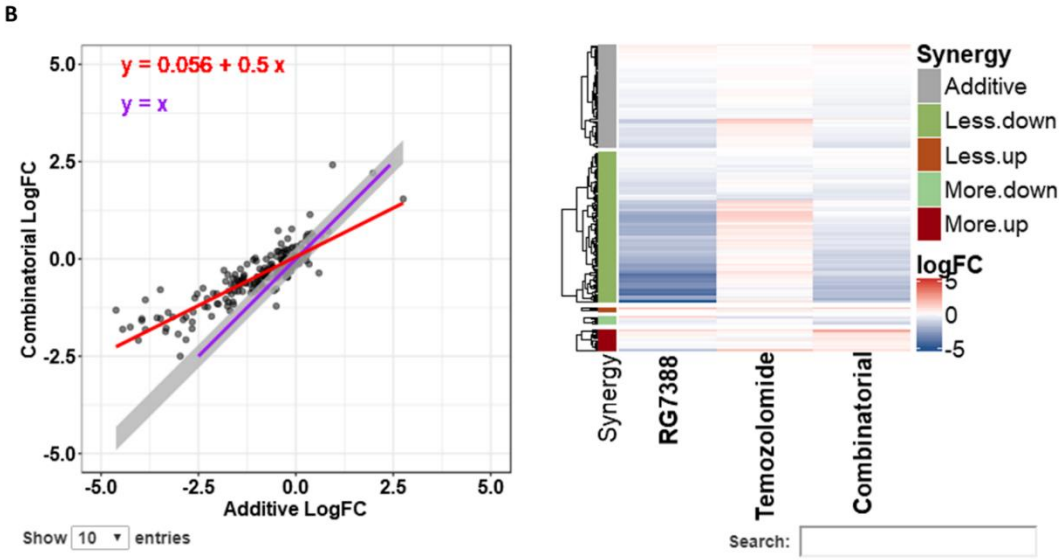

	Estimate	Std. Error	2.5 %	97.5 %	p Value(compared to y=x)
Intercept	0.0562	0.0284	0.000176	0.112	0.0493
Slope	0.501	0.0197	0.462	0.54	1.98e-67

Figure 3.57 Regression plot and heatmap of TP53 (A) and E2F4 (B)

Overrepresentation analysis enables the analysis of the synergy groups as well as up and downregulated genes separately. syneRgy performs overrepresentation analysis using Fisher's

exact test for the statistical analysis. The more.up synergy cluster was enriched with TP53 targets, overrepresented in RG7388 and combinatorial treatment (**Figure 3.58**). FOXM1, a TF part of the DREAM complex, is overrepresented in RG7388 down and temozolomide up genes and not in combinatorial treatment suggesting antagonism between these two treatments.

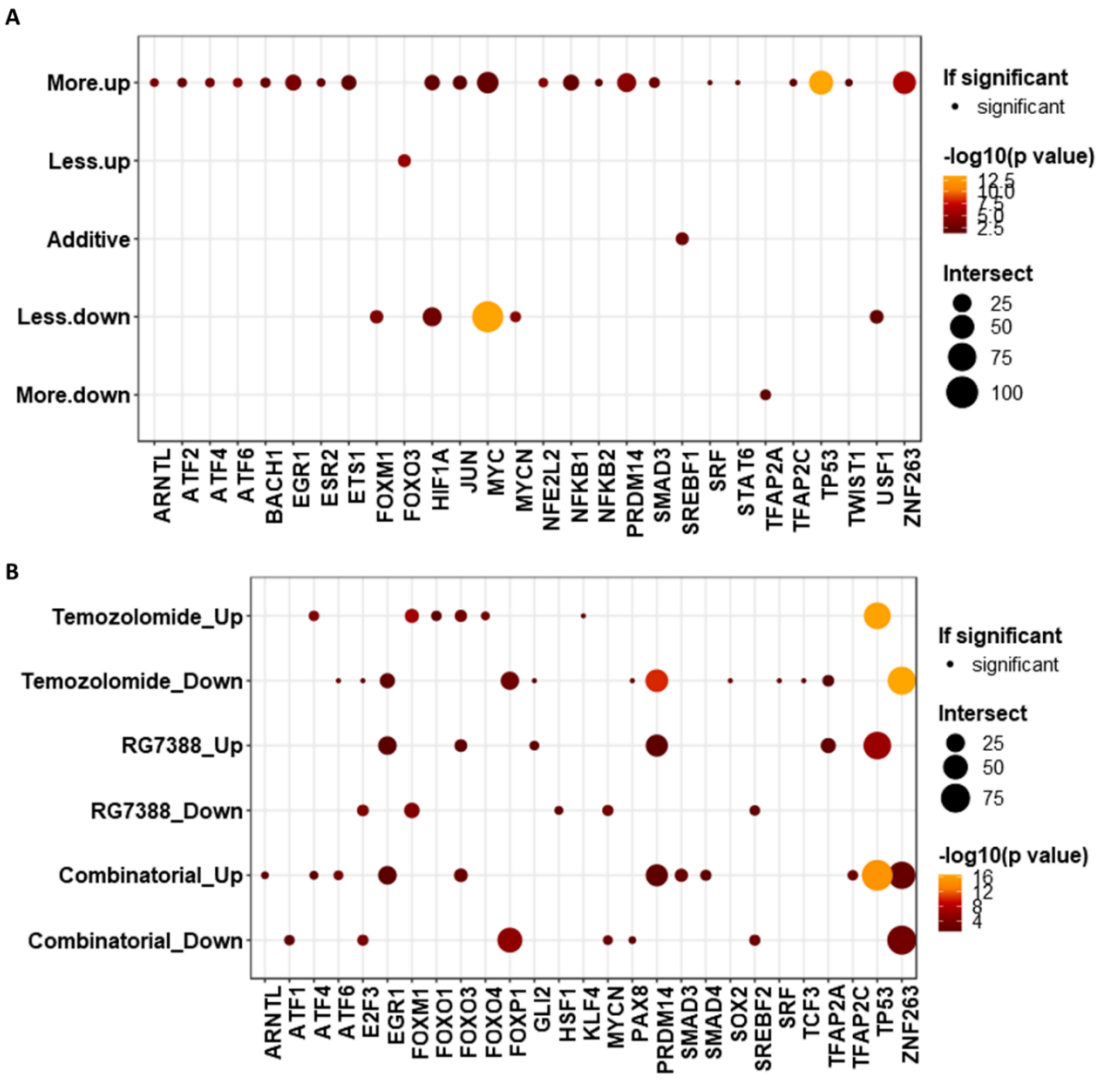

Figure 3.58 TF overrepresentation analysis results for synergy clusters (A) and treatments (B).

4 Conclusions and Discussion

4.1 Synergy analysis

Combinatorial treatment is a widely used technique both in clinics to increase the efficiency of the treatment and in scientific research to decipher cross-talk between proteins and pathways. Due to the complex nature of normal cellular function and diseases, the interaction between pathways becomes more important to study than single treatments. The ease of CRISPR technology and increased knowledge on ncRNAs enhance the modification capacity in *in-vitro* studies to provide deeper insights into molecular functioning. Therefore, there is an increasing number of studies combining genetic modifications, drugs, and knock-down/overexpression models, and transcriptomic profiling using microarrays or RNA-seq that have been frequently employed to understand the underlying mechanism (Diaz, et al., 2020; Kwon, et al., 2017; Nassiri, et al., 2019; Ord, et al., 2021; Vichas, et al., 2021). However, the existing methods are yet to be systematic except the recently published limma-based synergy analysis method (Schrode, et al., 2021). In the present thesis, a new regression-based model has been developed to assess the synergistic and additive behavior of the whole transcriptome and the selected gene sets, i.e., transcription factor (TF) targets.

Moreover, this method has been applied in three different contexts to assess the synergy between a) CHRNA5 and TP53 siRNAs in MCF7 cells; b) CHRNA5 siRNA and miR-495-5p mimic in MCF7 cells; c) RG7388 and temozolomide in the neuroblastoma cell line. The first two have complemented the TF-based molecular mechanisms driving the CHRNA5 action in breast cancer, and the third demonstrated the use of the synergy analysis with respect to an MDM2 inhibitor (TP53 activator) and DNA alkylating agent in neuroblastoma. The versatility of syneRgy via our novel methodology has shown that it is applicable to molecular and combinatorial drug treatments to microarrays or RNAseq transcriptomics datasets. syneRgy is the first application that provides TF target-based enrichment applicable to combinatorial treatment experiments and complements

the only published research by Schrode et al (Schrode, et al., 2021) and uses a novel regression based enrichment methodology.

4.1.1 Strength and limitations of each technique

Linear regression analysis is the oldest and one of the most widely used statistical methods to measure the prediction capacity of a variable over the outcome. Due to its simplicity in computation and biological interpretation, regression-based models have been proposed in different contexts, i.e., gene expression prediction through TF binding or expression level (Ibarra, et al., 2020; Kwong, et al., 2021; Lambert, et al., 2019; Liu, et al., 2019). Liu et al. (2019) applied a linear regression-based machine learning algorithm to predict the relation between the binding of a TF and the target gene expression using Oct4 binding during cell programming as a case study (Liu, et al., 2019). They have reported relatively low accuracy, 76%, which could be due to other factors, i.e., availability of other TFs, repressors, enhancers, and DNA shape. In another study, a regression-based model with the features related to DNA shape and the functional co-occurrence in ontologies to measure the cooperativity between TFs in their target expression was proposed (Ibarra, et al., 2020). They have identified cooperativity between FOXO and Ets family TFs. Linear regression models are not only used for TF binding but also to predict the gene expression from copy number alterations and methylation (Mallik, et al., 2020).

The slope of the regression line has been used to measure the strength of the relation between the variable and the outcome and, even in the multivariate sense, prioritize the variables. In the regular regression analysis, the slope's divergence from zero corresponds to the strength of the interaction. Stepaniants et al. (2014) have developed a model in which they measure the relationship between phenotype, emphysema, and gene expression level through the slope of the regression line to identify the genes that were functional in the emphysema (Stepaniants, et al., 2014). In a time-course study in mice, they fit a regression line between the gene expression levels in the mutant, HD94, and the control mice, and the shift in the slope between time points was used to measure the overall change in gene expression profile (Xu, et al., 2002). Although it is a widely used method, to our knowledge, the regression-based synergy analysis, which we called

synreg, is the first-time ever regression analysis method, applied in the context of transcriptome-based combinatorial treatment and predicting the overall synergistic effect of the combinatorial application.

In *synreg*, the regression analysis has been applied between the summation of the logFC values obtained from the individual treatments (additive) and the combinatorial treatment logFC values; hence the slope was used as a metric for the type and the degree of the synergy if different from 0. In *synreg*, the offset was defined as 1, and divergence from 1 was associated with the synergy coefficient, i.e., if the slope is significantly lesser than 1, the interplay is more antagonistic. The *synreg* analysis focuses on identifying the overall synergistic as well as the antagonistic interplay between treatments for the selected gene sets, yet it cannot further dissect the synergy status of the individual gene.

On the other hand, the recently published limma-based synergy method, which calculates the synergy coefficient for each gene, and therefore was used in the present thesis both as a complement and comparison to *synreg*. Limma is a widely-used, well-established differential gene expression analysis (DEG) method for both RNAseq and microarray data (Ritchie, et al., 2015). Schrode et al.(2021) has proposed using the limma method to calculate gene-wise synergy coefficient and stratify genes into five clusters according to synergy coefficient and combinatorial logFC values (Schrode, et al., 2021). However, to be able to expand the usage of the limma-based method in this thesis, I introduced several modifications that included: 1) adaptation to use with multiple control groups, such that the threshold for the synergy coefficient was only based on the results of the treatment groups while the downstream analysis has been freed from the synergy coefficient and additive logFC; and 2) extension of its use to microarrays from any platform, so that the synergy coefficient and additive logFC values have been calculated without any statistical test (FDR = 0.99), and the threshold for the synergy coefficient was pre-determined as 0.3. However, the obtained results were altered significantly with the change in the threshold for the synergy coefficient both in logFC data and count data. Although meanSE based threshold is statistically sound, further options, e.g. mean standard deviation, and mean coefficient of

variation, should be tested and included in the syneRgy app. Furthermore, the limitation that remains is the use of count data since any differential gene expression analysis for RNAseq data requires raw count data, and limma- and regression-based methods cannot accept RPKM, TPM, or any other form of normalized data. As with other transcriptome-based methods, the power of the analysis depends on the number of biological replicates and the depth of the RNAseq (Baccarella, et al., 2018).

Accordingly, the syneRgy app is applicable to the combinatorial transcriptome datasets (either count or DEG results provided by the user) using Schrode et al.'s modified and our newly developed *synreg* methods upon user's selection. syneRgy provides publication-ready tables and figures. The user can download both the limma for the downstream analysis and TF enrichment results. syneRgy also generates several types of figures, i.e., scatter plots, heatmaps, and dot plots, to enhance the visualization. These provide significant advantages and are possible via the use of Shiny (Chang). The limma-based method, on the other hand, provides more detailed information on the synergistic or additive effect on individual genes, yet it fails to detect the overall or gene-set-based linear impact of each treatment. This was partially overcome by including heatmaps to enhance dissection of the synergy clusters further, i.e., identifying the dominant treatment in the particular synergy cluster.

The syneRgy app is developed to perform transcriptome-based synergy analysis using both microarray and RNAseq data. The syneRgy app accommodates both synergy analysis methods and visualization options to overcome the abovementioned limitations of each method. To our knowledge, it is the first-ever online tool to perform such analysis.

4.1.2 TF enrichment analysis in syneRgy

To provide deeper mechanistic insight into the synergistic and additive interactions between individual treatments, it is fundamental to understand the changes in the transcription factor (TF) activity. Several methods have been proposed to identify altered TFs from gene expression data (Keenan, et al., 2019; Roopra, 2020; Rubin, et al., 2021). However, these tools were designed to

analyze a single geneset at a time, hence do not allow users to compare and contrast the enrichment results from different treatments with each other or their combination.

Therefore, the syneRgy app also contains a unique TF enrichment and overrepresentation analysis using two widely used TF-Target data, i.e., ChEA3 and DoRothEA. In addition to classical TF enrichment analysis methods, i.e., Viper, Fisher's exact test, and hypergeometric test, the *synreg* method also has been implemented for the TF-targets datasets to reveal the overall action of the treatments on the selected TF targeted genes and to determine the general direction and magnitude of TF activity modulation (Alvarez, et al., 2016; Keenan, et al., 2019; Shen L, 2021). Several linear model-based gene set tests have been proposed to overcome limitations of classical TF overrepresentation methods generally based on hypergeometric and Fisher's exact tests, which only consider the significantly regulated target number over the total number of TF targets in the background (Abatangelo, et al., 2009; Falcon S., 2008). Gatti et al. (2010) is the first proposed correlation-based gene set test method (Gatti, et al., 2010). Later Wu et al. (2012) proposed a well-known intergene correlation-based approach, Camera, in which the expression data was further normalized to remove the treatment effect (Wu and Smyth, 2012). In addition, Lasso and Elastic-net-based regression-models have also been developed to test multiple geneset in a given dataset (Frost and Amos, 2017; Zhang, et al., 2017). Although these methods overperform the overrepresentation analysis, they fail to compare two datasets. The *synreg* for TF targets in essence measures the shift of the TF activity between additive and the combinatorial treatment. It generates consistent results with existing tools included, yet it provides more biologically interpretable results. Its usage can be further expanded to the comparison between any two logFC profiles.

The syneRgy app considers not only synergy clusters (e.g., more.up, more.down) for the TF enrichment analysis but also treatment groups, i.e., up or downregulated genes in each treatment. The TF enrichment module analyzes individual and combinatorial treatments along with computed additive and synergy coefficients which allows users to visualize TF enrichment results for all groups on the same plot/table. It accelerates identifying differentially modulated TFs, the

direction of their activity, and the change in the expression levels of their targets using well-established and widely used methods (see Methods, for details). Similar visualization approaches have been applied for gene ontology terms (GO) and KEGG pathways and are proven to be valid by several studies with multiple comparison groups (Doldi, et al., 2015; Huang, et al., 2015; Khraiwesh, et al., 2015; Spinelli, et al., 2015; Wu, et al., 2021). Since syneRgy analysis is based on the comparison of individual and combinatorial treatments, it could be crucial to gain deeper insight into changes in transcriptional regulation.

4.2 TP53 signaling and DNA damage response in neuroblastoma cells

As an example of the application of *synreg* and syneRgy, I have used a public dataset GSE104917, in which two drugs were used individually and in combination. Briefly, the novel MDM2 antagonists RG7388 and/or temozolomide-treated neuroblastoma cell lines were studied (Chen, et al., 2019). Neuroblastoma is the most common cancer type in children younger than age five; and arises from immature neural crest cells and is found dispersed in many areas of the body but primarily the adrenal glands (Farina, et al., 2021; Park, et al., 2010). Low and intermediate-risk neuroblastoma can be treated with surgery alone, yet the survival rate for high-risk neuroblastoma with MYCN amplification remains less than 50% (Mahapatra and Challagundla, 2021). Moreover, most of the survivors suffer from severe side effects of long-term usage of the chemotherapeutic agents at a very early age (Friedman and Henderson, 2018). Therefore, there is an effort to decrease the toxicity and the exposure time to chemotherapy via increasing the efficiency of the therapy (Du, et al., 2012; Zage, et al., 2010). Although most neuroblastoma tumors harbor wild-type TP53, MYCN mediated inhibition of the TP53 pathway has been shown (Chen and Tweddle, 2012; Christiansen H, 2015). Therefore use of TP53 inducing agents, i.e., DNA damage inducers, MDM2 inhibitors, have been proposed as a therapeutic strategy for MYCN amplified neuroblastoma (Diskin, et al., 2014; Van Maerken, et al., 2009). Accordingly, the synergy analysis of this dataset was an important one to identify what happens to TF activity if these two drugs, RG7388 and temozolomide, were used in combination and whether any of the

TF activity can explain the synergistic effect observed by the authors. In addition, this example provided a use case for the syneRgy app and demonstrated its wide range of applications.

It is hypothesized that RG7388 as an MDM2 inhibitor would inhibit the MYCN mediated TP53 inactivation, and temozolomide would induce TP53 via DNA damage; hence together, they would result in increased stability of TP53 and therefore tumor growth inhibition through cell cycle arrest and/or apoptosis. Their synergy analysis using cell growth inhibition revealed a moderate synergism at a higher dosage (2x CI_{50}) and nearly additive at CI_{50} or lower dosages (Chen, et al., 2019). In accord with their in-vitro tumor growth inhibition and mice xenograft results, the use of *synreg* in syneRgy demonstrated that RG7388 exhibited a more dominant effect than temozolomide, and the overall action between the two treatments is moderately antagonistic (slope =0.7 and p-value 2e-16). The reasons for this would remain unclear; however, similar results were observed in another study with HDAC inhibitors, known to induce DNA damage, and MK-1775, a novel WEE1 inhibitor inducing G2/M arrest (Hoffmann, et al., 2021). They have also reported an antagonistic interplay between the two treatments and identified that both HDAC1 inhibitors and MK-1775 target the CDK1-CCNB1 complex to lead to cell death as a possible cause for antagonistic action. Therefore downstream analyses are required to understand the underlying mechanism further.

In the original study, as with many other combinatorial drug transcriptomic comparisons, the authors analyzed their RNAseq data through the Venn diagram approach; and they then employed GSEA for the functional analysis. GSEA analyses have identified TP53 and MYC targets. However, since they didn't analyze the individual treatments separately, it is hard to make any conclusion on the impact of each treatment and their synergy level. The TF enrichment analysis using DoRothEA data showed that TP53 was activated in both treatments and more in combinatorial treatment; however, their overall activity was lower than the sum of the individual treatments (slope =0.85, p-value = 2e-9). To dissect the effect of individual treatments further, heatmap representation was investigated, and the TP53 induction in temozolomide was to a lesser extent than RG7388, which is in accord with the qPCR results for TP53 targets in the original

paper. Interestingly, in addition to TP53 and MYC, which were found in the original study, syneRgy analysis identified that E2Fs (E2F1 and 4) and their co-regulators TFDP1 as activated in temozolomide while inhibited in both RG7388 and the combinatorial treatment. Temozolomide treatment even inhibited the RG7388 activity in the combinatorial treatment. The activation of E2Fs by temozolomide which wasn't identified in the original study could be the underlying mechanism of the antagonism between temozolomide and RG7388. Overall, syneRgy produces consistent results with the in-vitro and in-vivo results in the original data while providing a novel leads, e.g., E2Fs, as possible key players in the antagonistic interplay between two treatments, which can be tested further.

4.3 CHRNA5 and DNA damage response

CHRNA5 is a nicotinic cholinergic subunit expressed not only in the peripheral nervous system but also in many other tissues. Previously in our lab, CHRNA5 was successfully downregulated via three different siRNAs (siCHRNA5) in breast cancer cell lines, and the siCHRNA5 transcriptome in MCF7 cell lines was profiled using microarrays (Cingir Koker, et al., 2018). My analysis for the enriched KEGG pathways using the GSEA tool revealed that TP53 signaling was induced while various DNA damage repair and response pathways (DDR) were downregulated (Cingir Koker, et al., 2018). Previously, the polymorphisms in the CHRNA5-CHRNA3-CHRNB4 locus have been shown to be associated with DNA damage in lung tumors and patients with Alzheimer's disease (Dorszewska, et al., 2005; Tekpli, et al., 2013). Although studies on nACHRs and DNA damage are scarce, the correlation between cholinergic system activity and the accumulation of DNA damage in the brain has been reported (Cristofaro, et al., 2018; Di Bari, et al., 2015; Fayzullina and Martin, 2016; Ginzkey, et al., 2014; Verde Rodrigues, et al., 2014; Zhu, et al., 2015). Interestingly, both inhibition and the induction, through nicotine and its agonist, respectively, of the cholinergic system have been shown to increase the DNA damage. Therefore, I further analyzed the two most extensive breast cancer datasets, TCGA and METABRIC, for the expression levels of CHRNA5 along with DDR genes (Curtis, et al., 2012).

I found that CHRNA5 clustered together with those DDR genes upregulated in TP53 mutant tumors (Cingir Koker, et al., 2018; Knijnenburg, et al., 2018). Furthermore, to validate the relationship between CHRNA5 and DDR genes, I calculated the correlation between siCHRNA5 logFC values with the correlation coefficients between CHRNA5 and DDR genes. This type of coexpression method is widely used in the transcriptomics field (Liu, et al., 2020; Nath, et al., 2015; Peyre, et al., 2010). High negative correlations obtained from both TCGA and METABRIC datasets have further supported the possible causative relation or at least the association between CHRNA5 and DDR. In addition, the altered genome fraction percentage indicating the accumulation of DNA damage has been found to be positively correlated with CHRNA5 expression in TCGA and CCLE cell line dataset, which was not shown before.

CHRNA5 knockdown has been shown to increase the cytoplasmic calcium levels in bronchial cells (Krais, et al., 2011). Since calcium is the universal secondary messenger for several key pathways, there are an increasing number of studies focusing on identifying role of calcium in normal cell physiology (Humeau, et al., 2018; Kahl and Means, 2003; Takuwa, et al., 1995). Increased cytoplasmic calcium level in the cell has been associated with cell cycle arrest through calmodulins (Colomer, et al., 1994; Kahl and Means, 2004; Takuwa, et al., 1995). In addition, cellular calcium level has been associated with DNA damage through the release of reactive oxygen species (Delierneux, et al., 2020; Korzets, et al., 1999; Li and Cao, 2014; Palluzzi, et al., 2017; Rosenblatt, et al., 2021). Several others have shown the regulatory role of calcium on the DDR genes (Baek, et al., 2016; Bugreev and Mazin, 2004). Taken together, the increased cellular calcium level with CHRNA5 depletion could induce DNA damage yet decrease the DNA damage response through inhibition of nuclear localization of DDR proteins or direct inhibition.

4.3.1 Functional analysis with siTP53

Sahika Cingir-Koker has validated in-silico findings via in-vitro experiments, i.e., drug sensitivity assays using MTT, western blots, and qPCRs (Sahika Cingir-Koker, Ph.D. Thesis, 2019). The decrease in the p-CHEK1 level and increase in the g-H2AX, indicating increased DNA damage yet decreased DDR, in response to siCHRNA5, has been shown in the MCF7 cell line but not in

TP53 mutant BT20 and MDA-MB-231 cell lines. In accord with that, siCHRNA5 has increased the sensitivity to DNA damage-inducing agents, doxorubicin and camptothecin, in MCF7 cells but not in BT20 and MDA-MB-231 cell lines.

In-silico analysis along with in-vitro experiments have implicated the strong association between DDR and siCHRNA5 in TP53 wildtype MCF7 cells but not TP53 mutant cells. The disparity in response to siCHRNA5 in the context of DDR in TP53 mutant and wild-type cell lines has given rise to the hypothesis that siCHRNA5 may need a functional TP53 to suppress DDR, induce apoptosis, and result in drug sensitivity. Therefore, I treated cells with siCHRNA5 and siTP53 alone and in combination. I first optimized and validated the siTP53 treatment alone with increasing concentration. Visual inspection through DIC microscopy revealed an increase in cell number. In accord with previous results (Ermira Jahja, Ph.D. Thesis, 2017), the siCHRNA5 phenotype was still observable in combinatorial treatments indicating the partial EMT observed in siCHRNA5 treatment groups was TP53 independent.

I further profiled the siTP53 and siCHRNA5 transcriptome using RNAseq. The correlation and the regression analysis revealed the dominant effect of siTP53 in combination treatment. Furthermore, comparative transcriptomics analysis with TP53 inducers revealed that siCHRNA5 clustered together with TP53 inducers while combinatorial treatment clustered separately, further supporting the TP53 induction with siCHRNA5 rescued with siTP53. KEGG pathway enrichment analysis with synergy clusters revealed that DNA replication and DDR pathways were enriched in the less.down cluster. Interestingly, in heatmap representation, this cluster could be stratified into two: 1) downregulated in siTP53 and 2) upregulated or no change in siTP53. As expected, most of the DDR genes were found to be in cluster 2. The syneRgy app heatmap and KEGG analysis of the TP53-CHRNA5 combinatorial depletion experiment have provided strong support for this in-silico analysis. In addition, the pCHEK1 level, along with the total-CHEK1 levels, exhibited a rescue trend in combinatorial treatment. I also observed a decrease in BAX/BLC2 ratio, which is an apoptosis marker. These in vitro studies at the protein level complemented the abovementioned findings (**Figure 4.1**).

TP53 is an unstable protein in physiological conditions, and it is stabilized by DDR activity, i.e., ATR, CHEK1, and CHEK2 (Bartek and Lukas, 2003). Yet, we have observed the induction of TP53 with decreased pCHEK1 levels, indicating a possible reciprocal relationship between TP53 and CHEK1. Previously, the negative indirect regulatory role of TP53 on CHEK1 and CHEK2 in HCT116 cells has been reported (Gottifredi, et al., 2001). They have also shown that increased TP53 levels by ectopic expression could inhibit CHEK1 even without any DNA damage induction. Interestingly, in siCHRNA5 treated samples, not only TP53 target, CDKN1A but also TP53 itself were upregulated, further supporting increased stability of TP53 in siCHRNA5 treated MCF7 cells. Altogether our model indicates the TP53 can inhibit DDR, and the inhibition of DDR by siCHRNA5 requires functional TP53 supporting reciprocal interplay between DDR and TP53, yet future studies are needed (**Figure *4.1***).

4.3.2 SyneRgy TF analysis with siTP53 and siCHRNA5 and their combination

SyneRgy TF enrichment analysis was most valuable to identify TFs and downstream targets that might be driving the effects of CHRNA5 or TP53 knock-down or their combination. Based on Schode et al.'s methodology, TF analysis leading to the less.down cluster revealed an enrichment of FOXM1, E2F1, and MYBL2, which have been shown to be overexpressed/activated in TP53 mutant breast tumors (Pfister, et al., 2018). Indeed, FOXM1 targets were mostly downregulated in siCHRNA5 and changed in the opposite direction in siTP53. FOXM1 has been shown to be decreased upon DNA damage in TP53 dependent manner in MCF7 cells (Barsotti and Prives, 2009). I next investigated the change in the PLK1, which phosphorylates FOXM1 to activate its transcription activity, including PLK1 itself (Fu, et al., 2008; Marceau, et al., 2019). In the combinatorial treatment, a trend to recover the decrease in the PLK1 level in siCHRNA5 was observed. CDK2 is another regulatory factor for FOXM1 activity. Although there was no difference in siCHRNA5 and siTP53, a decreasing trend was observed in the combinatorial treatment. CDK2 is also a regulator for E2F along with CCND1, both of which also exhibited a decreasing trend. A decrease in CDK2 and CCND1 levels in TP53 knockout models in response

to DNA damage-inducing agents has been reported (Bacevic, et al., 2017). However, further studies are needed to understand the observed decrease in pRB, CDK2, and CCND1 levels and their relation to cell cycle distribution (**Figure 4.1**).

Since siCHRNA5 increases sensitivity to topoisomerase inhibitors, doxorubicin and camptothecin, only in TP53 wild-type MCF7 cells (Cingir Koker, et al., 2018), I further investigated the drug sensitivity in the absence of TP53. MCF7 cells were treated with an increasing dosage of doxorubicin ranging from 0.06uM to 0.250uM together with siCHRNA5 and/or siTP53 for 72h. The rescue trend was observed in the control group (DMSO-only) between siCHRNA5 and combinatorial treatment, whereas siTP53 exhibited an increasing trend. In 0.06uM and 0.125uM treatment groups, siTP53 treatment reverted the decrease the cell viability in siCHRNA5 treated groups. However, although there was a trend at the highest dosage, no significant difference was observed between treatment groups as previously shown in osteosarcoma cells (Sun, et al., 2016). Since TP53 is not stable in physiological conditions, siTP53 treatment without DNA damage induction was found to be ineffective in altering cell viability, while rescue effect was observed upon DNA damage induction (Huun, et al., 2017; Liu and Di Wang, 2019; Sun, et al., 2016). The rescue effect of siTP53 on siCHRNA5 further highlighted the siCHRNA5 profile on DDR partially depends on the functional TP53.

4.3.3 Cross-talk between estrogen signaling and TP53

Several studies have been reported focusing on the cross-talk between TP53 and estrogen (E2) signaling (Bailey, et al., 2012; Fritah, et al., 2005; Konduri, et al., 2010; Liao, et al., 2014; Liu, et al., 2006; Mandal and Davie, 2010). E2 treatment has been reported to revert the doxorubicin-mediated cell death, while inhibition of E2 signaling through Fulvestrant can further decrease the cell viability (Bailey, et al., 2012). In another study, ESR1 has been shown to bind to TP53 directly to prevent its transcriptional activity (Liu, et al., 2006). Furthermore, the TP53-ESR1 complex can recruit co-repressors, i.e., NCoR and HDAC, to promoters of the TP53 targets (Konduri, et al., 2010). The TP53-ESR1 complex, on the contrary, has been reported to enhance the expression of mitochondrial genes and functions (De Vitto, et al., 2020). Therefore, I also

included in my thesis the analysis of a dataset with E2, doxorubicin, TNF treatments alone and in combination to compare with the actions of siTP53 and siCHRNA5. Combinatorial treatment with doxorubicin and E2 exhibited a positive correlation with doxorubicin and other TP53 inducers, while negative one with E2 alone. In accord with our previous findings, siCHRNA5 positively correlated with doxorubicin and E2 combinatorial treatment while siTP53 and siCHRNA5 double knock-down group positively correlated with E2 and TNF. As it is important to support in silico findings with in vitro or in vivo experiments, I further investigated the expression levels of several ESR1 targets using qPCR. Except for SCNN1A and LAMC1, the siCHRNA5 effect has been reverted by siTP53 indicating a possible negative modulatory effect of TP53 on some of the ESR1 targets. Since both SCNN1A and LAMC1 are associated with epithelial to mesenchymal transition (EMT), I also investigated the change in the expression levels of AQP3 and CLDN1 (Chen, et al., 2014; Fujiwara, et al., 2007; Peixoto, et al., 2019). siTP53 enhanced the siCHRNA5 effect on both AQP3 and CLDN1. My results suggested, the siCHRNA5 action on EMT markers might be independent of TP53; however, further studies are required.

4.4 CHRNA5 in estrogen signaling

A novel interaction between CHRNA5 and E2 signaling has been studied in our lab since early 2010s (Sila Özdemir, MS Thesis, 2014, Huma Shehwana, Ph.D. Thesis, 2018; and this thesis). Eventually, CHRNA5 has been identified as an E2 response gene and exhibited differential expression in ER+ and ER- breast cancer tumors and cell lines (Shehwana, et al., 2021). My contribution to this finding was through in silico data analysis of public datasets relevant to the examination of this association. I have analyzed publicly available two ChIP-seq (GSE117941 and GSE14664) datasets for ESR1 and a GRO-seq (GSE27463) dataset for newly transcribed mRNAs. These datasets were analyzed first time in the literature together allowing us to extract primary targets that therefore increases the novelty of our study. Although the datasets were selected from the same cell line, MCF7, same exposure time, 40min, and similar growth conditions, the ESR1 targets were found to vary between datasets, i.e., only 9.4% (n=722) of the

total number of genes found in three datasets were common in all. In collaboration with Huma Shehwana, a limma-based secondary target score (PS score) was calculated using public GSE8597 (Bourdeau, et al., 2004). PS score, which is based on re-analysis and scoring of the results of the public dataset of E2 exposure in MCF7 with or without cycloheximide, also is a novel addition to the E2-ESR1 signaling research since we have found that it has prognostic significance (Shehwana, et al., 2021). Previous to this, there has not been a strong emphasis on the identification of the decoupling or coupling of primary and secondary signaling of E2-ESR1. Shehwana, Keskus et al. 2021 study has shed an intense light on how decoupled they are and also identified potential reasons why this could be the case rather than coupling.

In my studies, I also performed analyses with TCGA samples for primary and secondary estrogen targets showed a tighter clustering of secondary targets as opposed to the primary targets. This might suggest that there might be coordinated regulation of secondary targets with one or a few TFs or transcriptional regulators, i.e., FOXM1, E2Fs as TFs targeting more than 70%.

Starvation can induce cell cycle arrest and apoptosis, which can be reversed by E2 treatment (Mirzamohammadi, et al., 2016). Therefore, I further compared the expression profile of siCHRNA5 with E2 treatment and starvation datasets. The secondary targets were downregulated with siCHRNA5 and starvation while upregulated by E2 treatment. The primary targets with high PS scores (also secondarily induced) were downregulated, while those with low PS scores (pure primary targets) were either upregulated or not altered. The secondary targets downregulated by siCHRNA5 were also negatively correlated with CHRNA5 in TCGA dataset, while primary targets exhibited a more dispersed pattern. This could be because most of the secondary targets were regulated by E2Fs and/or FOXM1, a binding partner of ESR1, while the activity of ESR1 in primary targets depends on the availability of co-regulators (Shehwana, et al., 2021).

Again I used in vitro experiments to further decipher the link between siCHRNA5 and E2 signaling, MCF7 cells were treated with increasing dosage of siCHRNA5 for 72h and 10nm for 120h. The change in the expression levels of selected primary and secondary targets of ESR1 was measured with qPCR. In accord with microarray results, primary targets, except DTL, MYBL1,

TFF1, and FHL2, were upregulated in a time and dosage-dependent manner. DTL, MYBL1, and TFF1 also exhibited high PS scores indicating secondary activation and downregulated upon siCHRNA5 treatment. The increase in the primary target expression was reduced in 120h of siCHRNA5 treatment, supporting the presence of a negative feedback loop in E2 signaling (Ellison-Zelski, et al., 2009; Wang, et al., 2017; Yu-Rice, et al., 2016). AREG identified as a primary target in both ChIP-seq datasets but not in the Gro-Seq dataset and also in the literature with specific experiments was upregulated with siCHRNA5 treatment and clustered with the primary targets (Peterson, et al., 2015). These findings suggest that CHRNA5 depletion may induce primary targets but not all of them. The distinction here could be due to primary targets of estrogen can be modulated by other co-regulators and also through inhibition of secondary targets forming a negative feedback loop (Ellison-Zelski, et al., 2009; Xiao, et al., 2018). On the other hand, most of the secondary targets are downregulated, and this may be due to the downregulation of a primary target or through induction of TP53, whose knock-down rescued the siCHRNA5 effect (**Figure *4.1***). Future studies should consider CHRNA5 depletion in the absence of ESR1 and E2F family members and/or Rb1 to identify the synergism between these two crucial cross-talking molecules.

The cross-talk between estrogen signaling and the cholinergic system has previously been studied. A decrease in cognitive functions in the aging brain upon E2 depletion in menopause has been reported in rodents and non-human primates. Indeed, the maze learning rate decreased in rats undergone ovariectomy, a menopause model, and rescued with an E2 supplement (Gibbs, 2002; Gibbs, et al., 2004; Gibbs and Johnson, 2008). The rescue effect of E2 on post-menopausal women has been reported to be task-specific, i.e., the requirement of long and short-term memory (Binder, et al., 2001; Janowsky, et al., 2000; Phillips and Sherwin, 1992; Sherwin, 1988). The protective role of estrogen over cognitive functioning was proposed to be through the cholinergic system (Gibbs and Johnson, 2007; Johnson, et al., 2002; Luine and McEwen, 1983; Uppman, 1978). Although the involvement of E2 in cognition, the studies focusing on the underlying mechanism are limited, i.e., mitochondrial function and inflammation (Cipolla, et al., 2009;

Mosconi, et al., 2017). Therefore, our studies provide a novel link between the cholinergic system and E2 signaling in breast cancer, via the crosstalk with CHRNA5, which could be further studied in neurodegenerative disease in an aging brain, i.e., Alzheimer's disease.

4.5 CHRNA5 and 14q32.31 miRNA cluster

siCHRNA5 can induce cell cycle arrest, drug sensitivity, and apoptosis through induction of TP53 and inhibition of E2 signaling (Cingir Koker, et al., 2018; Shehwana, et al., 2021). To decipher further the regulatory components of the siCHRNA5 profile, we examined the changes in miRNA expression in response to siCHRNA5 (Basak Ozgursoy, MS Thesis, 2017, Sahika Cingir-Koker, Ph.D. Thesis, 2019, Rafed Said Tiryaki, MS Thesis, 2019; and this thesis). The main molecular assessment in the present dissertation was two-fold: a) finding which miRNAs were downregulated by CHRNA5 siRNA and b) testing whether upregulation of these downregulated miRNAs by using mimics rescues siCHRNA5 profile. This combinatorial treatment concept applied to a gene siRNA and miRNA mimic has been used in the literature and found to be helpful in dissecting the noncoding regulatory elements of a gene's action (Babu, et al., 2017; Larsson, et al., 2017; Wang, et al., 2021).

In our analysis, we had a striking finding such that chromosomal enrichment analysis results indicated siCHRNA5 decreased the expression level of the 14q32.31 miRNA cluster associated with tumorigenesis, metastasis, and drug resistance in several cancer types (Gattolliat, et al., 2011; Hill, et al., 2017; Hoppe, et al., 2016; Krokker, et al., 2021; Sellers, et al., 2019). In accord with the literature, expression analysis with TCGA and METABRIC revealed that 14q32.31 miRNAs were highly correlated with each other in our analysis, yet the expression level varies between miRNAs suggesting variation in the transcription efficiency and post-transcriptional regulations through lncRNAs (Gonzalez-Vallinas, et al., 2018; Hoppe, et al., 2016; Uppal, et al., 2015).

In this thesis, the 14q32.31 miRNA cluster was found to be less expressed in breast tumors than in healthy tissue. Among tumors, normal-like tumors exhibit the highest expression. Normal-like tumors have often been neglected in studies and considered contamination of normal breast tissue

due to their high molecular resemblance (Chen, et al., 2021; Parker, et al., 2009). However, several others classified them as triple-negative (Garrido-Castro, et al., 2019; Li, et al., 2015; Liu, et al., 2014; Zeng, et al., 2017). In my analysis, with estrogen targets, normal-like patients exhibited a distinct expression pattern compared to normal breast tissue and formed a tight cluster in which secondary targets were upregulated whereas primary targets were downregulated, indicating expression levels of estrogen targets can separate normal-like breast cancer cells from both basal-like and normal. The primary and secondary target geneset can be further analyzed and included in breast cancer subtype stratification, which could increase the prediction capacity.

4.5.1 Regulation of DLK1-MEG3 region

Several studies reported 14q32.31 miRNA cluster is regulated through the methylation and copy number alteration (CNA) of the DLK1-MEG3 region (for details, see Section 1.5.3.1). Methylation and CNA analysis showed that both methylation and deletion were increased in ER-negative patients (Shehwana, et al., 2021). I have also found that the 14q32.31 miRNA expression score was negatively correlated with ESR1 protein level in the LumA subtype. In addition, E2 treatment has been shown to exhibit chromosomal remodelling function using ATAC-Seq and in that data DLK1-MEG region has become available upon E2 treatment (Guan, et al., 2019). Therefore I examined the change in the DLK1 expression level in response to E2 and siCHRNA5. I found DLK1 decreased with siCHRNA5 but not with E2 treatment except ZR75. Differential binding of ESR1 to suboptimal binding regions in different breast cancer cell lines has been shown (Jia, et al., 2016; Joseph, et al., 2010). Besides, my in-silico analysis with time course E2 treatment datasets revealed that secondary target expression starts after 3h of E2 treatment. In the E2 treatment panel I used, cells were treated with E2 for 24h. Therefore DLK1 could be induced in ZR-75 secondarily.

E2F3 has been reported to regulate DLK1 expression in mice. However, among five human ChIP-seq datasets for E2F binding, I found a weak enrichment in DLK1 promoter in only one of the ChIP-seq datasets (McNair, et al., 2018). Since the DLK1-MEG3 region is controlled through methylation, several other factors might have played a critical role in the DLK1 regulation.

Multivariate analysis with TF expression and binding as well as DNA methylation status are required to further understand the regulatory factors for the 14q32.31 region.

4.5.2 miR495-3p as an anti-estrogen

Furthermore, transcriptomic profiling of miR495- 3p, miR376a-3p, and miR409-3p alone or in combination with siCHRNA5 with microarrays as well as *synreg* analysis revealed that siCHRNA5 exhibits a more dominant effect over the miRNAs. Ingenuity Pathway Analysis (IPA) showed that the estrogen-mediated S-phase entry pathway was downregulated in all groups, i.e., siCHRNA5, miR495-3p mimic, and their combination. In a xenograft study in mice, miR495-3p has been reported to induce cell cycle arrest and decrease tumorigenesis (Wang, et al., 2015). Previously, miR495-3p has been shown to cause G1/S arrest alone or with siCHRNA5 in MCF7 cells (Sahika Cıngır-Koker, Ph.D. Thesis, 2019). Therefore, I further analyzed the estrogen targets in response to miR495-3p treatment. miR495-3p exhibited a negative correlation with E2 and a positive one with SERM/SERDs except for tamoxifen, a partial agonist of E2. miR495-3p was found to be highly correlated with Fulvestrant, a selective estrogen degrader. These findings further highlight the anti-estrogenic action of miR495-3p. Although there are many studies on miRNAs modulating estrogen signaling through direct targeting of ESR1 or estrogen biosynthesis, to our knowledge, miR495-3p could be the first miRNA exhibiting anti-estrogenic activity. However, future in-vitro studies with E2 and fulvestrant treatment along with miR495-3p and siCHRNA5 are required.

Secondary targets of estrogen were downregulated in miR495-3p treated MCF7 cells. Although both siCHRNA5 and miR495-3p downregulated secondary targets, their impact was antagonistic, yet larger than either of them alone, in the combinatorial group. Protein-protein interaction network analysis with the altered genes in response to miR495-3p revealed that the E2F targets, also partially secondary estrogen targets, were downregulated. Targeting the same protein/network has been shown to lead the antagonistic action, as in the case of RG7388 and temozolomide in neuroblastoma cells (Cheng, et al., 2019; Diaz, et al., 2020; He, et al., 2021).

Therefore, the underlying mechanism of the partial antagonism between siCHRNA5 and miR495-3p on secondary targets could be both targeting E2F (**Figure 4.1**).

miR495-3p has been shown to inhibit FOXC1 through direct binding in endometrial cancer (Appendix 1) (Xu, et al., 2016). FOXC1 is an oncogenic transcription factor and also the primary target of ESR1 (Gilding and Somervaille, 2019). Several studies have also proposed that FOXC1 is also involved in the negative auto-feedback loop of estrogen signaling and tamoxifen resistance (Wang, et al., 2017; Yu-Rice, et al., 2016). Taken together, FOXC1 could be the link between miR495-3p and estrogen signaling (**Figure 4.1**).

4.6 Conclusions

This thesis focuses on deciphering the key modulatory components found in the siCHRNA5 expression profile using in-silico and in-vitro methods (**Figure 4.1**). In brief, I have demonstrated that CHRNA5 depletion can induce TP53 signaling, which inhibits DDR; hence the inhibition of TP53 could revert cell cycle arrest and apoptosis, yet not in full. Furthermore, TP53 depletion also rescues the expression of E2F targets, which are mainly the secondary estrogen targets. siCHRNA5 significantly modulates certain primary and most of the secondary targets of ESR1 in opposing directions which could be through the inhibition of the negative feedback loop between ESR1 secondary targets and primary targets. Furthermore, I have identified miR495-3p downregulated by siCHRNA5 along with other 14q32.31 miRNA cluster exhibits anti-estrogenic effects.

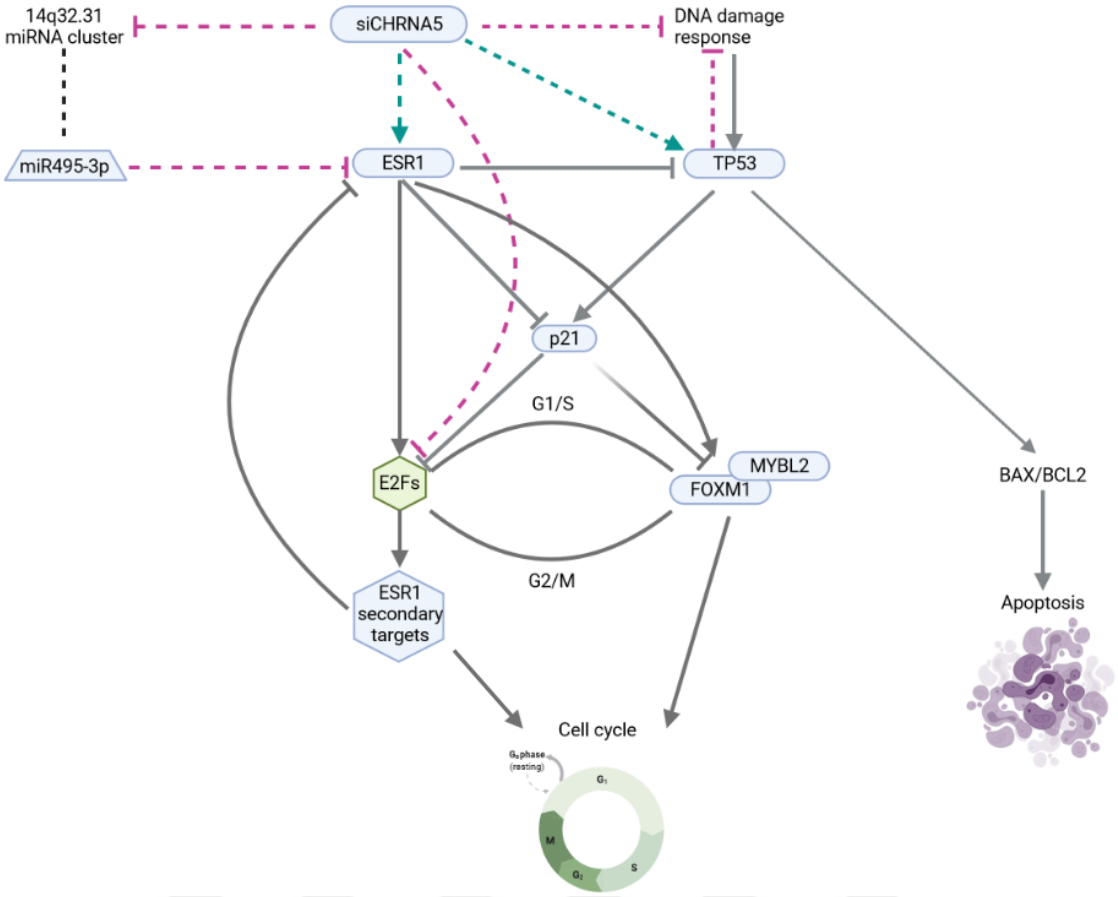

Figure 4.1 The summary of the findings and proposed mechanism. The known connections from the literature were shown with gray while novel interactions were colored as; pink and green for inhibition and induction, respectively. Direct relations through transcription or protein-protein binding were indicated with solid lines, and dashed lines were used for indirect relations.

4.7 Future Perspectives

- Enrichment and overrepresentation analyses for the other crucial regulatory factor, miRNAs, will be included in the syneRgy app.
- Some TFs require co-regulators to bind a group of their targets as ESR1. Therefore, enrichment analysis would be expanded to TF pairs and the master regulators.
- Network representation of TFs can be included to analyze further the shared targets between TFs and the co-regulatory TF modules driving synergy.

- Since regression analysis is applicable for linear relationships only, another widely used method to test the relationship between two variables, mutual information, could be tested and included in the syneRgy app.
- The expression level analysis with the TCGA dataset showed that PCPG, Pheochromocytoma, and Paraganglioma, which is a rare nerve tumor form in the adrenal gland, exhibits high CHRNA5 expression. Since its role in the nervous system is well studied, the CHRNA5 depletion studies can be extended to PCPG and other nervous system cancers, including low-grade glioma and glioblastoma.
- The cross-talk between ESR1 and TP53 signaling can be further studied in the siCHRNA5 and siTP53 model through E2 and SERM/SERD treatments. Although our findings suggest ESR1 signaling as downstream of TP53 through p21-E2F cascade future studies should investigate: 1) siCHRNA5 and fulvestrant (SERD) to test the change in the TP53 activity and 2) siCHRNA5, E2, and siTP53 to test expected rescue effect.
- The change in the cell cycle dynamics can be further studied using CDK4/6 inhibitors. E2Fs appeared to be the hub for the E2 and TP53 signaling as well as miR495-3p function. Therefore CDK4/6 inhibitors along with siCHRNA5 is needed to test the rescue effect.
- The siCHRNA5-mediated TP53 independent actions are yet to be explored. syneRgy analysis and qPCR data also revealed that not all siCHRNA5 profile has reverted by siTP53 treatment. syneRgy app can be employed for the identification of the TF candidates altered in siCHRNA5 and combinatorial but siTP53.
- The miR495-3p profile can be investigated in ER-positive and ER-negative cell lines through cell viability, cell cycle assays. All the in-vitro experiments so far were done in ER+ MCF7 cell line; therefore, the observed effects on estrogen signaling, cell cycle arrest needs to be further validated using other cell lines.
- The proposed anti-estrogenic effect of miR495-3p and siCHRNA5 can be further tested through treatment with E2 or SERMs/SERDs.

- The anti-estrogenic effect of miR495-3p can be further tested in the context of endocrine treatment resistance and could serve as a therapeutic marker for hormone receptor-positive breast tumors.
- The possible involvement of FOXC1 in miR495-3p/Estrogen signaling can be further tested through siFOXC1 and FOXC1 overexpression models.
- Since estrogen level has been associated with cognition, the miR495-3p can be further studied in the context of cognition and memory.

Appendix A. The summary table for the change in the miR495 in cancer cell lines and/or tumors, its function and targets

Cancer Type	Direction	Promotes	Inhibits	Targets	Cell Lines /Samples	Publication (DOI)
bladder cancer	up	cell proliferation, invasion and tumorgenesis	-	PTEN	J82, T24, UMUC3, TCCSUP, mouse xenograft, patient sample	10.1016/j.bbrc.2017.01.019
breast cancer	up	colony formation, invasion, tumorgenesis, hypoxia resistance	-	E-cadherin and REDD1.	breast cancer stem, mouse	10.1038/onc.2010.618
breast cancer	down	G1/S transition	tumorgenesis	Bmi-1	MCF-7 MDA-MB-231	10.1097/MD.0000000000000718
breast cancer	down	apoptosis	cell proliferation and migration	STAT3	MCF-7 HCC1973	10.3892/or.2017.5621
breast cancer	down	-	proliferation, invasion, and migration	HER2	SK-BR-3, MDA-MB-453, mouse xenograft	10.1002/jcb.26588
colorectal cancer	down	-	invasion and epithelial-mesenchymal transition	Annexin A3	SW620, SW480, HT29, HCT116	10.1159/000485877
esophageal squamous cell carcinoma	down	-	cell proliferation, epithelial-mesenchymal transition, migration and invasion	AKT1	ECA109, KYSE410, TE-1, Patient samples	10.18632/oncotarget.9981
gastric cancer	up	cell proliferation and angiogenesis	apoptosis	RUNX3	SNU5 SNU484	10.18632/oncotarget.5037
gastric cancer	down		migration and invasion	HMGA2	GES-1, SGC-7901, BGC-823, HGC-27	10.12659/msm.898740
gastric cancer	down	apoptosis	cell proliferation and migration	TWIST1	SGC-7901 BGC-823	10.3727/096504018X15223159811838
glioma	down	-	cell proliferation	CDK6	U87-MG T98	10.1186/1477-7819-11-87
glioma	down	-	cell proliferation, invasion	MYB	A172, U87, U251 U373, Patient samples	10.3892/mmr.2016.5327
glioma	down	-	cell proliferation, metabolic shift	GLUT1	U251 HEK293T	10.1097/SCS.0000000000001385
hepatocellular carcinoma	up	cell proliferation,tumorigenesis and metastasis		MAT1A	Hep3B HepG2, mouse xenograft	10.1172/JCI63861
hepatocellular carcinoma	down	-	cell proliferation and invasion	IGF1R	SMMC-7721, Hep3B, Huh7, THLE-3, Patient samples	10.3892/etm.2017.5467
malignant melanoma	down	-	cell proliferation, migration and invasion	PBX3	A375 MeWo	10.2147/OTT.S152362

medulloblastoma	down	-	-	GFI1	Patient samples	10.1159/000430308
non-small cell lung cancer	down	-	-	GRP78	Patient samples	10.1016/j.gene.2017.03.032
non-small cell lung cancer	down	-	cell proliferation, migration and invasion	TCF4	Patient samples	10.26355/eurrev_201811_16398
oral squamous cell carcinoma	down	-	cell proliferation, epithelial-mesenchymal transition, migration and invasion	IGF1	CA-83, SCC-4, SCC-9,HN-5, HOK, Patient samples	10.1016/j.joms.2018.12.021
osteosarcoma	down	apoptosis	cell proliferation and invasion	HMGN5	143B, SaOS-2, U2OS MG63,hFOB 293T, Patient samples	10.3892/or.2017.5715
renal cell carcinoma	down		cell proliferation and migration	SATB1	769-P, 786-O, A498, SN12-PM6,HK-2, Patient samples	PMID: **26692942**
gastric cancer	down	apoptosis	cell proliferation and migration	-	MKN28, MKN45, SNU216, SNU484, mouse xenograft, Patient samples	10.1002/path.4994
malignant melanoma	down	-	cell proliferation, migration and invasion	E2F3	HEMa-LP, A375, A2058, SK-MEL-28,HEK-293T, mouse xenograft	10.1002/jcp.28559
colorectal cancer	down	-	-	-	Patient Data	10.1016/j.amsu.2016.01.091
endometrial cancer	down	-	-	-	HT29, HCT116, SW620, SW480	10.3892/ol.2019.10508
cervical cancer	up	apoptosis	tumorgenesis	CDK1	C4-1, HeLa, SiHa,Caski, mouse xenograft	10.1007/s12094-021-02687-6
breast cancer	down	-	multidrug resistance	FOXC1, TGFB2	Novel TNBC cell line, MDA-MB-231, MCF7, MCF10A	10.1016/j.bcp.2021.114692
Low grade glioma	down	-	-	TOP2A	Patient samples	10.2147/CMAR.S314011
breast cancer	down	-	cell proliferation	CENPU	MDA-MB-468, BT-549, HCC1954, MCF-7, and MCF-10A	10.18632/aging.202909
gastric cancer	down	-	multidrug resistance, cell proliferation, autophagy	GRP78	SGC7901, Patient samples, mouse xenograft	10.1038/s41419-018-0950-x
prostate cancer	-	-	cell proliferation, tumor growth, migration and invasion	YTHDF2	LNCaP, C42, DU145, PC3, Patient samples, mouse xenograft	10.1186/s13046-020-01735-3
Oral squamous cell carcinoma	down	-	cell proliferation, epithelial-mesenchymal transition, tumor growth	HOXC6	Patient samples, Patient-derived cells	10.1186/s13287-020-1576-3
hepatocellular carcinoma	-	-	epithelial-mesenchymal transition, migration and invasion	ZNF503	Hep3B, Huh7, SMMC-7721, MHCC-97H, LO2, Patient samples	PMID: 31312355
non-small cell lung cancer	down	-	cell proliferation	HMGA2	A549, Patient Samples	10.3892/mmr.2018.9773

Oral squamous cell carcinoma	down	-	cell proliferation and invasion	NOTCH1	Tca8113, CAL-27, SCC-9, HOK, Patient Samples	10.3892/mmr.2018.9616
gastric cancer	down	apoptosis	cell proliferation and migration	-	MGC80-3	10.3892/or.2018.6722
gastric cancer	down	chemosensitivity and apoptosis	cell proliferation	HER2	-	10.12659/MSM.909458
nasopharyngeal carcinoma	up	radiosensitivity	invasion and epithelial-mesenchymal transition	GRP78	5–8F, Patient Samples	10.3892/or.2018.6538
colorectal cancer	down	-	cell proliferation, colony formation and migration	FAM83D	DLD-1, HCT-15, HT-29, SW480, Lovo, CaCo2, FHC, Patient samples	10.1016/j.biopha.2017.11.138
ovarian and gastric cancer	-	-	multidrug resistance	MDR1	MDR A2780DX5, MDR SGC7901R	10.1111/jcmm.13114
small cell lung cancer	-	apoptosis	drug resistance, cell proliferation, epithelial-mesenchymal transition, tumor growth	Etk/BMX	NCI-H446 and NCI-H69, Patient samples	PMCID: PMC5384991
small cell lung cancer	-	-	drug resistance,cell proliferation and tumor growth	TSPAN12	NCI-H69, NCI-H446	10.1016/j.bbrc.2017.03.044
prostate cancer	down		cell proliferation, migration, invasion and tumor growth	AKT, mTOR	LNCaP, PC-3,PZ-HPV-7, mouse xenograft	10.3109/07357907.2016.1156690
gallblader cancer	up	tumor growth	apoptosis	PHLPP	EH-GB1,GBC-SD, Patient samples, mouse xenograft	10.18632/oncotarget.3721
gastric cancer	up	-	migration and invasion	PRL3	SGC7901, MKN45, MKN28, BGC823, Patient samples	10.1016/j.bbrc.2014.11.083
gastric cancer	down		migration and invasion	PRL3	SGC7901, MKN45, MKN28, BGC823, Patient samples	10.1016/j.canlet.2012.03.029
breast cancer	up	migration		JAM-A	MCF7, MDA-MB-231	10.1007/s13238-014-0088-2
non-small cell lung cancer	down		cell proliferation, colony formation, migration	MTA3	A549, Calu-3, H460, H1299,H1650, SPC-A-1, Patient samples	10.1007/s13277-013-1460-1
chronic myelogenous leukemia	-	-	multidrug resistance	MDR1	K562	10.1371/journal.pone.0082062
non-small cell lung cancer		drug sensitivity		ATP7A	A549,H1299	10.1002/jcb.24665
hepatocellular carcinoma		tumor growth, metastasis	apoptosis	MAT1A	Hep3B, HepG2, mouse xenograft	10.1172/JCI63861

5 References

Abatangelo, L., *et al.* Comparative study of gene set enrichment methods. *BMC Bioinformatics* 2009;10:275.

Agrawal, A., *et al.* Regulation of the p14ARF-Mdm2-p53 pathway: an overview in breast cancer. *Exp Mol Pathol* 2006;81(2):115-122.

Ahmadi, A., *et al.* miR-199a-5p and miR-495 target GRP78 within UPR pathway of lung cancer. *Gene* 2017;620:15-22.

Al-Lazikani, B., Banerji, U. and Workman, P. Combinatorial drug therapy for cancer in the post-genomic era. *Nat Biotechnol* 2012;30(7):679-692.

Alqurashi, N., *et al.* miR-496, miR-1185, miR-654, miR-3183 and miR-495 are downregulated in colorectal cancer cells and have putative roles in the mTOR pathway. *Oncol Lett* 2019;18(2):1657-1668.

Alvarez, M.J., *et al.* Functional characterization of somatic mutations in cancer using network-based inference of protein activity. *Nat Genet* 2016;48(8):838-847.

Anders, S., Pyl, P.T. and Huber, W. HTSeq--a Python framework to work with high-throughput sequencing data. *Bioinformatics* 2015;31(2):166-169.

Andrade Fde, O., *et al.* Lipidomic fatty acid profile and global gene expression pattern in mammary gland of rats that were exposed to lard-based high fat diet during fetal and lactation periods associated to breast cancer risk in adulthood. *Chem Biol Interact* 2015;239:118-128.

Arps, D.P., *et al.* Invasive ductal carcinoma with lobular features: a comparison study to invasive ductal and invasive lobular carcinomas of the breast. *Breast Cancer Res Treat* 2013;138(3):719-726.

Arredondo, J., *et al.* Receptor-mediated tobacco toxicity: alterations of the NF-kappaB expression and activity downstream of alpha7 nicotinic receptor in oral keratinocytes. *Life Sci* 2007;80(24-25):2191-2194.

Aubrey, B.J., *et al.* How does p53 induce apoptosis and how does this relate to p53-mediated tumour suppression? *Cell Death Differ* 2018;25(1):104-113.

Babu, A., Munshi, A. and Ramesh, R. Combinatorial therapeutic approaches with RNAi and anticancer drugs using nanodrug delivery systems. *Drug Dev Ind Pharm* 2017;43(9):1391-1401.

Baccarella, A., *et al.* Empirical assessment of the impact of sample number and read depth on RNA-Seq analysis workflow performance. *BMC Bioinformatics* 2018;19(1):423.

Bacevic, K., *et al.* Cdk2 strengthens the intra-S checkpoint and counteracts cell cycle exit induced by DNA damage. *Sci Rep* 2017;7(1):13429.

Baek, K.H., *et al.* Calcium influx-mediated translocation of m-calpain induces Ku80 cleavage and enhances the Ku80-related DNA repair pathway. *Oncotarget* 2016;7(21):30831-30844.

Bai, Z., *et al.* The MiR-495/Annexin A3/P53 Axis Inhibits the Invasion and EMT of Colorectal Cancer Cells. *Cell Physiol Biochem* 2017;44(5):1882-1895.

Bailey, S.T., *et al.* Estrogen receptor prevents p53-dependent apoptosis in breast cancer. *Proc Natl Acad Sci U S A* 2012;109(44):18060-18065.

Bajic, V.B., *et al.* Dragon ERE Finder version 2: A tool for accurate detection and analysis of estrogen response elements in vertebrate genomes. *Nucleic Acids Res* 2003;31(13):3605-3607.

Balassiano, K., *et al.* Aberrant DNA methylation of cancer-associated genes in gastric cancer in the European Prospective Investigation into Cancer and Nutrition (EPIC-EURGAST). *Cancer Lett* 2011;311(1):85-95.

Bando, T., *et al.* Loss of heterozygosity of 14q32 in colorectal carcinoma. *Cancer Genet Cytogenet* 1999;111(2):161-165.

Barazetti, J.F., *et al.* From Micro to Long: Non-Coding RNAs in Tamoxifen Resistance of Breast Cancer Cells. *Cancers (Basel)* 2021;13(15).

Barroso-Sousa, R. and Metzger-Filho, O. Differences between invasive lobular and invasive ductal carcinoma of the breast: results and therapeutic implications. *Ther Adv Med Oncol* 2016;8(4):261-266.

Barsotti, A.M. and Prives, C. Pro-proliferative FoxM1 is a target of p53-mediated repression. *Oncogene* 2009;28(48):4295-4305.
Bartek, J. and Lukas, J. Chk1 and Chk2 kinases in checkpoint control and cancer. *Cancer Cell* 2003;3(5):421-429.
Bass, J.B., Jr., *et al.* Treatment of tuberculosis and tuberculosis infection in adults and children. American Thoracic Society and The Centers for Disease Control and Prevention. *Am J Respir Crit Care Med* 1994;149(5):1359-1374.
Beato, M., Chavez, S. and Truss, M. Transcriptional regulation by steroid hormones. *Steroids* 1996;61(4):240-251.
Becker, J.C., Schrama, D. and Houben, R. Merkel cell carcinoma. *Cell Mol Life Sci* 2009;66(1):1-8.
Bergman, L., *et al.* Risk and prognosis of endometrial cancer after tamoxifen for breast cancer. Comprehensive Cancer Centres' ALERT Group. Assessment of Liver and Endometrial cancer Risk following Tamoxifen. *Lancet* 2000;356(9233):881-887.
Bhatnagar, A.S., *et al.* Highly selective inhibition of estrogen biosynthesis by CGS 20267, a new non-steroidal aromatase inhibitor. *J Steroid Biochem Mol Biol* 1990;37(6):1021-1027.
Binder, E.F., *et al.* Effects of hormone replacement therapy on cognitive performance in elderly women. *Maturitas* 2001;38(2):137-146.
Bisio, A., *et al.* Cooperative interactions between p53 and NFkappaB enhance cell plasticity. *Oncotarget* 2014;5(23):12111-12125.
Blighe K, R.S., Lewis M 2021. EnhancedVolcano: Publication-ready volcano plots with enhanced colouring and labeling. R package version 1.10.0, . https://github.com/kevinblighe/EnhancedVolcano.
Bo, T., *et al.* LAT1 inhibitor JPH203 sensitizes cancer cells to radiation by enhancing radiation-induced cellular senescence. *Transl Oncol* 2021;14(11):101212.
Bordas, A., *et al.* Expression patterns for nicotinic acetylcholine receptor subunit genes in smoking-related lung cancers. *Oncotarget* 2017;8(40):67878-67890.
Bourdeau, V., *et al.* Genome-wide identification of high-affinity estrogen response elements in human and mouse. *Mol Endocrinol* 2004;18(6):1411-1427.
Bouzat, C., Barrantes, F. and Sine, S. Nicotinic receptor fourth transmembrane domain: hydrogen bonding by conserved threonine contributes to channel gating kinetics. *J Gen Physiol* 2000;115(5):663-672.
Brejc, K., *et al.* Crystal structure of an ACh-binding protein reveals the ligand-binding domain of nicotinic receptors. *Nature* 2001;411(6835):269-276.
Brettschneider, J., *et al.* Quality Assessment for Short Oligonucleotide Microarray Data. *Technometrics* 2008;50(3):241-264.
Brown, D.A. Muscarinic acetylcholine receptors (mAChRs) in the nervous system: some functions and mechanisms. *J Mol Neurosci* 2010;41(3):340-346.
Bruck, J., *et al.* Molecular characterization of temple syndrome families with 14q32 epimutations. *Eur J Med Genet* 2020;63(12):104077.
Budkova, Z., *et al.* Expression of ncRNAs on the DLK1-DIO3 Locus Is Associated With Basal and Mesenchymal Phenotype in Breast Epithelial Progenitor Cells. *Front Cell Dev Biol* 2020;8:461.
Bugreev, D.V. and Mazin, A.V. Ca2+ activates human homologous recombination protein Rad51 by modulating its ATPase activity. *Proc Natl Acad Sci U S A* 2004;101(27):9988-9993.
Cancer Genome Atlas, N. Comprehensive molecular portraits of human breast tumours. *Nature* 2012;490(7418):61-70.
Cao, M., *et al.* MicroRNA-495 induces breast cancer cell migration by targeting JAM-A. *Protein Cell* 2014;5(11):862-872.
Carroll, J.S., *et al.* Genome-wide analysis of estrogen receptor binding sites. *Nat Genet* 2006;38(11):1289-1297.
Carvajal, L.A. and Manfredi, J.J. Another fork in the road--life or death decisions by the tumour suppressor p53. *EMBO Rep* 2013;14(5):414-421.

Castelan, F., *et al.* Cytoplasmic regions adjacent to the M3 and M4 transmembrane segments influence expression and function of alpha7 nicotinic acetylcholine receptors. A study with single amino acid mutants. *J Neurochem* 2007;100(2):406-415.
Cauley, J.A. Estrogen and bone health in men and women. *Steroids* 2015;99(Pt A):11-15.
Cavailles, V., *et al.* Nuclear factor RIP140 modulates transcriptional activation by the estrogen receptor. *EMBO J* 1995;14(15):3741-3751.
Centeno, M.L., *et al.* Estradiol increases alpha7 nicotinic receptor in serotonergic dorsal raphe and noradrenergic locus coeruleus neurons of macaques. *J Comp Neurol* 2006;497(3):489-501.
Chang, L., *et al.* miRNet 2.0: network-based visual analytics for miRNA functional analysis and systems biology. *Nucleic Acids Res* 2020;48(W1):W244-W251.
Chang, W. shiny: Web Application Framework for R. Release 1.6.0
Cheang, M.C., *et al.* Ki67 index, HER2 status, and prognosis of patients with luminal B breast cancer. *J Natl Cancer Inst* 2009;101(10):736-750.
Chen, C.S., *et al.* Nicotine-induced human breast cancer cell proliferation attenuated by garcinol through down-regulation of the nicotinic receptor and cyclin D3 proteins. *Breast Cancer Res Treat* 2011;125(1):73-87.
Chen, F., Liu, L. and Wang, S. Long non-coding RNA NORAD exhaustion represses prostate cancer progression through inhibiting TRIP13 expression via competitively binding to miR-495-3p. *Cancer Cell Int* 2020;20:323.
Chen, G. and Xie, Y. miR-495 inhibits proliferation, migration, and invasion and induces apoptosis via inhibiting PBX3 in melanoma cells. *Onco Targets Ther* 2018;11:1909-1920.
Chen, J., *et al.* Acetylcholine receptors: Key players in cancer development. *Surg Oncol* 2019;31:46-53.
Chen, J., *et al.* Aquaporin 3 promotes epithelial-mesenchymal transition in gastric cancer. *J Exp Clin Cancer Res* 2014;33:38.
Chen, L., *et al.* Preclinical evaluation of the first intravenous small molecule MDM2 antagonist alone and in combination with temozolomide in neuroblastoma. *Int J Cancer* 2019;144(12):3146-3159.
Chen, L. and Tweddle, D.A. p53, SKP2, and DKK3 as MYCN Target Genes and Their Potential Therapeutic Significance. *Front Oncol* 2012;2:173.
Chen, S., *et al.* MicroRNA-495-3p inhibits multidrug resistance by modulating autophagy through GRP78/mTOR axis in gastric cancer. *Cell Death Dis* 2018;9(11):1070.
Chen, S.M., *et al.* MicroRNA-495 inhibits proliferation of glioblastoma multiforme cells by downregulating cyclin-dependent kinase 6. *World J Surg Oncol* 2013;11:87.
Chen, Y., *et al.* Demethylation of miR-495 inhibits cell proliferation, migration and promotes apoptosis by targeting STAT-3 in breast cancer. *Oncol Rep* 2017;37(6):3581-3589.
Chen, Y.J., *et al.* Molecular subtyping of breast cancer intrinsic taxonomy with oligonucleotide microarray and NanoString nCounter. *Biosci Rep* 2021;41(8).
Chen, Z., *et al.* Crucial role of p53-dependent cellular senescence in suppression of Pten-deficient tumorigenesis. *Nature* 2005;436(7051):725-730.
Cheng, F., Kovacs, I.A. and Barabasi, A.L. Network-based prediction of drug combinations. *Nat Commun* 2019;10(1):1197.
Cheng, K., *et al.* Acetylcholine release by human colon cancer cells mediates autocrine stimulation of cell proliferation. *Am J Physiol Gastrointest Liver Physiol* 2008;295(3):G591-597.
Chipuk, J.E., *et al.* Direct activation of Bax by p53 mediates mitochondrial membrane permeabilization and apoptosis. *Science* 2004;303(5660):1010-1014.
Chota, A., George, B.P. and Abrahamse, H. Interactions of multidomain pro-apoptotic and anti-apoptotic proteins in cancer cell death. *Oncotarget* 2021;12(16):1615-1626.
Chou, T.C. Drug combination studies and their synergy quantification using the Chou-Talalay method. *Cancer Res* 2010;70(2):440-446.
Chow, M.J., *et al.* Suppression of the dynamic interaction of estrogen receptor with chromatin is critical for therapeutic ligands to repress ER-mediated transcription activities. *Biotarget* 2020;4.
Christiansen H, C.N. Progressive Neuroblastoma: Innovation and Novel Therapeutic Strategies. *Pediatr Adolesc Med. Basel* 2015;20:59-80.

Chu, H., *et al.* MiR-495 regulates proliferation and migration in NSCLC by targeting MTA3. *Tumour Biol* 2014;35(4):3487-3494.
Chuang, S.C., *et al.* G Protein-Coupled Estrogen Receptor Mediates Cell Proliferation through the cAMP/PKA/CREB Pathway in Murine Bone Marrow Mesenchymal Stem Cells. *Int J Mol Sci* 2020;21(18).
Cingir Koker, S., *et al.* Cholinergic Receptor Nicotinic Alpha 5 (CHRNA5) RNAi is associated with cell cycle inhibition, apoptosis, DNA damage response and drug sensitivity in breast cancer. *PLoS One* 2018;13(12):e0208982.
Cipolla, M.J., Godfrey, J.A. and Wiegman, M.J. The effect of ovariectomy and estrogen on penetrating brain arterioles and blood-brain barrier permeability. *Microcirculation* 2009;16(8):685-693.
Colomer, J., *et al.* Calmodulin regulates the expression of cdks, cyclins and replicative enzymes during proliferative activation of human T lymphocytes. *Biochem Biophys Res Commun* 1994;200(1):306-312.
Cooke, J.P. Angiogenesis and the role of the endothelial nicotinic acetylcholine receptor. *Life Sci* 2007;80(24-25):2347-2351.
Cottone, E., *et al.* Role of coactivators and corepressors in steroid and nuclear receptor signaling: potential markers of tumor growth and drug sensitivity. *Int J Biol Markers* 2001;16(3):151-166.
Craig Parman, C.H., Robert Gentleman. affyQCReport
Cristofaro, I., *et al.* Activation of M2 muscarinic acetylcholine receptors by a hybrid agonist enhances cytotoxic effects in GB7 glioblastoma cancer stem cells. *Neurochem Int* 2018;118:52-60.
Cui, J., *et al.* MiR-873 regulates ERalpha transcriptional activity and tamoxifen resistance via targeting CDK3 in breast cancer cells. *Oncogene* 2015;34(30):3895-3907.
Cui, N., *et al.* LncRNA SNHG20 contributes to cell proliferation and invasion by upregulating ZFX expression sponging miR-495-3p in gastric cancer. *J Cell Biochem* 2019;120(3):3114-3123.
Culverhouse, R.C., *et al.* Variants in the CHRNA5-CHRNA3-CHRNB4 Region of Chromosome 15 Predict Gastrointestinal Adverse Events in the Transdisciplinary Tobacco Use Research Center Smoking Cessation Trial. *Nicotine Tob Res* 2020;22(2):248-255.
Curtis, C., *et al.* The genomic and transcriptomic architecture of 2,000 breast tumours reveals novel subgroups. *Nature* 2012;486(7403):346-352.
Dai, X., *et al.* Breast Cancer Cell Line Classification and Its Relevance with Breast Tumor Subtyping. *J Cancer* 2017;8(16):3131-3141.
Dai, X., *et al.* Breast cancer intrinsic subtype classification, clinical use and future trends. *Am J Cancer Res* 2015;5(10):2929-2943.
de Lencastre, A., *et al.* MicroRNAs both promote and antagonize longevity in C. elegans. *Curr Biol* 2010;20(24):2159-2168.
De Vitto, H., *et al.* Estrogen-related receptor alpha directly binds to p53 and cooperatively controls colon cancer growth through the regulation of mitochondrial biogenesis and function. *Cancer Metab* 2020;8(1):28.
Deciphering Developmental Disorders, S. Prevalence and architecture of de novo mutations in developmental disorders. *Nature* 2017;542(7642):433-438.
Delierneux, C., *et al.* Mitochondrial Calcium Regulation of Redox Signaling in Cancer. *Cells* 2020;9(2).
Deng, Q., *et al.* GPER/Hippo-YAP signal is involved in Bisphenol S induced migration of triple negative breast cancer (TNBC) cells. *J Hazard Mater* 2018;355:1-9.
Devor, E.J., *et al.* Global dysregulation of the chromosome 14q32 imprinted region in uterine carcinosarcoma. *Exp Ther Med* 2012;3(4):677-682.
Di Bari, M., *et al.* Cytotoxic and genotoxic effects mediated by M2 muscarinic receptor activation in human glioblastoma cells. *Neurochem Int* 2015;90:261-270.
Di Leva, G., *et al.* MicroRNA cluster 221-222 and estrogen receptor alpha interactions in breast cancer. *J Natl Cancer Inst* 2010;102(10):706-721.
Dias, K., *et al.* Claudin-Low Breast Cancer; Clinical & Pathological Characteristics. *PLoS One* 2017;12(1):e0168669.

Diaz, J.E., *et al.* The transcriptomic response of cells to a drug combination is more than the sum of the responses to the monotherapies. *Elife* 2020;9.
Diskin, S.J., *et al.* Rare variants in TP53 and susceptibility to neuroblastoma. *J Natl Cancer Inst* 2014;106(4):dju047.
Dobin, A., *et al.* STAR: ultrafast universal RNA-seq aligner. *Bioinformatics* 2013;29(1):15-21.
Doldi, V., *et al.* Integrated gene and miRNA expression analysis of prostate cancer associated fibroblasts supports a prominent role for interleukin-6 in fibroblast activation. *Oncotarget* 2015;6(31):31441-31460.
Dorszewska, J., *et al.* Polymorphisms of the CHRNA4 gene encoding the alpha4 subunit of nicotinic acetylcholine receptor as related to the oxidative DNA damage and the level of apoptotic proteins in lymphocytes of the patients with Alzheimer's disease. *DNA Cell Biol* 2005;24(12):786-794.
Downie Ruiz Velasco, A., *et al.* Posttranscriptional Regulation of 14q32 MicroRNAs by the CIRBP and HADHB during Vascular Regeneration after Ischemia. *Mol Ther Nucleic Acids* 2019;14:329-338.
Drago-Garcia, D., Espinal-Enriquez, J. and Hernandez-Lemus, E. Network analysis of EMT and MET micro-RNA regulation in breast cancer. *Sci Rep* 2017;7(1):13534.
Du, B.Y., *et al.* Synergistic effects of combination treatment with bortezomib and doxorubicin in human neuroblastoma cell lines. *Chemotherapy* 2012;58(1):44-51.
Du, C., *et al.* Activation of the KDM5A/miRNA-495/YTHDF2/m6A-MOB3B axis facilitates prostate cancer progression. *J Exp Clin Cancer Res* 2020;39(1):223.
Duan, B.X., Geng, X.R. and Wu, Y.Q. lncRNA RNCR2 facilitates cell proliferation and epithelial-mesenchymal transition in melanoma through HK2-mediated Warburg effect via targeting miR-495-3p. *Neoplasma* 2021;68(4):692-701.
Duffy, M.J., Synnott, N.C. and Crown, J. Mutant p53 in breast cancer: potential as a therapeutic target and biomarker. *Breast Cancer Res Treat* 2018;170(2):213-219.
Dumasia, K., *et al.* Estrogen, through estrogen receptor 1, regulates histone modifications and chromatin remodeling during spermatogenesis in adult rats. *Epigenetics* 2017;12(11):953-963.
Early Breast Cancer Trialists' Collaborative, G., *et al.* Relevance of breast cancer hormone receptors and other factors to the efficacy of adjuvant tamoxifen: patient-level meta-analysis of randomised trials. *Lancet* 2011;378(9793):771-784.
Edwards, E., *et al.* Phosphatidylinositol 3-kinase/Akt signaling in the response of vascular endothelium to ionizing radiation. *Cancer Res* 2002;62(16):4671-4677.
Ellison-Zelski, S.J., Solodin, N.M. and Alarid, E.T. Repression of ESR1 through actions of estrogen receptor alpha and Sin3A at the proximal promoter. *Mol Cell Biol* 2009;29(18):4949-4958.
Epis, M.R., *et al.* miR-331-3p and Aurora Kinase inhibitor II co-treatment suppresses prostate cancer tumorigenesis and progression. *Oncotarget* 2017;8(33):55116-55134.
Eun, J.W., *et al.* MicroRNA-495-3p functions as a tumor suppressor by regulating multiple epigenetic modifiers in gastric carcinogenesis. *J Pathol* 2018;244(1):107-119.
Falcon S., G.R. Hypergeometric Testing Used for Gene Set Enrichment Analysis. In: Bioconductor Case Studies. Use R!. In. New York: Springer; 2008.
Falvella, F.S., *et al.* Transcription deregulation at the 15q25 locus in association with lung adenocarcinoma risk. *Clin Cancer Res* 2009;15(5):1837-1842.
Farina, A.R., *et al.* Mechanisms involved in selecting and maintaining neuroblastoma cancer stem cell populations, and perspectives for therapeutic targeting. *World J Stem Cells* 2021;13(7):685-736.
Fayzullina, S. and Martin, L.J. DNA Damage Response and DNA Repair in Skeletal Myocytes From a Mouse Model of Spinal Muscular Atrophy. *J Neuropathol Exp Neurol* 2016;75(9):889-902.
Feng, X., *et al.* miR495 enhances the efficacy of radiotherapy by targeting GRP78 to regulate EMT in nasopharyngeal carcinoma cells. *Oncol Rep* 2018;40(3):1223-1232.
Feng, Y., *et al.* M3 muscarinic acetylcholine receptors regulate epithelial-mesenchymal transition, perineural invasion, and migration/metastasis in cholangiocarcinoma through the AKT pathway. *Cancer Cell Int* 2018;18:173.

Forbes, N., *et al.* Evidence for synergistic effects of PRNP and ATP7B mutations in severe neuropsychiatric deterioration. *BMC Med Genet* 2014;15:22.
Fragomeni, S.M., Sciallis, A. and Jeruss, J.S. Molecular Subtypes and Local-Regional Control of Breast Cancer. *Surg Oncol Clin N Am* 2018;27(1):95-120.
Frasor, J., *et al.* Selective estrogen receptor modulators: discrimination of agonistic versus antagonistic activities by gene expression profiling in breast cancer cells. *Cancer Res* 2004;64(4):1522-1533.
Friedman, D.N. and Henderson, T.O. Late Effects and Survivorship Issues in Patients with Neuroblastoma. *Children (Basel)* 2018;5(8).
Fritah, A., *et al.* p21WAF1/CIP1 selectively controls the transcriptional activity of estrogen receptor alpha. *Mol Cell Biol* 2005;25(6):2419-2430.
Frost, H.R. and Amos, C.I. Gene set selection via LASSO penalized regression (SLPR). *Nucleic Acids Res* 2017;45(12):e114.
Fu, W., *et al.* Bazedoxifene enhances paclitaxel efficacy to suppress glioblastoma via altering Hippo/YAP pathway. *J Cancer* 2020;11(3):657-667.
Fu, Z., *et al.* Plk1-dependent phosphorylation of FoxM1 regulates a transcriptional programme required for mitotic progression. *Nat Cell Biol* 2008;10(9):1076-1082.
Fucile, S., *et al.* Alpha 5 subunit forms functional alpha 3 beta 4 alpha 5 nAChRs in transfected human cells. *Neuroreport* 1997;8(11):2433-2436.
Fuentes, N. and Silveyra, P. Estrogen receptor signaling mechanisms. *Adv Protein Chem Struct Biol* 2019;116:135-170.
Fujimoto, N. and Kitamura, S. Effects of environmental estrogenic chemicals on AP1 mediated transcription with estrogen receptors alpha and beta. *J Steroid Biochem Mol Biol* 2004;88(1):53-59.
Fujiwara, H., *et al.* Regulation of mesodermal differentiation of mouse embryonic stem cells by basement membranes. *J Biol Chem* 2007;282(40):29701-29711.
Gao, J., *et al.* Integrative analysis of complex cancer genomics and clinical profiles using the cBioPortal. *Sci Signal* 2013;6(269):pl1.
Gao, J.J. and Swain, S.M. Luminal A Breast Cancer and Molecular Assays: A Review. *Oncologist* 2018;23(5):556-565.
Garcia-Alonso, L., *et al.* Benchmark and integration of resources for the estimation of human transcription factor activities. *Genome Res* 2019;29(8):1363-1375.
Gardiner, E., *et al.* Imprinted DLK1-DIO3 region of 14q32 defines a schizophrenia-associated miRNA signature in peripheral blood mononuclear cells. *Mol Psychiatry* 2012;17(8):827-840.
Garrido-Castro, A.C., Lin, N.U. and Polyak, K. Insights into Molecular Classifications of Triple-Negative Breast Cancer: Improving Patient Selection for Treatment. *Cancer Discov* 2019;9(2):176-198.
Gatti, D.M., *et al.* Heading down the wrong pathway: on the influence of correlation within gene sets. *BMC Genomics* 2010;11:574.
Gattolliat, C.H., *et al.* Expression of miR-487b and miR-410 encoded by 14q32.31 locus is a prognostic marker in neuroblastoma. *Br J Cancer* 2011;105(9):1352-1361.
Gautier, L., *et al.* affy--analysis of Affymetrix GeneChip data at the probe level. *Bioinformatics* 2004;20(3):307-315.
Geoffron, S., *et al.* Chromosome 14q32.2 Imprinted Region Disruption as an Alternative Molecular Diagnosis of Silver-Russell Syndrome. *J Clin Endocrinol Metab* 2018;103(7):2436-2446.
Gerzanich, V., *et al.* alpha 5 Subunit alters desensitization, pharmacology, Ca++ permeability and Ca++ modulation of human neuronal alpha 3 nicotinic receptors. *J Pharmacol Exp Ther* 1998;286(1):311-320.
Gibbs, R.B. Basal forebrain cholinergic neurons are necessary for estrogen to enhance acquisition of a delayed matching-to-position T-maze task. *Horm Behav* 2002;42(3):245-257.
Gibbs, R.B., *et al.* Effects of raloxifene and estradiol on hippocampal acetylcholine release and spatial learning in the rat. *Psychoneuroendocrinology* 2004;29(6):741-748.

Gibbs, R.B. and Johnson, D.A. Cholinergic lesions produce task-selective effects on delayed matching to position and configural association learning related to response pattern and strategy. *Neurobiol Learn Mem* 2007;88(1):19-32.
Gibbs, R.B. and Johnson, D.A. Sex-specific effects of gonadectomy and hormone treatment on acquisition of a 12-arm radial maze task by Sprague Dawley rats. *Endocrinology* 2008;149(6):3176-3183.
Gilding, L.N. and Somervaille, T.C.P. The Diverse Consequences of FOXC1 Deregulation in Cancer. *Cancers (Basel)* 2019;11(2).
Ginzkey, C., *et al.* Nicotine causes genotoxic damage but is not metabolized during long-term exposure of human nasal miniorgan cultures. *Toxicol Lett* 2014;229(1):303-310.
Goldman, M.J., *et al.* Visualizing and interpreting cancer genomics data via the Xena platform. *Nat Biotechnol* 2020;38(6):675-678.
Goncalves, A., *et al.* The CINSARC signature predicts the clinical outcome in patients with Luminal B breast cancer. *NPJ Breast Cancer* 2021;7(1):48.
Gonzalez-Vallinas, M., *et al.* Epigenetically Regulated Chromosome 14q32 miRNA Cluster Induces Metastasis and Predicts Poor Prognosis in Lung Adenocarcinoma Patients. *Mol Cancer Res* 2018;16(3):390-402.
Goss, P.E. and Tye, L.M. Anastrozole: a new selective nonsteroidal aromatase inhibitor. *Oncology (Williston Park)* 1997;11(11):1697-1703; discussion 1707-1698.
Gottifredi, V., *et al.* p53 down-regulates CHK1 through p21 and the retinoblastoma protein. *Mol Cell Biol* 2001;21(4):1066-1076.
Grady, S.R., *et al.* Low concentrations of nicotine differentially desensitize nicotinic acetylcholine receptors that include alpha5 or alpha6 subunits and that mediate synaptosomal neurotransmitter release. *Neuropharmacology* 2012;62(5-6):1935-1943.
Grando, S.A. Connections of nicotine to cancer. *Nat Rev Cancer* 2014;14(6):419-429.
Gregory, P.A., *et al.* The miR-200 family and miR-205 regulate epithelial to mesenchymal transition by targeting ZEB1 and SIP1. *Nat Cell Biol* 2008;10(5):593-601.
Groeneveld, S., *et al.* Snail mediates repression of the Dlk1-Dio3 locus in lung tumor-infiltrating immune cells. *Oncotarget* 2018;9(64):32331-32345.
Groot-Kormelink, P.J., Boorman, J.P. and Sivilotti, L.G. Formation of functional alpha3beta4alpha5 human neuronal nicotinic receptors in Xenopus oocytes: a reporter mutation approach. *Br J Pharmacol* 2001;134(4):789-796.
Gu, F., *et al.* Association Between Nicotine-dependent Gene Polymorphism and Smoking Cessation in Patients With Lung Cancer. *Clin Lung Cancer* 2020;21(2):171-176.
Gu, Z., Eils, R. and Schlesner, M. Complex heatmaps reveal patterns and correlations in multidimensional genomic data. *Bioinformatics* 2016;32(18):2847-2849.
Guan, J., *et al.* Therapeutic Ligands Antagonize Estrogen Receptor Function by Impairing Its Mobility. *Cell* 2019;178(4):949-963 e918.
Guan, Y.X., *et al.* Lnc RNA SNHG20 participated in proliferation, invasion, and migration of breast cancer cells via miR-495. *J Cell Biochem* 2018;119(10):7971-7981.
Guha, P., *et al.* Nicotine promotes apoptosis resistance of breast cancer cells and enrichment of side population cells with cancer stem cell-like properties via a signaling cascade involving galectin-3, alpha9 nicotinic acetylcholine receptor and STAT3. *Breast Cancer Res Treat* 2014;145(1):5-22.
Guo, J., *et al.* miR-346 Up-regulates Argonaute 2 (AGO2) Protein Expression to Augment the Activity of Other MicroRNAs (miRNAs) and Contributes to Cervical Cancer Cell Malignancy. *J Biol Chem* 2015;290(51):30342-30350.
Hafner, A., *et al.* The multiple mechanisms that regulate p53 activity and cell fate. *Nat Rev Mol Cell Biol* 2019;20(4):199-210.
Haga, C.L. and Phinney, D.G. MicroRNAs in the imprinted DLK1-DIO3 region repress the epithelial-to-mesenchymal transition by targeting the TWIST1 protein signaling network. *J Biol Chem* 2012;287(51):42695-42707.
Hah, N., *et al.* A rapid, extensive, and transient transcriptional response to estrogen signaling in breast cancer cells. *Cell* 2011;145(4):622-634.

Hajarnis, S., Lakhia, R. and Patel, V. MicroRNAs and Polycystic Kidney Disease. In: Li, X., editor, *Polycystic Kidney Disease*. Brisbane (AU); 2015.
Hallden, S., *et al.* Gene variance in the nicotinic receptor cluster (CHRNA5-CHRNA3-CHRNB4) predicts death from cardiopulmonary disease and cancer in smokers. *J Intern Med* 2016;279(4):388-398.
Hamilton, E.P., *et al.* A First-in-Human Study of the New Oral Selective Estrogen Receptor Degrader AZD9496 for ER(+)/HER2(-) Advanced Breast Cancer. *Clin Cancer Res* 2018;24(15):3510-3518.
Han, H., *et al.* Synergistic re-activation of epigenetically silenced genes by combinatorial inhibition of DNMTs and LSD1 in cancer cells. *PLoS One* 2013;8(9):e75136.
Hancock, D.B., *et al.* Genome-wide meta-analysis reveals common splice site acceptor variant in CHRNA4 associated with nicotine dependence. *Transl Psychiatry* 2015;5:e651.
Harris, S.L. and Levine, A.J. The p53 pathway: positive and negative feedback loops. *Oncogene* 2005;24(17):2899-2908.
He, G., *et al.* Induction of p21 by p53 following DNA damage inhibits both Cdk4 and Cdk2 activities. *Oncogene* 2005;24(18):2929-2943.
He, L., *et al.* Network-guided identification of cancer-selective combinatorial therapies in ovarian cancer. *Brief Bioinform* 2021.
He, Z., *et al.* NEAT1 promotes colon cancer progression through sponging miR-495-3p and activating CDK6 in vitro and in vivo. *J Cell Physiol* 2019;234(11):19582-19591.
Heeschen, C., *et al.* A novel angiogenic pathway mediated by non-neuronal nicotinic acetylcholine receptors. *J Clin Invest* 2002;110(4):527-536.
Heng, B., *et al.* Understanding the role of the kynurenine pathway in human breast cancer immunobiology. *Oncotarget* 2016;7(6):6506-6520.
Hennigs, A., *et al.* Prognosis of breast cancer molecular subtypes in routine clinical care: A large prospective cohort study. *BMC Cancer* 2016;16(1):734.
Herschkowitz, J.I., *et al.* Identification of conserved gene expression features between murine mammary carcinoma models and human breast tumors. *Genome Biol* 2007;8(5):R76.
Hill, K.E., *et al.* An imprinted non-coding genomic cluster at 14q32 defines clinically relevant molecular subtypes in osteosarcoma across multiple independent datasets. *J Hematol Oncol* 2017;10(1):107.
Himanshu Joshi, M.F.P. 22 - Molecular Oncology of Breast Cancer. In: Kirby I. Bland, E.M.C., V. Suzanne Klimberg, William J. Gradishar, editor, *The Breast (Fifth Edition)*,. Elsevier; 2018. p. 282-307.
Hoffmann, M.J., *et al.* Downregulation of Cell Cycle and Checkpoint Genes by Class I HDAC Inhibitors Limits Synergism with G2/M Checkpoint Inhibitor MK-1775 in Bladder Cancer Cells. *Genes (Basel)* 2021;12(2).
Holder, J.L., Jr., *et al.* A child with an inherited 0.31 Mb microdeletion of chromosome 14q32.33: further delineation of a critical region for the 14q32 deletion syndrome. *Am J Med Genet A* 2012;158A(8):1962-1966.
Hoppe, R., *et al.* Profiles of miRNAs matched to biology in aromatase inhibitor resistant breast cancer. *Oncotarget* 2016;7(44):71235-71254.
Hossain, D.M.S., *et al.* Dinaciclib induces immunogenic cell death and enhances anti-PD1-mediated tumor suppression. *J Clin Invest* 2018;128(2):644-654.
Hu, Y., *et al.* Analysis of key genes and signaling pathways involved in Helicobacter pylori-associated gastric cancer based on The Cancer Genome Atlas database and RNA sequencing data. *Helicobacter* 2018;23(5):e12530.
Huang, G.M., *et al.* LncRNA FAM83A-AS1 aggravates the malignant development of esophageal cancer by binding to miR-495-3p. *Eur Rev Med Pharmacol Sci* 2020;24(18):9408-9415.
Huang, L., *et al.* Eosinophils and IL-4 Support Nematode Growth Coincident with an Innate Response to Tissue Injury. *PLoS Pathog* 2015;11(12):e1005347.
Humeau, J., *et al.* Calcium signaling and cell cycle: Progression or death. *Cell Calcium* 2018;70:3-15.

Huun, J., Lonning, P.E. and Knappskog, S. Effects of concomitant inactivation of p53 and pRb on response to doxorubicin treatment in breast cancer cell lines. *Cell Death Discov* 2017;3:17026.
Hwang-Verslues, W.W., *et al.* miR-495 is upregulated by E12/E47 in breast cancer stem cells, and promotes oncogenesis and hypoxia resistance via downregulation of E-cadherin and REDD1. *Oncogene* 2011;30(21):2463-2474.
Ibarra, I.L., *et al.* Mechanistic insights into transcription factor cooperativity and its impact on protein-phenotype interactions. *Nat Commun* 2020;11(1):124.
Improgo, M.R., *et al.* ASCL1 regulates the expression of the CHRNA5/A3/B4 lung cancer susceptibility locus. *Mol Cancer Res* 2010;8(2):194-203.
Improgo, M.R., *et al.* Nicotinic acetylcholine receptors mediate lung cancer growth. *Front Physiol* 2013;4:251.
Jafari Ghods, F., *et al.* MiRNA and mRNA Profiling in Systemic Lupus Reveals a Novel Set of Cytokine - Related miRNAs and their Target Genes in Cases With and Without Renal Involvement. *Kidney Blood Press Res* 2017;42(6):1322-1337.
Janky, R., *et al.* iRegulon: from a gene list to a gene regulatory network using large motif and track collections. *PLoS Comput Biol* 2014;10(7):e1003731.
Janowsky, J.S., Chavez, B. and Orwoll, E. Sex steroids modify working memory. *J Cogn Neurosci* 2000;12(3):407-414.
Jeselsohn, R., *et al.* Abstract PD1-05: Results from the phase Ib/II clinical trial of bazedoxifene and palbociclib in hormone receptor positive metastatic breast cancer. *Cancer Research* 2019;79(4 Supplement):PD1-05-PD01-05.
Jia, M., *et al.* Estrogen Receptor alpha Promotes Breast Cancer by Reprogramming Choline Metabolism. *Cancer Res* 2016;76(19):5634-5646.
Jiang, W., *et al.* Overexpression of microRNA-495 suppresses the proliferation and invasion and induces the apoptosis of osteosarcoma cells by targeting high-mobility group nucleosome-binding domain 5. *Oncol Rep* 2017;38(2):1099-1107.
Jiang, X., *et al.* MiR-495 is a tumor-suppressor microRNA down-regulated in MLL-rearranged leukemia. *Proc Natl Acad Sci U S A* 2012;109(47):19397-19402.
Jin, X., Bermudez, I. and Steinbach, J.H. The nicotinic alpha5 subunit can replace either an acetylcholine-binding or nonbinding subunit in the alpha4beta2* neuronal nicotinic receptor. *Mol Pharmacol* 2014;85(1):11-17.
Jishnu, P.V., *et al.* Prognostic role of 14q32.31 miRNA cluster in various carcinomas: a systematic review and meta-analysis. *Clin Exp Metastasis* 2020;37(1):31-46.
Johansson, L., *et al.* The orphan nuclear receptor SHP utilizes conserved LXXLL-related motifs for interactions with ligand-activated estrogen receptors. *Mol Cell Biol* 2000;20(4):1124-1133.
Johnson, D.A., Zambon, N.J. and Gibbs, R.B. Selective lesion of cholinergic neurons in the medial septum by 192 IgG-saporin impairs learning in a delayed matching to position T-maze paradigm. *Brain Res* 2002;943(1):132-141.
Joseph, J.D., *et al.* The selective estrogen receptor downregulator GDC-0810 is efficacious in diverse models of ER+ breast cancer. *Elife* 2016;5.
Joseph, R., *et al.* Integrative model of genomic factors for determining binding site selection by estrogen receptor-alpha. *Mol Syst Biol* 2010;6:456.
Kabbani, N., *et al.* Are nicotinic acetylcholine receptors coupled to G proteins? *Bioessays* 2013;35(12):1025-1034.
Kahl, C.R. and Means, A.R. Regulation of cell cycle progression by calcium/calmodulin-dependent pathways. *Endocr Rev* 2003;24(6):719-736.
Kahl, C.R. and Means, A.R. Calcineurin regulates cyclin D1 accumulation in growth-stimulated fibroblasts. *Mol Biol Cell* 2004;15(4):1833-1842.
Kahraman, M., *et al.* Maximizing ER-alpha Degradation Maximizes Activity in a Tamoxifen-Resistant Breast Cancer Model: Identification of GDC-0927. *ACS Med Chem Lett* 2019;10(1):50-55.
Kalaitzidis, D. and Gilmore, T.D. Transcription factor cross-talk: the estrogen receptor and NF-kappaB. *Trends Endocrinol Metab* 2005;16(2):46-52.
Kanda, M., *et al.* Blockade of CHRNB2 signaling with a therapeutic monoclonal antibody attenuates the aggressiveness of gastric cancer cells. *Oncogene* 2021;40(36):5495-5504.

Kanehisa, M., *et al.* KEGG as a reference resource for gene and protein annotation. *Nucleic Acids Res* 2016;44(D1):D457-462.
Kang, S.H., *et al.* Cationic liposomal co-delivery of small interfering RNA and a MEK inhibitor for enhanced anticancer efficacy. *Pharm Res* 2011;28(12):3069-3078.
Karlin, A. Emerging structure of the nicotinic acetylcholine receptors. *Nat Rev Neurosci* 2002;3(2):102-114.
Keenan, A.B., *et al.* ChEA3: transcription factor enrichment analysis by orthogonal omics integration. *Nucleic Acids Res* 2019;47(W1):W212-W224.
Khraiwesh, B., *et al.* Genome-wide expression analysis offers new insights into the origin and evolution of Physcomitrella patens stress response. *Sci Rep* 2015;5:17434.
Kim, M.Y., *et al.* Acetylation of estrogen receptor alpha by p300 at lysines 266 and 268 enhances the deoxyribonucleic acid binding and transactivation activities of the receptor. *Mol Endocrinol* 2006;20(7):1479-1493.
Kim, Y.S., *et al.* miRNAs involved in LY6K and estrogen receptor alpha contribute to tamoxifen-susceptibility in breast cancer. *Oncotarget* 2016;7(27):42261-42273.
Knijnenburg, T.A., *et al.* Genomic and Molecular Landscape of DNA Damage Repair Deficiency across The Cancer Genome Atlas. *Cell Rep* 2018;23(1):239-254 e236.
Kohn, E.C., *et al.* Identification and molecular characterization of a m5 muscarinic receptor in A2058 human melanoma cells. Coupling to inhibition of adenylyl cyclase and stimulation of phospholipase A2. *J Biol Chem* 1996;271(29):17476-17484.
Komm, B.S., *et al.* Bazedoxifene acetate: a selective estrogen receptor modulator with improved selectivity. *Endocrinology* 2005;146(9):3999-4008.
Konduri, S.D., *et al.* Mechanisms of estrogen receptor antagonism toward p53 and its implications in breast cancer therapeutic response and stem cell regulation. *Proc Natl Acad Sci U S A* 2010;107(34):15081-15086.
Korzets, A., *et al.* H2O2 induces DNA repair in mononuclear cells: evidence for association with cytosolic Ca2+ fluxes. *J Lab Clin Med* 1999;133(4):362-369.
Kosmicki, J.A., *et al.* Refining the role of de novo protein-truncating variants in neurodevelopmental disorders by using population reference samples. *Nat Genet* 2017;49(4):504-510.
Krais, A.M., *et al.* CHRNA5 as negative regulator of nicotine signaling in normal and cancer bronchial cells: effects on motility, migration and p63 expression. *Carcinogenesis* 2011;32(9):1388-1395.
Krejcik, Z., *et al.* Aberrant expression of the microRNA cluster in 14q32 is associated with del(5q) myelodysplastic syndrome and lenalidomide treatment. *Cancer Genet* 2015;208(4):156-161.
Krokker, L., Patocs, A. and Butz, H. Essential Role of the 14q32 Encoded miRNAs in Endocrine Tumors. *Genes (Basel)* 2021;12(5).
Kruer, T.L., *et al.* Expression of the lncRNA Maternally Expressed Gene 3 (MEG3) Contributes to the Control of Lung Cancer Cell Proliferation by the Rb Pathway. *PLoS One* 2016;11(11):e0166363.
Kruse, J.P. and Gu, W. Modes of p53 regulation. *Cell* 2009;137(4):609-622.
Kulukian, A., *et al.* Preclinical Activity of HER2-Selective Tyrosine Kinase Inhibitor Tucatinib as a Single Agent or in Combination with Trastuzumab or Docetaxel in Solid Tumor Models. *Mol Cancer Ther* 2020;19(4):976-987.
Kumar, A., *et al.* Identification of miR-379/miR-656 (C14MC) cluster downregulation and associated epigenetic and transcription regulatory mechanism in oligodendrogliomas. *J Neurooncol* 2018;139(1):23-31.
Kumar, U., *et al.* MicroRNA-495/TGF-beta/FOXC1 axis regulates multidrug resistance in metaplastic breast cancer cells. *Biochem Pharmacol* 2021;192:114692.
Kuryatov, A., Berrettini, W. and Lindstrom, J. Acetylcholine receptor (AChR) alpha5 subunit variant associated with risk for nicotine dependence and lung cancer reduces (alpha4beta2)(2)alpha5 AChR function. *Mol Pharmacol* 2011;79(1):119-125.
Kuryatov, A., Onksen, J. and Lindstrom, J. Roles of accessory subunits in alpha4beta2(*) nicotinic receptors. *Mol Pharmacol* 2008;74(1):132-143.

Kwon, H.M., *et al.* Combinatorial effects of an epigenetic inhibitor and ionizing radiation contribute to targeted elimination of pancreatic cancer stem cell. *Oncotarget* 2017;8(51):89005-89020.
Kwong, J.M.K., *et al.* Differential Retinal Protein Expression in Primary and Secondary Retinal Ganglion Cell Degeneration Identified by Integrated SWATH and Target-Based Proteomics. *Int J Mol Sci* 2021;22(16).
Lambert, S.A., *et al.* Similarity regression predicts evolution of transcription factor sequence specificity. *Nat Genet* 2019;51(6):981-989.
Lappalainen, I., *et al.* The European Genome-phenome Archive of human data consented for biomedical research. *Nat Genet* 2015;47(7):692-695.
Larsson, M., *et al.* Local co-administration of gene-silencing RNA and drugs in cancer therapy: State-of-the art and therapeutic potential. *Cancer Treat Rev* 2017;55:128-135.
Le Novere, N., Corringer, P.J. and Changeux, J.P. The diversity of subunit composition in nAChRs: evolutionary origins, physiologic and pharmacologic consequences. *J Neurobiol* 2002;53(4):447-456.
Lebois, E.P., *et al.* Muscarinic receptor subtype distribution in the central nervous system and relevance to aging and Alzheimer's disease. *Neuropharmacology* 2018;136(Pt C):362-373.
Lee, C.H., *et al.* Crosstalk between nicotine and estrogen-induced estrogen receptor activation induces alpha9-nicotinic acetylcholine receptor expression in human breast cancer cells. *Breast Cancer Res Treat* 2011;129(2):331-345.
Lee, C.H., *et al.* Overexpression and activation of the alpha9-nicotinic receptor during tumorigenesis in human breast epithelial cells. *J Natl Cancer Inst* 2010;102(17):1322-1335.
Lee, S.H., *et al.* Targeting of RUNX3 by miR-130a and miR-495 cooperatively increases cell proliferation and tumor angiogenesis in gastric cancer cells. *Oncotarget* 2015;6(32):33269-33278.
Lee, S.Y., *et al.* miR-4463 regulates aromatase expression and activity for 17beta-estradiol synthesis in response to follicle-stimulating hormone. *Clin Exp Reprod Med* 2020;47(3):194-206.
Lettlova, S., *et al.* MiR-301a-3p Suppresses Estrogen Signaling by Directly Inhibiting ESR1 in ERalpha Positive Breast Cancer. *Cell Physiol Biochem* 2018;46(6):2601-2615.
Lewis-Wambi, J.S., *et al.* The selective estrogen receptor modulator bazedoxifene inhibits hormone-independent breast cancer cell growth and down-regulates estrogen receptor alpha and cyclin D1. *Mol Pharmacol* 2011;80(4):610-620.
Li, C., *et al.* Requirement of Sp1 and estrogen receptor alpha interaction in 17beta-estradiol-mediated transcriptional activation of the low density lipoprotein receptor gene expression. *Endocrinology* 2001;142(4):1546-1553.
Li, D. and Cao, W. Role of intracellular calcium and NADPH oxidase NOX5-S in acid-induced DNA damage in Barrett's cells and Barrett's esophageal adenocarcinoma cells. *Am J Physiol Gastrointest Liver Physiol* 2014;306(10):G863-872.
Li, J., *et al.* Essentiality and Transcriptome-Enriched Pathway Scores Predict Drug-Combination Synergy. *Biology (Basel)* 2020;9(9).
Li, J.Z., *et al.* MicroRNA-495 Regulates Migration and Invasion in Prostate Cancer Cells Via Targeting Akt and mTOR Signaling. *Cancer Invest* 2016;34(4):181-188.
Li, N., *et al.* MicroRNA-495 Confers Increased Sensitivity to Chemotherapeutic Agents in Gastric Cancer via the Mammalian Target of Rapamycin (mTOR) Signaling Pathway by Interacting with Human Epidermal Growth Factor Receptor 2 (ERBB2). *Med Sci Monit* 2018;24:5960-5972.
Li, Q., *et al.* Upregulation of miR-146b promotes porcine ovarian granulosa cell apoptosis by attenuating CYP19A1. *Domest Anim Endocrinol* 2021;74:106509.
Li, Q., *et al.* MiR-126* is a novel functional target of transcription factor SMAD4 in ovarian granulosa cells. *Gene* 2019;711:143953.
Li, Q., *et al.* Nicotine reduces TNF-alpha expression through a alpha7 nAChR/MyD88/NF-kB pathway in HBE16 airway epithelial cells. *Cell Physiol Biochem* 2011;27(5):605-612.
Li, Y., *et al.* Mirsynergy: detecting synergistic miRNA regulatory modules by overlapping neighbourhood expansion. *Bioinformatics* 2014;30(18):2627-2635.
Li, Z., *et al.* miR-495 and miR-551a inhibit the migration and invasion of human gastric cancer cells by directly interacting with PRL-3. *Cancer Lett* 2012;323(1):41-47.

Li, Z., *et al.* The differences in ultrasound and clinicopathological features between basal-like and normal-like subtypes of triple negative breast cancer. *PLoS One* 2015;10(3):e0114820.
Li, Z., *et al.* Methylation-associated silencing of miR-495 inhibit the migration and invasion of human gastric cancer cells by directly targeting PRL-3. *Biochem Biophys Res Commun* 2015;456(1):344-350.
Liang, Q., *et al.* Long non-coding RNA, HOTAIRM1, promotes glioma malignancy by forming a ceRNA network. *Aging (Albany NY)* 2019;11(17):6805-6838.
Liao, K., *et al.* The LGMN pseudogene promotes tumor progression by acting as a miR-495-3p sponge in glioblastoma. *Cancer Lett* 2020;490:111-123.
Liao, X.H., *et al.* Estrogen receptor alpha mediates proliferation of breast cancer MCF-7 cells via a p21/PCNA/E2F1-dependent pathway. *FEBS J* 2014;281(3):927-942.
Lin, C.H., *et al.* Nicotinic Acetylcholine Receptor Subunit Alpha-5 Promotes Radioresistance via Recruiting E2F Activity in Oral Squamous Cell Carcinoma. *J Clin Med* 2019;8(9).
Lin, G., *et al.* Overexpression of muscarinic receptor 3 promotes metastasis and predicts poor prognosis in non-small-cell lung cancer. *J Thorac Oncol* 2014;9(2):170-178.
Lin, S., *et al.* The lncRNA GATA3-AS1/miR-495-3p/CENPU axis predicts poor prognosis of breast cancer via the PLK1 signaling pathway. *Aging (Albany NY)* 2021;13(10):13663-13679.
Lin, W., *et al.* Role of alpha7-nicotinic acetylcholine receptor in normal and cancer stem cells. *Curr Drug Targets* 2012;13(5):656-665.
Lin, Z., *et al.* Novel estrogen receptor-alpha binding sites and estradiol target genes identified by chromatin immunoprecipitation cloning in breast cancer. *Cancer Res* 2007;67(10):5017-5024.
Lischka, J., *et al.* Circulating microRNAs 34a, 122, and 192 are linked to obesity-associated inflammation and metabolic disease in pediatric patients. *Int J Obes (Lond)* 2021;45(8):1763-1772.
Liu, C., *et al.* Genetic polymorphisms and lung cancer risk: Evidence from meta-analyses and genome-wide association studies. *Lung Cancer* 2017;113:18-29.
Liu, C., *et al.* MicroRNA 495 Inhibits Proliferation and Metastasis and Promotes Apoptosis by Targeting Twist1 in Gastric Cancer Cells. *Oncol Res* 2019;27(3):389-397.
Liu, F. and Di Wang, X. miR-150-5p represses TP53 tumor suppressor gene to promote proliferation of colon adenocarcinoma. *Sci Rep* 2019;9(1):6740.
Liu, J., *et al.* Identification of three molecular subtypes based on immune infiltration in ovarian cancer and its prognostic value. *Biosci Rep* 2020;40(10).
Liu, L., *et al.* GPR30-mediated HMGB1 upregulation in CAFs induces autophagy and tamoxifen resistance in ERalpha-positive breast cancer cells. *Aging (Albany NY)* 2021;13(12):16178-16197.
Liu, M.M., *et al.* Opposing action of estrogen receptors alpha and beta on cyclin D1 gene expression. *J Biol Chem* 2002;277(27):24353-24360.
Liu, Q., *et al.* Evaluation of drug combination effect using a Bliss independence dose-response surface model. *Stat Biopharm Res* 2018;10(2):112-122.
Liu, S., *et al.* Prediction of Gene Expression Patterns With Generalized Linear Regression Model. *Front Genet* 2019;10:120.
Liu, S. and Xi, X. LINC01133 contribute to epithelial ovarian cancer metastasis by regulating miR-495-3p/TPD52 axis. *Biochem Biophys Res Commun* 2020;533(4):1088-1094.
Liu, S.S., *et al.* The ERalpha-miR-575-p27 feedback loop regulates tamoxifen sensitivity in ER-positive Breast Cancer. *Theranostics* 2020;10(23):10729-10742.
Liu, W., *et al.* Estrogen receptor-alpha binds p53 tumor suppressor protein directly and represses its function. *J Biol Chem* 2006;281(15):9837-9840.
Liu, Z., Zhang, X.S. and Zhang, S. Breast tumor subgroups reveal diverse clinical prognostic power. *Sci Rep* 2014;4:4002.
Livak, K.J. and Schmittgen, T.D. Analysis of relative gene expression data using real-time quantitative PCR and the 2(-Delta Delta C(T)) Method. *Methods* 2001;25(4):402-408.
Llanos, S., *et al.* Stabilization of p53 by p14ARF without relocation of MDM2 to the nucleolus. *Nat Cell Biol* 2001;3(5):445-452.
Luine, V.N. Estradiol and cognitive function: past, present and future. *Horm Behav* 2014;66(4):602-618.

Luine, V.N. and McEwen, B.S. Sex differences in cholinergic enzymes of diagonal band nuclei in the rat preoptic area. *Neuroendocrinology* 1983;36(6):475-482.
Lv, C., *et al.* MicroRNA-495 suppresses human renal cell carcinoma malignancy by targeting SATB1. *Am J Transl Res* 2015;7(10):1992-1999.
Lv, L., *et al.* MicroRNA495 targets Notch1 to prohibit cell proliferation and invasion in oral squamous cell carcinoma. *Mol Med Rep* 2019;19(1):693-702.
Maenza, J. and Flexner, C. Combination antiretroviral therapy for HIV infection. *Am Fam Physician* 1998;57(11):2789-2798.
Mahapatra, S. and Challagundla, K.B. Neuroblastoma. In, *StatPearls*. Treasure Island (FL); 2021.
Mal, R., *et al.* Estrogen Receptor Beta (ERbeta): A Ligand Activated Tumor Suppressor. *Front Oncol* 2020;10:587386.
Mallik, S., *et al.* A Linear Regression and Deep Learning Approach for Detecting Reliable Genetic Alterations in Cancer Using DNA Methylation and Gene Expression Data. *Genes (Basel)* 2020;11(8).
Mandal, S. and Davie, J.R. Estrogen regulated expression of the p21 Waf1/Cip1 gene in estrogen receptor positive human breast cancer cells. *J Cell Physiol* 2010;224(1):28-32.
Mansoori, B., *et al.* miR-142-3p is a tumor suppressor that inhibits estrogen receptor expression in ER-positive breast cancer. *J Cell Physiol* 2019.
Mao, Y., *et al.* MiR-495 inhibits esophageal squamous cell carcinoma progression by targeting Akt1. *Oncotarget* 2016;7(32):51223-51236.
Marceau, A.H., *et al.* An order-to-disorder structural switch activates the FoxM1 transcription factor. *Elife* 2019;8.
Mardanshahi, A., *et al.* The PI3K/AKT/mTOR signaling pathway inhibitors enhance radiosensitivity in cancer cell lines. *Mol Biol Rep* 2021;48(8):1-14.
Marino, M., Galluzzo, P. and Ascenzi, P. Estrogen signaling multiple pathways to impact gene transcription. *Curr Genomics* 2006;7(8):497-508.
Martin, E.C., *et al.* MicroRNA-335-5p and -3p synergize to inhibit estrogen receptor alpha expression and promote tamoxifen resistance. *FEBS Lett* 2017;591(2):382-392.
Mathison, A., *et al.* Combined AURKA and H3K9 Methyltransferase Targeting Inhibits Cell Growth By Inducing Mitotic Catastrophe. *Mol Cancer Res* 2017;15(8):984-997.
Mayo, L.D., Turchi, J.J. and Berberich, S.J. Mdm-2 phosphorylation by DNA-dependent protein kinase prevents interaction with p53. *Cancer Res* 1997;57(22):5013-5016.
McGowan, E.M., *et al.* Evaluation of cell cycle arrest in estrogen responsive MCF-7 breast cancer cells: pitfalls of the MTS assay. *PLoS One* 2011;6(6):e20623.
McGowan, E.M., *et al.* p14ARF post-transcriptional regulation of nuclear cyclin D1 in MCF-7 breast cancer cells: discrimination between a good and bad prognosis? *PLoS One* 2012;7(7):e42246.
McNair, C., *et al.* Differential impact of RB status on E2F1 reprogramming in human cancer. *J Clin Invest* 2018;128(1):341-358.
Medjber, K., *et al.* Role of nicotinic acetylcholine receptors in cell proliferation and tumour invasion in broncho-pulmonary carcinomas. *Lung Cancer* 2015;87(3):258-264.
Mehta, A. and Baltimore, D. MicroRNAs as regulatory elements in immune system logic. *Nat Rev Immunol* 2016;16(5):279-294.
Meng, D., *et al.* MicroRNA-1280 modulates cell growth and invasion of thyroid carcinoma through targeting estrogen receptor alpha. *Cell Mol Biol (Noisy-le-grand)* 2016;62(3):1-6.
Mi, H., *et al.* PANTHER version 14: more genomes, a new PANTHER GO-slim and improvements in enrichment analysis tools. *Nucleic Acids Res* 2019;47(D1):D419-D426.
Mijit, M., *et al.* Role of p53 in the Regulation of Cellular Senescence. *Biomolecules* 2020;10(3).
Miller, T.E., *et al.* MicroRNA-221/222 confers tamoxifen resistance in breast cancer by targeting p27Kip1. *J Biol Chem* 2008;283(44):29897-29903.
Min, H.Y., *et al.* Smoking-associated lung cancer prevention by blockade of the beta-adrenergic receptor-mediated insulin-like growth factor receptor activation. *Oncotarget* 2016;7(43):70936-70947.

Mirzamohammadi, S., *et al.* Protective effect of 17beta-estradiol on serum deprivation-induced apoptosis and oxidative stress in bone marrow-derived mesenchymal stem cells. *Hum Exp Toxicol* 2016;35(3):312-322.
Molina-Pinelo, S., *et al.* Impact of DLK1-DIO3 imprinted cluster hypomethylation in smoker patients with lung cancer. *Oncotarget* 2018;9(4):4395-4410.
Montemurro, F., Valabrega, G. and Aglietta, M. Lapatinib: a dual inhibitor of EGFR and HER2 tyrosine kinase activity. *Expert Opin Biol Ther* 2007;7(2):257-268.
Morris, J.H., *et al.* clusterMaker: a multi-algorithm clustering plugin for Cytoscape. *BMC Bioinformatics* 2011;12:436.
Mosconi, L., *et al.* Perimenopause and emergence of an Alzheimer's bioenergetic phenotype in brain and periphery. *PLoS One* 2017;12(10):e0185926.
Moulder, D.E., *et al.* The Roles of p53 in Mitochondrial Dynamics and Cancer Metabolism: The Pendulum between Survival and Death in Breast Cancer? *Cancers (Basel)* 2018;10(6).
Murray-Zmijewski, F., Slee, E.A. and Lu, X. A complex barcode underlies the heterogeneous response of p53 to stress. *Nat Rev Mol Cell Biol* 2008;9(9):702-712.
Musgrove, E.A., *et al.* Cyclin D as a therapeutic target in cancer. *Nat Rev Cancer* 2011;11(8):558-572.
Mutalifu, N., *et al.* Circ_0000215 Increases the Expression of CXCR2 and Promoted the Progression of Glioma Cells by Sponging miR-495-3p. *Technol Cancer Res Treat* 2020;19:1533033820957026.
Nagaoka, K., *et al.* Deep immunophenotyping at the single-cell level identifies a combination of anti-IL-17 and checkpoint blockade as an effective treatment in a preclinical model of data-guided personalized immunotherapy. *J Immunother Cancer* 2020;8(2).
Naseri, M.H., *et al.* Up regulation of Bax and down regulation of Bcl2 during 3-NC mediated apoptosis in human cancer cells. *Cancer Cell Int* 2015;15:55.
Nassiri, I., *et al.* Regulatory Crosstalk of Doxorubicin, Estradiol and TNFalpha Combined Treatment in Breast Cancer-derived Cell Lines. *Sci Rep* 2019;9(1):15172.
Nath, A., *et al.* Elevated free fatty acid uptake via CD36 promotes epithelial-mesenchymal transition in hepatocellular carcinoma. *Sci Rep* 2015;5:14752.
Nathan, M.R. and Schmid, P. A Review of Fulvestrant in Breast Cancer. *Oncol Ther* 2017;5(1):17-29.
Nichols, W.A., *et al.* Mutation Linked to Autosomal Dominant Nocturnal Frontal Lobe Epilepsy Reduces Low-Sensitivity alpha4beta2, and Increases alpha5alpha4beta2, Nicotinic Receptor Surface Expression. *PLoS One* 2016;11(6):e0158032.
Nie, S., *et al.* miR-495 mediates metabolic shift in glioma cells via targeting Glut1. *J Craniofac Surg* 2015;26(2):e155-158.
Nikulenkov, F., *et al.* Insights into p53 transcriptional function via genome-wide chromatin occupancy and gene expression analysis. *Cell Death Differ* 2012;19(12):1992-2002.
Nishimura, M., *et al.* Therapeutic synergy between microRNA and siRNA in ovarian cancer treatment. *Cancer Discov* 2013;3(11):1302-1315.
Nishioka, T., *et al.* Nicotine exposure induces the proliferation of oral cancer cells through the alpha7 subunit of the nicotinic acetylcholine receptor. *Biochem Biophys Res Commun* 2019;509(2):514-520.
Nourbakhsh, M., *et al.* Nanolipoparticles-mediated MDR1 siRNA delivery reduces doxorubicin resistance in breast cancer cells and silences MDR1 expression in xenograft model of human breast cancer. *Iran J Basic Med Sci* 2015;18(4):385-392.
O'Hara, D.M., *et al.* LRRK2 and alpha-Synuclein: Distinct or Synergistic Players in Parkinson's Disease? *Front Neurosci* 2020;14:577.
O'Lone, R., *et al.* Genomic targets of nuclear estrogen receptors. *Mol Endocrinol* 2004;18(8):1859-1875.
Oddo, S. and LaFerla, F.M. The role of nicotinic acetylcholine receptors in Alzheimer's disease. *J Physiol Paris* 2006;99(2-3):172-179.
Olivier, M., Hollstein, M. and Hainaut, P. TP53 mutations in human cancers: origins, consequences, and clinical use. *Cold Spring Harb Perspect Biol* 2010;2(1):a001008.

Olivo-Marston, S.E., *et al.* Serum estrogen and tumor-positive estrogen receptor-alpha are strong prognostic classifiers of non-small-cell lung cancer survival in both men and women. *Carcinogenesis* 2010;31(10):1778-1786.
Ord, T., *et al.* Pharmacological or TRIB3-Mediated Suppression of ATF4 Transcriptional Activity Promotes Hepatoma Cell Resistance to Proteasome Inhibitor Bortezomib. *Cancers (Basel)* 2021;13(10).
Oshima, G., *et al.* DNA Methylation Controls Metastasis-Suppressive 14q32-Encoded miRNAs. *Cancer Res* 2019;79(3):650-662.
Pacini, L., *et al.* M2muscarinic receptors inhibit cell proliferation and migration in urothelial bladder cancer cells. *Cancer Biol Ther* 2014;15(11):1489-1498.
Paech, K., *et al.* Differential ligand activation of estrogen receptors ERalpha and ERbeta at AP1 sites. *Science* 1997;277(5331):1508-1510.
Paliwal, A., *et al.* Aberrant DNA methylation links cancer susceptibility locus 15q25.1 to apoptotic regulation and lung cancer. *Cancer Res* 2010;70(7):2779-2788.
Palluzzi, F., *et al.* A novel network analysis approach reveals DNA damage, oxidative stress and calcium/cAMP homeostasis-associated biomarkers in frontotemporal dementia. *PLoS One* 2017;12(10):e0185797.
Pandey, D.P. and Picard, D. miR-22 inhibits estrogen signaling by directly targeting the estrogen receptor alpha mRNA. *Mol Cell Biol* 2009;29(13):3783-3790.
Pardinas, A.F., *et al.* Common schizophrenia alleles are enriched in mutation-intolerant genes and in regions under strong background selection. *Nat Genet* 2018;50(3):381-389.
Park, J.R., Eggert, A. and Caron, H. Neuroblastoma: biology, prognosis, and treatment. *Hematol Oncol Clin North Am* 2010;24(1):65-86.
Park, S.M., *et al.* The miR-200 family determines the epithelial phenotype of cancer cells by targeting the E-cadherin repressors ZEB1 and ZEB2. *Genes Dev* 2008;22(7):894-907.
Parker, J.S., *et al.* Supervised risk predictor of breast cancer based on intrinsic subtypes. *J Clin Oncol* 2009;27(8):1160-1167.
Peixoto, P., *et al.* EMT is associated with an epigenetic signature of ECM remodeling genes. *Cell Death Dis* 2019;10(3):205.
Peng, J., Oo, M.L. and Andersen, J.K. Synergistic effects of environmental risk factors and gene mutations in Parkinson's disease accelerate age-related neurodegeneration. *J Neurochem* 2010;115(6):1363-1373.
Perez-Aguilar, B., *et al.* Acetylcholinesterase is associated with a decrease in cell proliferation of hepatocellular carcinoma cells. *Biochim Biophys Acta* 2015;1852(7):1380-1387.
Perkins, K.A., *et al.* Nicotinic acetylcholine receptor beta2 subunit (CHRNB2) gene and short-term ability to quit smoking in response to nicotine patch. *Cancer Epidemiol Biomarkers Prev* 2009;18(10):2608-2612.
Perou, C.M., *et al.* Molecular portraits of human breast tumours. *Nature* 2000;406(6797):747-752.
Peterson, E.A., *et al.* Amphiregulin Is a Critical Downstream Effector of Estrogen Signaling in ERalpha-Positive Breast Cancer. *Cancer Res* 2015;75(22):4830-4838.
Peyre, M., *et al.* Portrait of ependymoma recurrence in children: biomarkers of tumor progression identified by dual-color microarray-based gene expression analysis. *PLoS One* 2010;5(9):e12932.
Pfister, K., *et al.* Identification of Drivers of Aneuploidy in Breast Tumors. *Cell Rep* 2018;23(9):2758-2769.
Phillips, S.M. and Sherwin, B.B. Effects of estrogen on memory function in surgically menopausal women. *Psychoneuroendocrinology* 1992;17(5):485-495.
Poletto, M., *et al.* p53 coordinates base excision repair to prevent genomic instability. *Nucleic Acids Res* 2016;44(7):3165-3175.
Pommier, R.M., *et al.* Comprehensive characterization of claudin-low breast tumors reflects the impact of the cell-of-origin on cancer evolution. *Nat Commun* 2020;11(1):3431.
Prasasya, R., *et al.* Temple syndrome and Kagami-Ogata syndrome: clinical presentations, genotypes, models and mechanisms. *Hum Mol Genet* 2020;29(R1):R107-R116.
Prevost, M.S., *et al.* Concatemers to re-investigate the role of alpha5 in alpha4beta2 nicotinic receptors. *Cell Mol Life Sci* 2021;78(3):1051-1064.

Prossnitz, E.R. and Barton, M. The G-protein-coupled estrogen receptor GPER in health and disease. *Nat Rev Endocrinol* 2011;7(12):715-726.
Qian, J., *et al.* lncRNA LUNAR1 accelerates colorectal cancer progression by targeting the miR4953p/MYCBP axis. *Int J Oncol* 2020;57(5):1157-1168.
Qiu, Y., *et al.* Protein phosphatase PHLPP induces cell apoptosis and exerts anticancer activity by inhibiting Survivin phosphorylation and nuclear export in gallbladder cancer. *Oncotarget* 2015;6(22):19148-19162.
Qiu, Y.A., *et al.* GPER-Induced ERK Signaling Decreases Cell Viability of Hepatocellular Carcinoma. *Front Oncol* 2021;11:638171.
Quik, M., *et al.* Targeting nicotinic receptors for Parkinson's disease therapy. *CNS Neurol Disord Drug Targets* 2011;10(6):651-658.
Rakha, E.A., Reis-Filho, J.S. and Ellis, I.O. Basal-like breast cancer: a critical review. *J Clin Oncol* 2008;26(15):2568-2581.
Ramirez-Latorre, J., *et al.* Functional contributions of alpha5 subunit to neuronal acetylcholine receptor channels. *Nature* 1996;380(6572):347-351.
Rao, X., *et al.* MicroRNA-221/222 confers breast cancer fulvestrant resistance by regulating multiple signaling pathways. *Oncogene* 2011;30(9):1082-1097.
Raynal, N.J., *et al.* Repositioning FDA-Approved Drugs in Combination with Epigenetic Drugs to Reprogram Colon Cancer Epigenome. *Mol Cancer Ther* 2017;16(2):397-407.
Rinner, I., *et al.* Cholinergic stimulation modulates apoptosis and differentiation of murine thymocytes via a nicotinic effect on thymic epithelium. *Biochem Biophys Res Commun* 1994;203(2):1057-1062.
Ristori, E., *et al.* A Dicer-miR-107 Interaction Regulates Biogenesis of Specific miRNAs Crucial for Neurogenesis. *Dev Cell* 2015;32(5):546-560.
Ritchie, M.E., *et al.* limma powers differential expression analyses for RNA-sequencing and microarray studies. *Nucleic Acids Res* 2015;43(7):e47.
Roopra, A. MAGIC: A tool for predicting transcription factors and cofactors driving gene sets using ENCODE data. *PLoS Comput Biol* 2020;16(4):e1007800.
Rosa, A.L., *et al.* Allele-specific methylation of a functional CTCF binding site upstream of MEG3 in the human imprinted domain of 14q32. *Chromosome Res* 2005;13(8):809-818.
Rosenblatt, R.B., Frank, J.A. and Burks, S.R. Cytosolic Ca(2+) transients during pulsed focused ultrasound generate reactive oxygen species and cause DNA damage in tumor cells. *Theranostics* 2021;11(2):602-613.
Rubin, J.D., *et al.* Transcription factor enrichment analysis (TFEA) quantifies the activity of multiple transcription factors from a single experiment. *Commun Biol* 2021;4(1):661.
Rufini, A., *et al.* Senescence and aging: the critical roles of p53. *Oncogene* 2013;32(43):5129-5143.
Safe, S. Transcriptional activation of genes by 17 beta-estradiol through estrogen receptor-Sp1 interactions. *Vitam Horm* 2001;62:231-252.
Samocha, K.E., *et al.* A framework for the interpretation of de novo mutation in human disease. *Nat Genet* 2014;46(9):944-950.
Sarver, A.L., *et al.* MicroRNAs at the human 14q32 locus have prognostic significance in osteosarcoma. *Orphanet J Rare Dis* 2013;8:7.
Scherf, D.B., *et al.* Epigenetic screen identifies genotype-specific promoter DNA methylation and oncogenic potential of CHRNB4. *Oncogene* 2013;32(28):3329-3338.
Schrode, N., *et al.* Synergistic effects of common schizophrenia risk variants. *Nat Genet* 2019;51(10):1475-1485.
Schrode, N., *et al.* Analysis framework and experimental design for evaluating synergy-driving gene expression. *Nat Protoc* 2021;16(2):812-840.
Schuller, H.M. Is cancer triggered by altered signalling of nicotinic acetylcholine receptors? *Nat Rev Cancer* 2009;9(3):195-205.
Sellers, Z.P., *et al.* Increased methylation upstream of the MEG3 promotor is observed in acute myeloid leukemia patients with better overall survival. *Clin Epigenetics* 2019;11(1):50.
Shannon, P., *et al.* Cytoscape: a software environment for integrated models of biomolecular interaction networks. *Genome Res* 2003;13(11):2498-2504.

Shatz, M., *et al.* p53 amplifies Toll-like receptor 5 response in human primary and cancer cells through interaction with multiple signal transduction pathways. *Oncotarget* 2015;6(19):16963-16980.
Shehwana, H., *et al.* CHRNA5 belongs to the secondary estrogen signaling network exhibiting prognostic significance in breast cancer. *Cell Oncol (Dordr)* 2021;44(2):453-472.
Shen L, S.I. 2021. GeneOverlap: Test and visualize gene overlaps. R package version 1.28.0, . http://shenlab-sinai.github.io/shenlab-sinai/.
Sherwin, B.B. Estrogen and/or androgen replacement therapy and cognitive functioning in surgically menopausal women. *Psychoneuroendocrinology* 1988;13(4):345-357.
Shibahara, Y., *et al.* Aromatase inhibitor treatment of breast cancer cells increases the expression of let-7f, a microRNA targeting CYP19A1. *J Pathol* 2012;227(3):357-366.
Shivram, H., Le, S.V. and Iyer, V.R. PRC2 activates interferon-stimulated genes indirectly by repressing miRNAs in glioblastoma. *PLoS One* 2019;14(9):e0222435.
Silva, M.R., *et al.* Polymorphisms of CHRNA3 and CHRNA5: Head and neck cancer and cigarette consumption intensity in a Brazilian population. *Mol Genet Genomic Med* 2019;7(12):e998.
Simoes, B.M., *et al.* Anti-estrogen Resistance in Human Breast Tumors Is Driven by JAG1-NOTCH4-Dependent Cancer Stem Cell Activity. *Cell Rep* 2015;12(12):1968-1977.
Sims, A.H., *et al.* Origins of breast cancer subtypes and therapeutic implications. *Nat Clin Pract Oncol* 2007;4(9):516-525.
Slamon, D.J., *et al.* Human breast cancer: correlation of relapse and survival with amplification of the HER-2/neu oncogene. *Science* 1987;235(4785):177-182.
Slamon, D.J., *et al.* Use of chemotherapy plus a monoclonal antibody against HER2 for metastatic breast cancer that overexpresses HER2. *N Engl J Med* 2001;344(11):783-792.
Smith, C.L. and O'Malley, B.W. Coregulator function: a key to understanding tissue specificity of selective receptor modulators. *Endocr Rev* 2004;25(1):45-71.
Smith, M.L. and Seo, Y.R. p53 regulation of DNA excision repair pathways. *Mutagenesis* 2002;17(2):149-156.
Song, L., *et al.* miR-495 enhances the sensitivity of non-small cell lung cancer cells to platinum by modulation of copper-transporting P-type adenosine triphosphatase A (ATP7A). *J Cell Biochem* 2014;115(7):1234-1242.
Song, P. and Spindel, E.R. Basic and clinical aspects of non-neuronal acetylcholine: expression of non-neuronal acetylcholine in lung cancer provides a new target for cancer therapy. *J Pharmacol Sci* 2008;106(2):180-185.
Song, Q., *et al.* miR-21 synergizes with BMP9 in osteogenic differentiation by activating the BMP9/Smad signaling pathway in murine multilineage cells. *Int J Mol Med* 2015;36(6):1497-1506.
Song, Y., *et al.* EPAS1 targeting by miR-152-3p in Paclitaxel-resistant Breast Cancer. *J Cancer* 2020;11(19):5822-5830.
Spinelli, L., *et al.* BubbleGUM: automatic extraction of phenotype molecular signatures and comprehensive visualization of multiple Gene Set Enrichment Analyses. *BMC Genomics* 2015;16:814.
Stegemann, A. and Bohm, M. Tropisetron via alpha7 nicotinic acetylcholine receptor suppresses tumor necrosis factor-alpha-mediated cell responses of human keratinocytes. *Exp Dermatol* 2019;28(3):276-282.
Stepaniants, S., *et al.* Genes related to emphysema are enriched for ubiquitination pathways. *BMC Pulm Med* 2014;14:187.
Stevens, M.L., *et al.* Genomic integration of Wnt/beta-catenin and BMP/Smad1 signaling coordinates foregut and hindgut transcriptional programs. *Development* 2017;144(7):1283-1295.
Stokes, C. and Papke, R.L. Use of an alpha3beta4 nicotinic acetylcholine receptor subunit concatamer to characterize ganglionic receptor subtypes with specific subunit composition reveals species-specific pharmacologic properties. *Neuropharmacology* 2012;63(4):538-546.
Subramanian, A., *et al.* Gene set enrichment analysis: a knowledge-based approach for interpreting genome-wide expression profiles. *Proc Natl Acad Sci U S A* 2005;102(43):15545-15550.

Sun, H.J., Jia, Y.F. and Ma, X.L. Alpha5 Nicotinic Acetylcholine Receptor Contributes to Nicotine-Induced Lung Cancer Development and Progression. *Front Pharmacol* 2017;8:573.
Sun, J., *et al.* MiR495 suppresses cell proliferation by directly targeting HMGA2 in lung cancer. *Mol Med Rep* 2019;19(3):1463-1470.
Sun, Y., *et al.* Silencing c-Jun inhibits autophagy and abrogates radioresistance in nasopharyngeal carcinoma by activating the PI3K/AKT/mTOR pathway. *Ann Transl Med* 2021;9(13):1085.
Sun, Y., *et al.* P53 is required for Doxorubicin-induced apoptosis via the TGF-beta signaling pathway in osteosarcoma-derived cells. *Am J Cancer Res* 2016;6(1):114-125.
Sung, H., *et al.* Global Cancer Statistics 2020: GLOBOCAN Estimates of Incidence and Mortality Worldwide for 36 Cancers in 185 Countries. *CA Cancer J Clin* 2021;71(3):209-249.
Szklarczyk, D., *et al.* STRING v11: protein-protein association networks with increased coverage, supporting functional discovery in genome-wide experimental datasets. *Nucleic Acids Res* 2019;47(D1):D607-D613.
Takuwa, N., Zhou, W. and Takuwa, Y. Calcium, calmodulin and cell cycle progression. *Cell Signal* 1995;7(2):93-104.
Tan, M., *et al.* microRNA-495 promotes bladder cancer cell growth and invasion by targeting phosphatase and tensin homolog. *Biochem Biophys Res Commun* 2017;483(2):867-873.
Tang, J., *et al.* MiR-495-3p and miR-143-3p co-target CDK1 to inhibit the development of cervical cancer. *Clin Transl Oncol* 2021.
Tang, J.M., *et al.* Acetylcholine induces mesenchymal stem cell migration via Ca2+ /PKC/ERK1/2 signal pathway. *J Cell Biochem* 2012;113(8):2704-2713.
Tapia, L., Kuryatov, A. and Lindstrom, J. Ca2+ permeability of the (alpha4)3(beta2)2 stoichiometry greatly exceeds that of (alpha4)2(beta2)3 human acetylcholine receptors. *Mol Pharmacol* 2007;71(3):769-776.
Tekpli, X., *et al.* Functional effect of polymorphisms in 15q25 locus on CHRNA5 mRNA, bulky DNA adducts and TP53 mutations. *Int J Cancer* 2013;132(8):1811-1820.
Thorgeirsson, T.E., *et al.* A rare missense mutation in CHRNA4 associates with smoking behavior and its consequences. *Mol Psychiatry* 2016;21(5):594-600.
Tolaymat, M., *et al.* The Role of M3 Muscarinic Receptor Ligand-Induced Kinase Signaling in Colon Cancer Progression. *Cancers (Basel)* 2019;11(3).
Treuter, E., *et al.* Competition between thyroid hormone receptor-associated protein (TRAP) 220 and transcriptional intermediary factor (TIF) 2 for binding to nuclear receptors. Implications for the recruitment of TRAP and p160 coactivator complexes. *J Biol Chem* 1999;274(10):6667-6677.
Tu, S.H., *et al.* Protein phosphatase Mg2+/Mn2+ dependent 1F promotes smoking-induced breast cancer by inactivating phosphorylated-p53-induced signals. *Oncotarget* 2016;7(47):77516-77531.
Uppal, A., *et al.* 14q32-encoded microRNAs mediate an oligometastatic phenotype. *Oncotarget* 2015;6(6):3540-3552.
Uppman, S. Social education of staff for audiological work. *Scand Audiol Suppl* 1978(Suppl 8):168-171.
Van Maerken, T., *et al.* Escape from p53-mediated tumor surveillance in neuroblastoma: switching off the p14(ARF)-MDM2-p53 axis. *Cell Death Differ* 2009;16(12):1563-1572.
Vasan, N., Baselga, J. and Hyman, D.M. A view on drug resistance in cancer. *Nature* 2019;575(7782):299-309.
Vegeto, E., Benedusi, V. and Maggi, A. Estrogen anti-inflammatory activity in brain: a therapeutic opportunity for menopause and neurodegenerative diseases. *Front Neuroendocrinol* 2008;29(4):507-519.
Verde Rodrigues, L.C., *et al.* Neurotoxicological profile assessment of lobeline after acute treatment in mice. *Basic Clin Pharmacol Toxicol* 2014;114(6):485-489.
Vichas, A., *et al.* Integrative oncogene-dependency mapping identifies RIT1 vulnerabilities and synergies in lung cancer. *Nat Commun* 2021;12(1):4789.
Vilquin, P., *et al.* MicroRNA-125b upregulation confers aromatase inhibitor resistance and is a novel marker of poor prognosis in breast cancer. *Breast Cancer Res* 2015;17:13.

Vogel, V.G., *et al.* Effects of tamoxifen vs raloxifene on the risk of developing invasive breast cancer and other disease outcomes: the NSABP Study of Tamoxifen and Raloxifene (STAR) P-2 trial. *JAMA* 2006;295(23):2727-2741.
Wakeling, A.E. and Bowler, J. Novel antioestrogens without partial agonist activity. *J Steroid Biochem* 1988;31(4B):645-653.
Wang, C., *et al.* MiR-495 is a Predictive Biomarker that Downregulates GFI1 Expression in Medulloblastoma. *Cell Physiol Biochem* 2015;36(4):1430-1439.
Wang, F., *et al.* Assembly of human neuronal nicotinic receptor alpha5 subunits with alpha3, beta2, and beta4 subunits. *J Biol Chem* 1996;271(30):17656-17665.
Wang, G., *et al.* FAM83A and FAM83A-AS1 both play oncogenic roles in lung adenocarcinoma. *Oncol Lett* 2021;21(4):297.
Wang, H., *et al.* Multivalent rubber-like RNA nanoparticles for targeted co-delivery of paclitaxel and MiRNA to silence the drug efflux transporter and liver cancer drug resistance. *J Control Release* 2021;330:173-184.
Wang, H., *et al.* MicroRNA-495 Inhibits Gastric Cancer Cell Migration and Invasion Possibly via Targeting High Mobility Group AT-Hook 2 (HMGA2). *Med Sci Monit* 2017;23:640-648.
Wang, H., Lu, Y. and Wang, Z. Function of cardiac M3 receptors. *Auton Autacoid Pharmacol* 2007;27(1):1-11.
Wang, J., *et al.* MicroRNA495 regulates human gastric cancer cell apoptosis and migration through Akt and mTOR signaling. *Oncol Rep* 2018;40(6):3654-3662.
Wang, J., *et al.* Human esophageal smooth muscle cells express muscarinic receptor subtypes M(1) through M(5). *Am J Physiol Gastrointest Liver Physiol* 2000;279(5):G1059-1069.
Wang, J., *et al.* The antidepressant and anxiolytic effect of GPER on translocator protein (TSPO) via protein kinase a (PKA) signaling in menopausal female rats. *J Steroid Biochem Mol Biol* 2021;207:105807.
Wang, J., *et al.* FOXC1 is associated with estrogen receptor alpha and affects sensitivity of tamoxifen treatment in breast cancer. *Cancer Med* 2017;6(1):275-287.
Wang, L., *et al.* miR-9-5p facilitates hepatocellular carcinoma cell proliferation, migration and invasion by targeting ESR1. *Mol Cell Biochem* 2021;476(2):575-583.
Wang, L., *et al.* Downregulated miR-495 [Corrected] Inhibits the G1-S Phase Transition by Targeting Bmi-1 in Breast Cancer. *Medicine (Baltimore)* 2015;94(21):e718.
Wang, M., *et al.* Comprehensive Bioinformatics Analysis of mRNA Expression Profiles and Identification of a miRNA-mRNA Network Associated with the Pathogenesis of Low-Grade Gliomas. *Cancer Manag Res* 2021;13:5135-5147.
Wang, W. Emergence of a DNA-damage response network consisting of Fanconi anaemia and BRCA proteins. *Nat Rev Genet* 2007;8(10):735-748.
Wang, X., Zhang, H. and Chen, X. Drug resistance and combating drug resistance in cancer. *Cancer Drug Resist* 2019;2:141-160.
Wang, Y., *et al.* MiR-495/IGF-1/AKT Signaling as a Novel Axis Is Involved in the Epithelial-to-Mesenchymal Transition of Oral Squamous Cell Carcinoma. *J Oral Maxillofac Surg* 2019;77(5):1009-1021.
Wang, Y., *et al.* MEF2A Regulates the MEG3-DIO3 miRNA Mega Cluster-Targeted PP2A Signaling in Bovine Skeletal Myoblast Differentiation. *Int J Mol Sci* 2019;20(11).
Wang, Y., *et al.* Association of CHRNA5-A3-B4 variation with esophageal squamous cell carcinoma risk and smoking behaviors in a Chinese population. *PLoS One* 2013;8(7):e67664.
Wardell, S.E., Kazmin, D. and McDonnell, D.P. Research resource: Transcriptional profiling in a cellular model of breast cancer reveals functional and mechanistic differences between clinically relevant SERM and between SERM/estrogen complexes. *Mol Endocrinol* 2012;26(7):1235-1248.
Wei, T., *et al.* miR-495 promotes the chemoresistance of SCLC through the epithelial-mesenchymal transition via Etk/BMX. *Am J Cancer Res* 2017;7(3):628-646.
Welboren, W.J., *et al.* ChIP-Seq of ERalpha and RNA polymerase II defines genes differentially responding to ligands. *EMBO J* 2009;28(10):1418-1428.
Wen, L., *et al.* Contribution of Variants in CHRNA5/A3/B4 Gene Cluster on Chromosome 15 to Tobacco Smoking: From Genetic Association to Mechanism. *Mol Neurobiol* 2016;53(1):472-484.

Wessler, I. and Kirkpatrick, C.J. Acetylcholine beyond neurons: the non-neuronal cholinergic system in humans. *Br J Pharmacol* 2008;154(8):1558-1571.
Widodo, Djati, M.S. and Rifa'i, M. Role of MicroRNAs in carcinogenesis that potential for biomarker of endometrial cancer. *Ann Med Surg (Lond)* 2016;7:9-13.
Winter, J., *et al.* Many roads to maturity: microRNA biogenesis pathways and their regulation. *Nat Cell Biol* 2009;11(3):228-234.
Wu, D. and Smyth, G.K. Camera: a competitive gene set test accounting for inter-gene correlation. *Nucleic Acids Res* 2012;40(17):e133.
Wu, H., *et al.* Is susceptibility locus for lung cancer in the 15q25 nicotinic acetylcholine receptor gene cluster CHRNA5-A3-B4 associated with risk of gastric cancer? *Med Oncol* 2013;30(2):576.
Wu, T., *et al.* clusterProfiler 4.0: A universal enrichment tool for interpreting omics data. *The Innovation* 2021;2(3).
Xi, H.J., *et al.* Role of acetylcholinesterase in lung cancer. *Thorac Cancer* 2015;6(4):390-398.
Xia, Y., *et al.* lncRNA NEAT1 facilitates melanoma cell proliferation, migration, and invasion via regulating miR-495-3p and E2F3. *J Cell Physiol* 2019;234(11):19592-19601.
Xiao, C., *et al.* Neural circuits and nicotinic acetylcholine receptors mediate the cholinergic regulation of midbrain dopaminergic neurons and nicotine dependence. *Acta Pharmacol Sin* 2020;41(1):1-9.
Xiao, T., *et al.* Estrogen-regulated feedback loop limits the efficacy of estrogen receptor-targeted breast cancer therapy. *Proc Natl Acad Sci U S A* 2018;115(31):7869-7878.
Xu, C., *et al.* Pulmonary Codelivery of Doxorubicin and siRNA by pH-Sensitive Nanoparticles for Therapy of Metastatic Lung Cancer. *Small* 2015;11(34):4321-4333.
Xu, Q., *et al.* Site-specific regulation of gene expression by estrogen in the hypothalamus of adult female rats. *Neurosci Lett* 2008;436(1):35-39.
Xu, X.L., Olson, J.M. and Zhao, L.P. A regression-based method to identify differentially expressed genes in microarray time course studies and its application in an inducible Huntington's disease transgenic model. *Hum Mol Genet* 2002;11(17):1977-1985.
Xu, Y., *et al.* Identification of Potential Driver Genes Based on Multi-Genomic Data in Cervical Cancer. *Front Genet* 2021;12:598304.
Xu, Y., *et al.* Changes in the expression of miR-381 and miR-495 are inversely associated with the expression of the MDR1 gene and development of multi-drug resistance. *PLoS One* 2013;8(11):e82062.
Xu, Y., *et al.* Combinatorial microRNAs suppress hypoxia-induced cardiomyocytes apoptosis. *Cell Physiol Biochem* 2015;37(3):921-932.
Xu, Y.Y., *et al.* MicroRNA-495 downregulates FOXC1 expression to suppress cell growth and migration in endometrial cancer. *Tumour Biol* 2016;37(1):239-251.
Yan, L., Yao, J. and Qiu, J. miRNA-495 suppresses proliferation and migration of colorectal cancer cells by targeting FAM83D. *Biomed Pharmacother* 2017;96:974-981.
Yang, H., *et al.* MicroRNAs regulate methionine adenosyltransferase 1A expression in hepatocellular carcinoma. *J Clin Invest* 2013;123(1):285-298.
Yang, Z., *et al.* CircKRT1 drives tumor progression and immune evasion in oral squamous cell carcinoma by sponging miR-495-3p to regulate PDL1 expression. *Cell Biol Int* 2021;45(7):1423-1435.
Yao, W., *et al.* Taxifolin Targets PI3K and mTOR and Inhibits Glioblastoma Multiforme. *J Oncol* 2021;2021:5560915.
Ye, M., *et al.* TSPAN12 promotes chemoresistance and proliferation of SCLC under the regulation of miR-495. *Biochem Biophys Res Commun* 2017;486(2):349-356.
Ye, Y., *et al.* MicroRNA-495 suppresses cell proliferation and invasion of hepatocellular carcinoma by directly targeting insulin-like growth factor receptor-1. *Exp Ther Med* 2018;15(1):1150-1158.
Yi, X., *et al.* The relationship between CHRNA5/A3/B4 gene cluster polymorphisms and lung cancer risk: An updated meta-analysis and systematic review. *Medicine (Baltimore)* 2021;100(6):e24355.

Yin, G., *et al.* ZNF503 accelerates aggressiveness of hepatocellular carcinoma cells by down-regulation of GATA3 expression and regulated by microRNA-495. *Am J Transl Res* 2019;11(6):3426-3437.
You, X., *et al.* MicroRNA-495 confers inhibitory effects on cancer stem cells in oral squamous cell carcinoma through the HOXC6-mediated TGF-beta signaling pathway. *Stem Cell Res Ther* 2020;11(1):117.
Youngs, E.L., Hellings, J.A. and Butler, M.G. A clinical report and further delineation of the 14q32 deletion syndrome. *Clin Dysmorphol* 2011;20(3):143-147.
Yu-Rice, Y., *et al.* FOXC1 is involved in ERalpha silencing by counteracting GATA3 binding and is implicated in endocrine resistance. *Oncogene* 2016;35(41):5400-5411.
Yu, H., *et al.* Acetylcholine acts through M3 muscarinic receptor to activate the EGFR signaling and promotes gastric cancer cell proliferation. *Sci Rep* 2017;7:40802.
Yu, L., *et al.* Dual HER2 Blockade versus a Single Agent in Trastuzumab-Containing Regimens for HER2-Positive Early Breast Cancer: A Systematic Review and Meta-Analysis of Randomized Controlled Trials. *J Oncol* 2020;2020:5169278.
Yu, Q., *et al.* An estradiol-17beta/miRNA-26a/cyp19a1a regulatory feedback loop in the protogynous hermaphroditic fish, Epinephelus coioides. *Mol Cell Endocrinol* 2020;504:110689.
Yuan, C.X., *et al.* The TRAP220 component of a thyroid hormone receptor- associated protein (TRAP) coactivator complex interacts directly with nuclear receptors in a ligand-dependent fashion. *Proc Natl Acad Sci U S A* 1998;95(14):7939-7944.
Zaccara, S., *et al.* p53-directed translational control can shape and expand the universe of p53 target genes. *Cell Death Differ* 2014;21(10):1522-1534.
Zafar, E., *et al.* A comprehensive review on anticancer mechanism of bazedoxifene. *Biotechnol Appl Biochem* 2021.
Zage, P.E., *et al.* A novel therapeutic combination for neuroblastoma: the vascular endothelial growth factor receptor/epidermal growth factor receptor/rearranged during transfection inhibitor vandetanib with 13-cis-retinoic acid. *Cancer* 2010;116(10):2465-2475.
Zehavi, L., *et al.* Silencing of a large microRNA cluster on human chromosome 14q32 in melanoma: biological effects of mir-376a and mir-376c on insulin growth factor 1 receptor. *Mol Cancer* 2012;11:44.
Zeng, Z., *et al.* Mammography and ultrasound effective features in differentiating basal-like and normal-like subtypes of triple negative breast cancer. *Oncotarget* 2017;8(45):79670-79679.
Zhang, B., *et al.* Uncovering the transcriptomic and epigenomic landscape of nicotinic receptor genes in non-neuronal tissues. *BMC Genomics* 2017;18(1):439.
Zhang, B., *et al.* Hsa-miR-495 acts as a tumor suppressor gene in glioma via the negative regulation of MYB. *Mol Med Rep* 2016;14(1):977-982.
Zhang, C., *et al.* Blockade of alpha7 nicotinic acetylcholine receptors inhibit nicotine-induced tumor growth and vimentin expression in non-small cell lung cancer through MEK/ERK signaling way. *Oncol Rep* 2017;38(6):3309-3318.
Zhang, H., *et al.* Curcumin Suppresses In Vitro Proliferation and Invasion of Human Prostate Cancer Stem Cells by Modulating DLK1-DIO3 Imprinted Gene Cluster MicroRNAs. *Genet Test Mol Biomarkers* 2018;22(1):43-50.
Zhang, L.N., Li, J.Y. and Xu, W. A review of the role of Puma, Noxa and Bim in the tumorigenesis, therapy and drug resistance of chronic lymphocytic leukemia. *Cancer Gene Ther* 2013;20(1):1-7.
Zhang, R., Wang, T. and Lin, J. Synergistic Effect of Bazedoxifene and PARP Inhibitor in the Treatment of Ovarian Cancer Regardless of BRCA Mutation. *Anticancer Res* 2021;41(5):2277-2286.
Zhang, S., Xie, D. and Zhang, Q. Mesenchymal stem cells plus bone repair materials as a therapeutic strategy for abnormal bone metabolism: Evidence of clinical efficacy and mechanisms of action implied. *Pharmacol Res* 2021;172:105851.
Zhang, Y., *et al.* Reciprocal activation of alpha5-nAChR and STAT3 in nicotine-induced human lung cancer cell proliferation. *J Genet Genomics* 2017;44(7):355-362.
Zhang, Y., *et al.* alpha5-nAChR and survivin: Two potential biological targets in lung adenocarcinoma. *J Cell Physiol* 2021;236(3):1787-1797.

Zhang, Y., *et al.* FUNNEL-GSEA: FUNctioNal ELastic-net regression in time-course gene set enrichment analysis. *Bioinformatics* 2017;33(13):1944-1952.
Zhao, C., *et al.* A feedback regulatory loop involving microRNA-9 and nuclear receptor TLX in neural stem cell fate determination. *Nat Struct Mol Biol* 2009;16(4):365-371.
Zhao, J., *et al.* Synergy between next generation EGFR tyrosine kinase inhibitors and miR-34a in the inhibition of non-small cell lung cancer. *Lung Cancer* 2017;108:96-102.
Zhao, J.J., *et al.* MicroRNA-221/222 negatively regulates estrogen receptor alpha and is associated with tamoxifen resistance in breast cancer. *J Biol Chem* 2016;291(43):22859.
Zhao, Q., *et al.* Inactivation of M2 AChR/NF-kappaB signaling axis reverses epithelial-mesenchymal transition (EMT) and suppresses migration and invasion in non-small cell lung cancer (NSCLC). *Oncotarget* 2015;6(30):29335-29346.
Zhao, Y., *et al.* Synergistic regulatory effects of microRNAs on brain glioma cells. *Mol Med Rep* 2017;16(2):1409-1416.
Zhao, Y., *et al.* Nicotine activates YAP1 through nAChRs mediated signaling in esophageal squamous cell cancer (ESCC). *PLoS One* 2014;9(3):e90836.
Zheng, H.E., *et al.* MicroRNA-495 inhibits the progression of non-small-cell lung cancer by targeting TCF4 and inactivating Wnt/beta-catenin pathway. *Eur Rev Med Pharmacol Sci* 2018;22(22):7750-7759.
Zhou, X., *et al.* MiR-141 Inhibits Gastric Cancer Proliferation by Interacting with Long Noncoding RNA MEG3 and Down-Regulating E2F3 Expression. *Dig Dis Sci* 2015;60(11):3271-3282.
Zhu, H., *et al.* Fluoxetine is neuroprotective in slow-channel congenital myasthenic syndrome. *Exp Neurol* 2015;270:88-94.
Zhu, J., *et al.* Downregulation of microRNA-27b-3p enhances tamoxifen resistance in breast cancer by increasing NR5A2 and CREB1 expression. *Cell Death Dis* 2016;7(11):e2454.
Zhu, M., *et al.* The future of antibiotics begins with discovering new combinations. *Ann N Y Acad Sci* 2021;1496(1):82-96.
Zhu, W., *et al.* Meg3-DMR, not the Meg3 gene, regulates imprinting of the Dlk1-Dio3 locus. *Dev Biol* 2019;455(1):10-18.
Zhu, W., *et al.* Dissection of protein interactomics highlights microRNA synergy. *PLoS One* 2013;8(5):e63342.
Zhuo, H., *et al.* The aberrant expression of MEG3 regulated by UHRF1 predicts the prognosis of hepatocellular carcinoma. *Mol Carcinog* 2016;55(2):209-219.
Zou, Z., *et al.* miR-495 sensitizes MDR cancer cells to the combination of doxorubicin and taxol by inhibiting MDR1 expression. *J Cell Mol Med* 2017;21(9):1929-1943.

COPY RIGHT PERMISSIONS

JOHN WILEY AND SONS LICENSE
TERMS AND CONDITIONS

Aug 31, 2021

This Agreement between Ms. Ayse Keskus ("You") and John Wiley and Sons ("John Wiley and Sons") consists of your license details and the terms and conditions provided by John Wiley and Sons and Copyright Clearance Center.

License Number	5139340382720
License date	Aug 31, 2021
Licensed Content Publisher	John Wiley and Sons
Licensed Content Publication	BioEssays
Licensed Content Title	Are nicotinic acetylcholine receptors coupled to G proteins?
Licensed Content Author	David J. Adams, Victoria A. Seymour, Amarda Shehu, et al
Licensed Content Date	Oct 8, 2013
Licensed Content Volume	35
Licensed Content Issue	12
Licensed Content Pages	10
Type of use	Dissertation/Thesis
Requestor type	University/Academic
Format	Electronic
Portion	Figure/table
Number of figures/tables	1

ELSEVIER LICENSE
TERMS AND CONDITIONS

Aug 31, 2021

This Agreement between Ms. Ayse Keskus ("You") and Elsevier ("Elsevier") consists of your license details and the terms and conditions provided by Elsevier and Copyright Clearance Center.

License Number	5139650980669
License date	Aug 31, 2021
Licensed Content Publisher	Elsevier
Licensed Content Publication	Elsevier Books
Licensed Content Title	Advances in Protein Chemistry and Structural Biology
Licensed Content Author	Nathalie Fuentes,Patricia Silveyra
Licensed Content Date	Jan 1, 2019
Licensed Content Pages	36
Start Page	135
End Page	170
Type of Use	reuse in a thesis/dissertation
Portion	figures/tables/illustrations
Number of figures/tables/illustrations	1
Format	both print and electronic

SPRINGER NATURE LICENSE
TERMS AND CONDITIONS

Oct 03, 2021

This Agreement between Ms. Ayse Keskus ("You") and Springer Nature ("Springer Nature") consists of your license details and the terms and conditions provided by Springer Nature and Copyright Clearance Center.

License Number	5161460968853
License date	Oct 03, 2021
Licensed Content Publisher	Springer Nature
Licensed Content Publication	Cellular Oncology
Licensed Content Title	CHRNA5 belongs to the secondary estrogen signaling network exhibiting prognostic significance in breast cancer
Licensed Content Author	Huma Shehwana et al
Licensed Content Date	Jan 19, 2021
Type of Use	Thesis/Dissertation
Requestor type	academic/university or research institute
Format	print and electronic
Portion	figures/tables/illustrations
Number of figures/tables /illustrations	3
Will you be translating?	no